AD-A166 596 VECTORED THRUST DIGITAL FLIGHT CONTROL FOR CREW ESCAPE 1/3
VOLUME 2(U) SCIENTIFIC SYSTEMS INC CAMBRIDGE MA
J V CARROLL ET AL. DEC 85 AFWAL-TR-85-3116-VOL-2
UNCLASSIFIED F33615-82-C-3402 F/G 1/4 NL

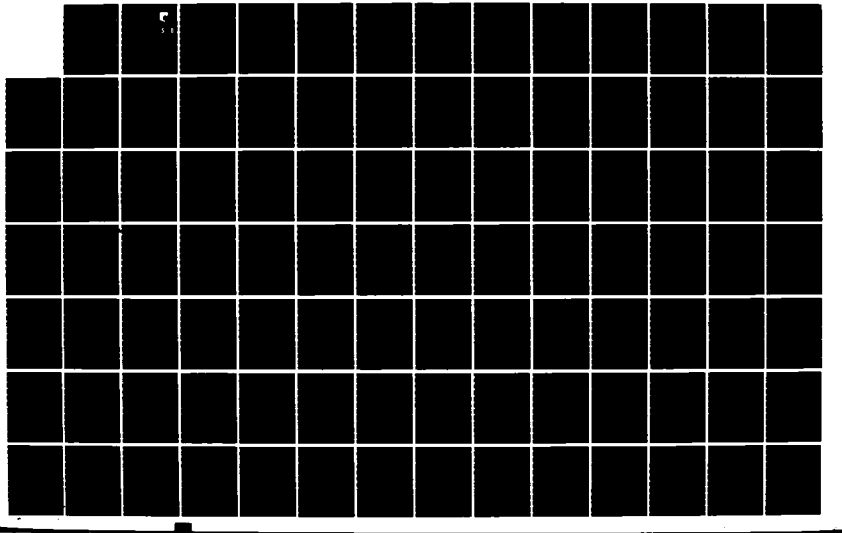

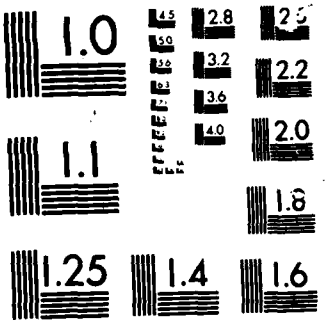

MICROCOPY CHART

AFWAL-TR-85-3116
Volume II

VECTORED THRUST DIGITAL FLIGHT CONTROL FOR CREW ESCAPE

James V. Carroll
Robert F. Gendron

Scientific Systems Inc.
54 Cambridge Park Extension
Cambridge MA 02140

December 1985

Final Report for Period June 1982 - February 1985

FLIGHT DYNAMICS LABORATORY
AIR FORCE WRIGHT AERONAUTICAL LABORATORIES
AIR FORCE SYSTEMS COMMAND
WRIGHT-PATTERSON AIR FORCE BASE, OHIO 45433

NOTICE

When Government drawings, specifications, or other data are used for any purpose other than in connection with a definitely related Government procurement operation, the United States Government thereby incurs no responsibility nor any obligation whatsoever; and the fact that the government may have formulated, furnished, or in any way supplied the said drawings, specifications, or other data, is not to be regarded by implication or otherwise as in any manner licensing the holder or any other person or corporation, or conveying any rights or permission to manufacture use, or sell any patented invention that may in any way be related thereto.

This report has been reviewed by the Office of Public Affairs (ASD/PA) and is releasable to the National Technical Information Service (NTIS). At NTIS, it will be available to the general public, including foreign nations.

This technical report has been reviewed and is approved for publication.

Lanny A. Jines

LANNY A. JINES, P.E.
Project Engineer

B. J. WHITE
Group Leader
Aircrew Escape Group

FOR THE COMMANDER

RUDI BERNDT
Acting Chief
Vehicle Equipment Division

"If your address has changed, if you wish to be removed from our mailing list, or if the addressee is no longer employed by your organization please notify AFWAL/FIER, *W-PAFB, OH 45433 to help us maintain a current mailing list".*

Copies of this report should not be returned unless return is required by security considerations, contractual obligations, or notice on a specific document.

UNCLASSIFIED

SECURITY CLASSIFICATION OF THIS PAGE

AD A166596

REPORT DOCUMENTATION PAGE

1a. REPORT SECURITY CLASSIFICATION UNCLASSIFIED	1b. RESTRICTIVE MARKINGS
2a. SECURITY CLASSIFICATION AUTHORITY	3. DISTRIBUTION/AVAILABILITY OF REPORT Approved for public release; distribution is unlimited.
2b. DECLASSIFICATION/DOWNGRADING SCHEDULE	
4. PERFORMING ORGANIZATION REPORT NUMBER(S)	5. MONITORING ORGANIZATION REPORT NUMBER(S) AFWAL-TR-85-3116, Vol II
6a. NAME OF PERFORMING ORGANIZATION Scientific Systems Inc. — 6b. OFFICE SYMBOL (If applicable)	7a. NAME OF MONITORING ORGANIZATION Flight Dynamics Laboratory (FIER) AF Wright Aeronautical Laboratories, AFSC
6c. ADDRESS (City, State and ZIP Code) 54 Cambridge Park Extension Cambridge MA 02140	7b. ADDRESS (City, State and ZIP Code) Wright-Patterson AFB OH 45433-6553
8a. NAME OF FUNDING/SPONSORING ORGANIZATION Flight Dynamics Laboratory — 8b. OFFICE SYMBOL (If applicable) AFWAL/FIER	9. PROCUREMENT INSTRUMENT IDENTIFICATION NUMBER F33615-C-82-3402
8c. ADDRESS (City, State and ZIP Code) Wright-Patterson AFB, Ohio 45433	10. SOURCE OF FUNDING NOS.

PROGRAM ELEMENT NO.	PROJECT NO.	TASK NO.	WORK UNIT NO.
62201F	2402	240203	24020342

11. TITLE (Include Security Classification) Vectored Thrust Digital Flight Control for Crew Escape Vol II (Uncl)

12. PERSONAL AUTHOR(S) Carroll, James V. Gendron, Robert F.

13a. TYPE OF REPORT	13b. TIME COVERED	14. DATE OF REPORT (Yr., Mo., Day)	15. PAGE COUNT
Final	FROM 82 Jun 01 TO 85 Feb 28	December 1985	187 through 378

16. SUPPLEMENTARY NOTATION
AFWAL-TR-85-3116 consist of Vols I, II, III, and IV Vols III & IV are computer software

17. COSATI CODES		
FIELD	GROUP	SUB. GR
0607		

18. SUBJECT TERMS (Continue on reverse if necessary and identify by block number)
Modern Control Theory, Acceleration Control, Model Algorithmic Control, Ejection Seat Control.

19. ABSTRACT (Continue on reverse if necessary and identify by block number)
Work of Meyer and Cicolani was adapted for application to open seat escape systems in current Air Force fighter aircraft. The control system design is a fully self-contained system whose major on-seat components are: acceleration, rate, attitude and altitude sensors, real-time control logic imbedded on a microprocessor chip, rocket thrusters with thrust vectoring and throttling capability, and various avionics and support subsystem hardware items (e.g., power supply). The control concept is based on a comparison of measured translational and rotational accelerations with desired values; the propulsion system is then configured to provide adequate energy to follow the desired trajectory and simultaneously eliminate acceleration errors. The concept uses nonlinear models and incorporates state and control constraints. Volume I contains the detailed documentation of specification development, control logic design, hardware identification, and trade study efforts. Volume II contains a description of the prototype design, real time breadboard simulation, and the results and analysis of the verification task. Volume III

20. DISTRIBUTION/AVAILABILITY OF ABSTRACT	21. ABSTRACT SECURITY CLASSIFICATION
UNCLASSIFIED UNLIMITED ☒ SAME AS RPT ☐ DTIC USERS ☐	UNCLASSIFIED

22a. NAME OF RESPONSIBLE INDIVIDUAL	22b. TELEPHONE NUMBER (Include Area Code)	22c. OFFICE SYMBOL
Lanny A. Jines	(513) 255-3305	AFWAL/FIER

DD FORM 1473, 83 APR EDITION OF 1 JAN 73 IS OBSOLETE

UNCLASSIFIED

SECURITY CLASSIFICATION OF THIS PAGE

contains the supporting appendices for Volumes I and II. Volume IV details the results of the real time hybrid computer simulation effort.

FOREWORD

The design study described in this report was conducted by Scientific Systems, Inc. (SSI), Cambridge, Mass., under Contract F33615-82-C-3402. The project was administered by Mr. Lanny A. Jines in the Crew and Escape Subsystems Branch of the Vehicle Equipment Division, Flight Dynamics Laboratory, Air Force Wright Aeronautical Laboratories, Wright-Patterson Air Force Base, Ohio. SSI was supported in this project by the following subcontractors: Stencel Aero Engineering Corp., Martin Marietta Orlando Aerospace, Boeing Military Airplane Co., and Unidynamics/Phoenix.

Dr. James V. Carroll of SSI was Program Manager. His co-workers were R. Gendron, D. Martin, and B. Chan. Dr. Raman Mehra, President of SSI, played an active technical role in the early phases of the project. Key subcontractor participants were: Dr. C. Kylstra of Stencel, S. Baumgartner of Boeing, M. K. Klukis, A. J. Ciaponi and W. Hester of Martin Marietta, and J. Roane of Unidynamics.

The timely and efficient support of the SSI Publications Department, led by Alina Bernat, was greatly appreciated.

TABLE OF CONTENTS

VOLUME I (Under Separate Cover)

TABLE OF CONTENTS (cont'd)

VOLUME I (Under Separate Cover)

VOLUME II

TABLE OF CONTENTS (continued)

LIST OF FIGURES

LIST OF TABLES

CHAPTER 6

TASK 4: PROTOTYPE DESIGN; REAL TIME BREADBOARD SIMULATION

This volume is the second of four which collectively summarize the results from the development of a control strategy for ejection seats for the Air Force Program entitled "Vectored Thrust Digital Flight Control for Crew Escape." Volume I of this effort concentrated on posing the fundamental control problem and reviewed several control synthesis techniques for potential application to this problem. The "acceleration control" approach based on Meyer (1975) best met the stringent time requirements in dealing directly with the life-threatening accelerations typical in the high dynamic environment of ejection seat deployment. Subsequent discussion dealt with adapting Meyer's approach to the specific requirements of the ejection seat problem and detailed the benefits of the selected control design. Also discussed in Volume I was the result of a technology survey that investigated the current availability of sensors, actuators, and microprocessors to meet the respective state estimation accuracy, control energy and computational requirements inherent in the implementation of the new control design.

Volume II focuses on the description of the simulation effort and results obtained using the "acceleration control" approach applied to the ACES II ejection seat given the confines of existing technologies. The primary goal of Task 4 is the evaluation of the feasibility of real-time operation of a microprocessor based implementation of the control design when applied to a wide variety of escape conditions ranging from benign to immediately life threatening.

Given the enormous computational overhead in generating the truth model for high fidelity flight simulations, standard digital computers are typically unsuitable for real-time operation. That is, the truth models require generation of the necessary sensor inputs for use by the control law and the evaluation of the subsequent airframe response to control outputs. For high dimensional models operating at fast rates (on the order of 50 to 100 Hz), the requirements would exceed the capacity of most digital computers with the exception of large dedicated main frames.

The approach taken here is to simulate in analog hardware as many of the models as practicable with the exception of the digital control law under test. The analog computer is by nature a parallel processing device so that real-time simulation of even enormously complex system models is feasible. In this "hybrid" mode, the microprocessor based system solicits sensor inputs directly over an analog to digital converter (ADC) interface and delivers the quantized control outputs to the actuation system via digital to analog converters (DAC). The interfaces then accurately reflect the actual communication medium of the operational host system. That is, the effect of signal quantization, sampling error, ambient electrical noise, hardware response time and control cycle timing are all implicit in system operation.

The simulation test cases examined are meant to exercise the control law over the entire spectrum of flight conditions for which it is designed. In the low altitude regime the flight scenarios exercise "adverse attitude" conditions, i.e., conditions in which ground collision is likely if the opportunity for immediate corrective action is delayed. High dynamic pressure operation is demonstrated in low altitude and high altitude situations while other test cases are aimed at examining the sensitivity of control performance to large angle variations in initial attitude. Of paramount importance in the evaluations is the control system effectiveness in maintaining

the "acceleration radical" below the lethal or high probability of injury limit while demonstrating proper terminal attitude control for subsequent phases of chute deployment and recovery.

Volume II is subdivided into three chapters, 6 through 8. Chapter 6 is devoted to the description of the hybrid simulation models and includes a discussion of the aerodynamics, dynamics equations, plus sensor and actuator models comprising the analog segment of the simulation (6.2). The digital segment representing the control and actuator element logic is discussed in section 6.3. The allocation of hardware to perform the hybrid processing is described in section 6.4 and includes a brief description of the Martin Marietta computing configuration as well as the microprocessor based system developed by Unidynamics. Overlap with some material presented in other volumes of this report is inevitable but for the sake of continuity and completeness some information is repeated when necessary.

Chapter 7 represents the main body of the results. The purpose of Chapter 7 is to demonstrate that the major control objectives are met when evaluated in "difficult" situations. Aside from the emphasis on control system performance, other results are presented that demonstrate consistency between alternate analog simulation models. For example, the hybrid simulation allows for generation of results through the use of a main frame computer replacing the microprocessor implementation of the control algorithm. Close agreement in the results is obtained with the alternate configurations as demonstrated in section 7.2. Also included as a comparison in the results are the effects of "open loop" operation of the system. Here "open loop" refers to fixed force magnitude of the main thruster with no means of attitude control corresponding to current ACES II performance due to the omission of the STAPAC and the drogue from the system. These comparisons vividly demonstrate the direct benefits of intelligent ejection seat control.

The results exercising the MIL-SPEC cases as defined in are presented in section 7.3 . Those cases reflect the "adverse attitude" cases previously mentioned. Section 7.4 is devoted to examining the alternate 20 cases as required by SOW paragraph 4.5.4.2 which exercises the control law over a wide range of initial speed, altitude and attitude conditions.

Paragraph 7.6 is a discussion of the memory and throughput measurements for the Motorola 68000 microprocessor (MC 68000) in this control application. The original intent of implementing the control algorithm in a higher order language (PASCAL) has proven to yield results far from satisfactory with respect to system timing. However an assembly version of the control code has proven successful in meeting the stringent timing requirements of the duty cycle.

Paragraph 7.7 analyzes the stability of the control system to variations in parameters such as gains, sensor and actuator bandwidths, as well as sensitivity to initial conditions and uncertainty in moment of inertia and CG location.

Finally, paragraph 7.8 is a stand alone section which evaluates the effects of pilot CG motion on control system performance. Due to limitations in the pilot harness restraints, some limited pilot motion when subjected to high g's is inevitable. As a consequence the net seat/pilot center of gravity and moment of inertia is actually a time varying quantity. The control law maintains a constant estimate of these key system parameters so that the variations in performance is of some issue in determining robustness of the control approach. The results included in paragraph 7.8 demonstate an insignificant level of sensitivity to pilot motion disturbance.

Chapter 8 offers some basic conclusions on the overall system performance plus indicated restrictions for deployment and offers recommendations for further studies of and enhancements in the control

system design.

6.1 Overview of the hybrid simulation model.

The hybrid simulation for the ejection seat problem is a collection of modules that model the dynamics and response for the components of the ACES II ejection seat flight system. Three classifications of models are evident: 1) environment models, 2) sensor and actuation system models and 3) the digital control algorithm. The environment models are concerned with representing with the highest degree of realism the effects of the aerodynamic forces and torques acting on the ejection seat as a function of the specific flight conditions, i.e., ejection seat altitude, speed and attitude. The sensor models receive the best estimate of the "truth" from the ejection seat dynamics model and in turn generate realistic signals which incorporate the major sources of instrument error. Here the most pressing source of error is instrument delay since the control system response time is critical in alleviating the life-threatening forces acting on the pilot's body. The actuation system models are similarly concerned with imposing the natural instrument delay in responding to control law command inputs. Hence, the actual forces and torques sensed by the seat differ from the idealized commands due to the limitations of the actuation system. The digital control law accepts the raw instrument inputs and, given certain control parameters (gains, time constants, trajectory profile specifications), generates the idealized control signals for use by the actuation system just mentioned.

In digital simulations of continuous time systems the model components are discrete in form, i.e., at each discrete time step the individual modules evaluate an average value for projection over the ensuing time step which are mathematically combined to propagate the system states. In the hybrid simulation the approach is to reduce the mathematical model to equivalent analog circuitry and as a result

represent the system states continuously in time. The digital control law under test is by definition a discrete evaluation entity so that the continuous system states are sampled at fixed intervals in time and the associated quantized control outputs generated for subsequent use in state propagation by continuous time models.

The integrated model components of the hybrid ejection seat simulation and control system is illustrated in Figure 6.1 while the associated parameters of the models as well as those in the following paragraphs are defined in Table 6.1. A qualitative description of the system in Figure 6.1 is warranted to clarify the necessity of the illustrated model components.

At the heart of the integrated simulation is the six degree of freedom flight model (6DOF) which serves as the "truth" model for evolution of the key system states. With the initial conditions for the ejection seat defined, the 6DOF flight model integrates the combined aerodynamic forces and torques with the achieved actuator forces and torques to update the "truth" values of the vehicle dynamic states $(u,v,w,x,y,z,\phi,\theta,\psi,p,q,r)$. The truth values of the states are represented in body coordinates $(\phi,\theta,\psi,a_i^b, v_i^b, \omega_i^b, \dot{\omega}_i^b)$ and are processed by sensor models $(G_{\alpha_i}, G_{a_i}, G_{v_i}, G_{\omega_i}, G_{\dot{\omega}_i})$ which incorporate instrument error sources to form the final sensor estimates $(\hat{\phi},\hat{\theta},\hat{\psi},\hat{a}_i^b, \hat{v}_i^b, \hat{\omega}_i^b, \hat{\dot{\omega}}_i^b)$ for use by the control algorithm.

The control algorithm accepts the instrument estimates of the vehicle dynamic states plus specific control law parameters and evaluates the ideal desired body forces and torques (f_c^B, τ_c^B) necessary for seat control. These idealized commands (f_c^B, τ_c^B) are transformed into the desired individual actuation system element commands $(u = P^{-1}[f_c^B, \tau_c^B])$ which for the particular system under investigation are specifically rocket force magnitudes $(f_c^{N_i})$ and the associated pointing angles $(\theta_c^{N_i}, \psi_c^{N_i})$ which drive the actual outputs of thrust jet control elements. The transformations from (f_c^B, τ_c^B) to control

TABLE 6.1 Definition of Terms in Hybrid Simulation

Block	Model	Symbol	Definition	Units
B1	Aero	α	angle of attack	degrees
		β	side slip angle	degrees
		C_x	axial force coefficient	none
		C_y	side force coefficient	none
		C_z	normal force coefficient	none
		C_ℓ	rolling moment coefficient	S^2
		C_m	pitching moment coefficient	S^2
		C_n	yawing moment coefficient	S^2
B2	6 DOF	u, u_0	velocity projected onto the seat x axis	fps
		v, v_0	velocity projectd onto the seat y axis	fps
		w, w_0	velocity projected onto the seat z axis	fps
		p, p_0	rotation rate about the seat x axis	R/S
		q, q_0	rotation rate about the seat y axis	R/S
		r, r_0	rotation rate about the seat z axis	R/S
		x, x_0	inertial x position	ft
		y, y_0	inertial y position	ft
		x, z_0	inertial z position	ft
		ϕ, ϕ_0	inertial roll angle	R
		θ, θ_0	inertial pitch angle	R
		ψ, ψ_0	inertial yaw angle	R
		V_0	wind speed	fps
		$\dot{u}$	acceleration for x seat axis for rotating observer	fps^2

TABLE 6.1 Definition of Terms in Hybrid Simulation (Continued)

Block Model	Symbol	Definition	Units
B2 6 DOF	$\dot{v}$	acceleration for y seat axis for rotating observer	fps^2
	$\dot{w}$	acceleration for z seat axis for rotating observer	fps^2
	$\dot{p}$	rotational acceleration about the x seat axis	R/S^2
	$\dot{q}$	rotational acceleration about the y seat axis	R/S^2
	$\dot{r}$	rotational acceleration about the z seat axis	R/S^2
	$\dot{x}$	x component of inertial velocity	fps
	$\dot{y}$	y component of inertial velocity	fps
	$\dot{z}$	z component of inertial velocity	fps
	$\dot{\phi}$	roll rate	R/S
	$\dot{\theta}$	pitch rate	R/S
	$\dot{\psi}$	yaw rate	R/S
	I_x, I_y, I_z	moment of inertia about the x,y,z seat axes	$slug\text{-}ft^2$
	I_{xz}, I_{xy}, I_{yz}	cross product of inertia	$slug\text{-}ft^2$
	M	Mach number	none
	$\bar{q}$	dynamic pressure	lb/ft^2
	S	seat reference cross section area	ft^2
	m	seat mass	slugs

TABLE 6.1 Definition of Terms in Hybrid Simulation (Continued)

Block	Model	Symbol	Definition	Units
B2	6 DOF	g	local gravity acceleration magnitude	lb
		f_x^R	x component of resultant of rocket force	lb
		f_y^R	y component of resultant of rocket force	lb
		f_z^R	z component of resultant of rocket force	lb
		a_i^b	vector of inertial accelerations expressed in body	fps^2
		x_{CG}	seat center of gravity in seat units (x component)	ft
		y_{CG}	seat center of gravity in seat units (y component)	ft
		z_{CG}	seat center of gravity in seat units (z component)	ft
		τ_x^R	x component of rocket resultant torques	ft-lb
		τ_y^R	y component of rocket resultant torques	ft-lb
		τ_z^R	z component of rocket resultant torques	ft-lb
B4	CONTROL	θ, ϕ, ψ	estimates of pitch, roll, yaw	R
		$\hat{a}_i^b$	estimate of inertial acceleration expressed in body	fps^2
		$\hat{v}_i^b$	estimate of inertial velocity expressed in body	fps

TABLE 6.1 Definition of Terms in Hybrid Simulation (Continued)

Block	Model Symbol	Definition	Units
B4 CONTROL	$\hat{\omega}_i^b$	estimate of inertial angular velocity in body	R/S
	$\dot{\hat{\omega}}_i^b$	estimate of inertial angular acceleration in body	R/S^2
	ω_d^b	vector of desired angular velocities	R/S
	V_d^b	desired velocity in body	fps
	a_d^b	desired acceleration in body	fps^2
	$\dot{\omega}_d^b$	vector of desired angular accelerations	R/S^2
	$K_{c_{p0}}$	control gain for cross product steering	$1/S^2$
	$K_{c_{p1}}$	control gain for cross product steering	1/S
	k_1	translational acceleration control gain	none
	k_2	translational acceleration control gain	1/S
	k_3	rotational acceleration control gain	none
	k_4	rotational acceleration control gain	1/S
	τ_r	rocket burn time constant	S
	Δt	simulation time step	S
	m	seat mass	slugs

TABLE 6.1 Definition of Terms in Hybrid Simulation (Continued)

Block	Model	Symbol	Definition	Units
B4	CONTROL	I	moment of inertia	slug-ft^2
		t_{k_1}	control time constant for acceleration	1/S
		θ_F	final inertial pitch angle	R
		ϕ_F	final inertial roll angle	R
		a_F	final inertial acceleration	fps^2
		f_c	idealized control forces in body	lb
		τ_c	idealized control torques in body	lb-ft
B5	Configuration	p^{-1}	inverse of control gradient matrix	dependent
		$\overline{f}_c^{N_1}$	commanded force magnitude for rocket 1	lb
		$\overline{f}_c^{N_2}$	commanded force magnitude for rocket 2	lb
		$\overline{f}_c^{N_3}$	commanded force magnitude for rocket 3	lb
		$\psi_c^{N_1}$	commanded pointing angle ψ for rocket 1	R
		$\theta_c^{N_1}$	commanded pointing angle θ for rocket 1	R
		$\psi_c^{N_2}$	commanded pointing angle ψ for rocket 2	R
		$\theta_c^{N_2}$	commanded pointing angle θ for rocket 2	R
		$U_c = [\overline{f}_c^{N_1}, \ldots, \theta_c^{N_2}]$	control vector	

TABLE 6.1 Definition of Terms of Hybrid Simulation (Continued)

Block	Model	Symbol	Definition	Units
B6	ACTUATOR	ψ^{N1}	achieved ψ pointing angle for rocket 1	R
		ψ^{N2}	achieved ψ pointing angle for rocket 2	R
		θ^{N1}	achieved θ pointing angle for rocket 1	R
		θ^{N2}	achieved θ pointing angle for rocket 2	R
		$\underline{f}^{N1}$	achieved rocket force magnitude for rocket 1	lb
		$\underline{f}^{N2}$	achieved rocket force magnitude for rocket 2	lb
		$\underline{f}^{N3}$	achieved rocket force magnitude for rocket 3	lb
B7	RESULTANT	$\delta r_x^{N1}, \delta r_y^{N1}, \delta r_z^{N1}$	displacement of rocket 1 from c.g. in seat units	ft
		$\delta r_x^{N3}, \delta r_y^{N3}, \delta r_z^{N3}$	displacement of rocket 3 from c.g. in seat units	ft
		$\delta r_x^{N2}, \delta r_y^{N2}, \delta r_z^{N2}$	displacement of rocket 2 from c.g. in seat units	ft
		$f_{R_x}^{b}, f_{R_y}^{b}, f_{R_z}^{b}$	components of resultant rocket forces in body	lb
		$\tau_{R_x}^{b}, \tau_{R_y}^{b}, \tau_{R_z}^{b}$	components of resultant rocket torques in body	lb-ft
		$C_{N_1}^{b}$	direction cosine matrix from rocket N_1 to body	

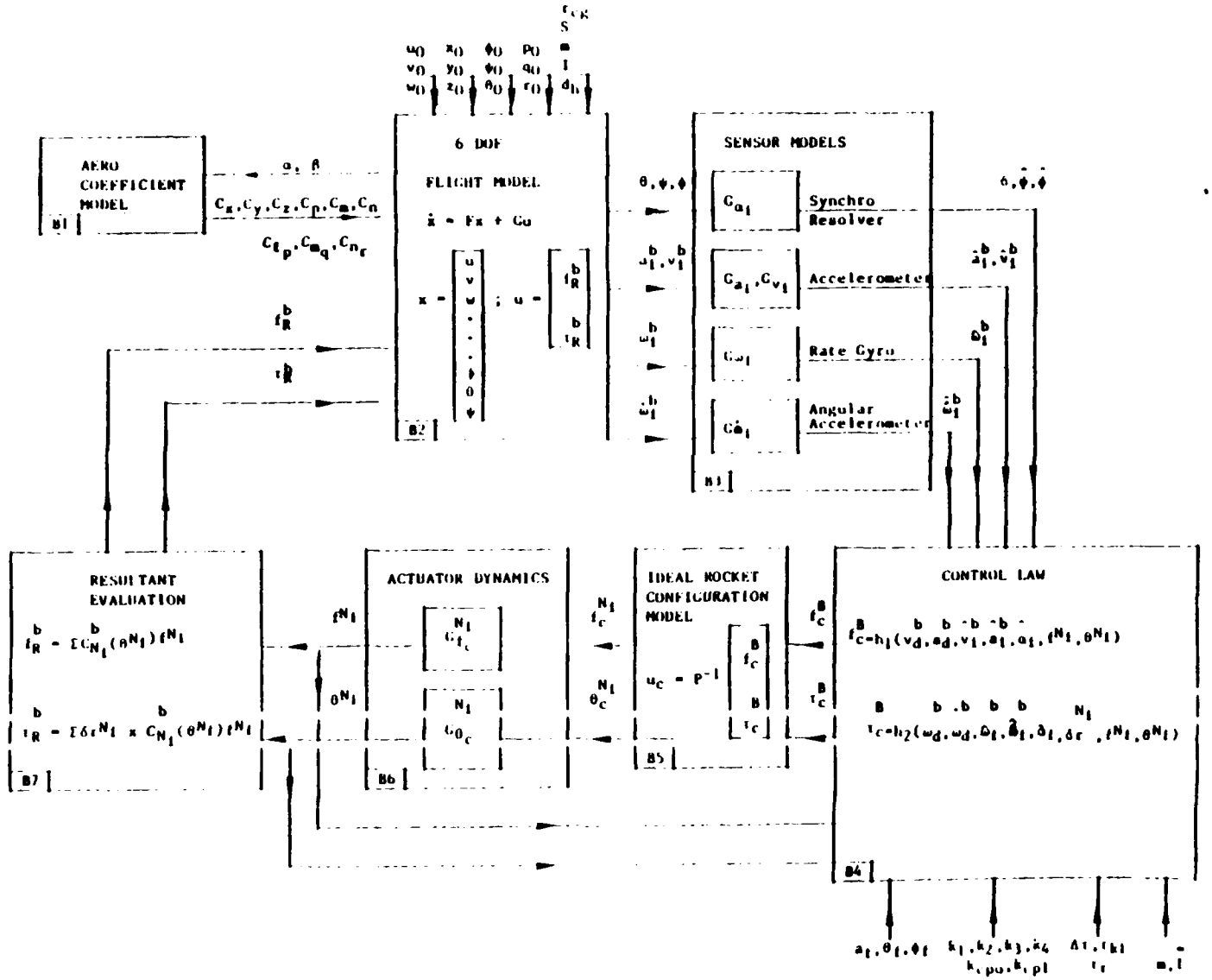

Figure 6.1. EJECTION SEAT SIMULATION/CONTROL SYSTEM

vector u_c is obviously dependent upon the constraints inherent in the particular actuation configuration employed. Results employing alternate actuator configuration schemes are presented in Chapter 7. The actual rocket forces and pointing angles ($\bar{f}^{N_i}, \vartheta^{N_i}$) attained are determined by actuation system transfer functions ($G_{f_c}^{N_i}, G_{\vartheta_c}^{N_i}$) acting on the idealized commands ($\bar{f}_c^{N_i}, \vartheta_c^{N_i}$).

The measures for evaluation of the control performance can be divided into two distinct classes: (1) the performance of the control law in steering the ejection seat along a prescribed trajectory, (2) the performance of the control law in bounding the lethality measure or acceleration radical given the constraints of the prescribed trajectory. In this particular application the "prescribed trajectory" has the loose meaning of ground collision avoidance, dynamic pressure reduction, and control of the vehicle to terminal attitude conditions conducive to succeeding phases of chute deployment. The acceleration radical employed in this study is given by:

$$a_L = \left| a \cdot \left(\omega_i^b \times \omega_i^b \times R - \omega_i^b \times v_i^b - \dot{v}_i^b + \dot{\omega}_i^b \times R \right) \right|^{1/2} \qquad (6.1)$$

The radical coefficients (a) in equation 6.1 represent the relative sensitivity to injury of the pilot by mutually orthogonal acceleration components acting normal to the chest, laterally and down the spine. The specific values for coefficients (a) expressed in the square of g are:

$$a = [(1/30g)^2, (1/12g)^2, (1/17g)^2]$$

The acceleration radical a_L is assumed to be lethal or at least implies a high probability of serious injury whenever $a_L > 1$.

The simulation segments from Figure 6.1 mechanized in equivalent analog circuitry are: (1) Aerodynamic Coefficients (Block B1), (2) 6DOF Flight Model (Block B2), (3) Sensor Models (Block B3), (4) Actuator Dynamics Model (Block B6), and (5) Resultant Evaluation (Block B7). The ensuing description (paragraphs 6.2.1-6.2.6) dicusses the mathematical models employed and defines the parameters utilized. Digital operations is reserved for mechanizations of (6) Control Algorithm (Block B4) and (7) Idealized Rocket Configuration (Block B5) discussed in paragraphs 6.3.1-6.3.2.

6.2 Analog simulation models.

6.2.1 Aerodynamic Model. The source of aerodynamical coefficients for the ejection seat is taken from the report entitled "Aeromechanical Properties of Ejection Seat Escape Systems", B.J. White (1974). That report dealt with introductory technical discussions on aerodynamical coefficients, forces and moments with an emphasis on presenting the measurements of aerodynamical coefficients for crew escape systems performed at the Air Force Flight Dynamics Laboratory, Wright Patterson AFB. Intensive aerodynamic measurements of the F-101 and F-106 manned/unmanned ejection seat systems were performed over a wide range of aerodynamic conditions (0.2-1.5 Mach, 0-360 deg attack angle, 0-45 deg sideslip angle) resulting in the most extensive compendium of such data to our knowledge.

The B.J. White data for the manned ACES ejection seat form the basis for the aerodynamical model for the results presented herein. The raw aerodynamical coefficients are defined in the following table:

Table 6.2 Definition of Fundamental Aerodynamical Coefficients.

Coefficient	Definition
C_x	axial force coefficient
C_y	side force coefficient
C_z	normal force coefficient
C_l	rolling moment coefficient
C_m	pitching moment coefficient
C_n	yawing moment coefficient
C_{l_p}	roll acceleration damping coefficient
C_{m_q}	pitch acceleration damping coefficient
C_{n_r}	yaw acceleration damping coefficient

The aerodynamical forces (f_A^b) and torques (τ_A^b) expressed in the ejection seat body frame are related to the reference coefficients in Table 6.2 by:

$$f_A^b = Q\,s \begin{bmatrix} C_x(\alpha,\beta,n) \\ Cy(\alpha,\beta,n) \\ Cz(\alpha,\beta,n) \end{bmatrix}$$

$$\tau_A^b = Q\,s \begin{bmatrix} C_l(\alpha,\beta,n) + p\,C_{l_p}\frac{dh^2}{2V} + z_{CG}\,C_y - y_{CG}\,C_z \\ C_m(\alpha,\beta,n) + q\,C_{m_q}\frac{dh^2}{2V} + x_{CG}\,C_z - z_{CG}\,C_x \\ C_n(\alpha,\beta,n) + r\,C_{n_r}\frac{dh^2}{2V} + y_{CG}\,C_x - x_{CG}\,C_y \end{bmatrix}$$

The aerodynamic pressure Q is defined by the familiar expression:

$$Q = \tfrac{1}{2}\,\rho\,(h,T)V_w^2$$

where

ρ atmospheric density at altitude

h altitude of vehicle

T reference temperature at altitude

The atmospheric density as a function of altitude is generated by look-up tables equivalent to the method employed in the EASIEST simulation model (1980).

Actual generation of aerodynamical coefficients for intermidiary points lying between those given by White are generated by linear interpolation over the appropriate Mach, α , β interval since justification of a higher order model is not apparent from inspection of the data. The relative insensitivity of the B.J. White coefficients over the 0.5 - 1.2 Mach regime is indicative of turbulent aerodynamic flow for most flight conditions of interest in this study. Further, it should be noted that the control synthesis method discussed in Volume I is highly reliant on the sensor inputs while avoiding any explicit estimation schemes dependent on aerodynamical coefficients. Hence, aerodynamic effects are treated as disturbances in the control algorithm which manifest their influence as undesirable state dynamics to be damped out by considering the variations in the observables.

6.2.2 Six Degree of Freedom Flight Model (6 DOF). The 6 DOF flight equations are the differential equations of motion representing the evolution of the system states in body coordinates according to Newton's laws of motion. The inertial forces and torques acting on the body are identifiably from three distinct sources: (1) aerodynamic forces and torques (paragraph 6.2.1), (2) resultant rocket forces and torques (paragraph 6.2.5) and (3) gravitational force. All other terms contributing to the translational and rotational state dynamics are merely consequences of the particular frame selected for the mechanization. Selection of the body frame for the representation of rotational motion significantly simplifies the differential

equations since in that frame the moment of inertia is constant. Hence, it is the natural frame of choice for implementation of control strategies and modeling of the dynamics of the rigid body. Excellent presentations of the basic theory of dynamics may be found in Goldstein (1981) or Etkin (1972).

The non-linear 6DOF equations in the ejection seat body frame for this problem are summarized in Figure 6.2. The symbols in Figure 6.2 were previously defined in Table 6.1. Notice that the first six equations in Figure 6.2 are the expression of Newton's laws in the rotating body frame while equations 7-9 are the inertial velocity components expressed as functions of the body velocity. Finally, equations 10-12 are the kinematic equations for the inertial Euler angles as a function of body angular rates and orientation. The essential singularity in equations 10-12 occures at $\theta = 90$ degrees due to the order of definition of the Euler angles so that the pitch angle limit in examining control law performance is inherently bounded to less than the straight-up direction.

6.2.3 Sensor Models. The "acceleration control" approach requires that rapid reliable estimates of inertial forces and torques acting on the ejection seat be available for generating immediate control terms that neutralize undesirable state dynamics. In addition the control approach is reliant upon direct estimates of the inertial Euler angles for generation of control torques proportional to attitude error in order to steer the ejection seat to a desired terminal attitude. The requirement to directly estimate inertial torque imposes at a minimum that measurements of inertial rotational rate and acceleration be continuously available. Rate gyros and angular accelerometers are standard inertial instruments that provide these measurements and are small in size, low in power with large mean time between failures. Similar considerations apply for the estimate of inertial forces and velocities imposing the additional requirement of three axis accelerometer readout. The attitude estimates are

$$\begin{bmatrix} \dot{u} \\ \dot{v} \\ \dot{w} \end{bmatrix} = \begin{bmatrix} \\ a_f^b \\ \\ \end{bmatrix} + \begin{bmatrix} vr - wq \\ wp - ur \\ uq - vp \end{bmatrix} \qquad [1\text{-}3]$$

$$\begin{bmatrix} \dot{p} \\ \dot{q} \\ \dot{r} \end{bmatrix} = I^{-1} \begin{Bmatrix} (I_y - I_z)qr + I_{yz}(q^2 - r^2) + p(I_{xz}q - I_{xy}r) + \bar{q}s\left[d_h C_{\ell} + \left(\frac{d_h^2}{2v_w}\right) pC_{\ell_p} + z_{cG}C_y - y_{cG}C_z\right] + \tau_x^R \\ (I_z - I_x)pr + I_{xz}(r^2 - p^2) + q(I_{xy}r - I_{xz}p) + \bar{q}s\left[d_h C_m + \left(\frac{d_h^2}{2v_w}\right) qC_{m_q} + x_{cG}C_z - z_{xG}C_x\right] + \tau_y^R \\ (I_x - I_y)qp + I_{xy}(p^2 - q^2) + r(I_{yz}p - I_{xz}q) + \bar{q}s\left[d_h C_n + \left(\frac{d_h^2}{2v_w}\right) rC_{n_r} + v_{cG}C_x - X_{cG}C_y\right] + \tau_z^R \end{Bmatrix} \qquad [4\text{-}6]$$

$$\dot{x} = C\psi C\theta \; u + (C\psi S\theta S\psi - S\psi C\phi) \; v + (C\psi S\theta C\phi + S\psi S\phi) \; w$$

$$\dot{y} = S\psi C\theta \; u + (S\psi S\theta S\phi + C\psi C\phi) \; v + (S\psi S\theta C\phi - C\psi S\phi) \; w \qquad [7\text{-}9]$$

$$\dot{z} = -S\theta \; u + C\theta S\phi \; v + C\theta C\phi \; w$$

$$\dot{\phi} = p + (q \sin\phi + r \cos\phi) \tan\theta - p + \dot{\psi} \sin\theta$$

$$\dot{\theta} = q \cos\phi - r \sin\phi \qquad [10\text{-}12]$$

$$\dot{\psi} = (q \sin\phi + r \cos\phi) \sec\theta$$

$$I^{-1} = \begin{bmatrix} 0.05806 & 0.00095903 & 0.02777158 \\ 0.00095903 & 0.0476022 & -0.00172473 \\ 0.02777158 & -0.00172473 & 0.14833678 \end{bmatrix}$$

Figure 6.2 Six Degrees of Freedom Differential Equations

either directly available as synchro resolver outputs or derivable from the integrated outputs of the rate gyros with proper initialization prior to ejection time from navigational estimates from the host aircraft. Volume I, section 5.1 summarizes the results of a literature survey of currently available inertial instruments that fulfill the sensor requirements. The objective in Volume II is to relate the mathematical form of the sensor models and to establish the level of error implied by the measurements.

6.2.3.1 Sensor Accuracy Limitations. The hybrid simulation environment necessitates the use of interfacing electronics that samples the continuous analog representation of input variables and delivers the quantized "snapshot" estimate to the digital control algorithm. The analog to digital converter (ADC) is the standard device for such purposes. The ADC accepts as input an analog signal specified over a limited range in voltage magnitude and outputs the digital signal equivalent in the form of the number of quanta expressed in the base unit of the device. The maximum number of quanta is given by 2^N where N is the number of bits of accuracy in ADC resolution so that the base unit is $1/2^N$ if the magnitude of the signal is bounded by 0 and 1.

The actual accuracy delivered by ADCs is dependent on the electrical noise environment where it operates and may in fact be substantially less than the N bits of precision guaranteed due to the presence of stray electrical noise at the analog interface. The ADCs used here are rated as 12 bit devices while actual noise measurements at the +/- 10 V interface indicate ambient electrical noise at the 40 mV level. Hence, at best the ADCs can be expected to deliver 10 bits of precision for a base unit of $1/2^{10}$ rather than the $1/2^{12}$ rating.

Table 6.3 specifies each input to the control algorithm illustrated in Figure 6.1 with associated maximum input analog bounds, corresponding real scale factor, base unit assumed and resulting

quantization error.

Table 6.3 Inertial Instrument Accuracy Limits.

Sensor	Variable	Analog Voltage Bounds	Real Scale Factor	Base Unit	Quantization Error
Synchro Resolver	Yaw	+/- 10 V	+/- 200 deg	1/1024	+/- 0.2 deg
Synchro Resolver	Pitch	+/- 10 V	+/- 200 deg	1/1024	+/- 0.2 deg
Synchro Resolver	Roll	+/- 10 V	+/- 1000 deg	1/1024	+/- 1.0 deg
Accelerometer		+/- 10 V	+/- 2000 fps^2	1/1024	+/- 2 fps^2
Rate Gyro		+/- 10 V	+/- 10 R/s	1/1024	+/- 0.5 deg/s
Angular Accelerometer		+/- 10 V	+/- 500 R/s^2	1/1024	+/- 30 deg/s^2

It is evident from Table 6.3 that the quantization error alone would qualify the sensors as crude when compared with the high accuracy of modern inertial instruments.

A more complete discussion of the hardware interface specifications for the hybrid simulation is presented in paragraph 6.4. This segment is included to quantify the sources of error beyond the intended sources of error explicitly modeled.

6.2.3.2 Sensor Dynamics Model. For inertial navigational applications it is usual to consider sources of error in sensor modeling which will cause apparent velocity and position error growth when integrated over the long term (1 hour). For accelerometers and gyros the major sources of error include constant bias, random bias, scale factor error, non-linearity of the scale factors and misalignment. For typical high accuracy inertial instruments in a low dynamic environment the resultant navigation errors are generally in the vicinity of 1 nm position error and 2 fps velocity error after an hour of operation.

Given the extremely brief interval of this application (at most 2 sec) many of the mentioned sources of instrument error are negligible. In light of the discussion of the previous paragraph the sources of error associated with bias, g-sensitivity, scale factors and misalignment are moot when compared with the quantization error in Table 6.3.

Of far greater consequence in the ejection seat problem is the delay imposed by the sensors given the reliance of the control strategy on the availability of vehicle state estimates and the need to respond immediately. The emphasis on sensor modeling in this study then is to consider the effects of sensor delay on the control system. The highest fidelity models for sensors generally are high order (up to sixth) which generate with considerable resolution the sensor dynamics. In the interest of simplicity the delay models utilized here are of first order which is meant to capture the essence of system delay on control performance.

Table 6.4 defines the relationships between the sensor estimates ($\hat{x}$, $\hat{a}_i^b$, $\hat{v}_i^b$, $\hat{\omega}_i^b$, $\hat{\dot{\omega}}_i^b$) to the truth values (x, a_i^b, v_i^b, ω_i^b, $\dot{\omega}_i^b$) as well as the transfer functions (G_{x_i}, G_{a_i}, G_{ω_i}, $G_{\dot{\omega}_i}$) with the associated time constants (τ_{x_i}, τ_{a_i}, τ_{ω_i}, $\tau_{\dot{\omega}_i}$). Notice that all transfer functions are defined in the frequency domain while the error in the velocity

estimate $\hat{v}_i^b(s)$ is derived from the acceleration error ($\hat{a}_i^b(s)$ - $a_i^b(s)$). The time constants in Table 6.4 are representative values for sensors deployed in missile guidance applications. It should be noted that the control scheme was evaluated with the time constants $\tau_{\alpha_i}, \ldots, \tau_{\dot{\omega}_i}$=0.01 sec (well within current sensor bandwidths) and yielded results similar to those presented in Chapter 7.

Table 6.4 Sensor Transfer Functions and Response Times.

$$\hat{\alpha}_i(s) = G_{\alpha_i}\ \alpha_i\ (s)$$
$$\hat{a}_i^b(s) = G_{a_i}\ a_i^b(s)$$
$$\hat{v}_i^b(s) = v_i^b(s) + \frac{1}{s}\ (\hat{a}_i^b(s) - a_i^b(s))$$
$$\hat{\omega}_i^b(s) = G_{\omega_i}\ \omega_i^b\ (s)$$
$$\dot{\omega}_i^b(s) = G_{\dot{\omega}_i}\ \dot{\omega}_i^b\ (s)$$

Sensor	Transfer Function	Time Constant
Synchro Resolver	$G_{\alpha_i} = \frac{1}{1 + \tau_{\alpha_i} s}$	$\tau_{\alpha_i} = 0.00025$
Accelerometer	$G_{a_i} = \frac{1}{1 + \tau_{a_i} s}$	$\tau_{a_i} = 0.0025$
Rate Gyro	$G_{\omega_i} = \frac{1}{1 + \tau_{\omega_i} s}$	$\tau_{\omega_i} = 0.0025$
Angular Accelerometer	$G_{\dot{\omega}_i} = \frac{1}{1 + \tau_{\dot{\omega}_i} s}$	$\tau_{\dot{\omega}_i} = 0.0025$

6.2.4 Actuator Dynamics Model. The actuation system elements in ejection seat control are rocket nozzle thrusters either fixed in orientation with respect to the ejection seat or gimballed to allow for some degree of freedom in force vectoring. Emerging technologies in rocket propulsion systems also allow for generation of variable force magnitudes from the rocket elements. The summary of a

technology survey for currently available actuators was presented in Volume I, paragraph 5.5.2. This paragraph is concerned with the response model of these rocket elements to input commands. It is apparent that the actuation system elements have finite bandwidth and representing the delays imposed are important in evaluating the control system robustness to such restrictions.

The idealized actuator configuration discussed in detail in Volume I consisted of three rocket thrusters, all with all with variable force magnitudes, one fixed in orientation with respect to the seat (main thruster) and the other two gimballed with two degrees of freedom. The independent command input variables with this configuration total seven: three force magnitudes ($\bar{f}_c^{N1}, \bar{f}_c^{N2}, \bar{f}_c^{N3}$) and four rocket pointing angles ($\theta_c^{N1}, \psi_c^{N1}, \theta_c^{N2}, \psi_c^{N2}$), i.e., two angles each for two rockets. The relationships for generating ($\bar{f}_c^{N1}, \bar{f}_c^{N2}, \bar{f}_c^{N3}, \theta_c^{N1}, \psi_c^{N1}, \theta_c^{N2}, \psi_c^{N2}$) from the idealized control forces (f_c^B) and torques (τ_c^B) indicated in Figure 6.1 are developed in Volume I, paragraph 3.2 and summarized in paragraph 6.3.2 of this volume.

In the interest of ease in implementation first order models are incorporated to corrupt the idealized input commands generated by the control algorithm. Table 6.5 relates outputs to inputs and defines the transfer functions and response times utilized in generating the achieved actuation.

Table 6.5 Actuator Transfer Functions and Response Times.

Actuator Update

$$\psi^{N_i} = G_{\psi N_i}\, \psi_c^{N_i}$$

$$\vartheta^{N_i} = G_{\theta N_i}\, \theta_c^{N_i}$$

$$\bar{f}^{N_i} = G_{fN_i}\, \bar{f}_c^{N_i}$$

Actuator Element	Transfer Function	Time Constants
Pointing Angle	$G_{\psi N_i} = \frac{1}{1+\tau_{\psi N_i} S}$; $G_{\vartheta N_i} = G_{\psi N_i}$	$\tau_{\psi N_i} = 0.015$ sec
Force Magnitude	$G_{\bar{f}N_i} = \frac{1}{1+\tau_{\bar{f}N_i} S}$	$\tau_{\bar{f}N_i} = 0.0025$ sec

The commanded values in Table 6.5 are quantized consistent with the 12 bit DACs and real scale factors. In actuality the DAC performance is limited by ambient electrical noise at the output channels analogous to noise input corruption for the sensors. Direct measurements of the noise levels implied at best 11 bit delivery. Table 6.6 defines the output variables along with real scale factor, base unit and the resulting maximum quantization error.

Table 6.6 Actuator Element Accuracy.

Variable	Definition	Base Unit	Scale Factor	Quantization Error
$\theta_c^{N_i}$	pitch pointing angle for rocket N_i	1/2048	$\pm \pi R$	$\pm$ 0.2 degree
$\psi_c^{N_i}$	yaw pointing angle for rocket N_i	1/2048	$\pm \pi R$	$\pm$ 0.2 degree
$f_c^{N_i}$	force magnitude for rocket N_i	1/2048	$\pm$ 10000 lb	$\pm$ 10 lb

6.2.5 Resultant Evaluation. The 6 DOF flight model discussed in section 6.2.2 required the resultant inertial forces and torques acting on the ejection seat in order to propagate the state according to the differential equations of motion. The inertial rocket force (f_r^b) and torque (τ_r^b) resultants expressed in body appear directly in the 6DOF equations as drivers of the system states. The resultants (f_r^b, τ_r^b) are simply the summation of the individual rocket inertial components transformed to body coordinates. As such they may be expressed succintly as:

$$f_r^b = \sum_{N_i} C_{N_i}^b(\theta^{N_i}, \psi^{N_i}) f^{-N_i} \qquad (6.2)$$

$$\tau_r^b = \sum_{N_i} \delta r^{N_i} \times C_{N_i}^b(\theta^{N_i}, \psi^{N_i}) f^{-N_i} \qquad (6.3)$$

In equations 6.2-6.3 f^{-N_i}, θ^{N_i}, ψ^{N_i} are of course the achieved actuation signals while $C_{N_i}^b$ are the vectors of direction cosines from rocket N_i to body. The parameter δr^{N_i} is the rocket N_i displacement from the seat c.g. expressed in body coordinates. Rockets N_1, N_2 are gimballed with pointing angles $(\theta^{N_1}, \psi^{N_1}, \theta^{N_2}, \psi^{N_2})$ while N_3 is fixed leading to expressions for $C_{N_i}^b$:

$$C = \begin{bmatrix} C_\theta N_i C_\psi N_i \\ S_\psi N_i \\ S_\theta N_i C_\psi N_i \end{bmatrix} \qquad i=1,2 \; ; \quad C_{N_3}^b = \begin{bmatrix} 1 \\ 0 \\ \tan \theta^{N_3} \end{bmatrix} .$$

The motivation for selection of this particular actuation configuration and the development of the theory may be found in Volume I, section 3.2.

6.2.6 Summary of Analog Simulation Models. The preceding paragraphs provided a synopsis of the mathematical form of the analog models while omitting completely the analog schematics which implement the circuit representation of those models. The detailed description of the analog hardware is contained in Volume IV, Appendix F, entitled "ACES II Hybrid Simulation Report" prepared by the Technical Computing Center of MMOA. Some of the information presented herein are excerpts from the material contained in Appendix F. As a matter of correlating the information in Volumes II and IV Table 6.7 defines the cross-reference index relating the analog schematic representations of Volume IV to the mathematical form of Volume II.

Table 6.7 Correspondence of Mathematical Model to Analog Schematics

Paragraph	Volume II Subject	Volume IV Analog Schematic Form
6.2.1	Aerodynamic Model	NDE
6.2.2	6DOF Flight Model	pp. 115-121
6.2.3	Sensor Models	p. 121,124
6.2.4	Actuator Dynamics Model	p. 122
6.2.5	Resultant Evaluation	p. 123,125

NDE=no direct equivalent

It should be noted that the Aerodynamical Model in Table 6.7 has no direct analog equivalent. The evaluation of aerodynamic coefficients is implemented on a parallel processor (AD-10) configured with an (ADC/DAC) interface to the 6DOF flight model.

This concludes the discussion of the Analog Simulation requirements for the Hybrid Simulation development. The digital segment is concerned with generation of the control signals ($\bar{f}_c^{N_i}$, $\theta_c^{N_i}$) given the sensor inputs ($\hat{\phi}$, $\hat{\theta}$, $\hat{\psi}$, $\hat{a}_i^b$, $\hat{v}_i^b$, $\hat{\omega}_i^b$, $\hat{\dot{\omega}}_i^b$) which is the subject of the next paragraph.

6.3 Digital Algorithms.

The digital segment of the hybrid simulation is the realization of real-time control algorithms which process sensor measurements and produce control commands for use by the actuation system in steering the ejection seat along a prescribed trajectory. The rapid update rate (50Hz) mandates the use of numerically efficient algorithms which evaluate inertial torques and forces and apply corrective terms in order to meet the trajectory specifications.

The sensor inputs were dealt with in paragraph 6.2.3 and paragraph 6.2.4 defined the dynamics of the actuation system elements. The objective here is to summarize the processing by the control algorithms that generate the idealized body forces (f_c^b) and torques (τ_c^b) and transform them into desired actuation signals.

6.3.1 Control Algorithm. Development of the control system methodology was a major topic of Volume I. In that discussion the exigency of the ejection seat control problem was emphasized which led to the "acceleration control" concept. The conclusion of that investigation was the necessity for prompt neutralization of the translation and rotational accelerations which led to specific sensor and actuator system requirements. Given that the aerodynamic effects

are reduced to acceptable levels the problem of meeting terminal attitude constraints is a residual dynamics problem amenable to standard attitude control methods such as "cr ss product steering". The translational problem is best dealt with by selecting desired acceleration profiles and generating the associated steering commands to meet the profile constraints. The final control logic resulting from the above considerations is detailed in Volume I, paragraph 4.3. In addition the mechanization of that control logic is also summarized in Volume IV, pp. 8-13.

The control logic is briefly reviewed here to allow for continuity in the discussion. Given the terminal attitude constraints (ϕ_F , θ_F), the intent is to steer the ejection seat from some attitude (ϕ , θ) to the terminal conditions. Small angle errors may be corrected effectively by "cross product steering". In that method torque terms proportional to angular error and its rate are returned as feedback to achieve and maintain the desired regulated attitude.

Figure 6.3 sketches the attitude control logic for cross product steering. The objective is to align the unit vertical body vector z_o^b with the terminal desired body vector $z_F^b(\phi_F, \theta_F)$. The error signal is generated by $z_0^b \times z_x^b$, exact for small attitude deviations and hence the use of the term "cross product". Step 3 in Figure 6.3 defines the evaluation of the desired angular acceleration proportional to attitude error and its rate. That is k_{CP0} is the position gain while k_{CP_1} serves as the velocity gain. Step 4 determines the desired rotation rate from the angular acceleration scaled by "time to go" as an approximation to the exact integral. The nonlinear form of the control is evident in step 5 which also directly cancels the inertial torques acting on the seat ($-I\hat{\dot{\omega}}_i^b - \hat{\omega}_i^b \times I\hat{\omega}_i^b$). The expression (5) is the major driver for attitude steering while the linear contributions in (6) become apparent for large deviations from the nominal trajectory.

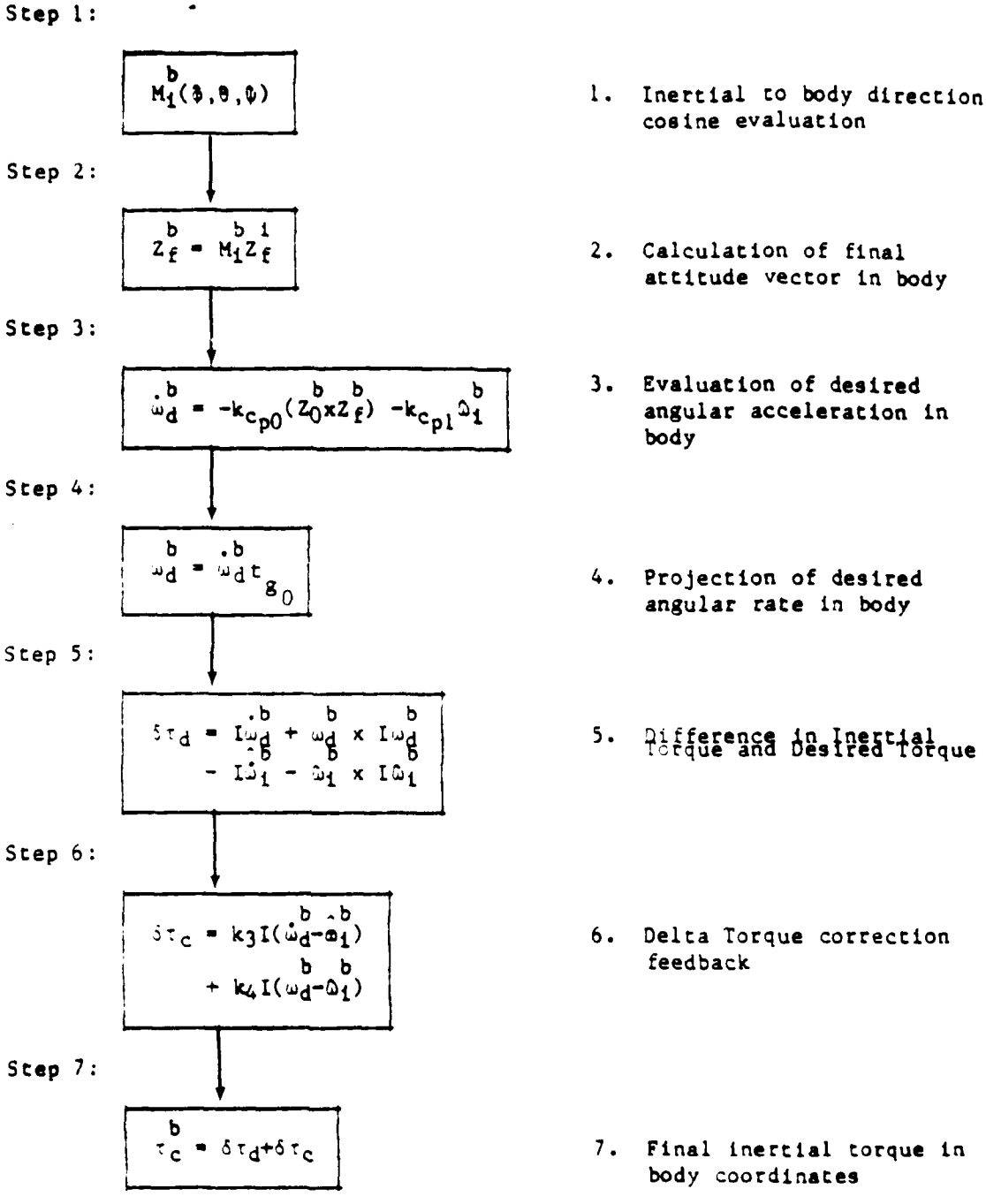

Figure 6.3 Attitude Steering Logic for Cross-Product Law

The brief description above related to the small angle error case while the considerations for the large angle case is similar with some modifications in steps 2-3. The large angle error case by comparison considers only the angular error in step 3 to arrive at the desired angular acceleration while preserving the form (4-7). The nonlinear compensation (5) performs similar to linear control for small deviations from the nominal trajectory while generating quadratic correction feedback of acceleration for angular rate error in response to linear growth.

The translational logic is illustrated in Figure 6.4. The desired inertial velocity v_d^i is analytically the integral of the desired inertial acceleration a_d^i. The dynamic values for v_d^i, a_d^i in turn reflect the initial and terminal desired acceleration and velocity conditions to which they converge over the ejection control interval. The variables v_d^i, a_d^i at ejection time are the initial values of velocity and acceleration and are selected to change slowly in time approaching the terminal conditions. As a result a smooth transition from the initial to the final desired values is realized.

The commanded forces are generated in the body frame while the updates of a_d^i and v_d^i are strictly inertial (step 2). Expression (3) cancels acting inertial forces ($-m\,\hat{a}_i^b$) and supplants the same with the desired dynamics imbedded within the commanded acceleration a_d^b. Expression (4) is proportional and integral compensation for error drift from the nominal velocity and acceleration profile resulting in the dominance of a_d^b in the terminal conditions.

The feedback forces (f_c^B) and torques (τ_c^B) of Figures 6.3-6.4 form the idealized commands in the body frame and are synonymous with those defined in Figure 6.1. In any implementation of controllers for ejection seats the idealized commands need be converted to actuation system element commands. The discussion of the actuation system mechanization is the subject of the next paragraph.

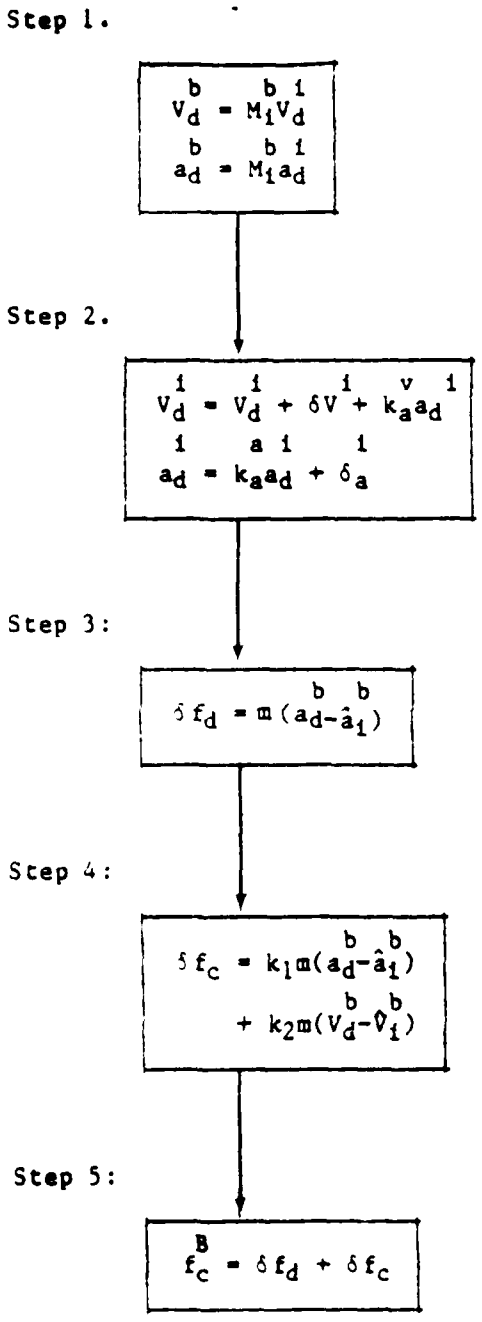

1. Desired Velocity, force in body from inertial components
2. Update of desired inertial acceleration and velocity components
3. Difference in inertial force and desired force
4. Delta Force Correction Feedback
5. Final inertial force in body coordinates

Figure 6.4 Force Steering Logic in Translational Control

6.3.2 Idealized Actuator Configuration Model. The actuation system employed is discussed in detail in Volume I, section 3.2.2.3. Similarly the processing steps are summarized in Volume IV, pp. 13-14. The excerpt from Volume IV is included to reduce the necessity of cross-reference in pursuing this discussion.

The problem here is to convert the idealized commands (f_c^B, τ_c^B) into the nearest equivalent set of rocket commands $(\bar{f}_c^{N_i}, \theta_c^{N_i}, \psi_c^{N_i})$. The term $\bar{f}_c^{N_i}$ is the rocket force magnitude while $\theta_c^{N_i}, \psi_c^{N_i}$ are the rocket pitch and yaw pointing angles respectively. Previously defined in paragraph 6.2.3.2, there are a total of seven control elements to be considered: $(\bar{f}_c^{N_1}, \bar{f}^{N_2}, \bar{f}_c^{N_3}, \theta_c^{N_1}, \psi_c^{N_1}, \theta_c^{N_2}, \psi_c^{N_2})$, i.e., three force magnitudes and four rocket pointing angles.

Conceptually the problem may be seen as choosing the parameters $(\bar{f}_c^{N_i}, \theta_c^{N_i}, \psi_c^{N_i})$ to simultaneously meet the decoupled idealized commands $(f_c^B, 0)$ and $(0, \tau_c^B)$. That is, rocket commands allocated to meet the resultant force f_c^B will generate no disturbance torques. An analogous statement applies for the command pair $(0, \tau_c^B)$ so that the rockets would deliver exact force command pair cancellation resulting in no effect on CG translational motion.

Figure 6.5 defines the relationships for producing the six dimensional force vector $(f_1, \ldots, f_6)$ from any given command pair (f_c^B, τ_c^B). The terms Q_{ij} are the inverse terms of the control gradient matrix P which relates each rocket contribution to the command pair resultant. Once available the force vector $(f_1, \ldots, f_6)$ are converted to the actuator signals $(\bar{f}_c^{N_i}, \theta_c^{N_i}, \psi_c^{N_i})$ as defined in Figure 6.6. There is an apparent discrepancy in dimension between the input vector (dimension six) and the output vector (dimension 7). The extra degree of freedom is removed by the arbitrary assignment of rocket 1,2 sharing of element f_4 evident in expressions 1-2 of Figure 6.6. This assignment also affects the generation of the rocket pointing angles in expressions (5,7).

Evaluate ideal rocket times and pointing angles

$$f_1^R = Q_{11} f_x^B + Q_{12} f_y^B + Q_{13} f_z^B + Q_{15} \tau_y^B + Q_{16} \tau_z^B$$

$$f_2^R = Q_{21} f_x^B + Q_{22} f_y^B + Q_{23} f_z^B + Q_{25} \tau_y^B + Q_{26} \tau_z^B$$

$$f_3^R = Q_{31} f_x^B + Q_{35} \tau_{y_B} + Q_{34} f_z^B$$

$$f_4^R = Q_{42} f_y^B$$

$$f_5^R = Q_{51} f_x^B + Q_{52} f_y^B + Q_{53} f_z^B + Q_{54} \tau_x^B + Q_{55} \tau_y^B$$

$$f_6^R = Q_{61} f_x^B + Q_{62} f_y^B + Q_{63} f_z^B + Q_{64} \tau_x^B + Q_{65} \tau_y^B$$

where $Q = \begin{bmatrix} \frac{\mu^1 + z}{2\mu^1} & -\frac{x}{2y} & -\frac{x}{2\mu^1} & 0 & -\frac{1}{2\mu^1} & \frac{1}{2y} \\ \frac{\mu^1 + z}{2\mu^1} & \frac{x}{2y} & -\frac{x}{2\mu^1} & 0 & -\frac{1}{2\mu^1} & -\frac{1}{2y} \\ -\frac{z}{\mu^1} & 0 & \frac{x}{\mu^1} & 0 & \frac{1}{\mu^1} & 0 \\ 0 & 1 & 0 & 0 & 0 & 0 \\ \frac{\lambda z}{2\mu^1} & -\frac{z}{2y} & \frac{\mu - z}{2\mu^1} & -\frac{1}{2y} & -\frac{\lambda}{2\mu^1} & 0 \\ \frac{\lambda z}{2\mu^1} & \frac{z}{2y} & \frac{\mu - z}{2\mu^1} & \frac{1}{2y} & -\frac{\lambda}{2\mu^1} & 0 \end{bmatrix} = \begin{bmatrix} 1 & 1 & 1 & 0 & 0 & 0 \\ 0 & 0 & 0 & 1 & 0 & 0 \\ 0 & 0 & \lambda & 0 & 1 & 1 \\ 0 & 0 & 0 & -z & -y & y \\ z & z & \mu & 0 & -x & -x \\ y & -y & 0 & x & 0 & 0 \end{bmatrix}^{-1} = P^{-1}$$

$$\lambda = \tan \theta^{N_1} \quad ; \quad x = \delta r_x^{N_2} \; ; \quad z = \delta r_z^{N_2}$$

$$\mu = \delta r_z^{N_1} - \lambda \delta r_x^{N_1} \; ; \quad y = \delta r_y^{N_2} \; ; \quad \mu^1 = \mu - z + \lambda x$$

Figure 6.5 Evaluation of Idealized Command Force Vector

$$\bar{f}_c^{N_1} = \sqrt{(f_1^R)^2 + (0.5\, f_4)^2 + (f_5)^2} \qquad (1)$$

$$\bar{f}_c^{N_2} = \sqrt{(f_2^R)^2 + (0.5\, f_4)^2 + (f_6)^2} \qquad (2)$$

$$\bar{f}_c^{N_3} = f_3^R \qquad (3)$$

$$\theta_c^{N_1} = \tan^{-1}\,(f_5^R/f_1^R) \qquad (4)$$

$$\psi_c^{N_1} = \sin^{-1}\,(0.5\, f_4^R/\bar{f}_c^{N_1}) \qquad (5)$$

$$\theta_c^{N_2} = \tan^{-1}\,(f_6^R/f_2^R) \qquad (6)$$

$$\psi_c^{N_2} = \sin^{-1}\,(0.5\, f_4^R/\bar{f}_c^{N_2}) \qquad (7)$$

$$(f_1 = f_x^{N_1},\ f_2 = f_x^{N_2},\ f_3 = \bar{f}^{N_3},\ f_4 = \bar{f}_y,\ f_5 = f_z^{N_1},\ f_6 = f_z^{N_2})$$

Figure 6.6 Update Equations for Actuation System Control Elements

The generation of the rocket commands completes the description of the processing requirements by the digital algorithms. The hardware allocation to support the processing of the Analog and Digital models is described next.

6.4 Hardware description.

6.4.1 Requirements. At a minimum the hybrid simulation requires the use of analog computing facilities for implementation of the analog models of section 6.2, the development of a microprocessor based hardware controller with associated interfacing electronics plus some means for displaying the state variables and system performance measures. The hybrid computing facility at MMOA has at its disposal a powerful array of parallel processors, digital and analog computers and chart recorders for hosting complex hybrid simulations. Unidynamics of Phoenix Arizona (UPHX) was tasked with the development of the hardware controller board that supported the interface and computational requirements for the Motorola 68000 microprocessor. In this phase of the effort SSI provided the system specification and was responsible for development of the microprocessor based control algorithms.

Figure 6.7 illustrates the division of responsibility for the implementation of the integrated simulation and control system. Inspection of Figure 6.7 indicates the hardware allocation to meet system requirements. The following paragraphs describe the various processors in use.

6.4.2 MMOA Analog Hardware Description. Volume IV details the hardware sub-systems and applications software necessary for operation of the analog segment of the system in Figure 6.7. A brief synopsis of those hardware elements is given here for completeness.

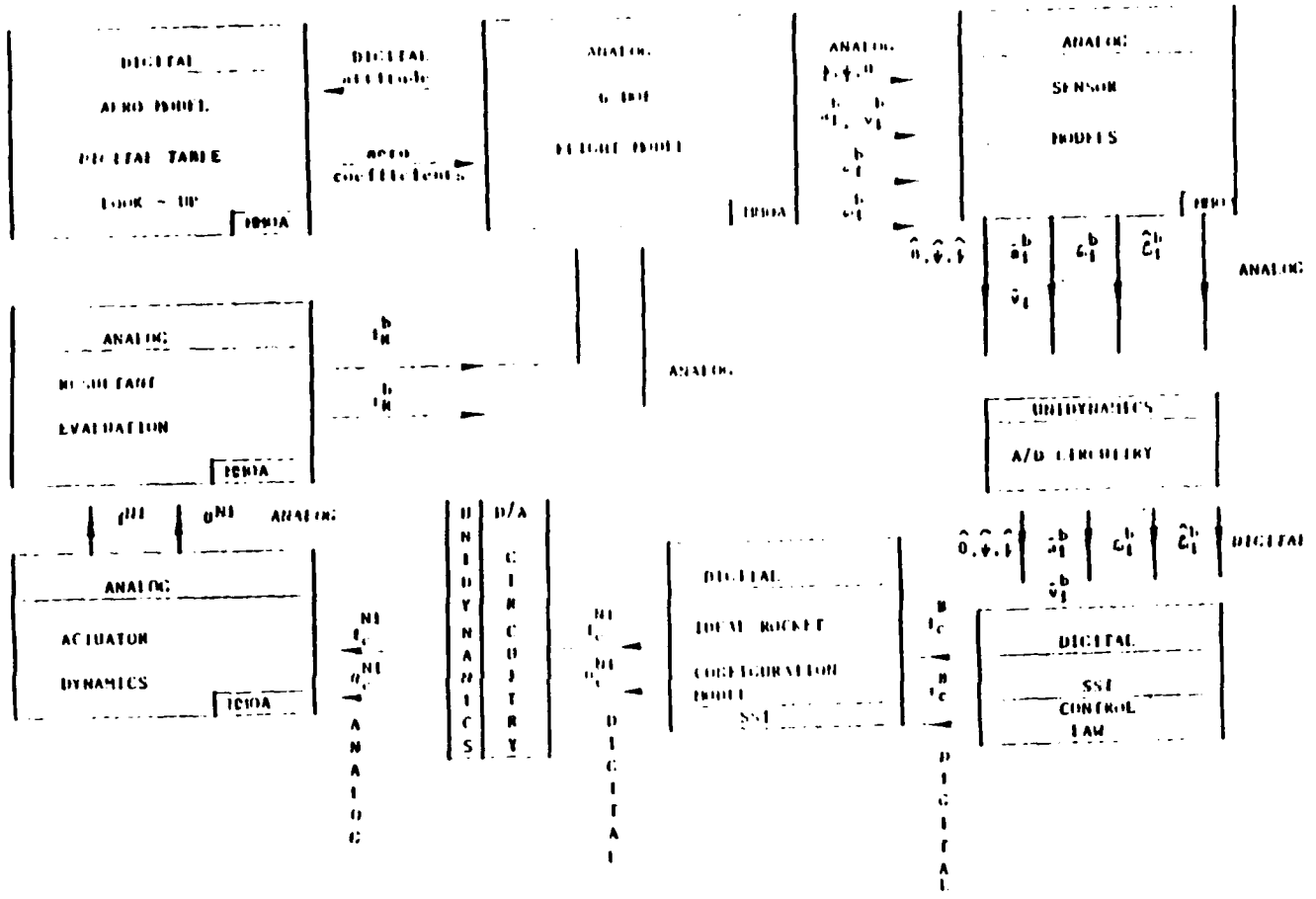

Figure 6.7 Illustration of Integrated DIGITAL/ANALOG SIMULATION/CONTROL SYSTEM

Table 6.8 Definition of Processors in MMOA Analog Simulation.

Hardware Component	Definition	Quantity
AD-10	Applied Dynamics AD-10 Parallel Processor	1
EA-8800	Electronic Associates 8800 Analog Computer	3
PE 8/32	Perkin Elmer 8/32 Digital Computer	1
Strip Chart Recorders		7

The three EA-8800 analog computers support the implementation of all analog models with appropriate ADC/DAC interfaces for communication with the AD-10, PE 8/32 and the Unidynamics controller board. The PE 8/32 defined in Table 6.8 does not explicitly appear in Figure 6.7. The MMOA analog simulation allows the use of the PE 8/32 to serve as substitute in place of the hardware controller microprocessor based system under test. Section 6.4.4, Modes of Operation, describes the use of this alternate system for the generation of results. The strip chart recorders allow for visibility of dynamic variables each with preset maximum values divisible over a 100 to 1 scaling range facilitating the observation of small signal dynamics for key variables of interest.

6.4.3 Unidynamics Hardware Controller Board Description. The general requirements for the fabrication of the microprocessor controller board are: (1) interface electronics to allow for access of sensor inputs, (2) sufficient RAM memory to support the control algorithms, (3) a system clock with a suitable rating to support real-time operation, (4) interface electronics to allow for control of actuation system elements and (5) a communications interface to support file downloads to the 68000 microprocessor.

Figure 6.8 illustrates the system specification for the Unidynamics hardware controller board. The system input module consists of a parallel 16 channel 12 bit ADC interface. The channels receive the raw analog signals from the MMOA simulation and deliver the digital equivalent to the algorithms hosted on the microprocessor. The system outputs are serviced by a parallel 12 channel 12 bit DAC interface with sample and hold circuits. The assigned control system variables are indicated in Figure 6.8. Note that the current configuration requires 7 channels to service outputs allowing for expansion in modeling alternate actuation system configurations.

The RS-232 terminal port allows for direct communication with the development system (VAX) to support fast download of executable files in the prescribed Motorola format. The internal memory allocation of the microprocessor allows for volatile all RAM operation (64K) or permanent program storage with the non volatile ROM (64K) memory.

The operation of the sub-system given in Figure 6.8 proceeds as follows. At the start of an execution cycle each sensor input is requested sequentially over the parallel input communication interface. With appropriate scaling of the sensor inputs the controller performs calculations to generate the control commands for the individual control elements. Each of the digital controls to the actuation system elements are converted sequentially by the parallel output interface to analog form for use by subsequent analog models. Hence the inputs capture all state estimates at nearly the same instant in time and the outputs are available for the actuation system as soon as practicable with near simultaneity. The sample and hold circuitry maintains the control signals at the commanded level until refreshed by the ensuing control cycle.

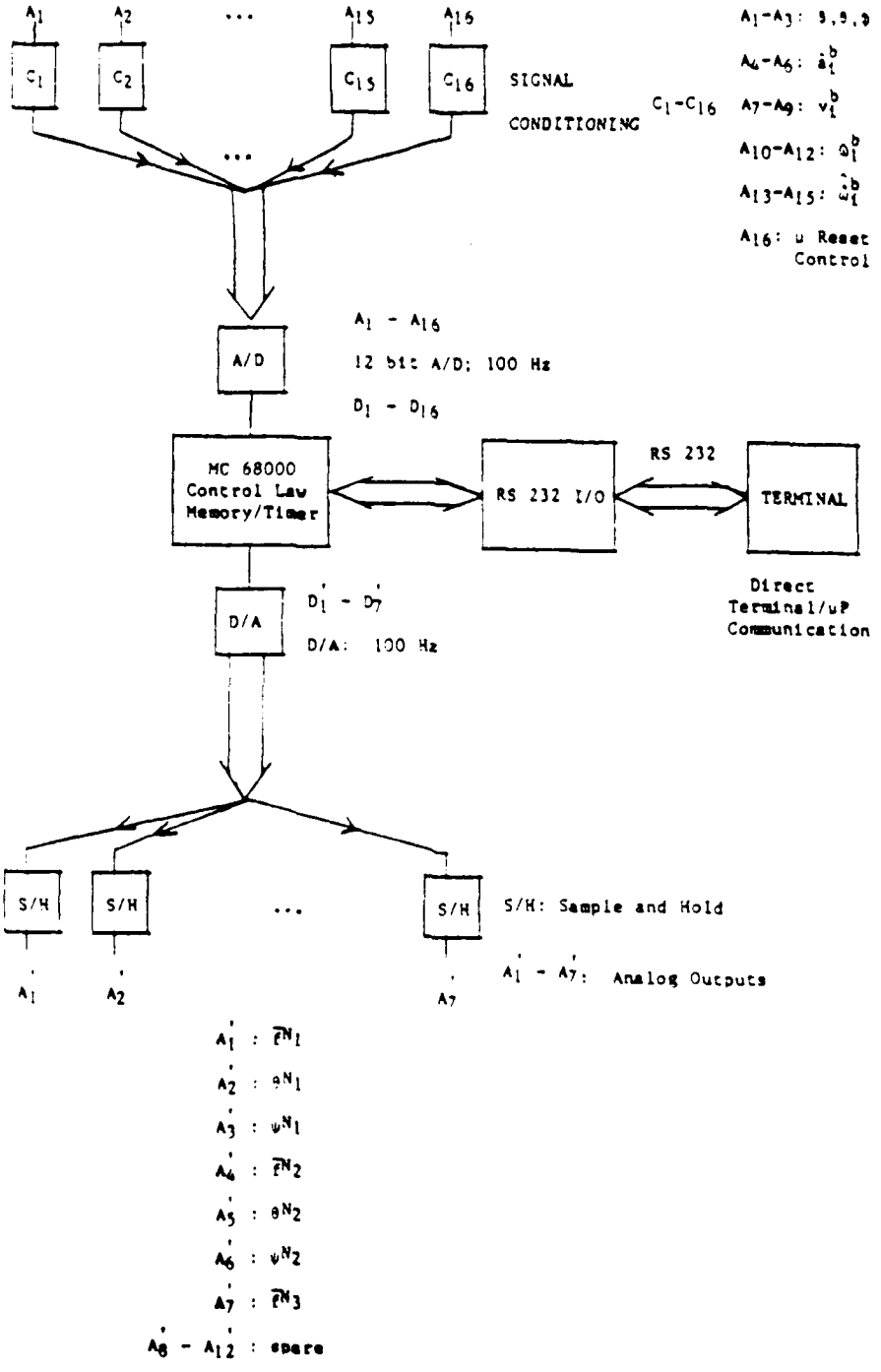

Figure 6.8 CONTROLLER BOARD INTERFACE REQUIREMENTS

The RS-232 terminal to microprocessor communication interface allows for the control algorithm to be interrupted in order to view the status of input and output variables or internal dynamic quantities in debugging when problems do arise.

6.4.4 Modes of Hybrid Simulation Operation. The MMOA analog system described above alluded to direct use of a PE 8/32 digital computer to support control system functions as an alternative to microprocessor hardware in the loop operation. The PE 8/32 operating mode executes an all FORTRAN implementation of the control concept replacing the digital control segment in Figure 6.7. This mechanization is extremely useful as it allows for direct comparisons with microprocessor in the loop results and simplifies alterations in the control logic for the evaluation of alternative control designs. In addition the PE operation mode allows for advanced debugging for isolation of potential sources of system mal-functions, both hardware and software.

The second mode of hybrid operation is of course with the microprocessor controller in the loop. This mode of operation is primarily concerned with verification of proper operation of the microprocessor based code and to provide for throughput estimates. While the variables assigned to the ADC/DAC interface are directly observable in this operating mode the internal controller dynamic variables are unobservable due to limited communication so that the PE 8/32 does provide for a more complete picture of controller operation. With that in mind the stand alone PE 8/32 operating mode is actually preferable for the examination of the results.

CHAPTER 7

RESULTS AND ANALYSIS

7.1 Overview of Chapter 7.

Chapter 7 examines the results obtained with the proposed control algorithm when exercised in the real time hybrid simulation environment. The major goal in all cases is to demonstrate acceptable performance of the control concept with respect to the following measures: (1) avoidance of ground collisions for low altitude ejection, (2) containment of the acceleration radical to survivable limits and (3) guarantee that in steady state that the terminal attitude constraints are met. The cases under investigation vary over a wide range of the flight envelope expected in emergency ejection. These conditions include low altitude ejection at high dynamic pressure, low altitude ejection at "adverse attitude" and high altitude, high dynamic pressure ejection. It is important to emphasize that the results discussed below utilize a single set of control parameters in the evaluation of all the test conditions. That is, no specific tuning of parameters to the specific ejection conditions are inherent in the following results. Any viable scheme necessarily would only require a minimal set of parameters to be selected if the approach is truly applicable to a wide region of the ejection envelope.

7.2 Comparison of Alternative Operational Modes of the Hybrid Simulation.

Three operational modes are examined with the hybrid simulation model. The first illustrates the negative consequences of open loop ejection where there is no direct control of the life threatening

forces and torques in ejection nor are any position or attitude constraints enforced. In this simplistic mode of operation, the main thruster is deployed at a constant thrust level throughout the scenario and all other control elements are constrained off. The second mode of operation exercises the control logic hosted on a mainframe computer (PE 8/32) which serves as substitute for the microprocessor based controller (see paragraph 6.4.4). In this mode of operation all control functions are exercised to simultaneously contain the acceleration radical and to provide corrective attitude steering to the terminal constraint values. The results obtained with the PE 8/32 represent the nominal performance to be expected when the controller is deployed actively in emergency ejection. In the PE 8/32 mode of hybrid operation the control logic is implemented in the FORTRAN language and is a wholly real time operational mode. The third mode of hybrid operation is with the control law hosted on a Motorola 68000 microprocessor which exercises all control functions and represents the performance to be expected with actual hardware in the loop operation with accuracy limited to 16 bit precision.

In summary it would be expected that the open loop mode of operation would typically fail with respect to all performance measures for "difficult" ejection situations. The PE 8/32 and 68000 implementations are expected to deliver acceptable performance with nearly identical results since both modes of operation are realizations of hardware implementations of the control concept under test.

7.2.1 Interpretation of Strip Chart Results.

The outputs of the hybrid simulation are most easily assimilated as direct strip chart outputs of the internal analog variable values. A typical performance evaluation strip chart is illustrated in Figure 7.1. The key variables of interest in evaluation of the performance measures are included in the figure. Other output variables are

U=UNCONTROLLED, S=SIMULATION (PE 8/32). H=HARDWARE (MC 68000)

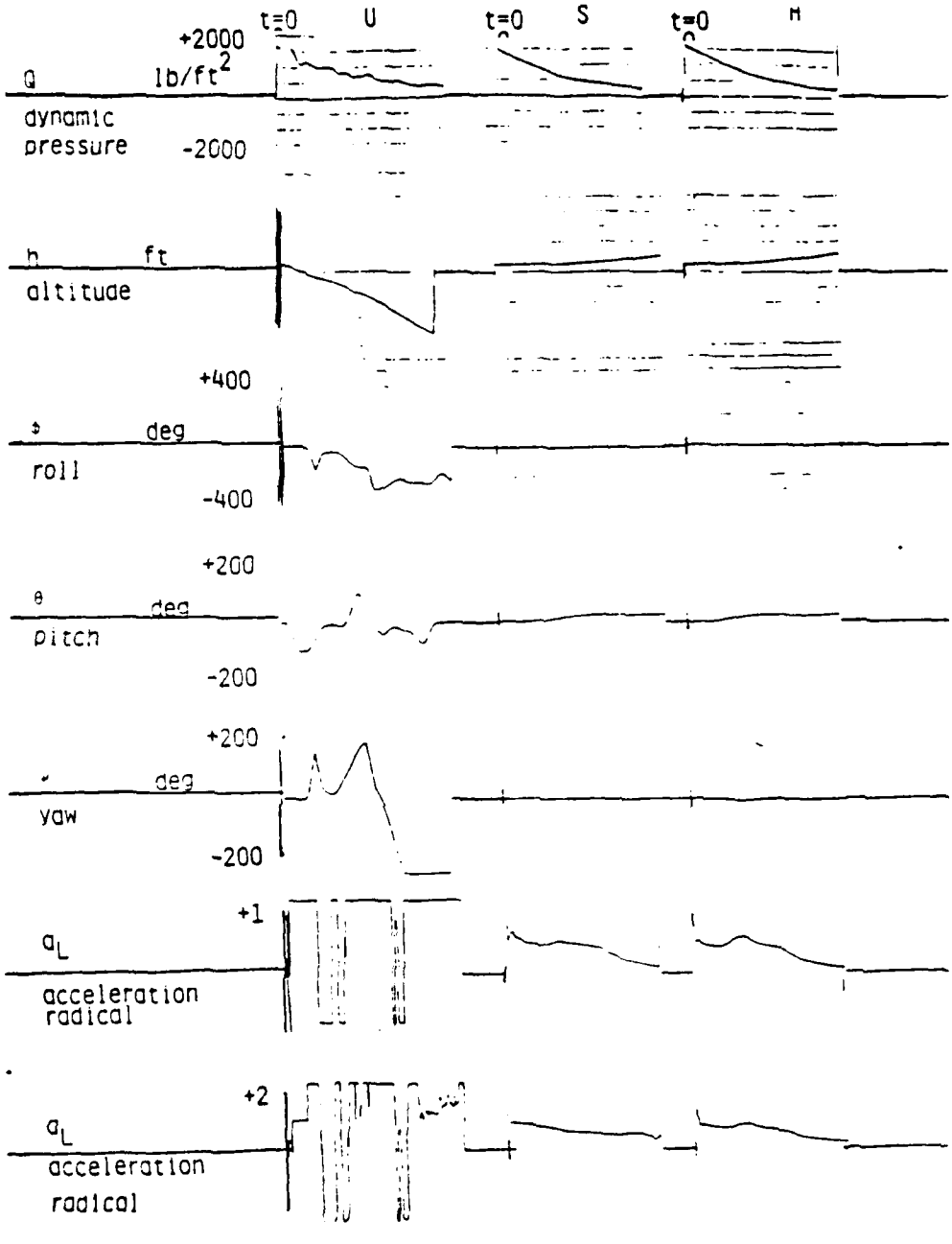

Figure 7.1 HIGH DYNAMIC PRESSURE RESULTS

available from the hybrid simulation but are omitted in the interest of summarizing performance in limited space. Each strip chart is divided into three sequential evaluations, one for each mode of operation identified in the last paragraph. In Figure 7.1, each execution mode is identified at the top of the figure by the abbreviations "U","S", and "H". Case "U" is the "uncontrolled" response of the ejection seat and represents the performance of fixed thrust schemes with the omission of STAPAC from the ACES II ejection seat. Case "S" outputs represents "simulated" controller performance and are the results of the PE 8/32 mode of operation. Finally the case "H" results are the outputs obtained with the Motorola 68000 "hardware" in the loop mode of operation. All of the results examined in this section are of 2 seconds duration.

For the particular results illustrated in Figure 7.1, the initial flight conditions are as follows: (1) initial speed = 687 KEAS, (2) roll,pitch,yaw = (0,0,0), (3) euler rates p,q,r =(0,0,0) at (4) altitude 100 feet. The desired terminal conditions desired are given by: roll,pitch,yaw=(0,10,0 deg) with ground collision to be avoided. The ambient dynamic pressure in this case is approximately 1600 lb/ft**2 representing a high dynamic pressure ejection resulting in a lethal condition if the resultant inertial forces and torques are inadequately controlled.

In general the roll euler angle is essentially a "free" control variable since rotations about the velocity vector induce no injurious force and torque contributions of any consequence. The pitch euler angle is subject to enormous environmental torquing dynamics so that it is imperative that tight pitch control be maintained to insure ejection seat body stability. Particularly threatening are changes in the yaw euler angle from the initial condition which cause large lateral force components to act directly along the most sensitive pilot body direction. It is apparent that the yaw euler angle should be tightly regulated to the initial value in order to minimize the

growth of the lateral acceleration component.

Examination of the results for the uncontrolled ejection seat labelled "U" in Figure 7.1 indicates no hope of pilot survival for the given initial flight condition. First, ground collision is near immediate eliminating all hope for ejection success. Next, the uncontrolled pitch and yaw dynamics illustrate the highly unstable oscillatory modes that are to be expected in the absence of active attitude control. The acceleration radical evaluation illustrated at the bottom of the figure with scalings (+/- 1,+/- 2) indicate that the lethal limit is attained immediately (radical>1) with no hope for recovery. A thorough inspection of auxiliary hybrid outputs not illustrated in Figure 7.1 indicates that the maximum analog values for several variables are exceeded almost immediately leading to the loss of simulation fidelity in generation of the final results. It should be noted that the acceleration radical evaluations appear less than 0 in the strip chart outputs due to severe violations of allowable variable bounds in the analog circuitry. An all digital VAX simulation of this scenario for the uncontrolled case indicated that the maximum value of the acceleration radical exceeded 10.

The PE 8/32 simulated performance labelled "S" in Figure 7.1 illustrates clearly the advantages of active translation and attitude control when compared to the uncontrolled performance labelled "U". Ground collision is clearly avoided given the monotonically increasing altitude history. The desired 0 degree roll and yaw angles are tightly regulated indicating proper attitude control and resulting ejection seat rotational stability. The pitch euler angle history is indicative of successful pitch angle control given the well controlled history from the initial 0 degree value to the desired nominal terminal value of 10 degrees. The rapid reaction of the control system to the environmental translational forces and rotational torques are evident in this case which completely avoids all the negative aspects of the uncontrolled ejection seat. The resulting

acceleration radical is bounded to less than 1 throughout the 2 second ejection duration with a terminal reduction by an order of magnitude of the acceleration radical and dynamic pressure by mission completion when compared with the starting values.

The microprocessor hardware in the loop operation labelled "H" results in a close match with the simulated PE 8/32 results labelled "S". Some discrepancy is observable in the acceleration radical history between the "H" and "S" results. A close examination of the euler time histories at a finer strip chart scale than that illustrated in Figure 7.3 indicated some variation particularly noticeable in the yaw channel. The primary disturbance responsible for this variation is the ambient electrical noise at the simulated sensor ADC interface. The PE 8/32 operates with an interface voltage of +/- 100 V range for all process variables generated by the analog computer while the Motorola 68000 ADC interface is bounded by a +/- 10 V range. The RMS electrical noise level at the electrical interfaces are comparable for both systems implying an order of magnitude poorer signal to noise ratio for the Motorola 68000 sensor measurements when compared to those available to the PE 8/32.

7.3 Low Altitude Escape Conditions.

The initial ejection seat flight conditions forming the MIL-S-9479B test cases are defined in Table 7.1. The corresponding figure identifiers illustrating the results of each case are also indicated in the figure.

TABLE 7.1

Low Altitude Escape Conditions (1)

MIL Case	Attitude Pitch (Deg)	Attitude Roll (Deg)	Speed (KEAS)	Altitude (feet)	Results Illustration
1	0	60	120	0 (2)	Figure 7.2
2	0	180	150	200	Figure 7.3
3	0	0	150	300 (3)	Figure 7.4
4	-60	0	200	500	Figure 7.5
5	-30	0	450	500	Figure 7.6
6	-60	60	200	550	Figure 7.7
7	-45	180	250	600	Figure 7.8

(1) Conditions at start of escape sequence

(2) Impact occurs at instant of seat/aircraft separation

(3) 10000 feet per minute sink rate.

All the cases indicated above are likely to result in ground collisions if the opportunity for immediate corrective control action is missed. Particularly pressing are MIL Case 3 with a high sink rate and MIL Case 7 with inverted roll and steep pitch orientated to cause ground impact in the absence of direct control. All the above cases are essentially at low dynamic pressure with the exception of MIL Case 5 with moderate dynamic pressure.

Inspection of the results of the following pages for the "U" or the "uncontrolled" class of response dynamics demonstrates unacceptable performance for a variety of reasons. In all cases, the attitude is highly unstable leading to high attitude rates with corresponding effects observable as oscillations in the acceleration radical. The altitude performance is unpredictable with cases 2, 5, 7, leading to obvious ground collisions. Ground collision avoidance in

U=UNCONTROLLED, S=SIMULATION (PE 8/32), H=HARDWARE (MC 68000)

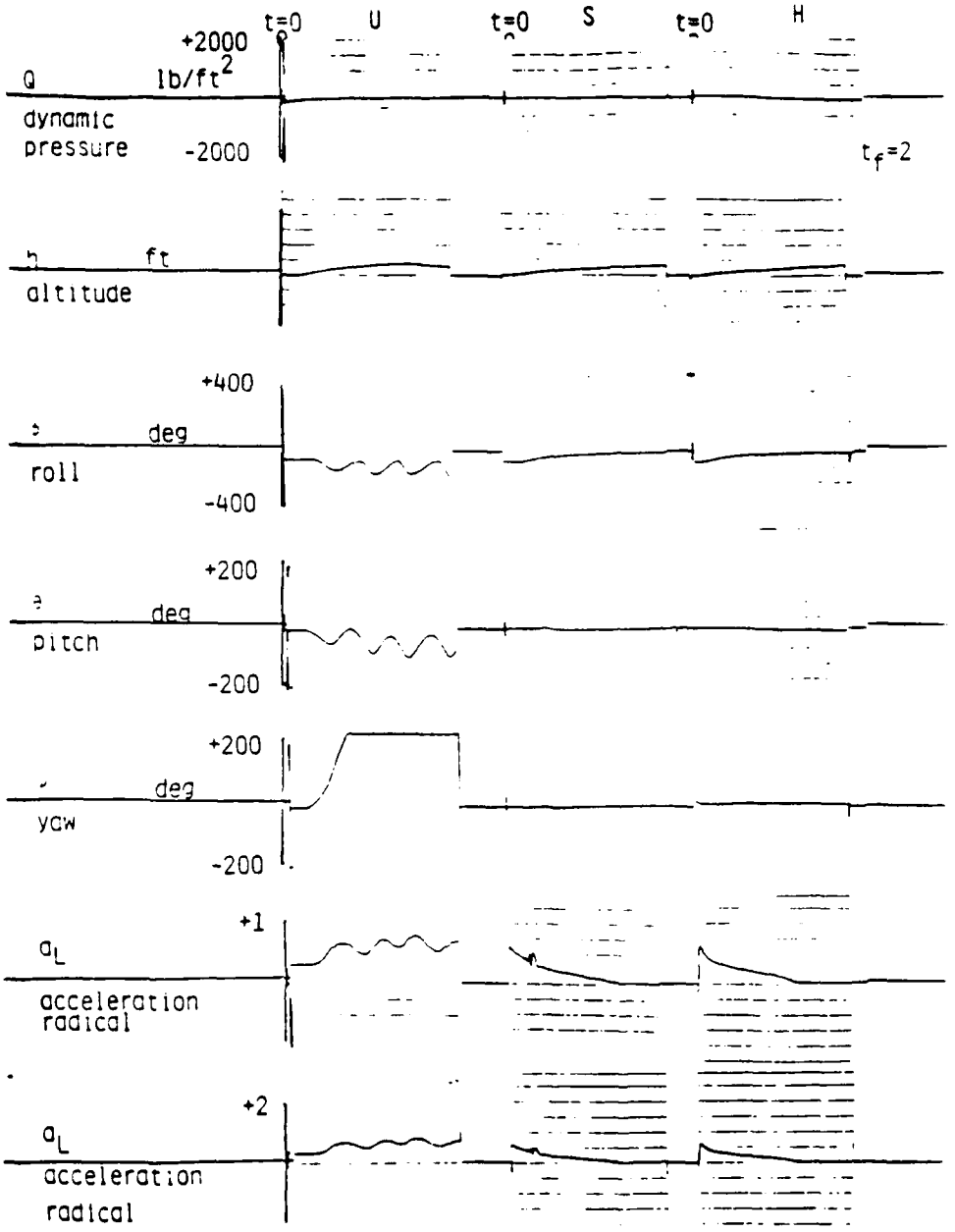

Figure 7.2 LOW ALTITUDE ESCAPE CONDITIONS

U=UNCONTROLLED, S=SIMULATION (PE 8/32), H=HARDWARE (MC 68000)

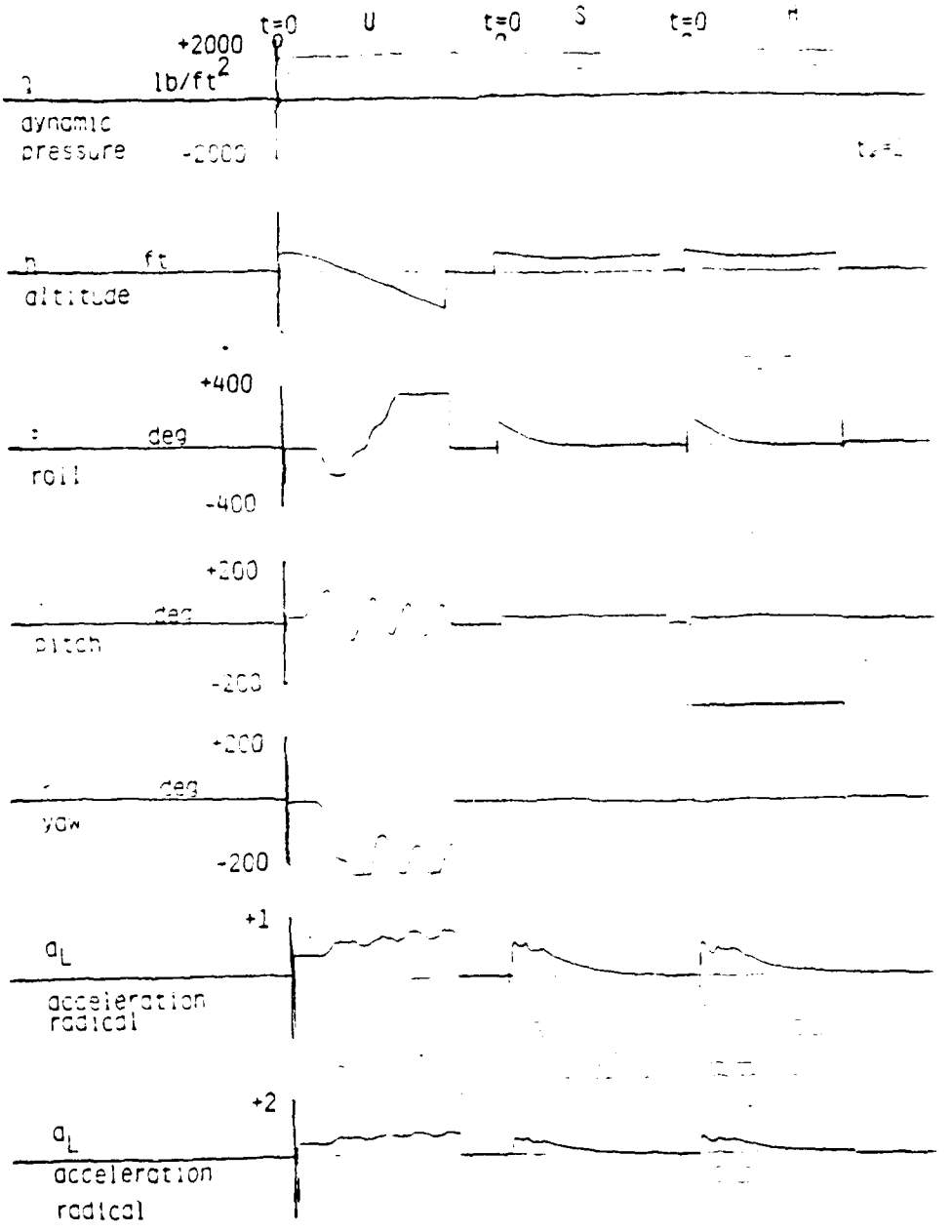

Figure 7.3 LOW ALTITUDE ESCAPE CONDITIONS

U=UNCONTROLLED, S=SIMULATION (PE 8/32), H=HARDWARE (MC 68000)

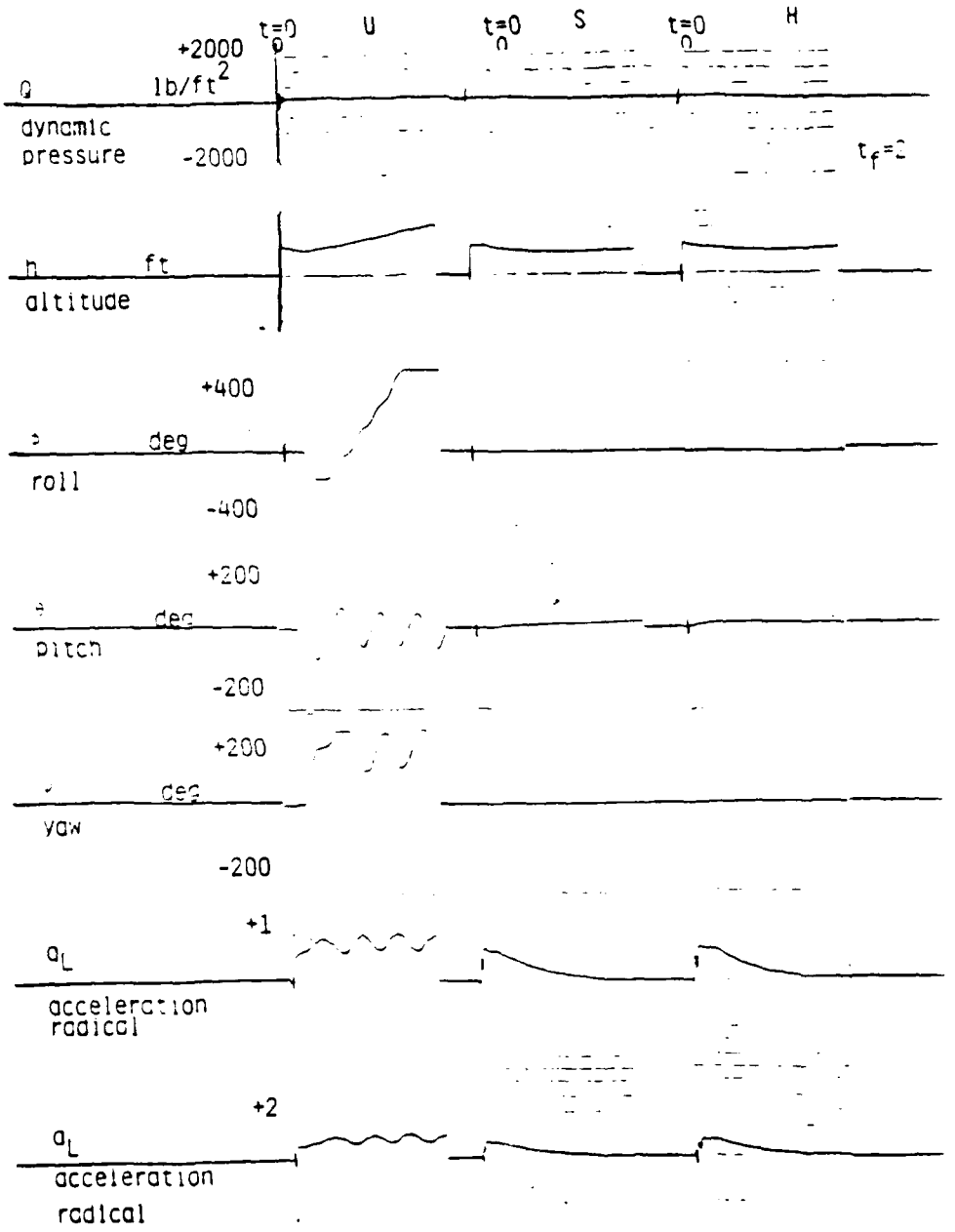

Figure 7.4 LOW ALTITUDE ESCAPE CONDITIONS

U=UNCONTROLLED, S=SIMULATION (PE 8/32), H=HARDWARE (MC 68000)

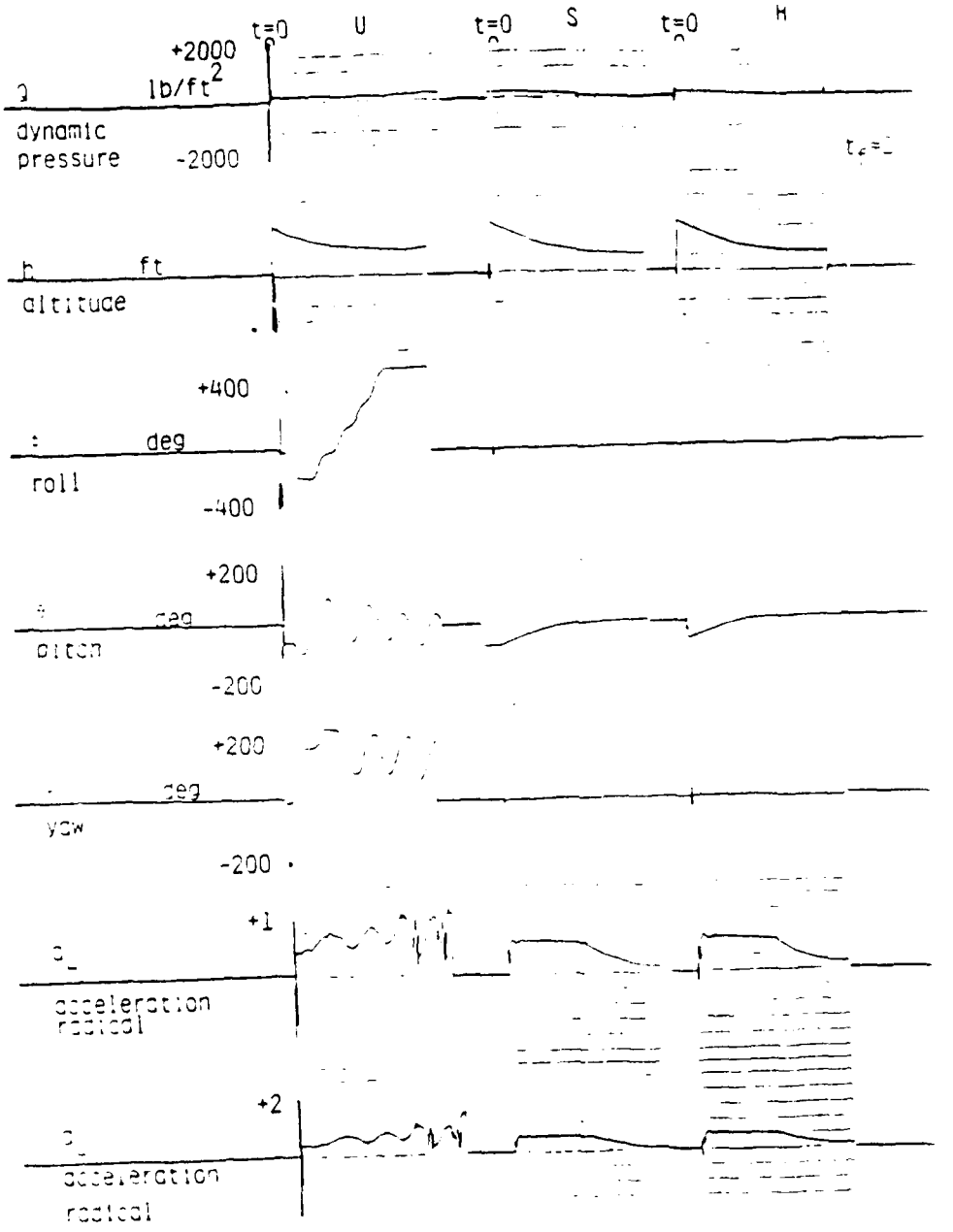

Figure 7.5 LOW ALTITUDE ESCAPE CONDITIONS

U=UNCONTROLLED, S=SIMULATION (PE 8/32). H=HARDWARE (MC 68000)

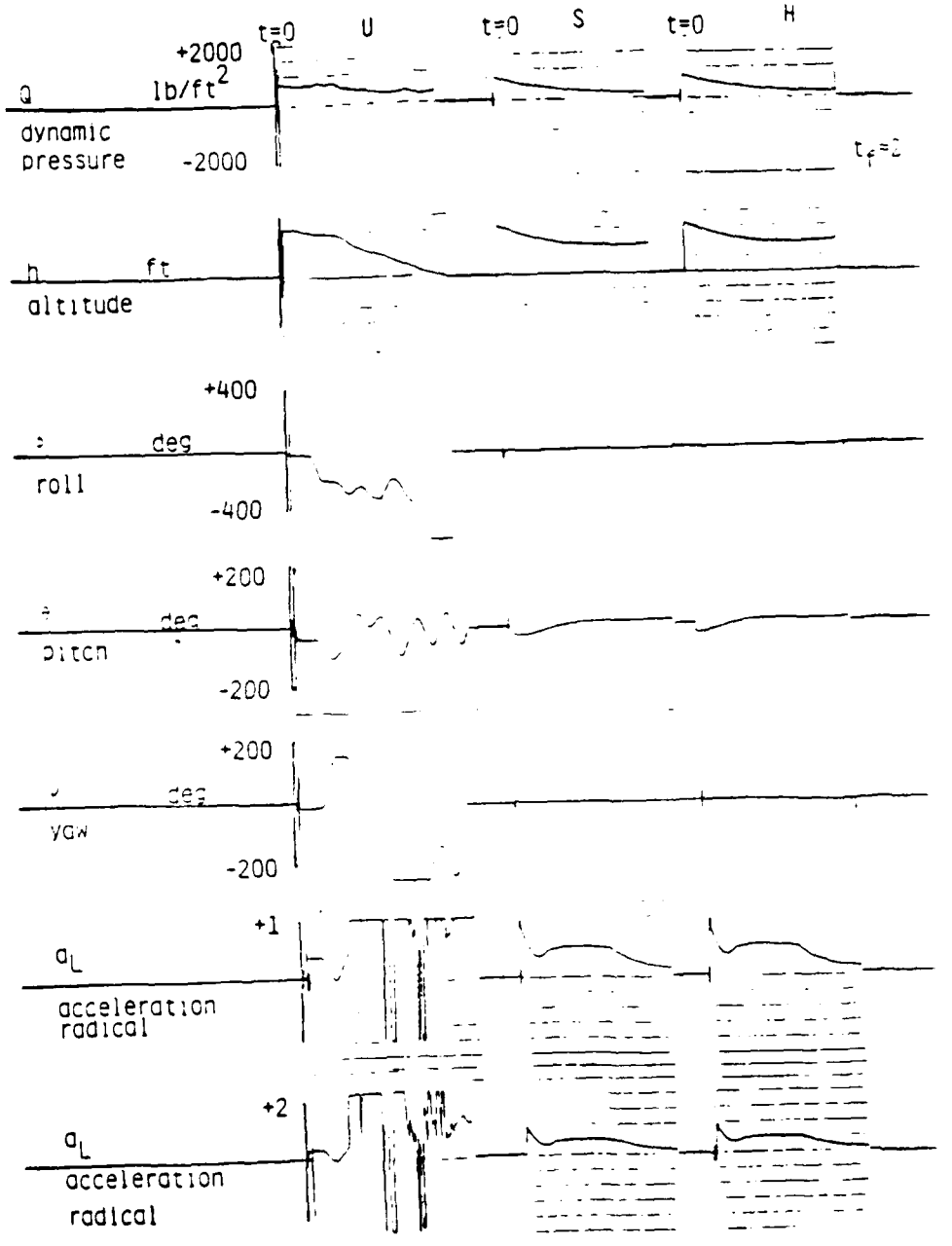

Figure 7.6 LOW ALTITUDE ESCAPE CONDITIONS

U=UNCONTROLLED, S=SIMULATION (PE 8/32), H=HARDWARE (MC 68000)

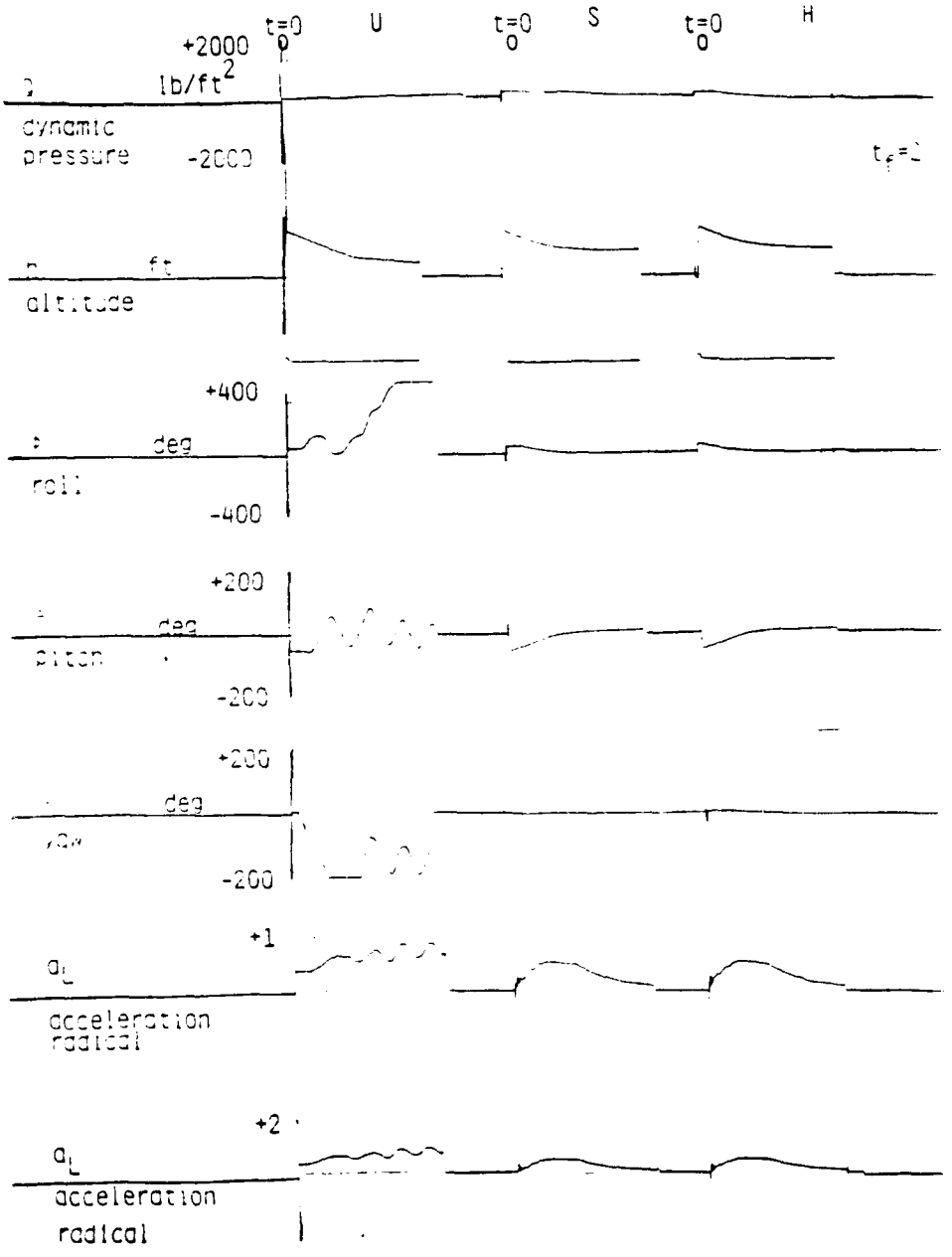

Figure 7.7 LOW ALTITUDE ESCAPE CONDITIONS

U=UNCONTROLLED, S=SIMULATION (PE 8/32). H=HARDWARE (MC 68000)

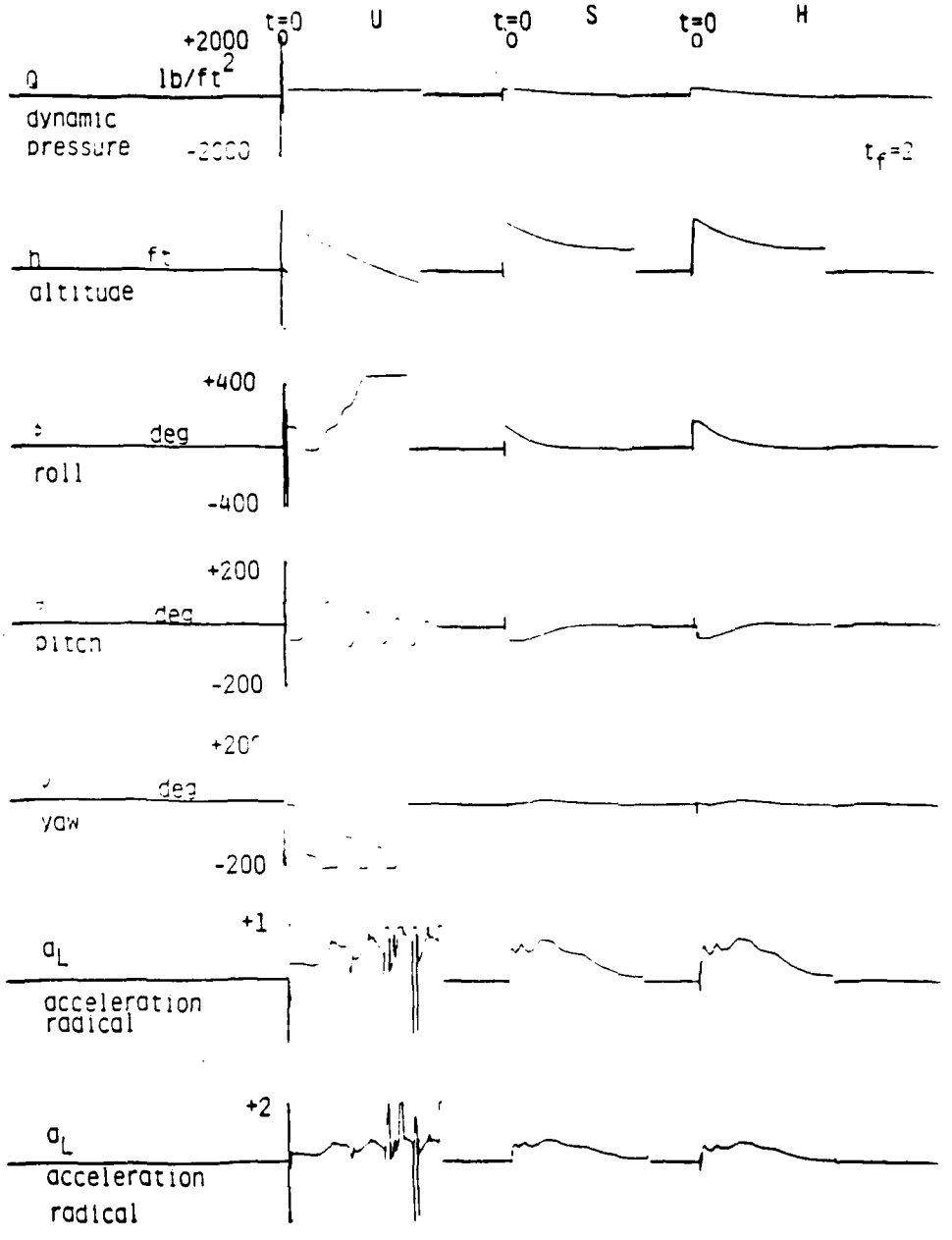

Figure 7.8 LOW ALTITUDE ESCAPE CONDITIONS

other cases are effectively accidental. In all instances the mean acceleration radical is an increasing function of time indicative of a poorly controlled situation.

The "S" or simulated hardware (PE 8/32) results by contrast have well controlled attitude profiles and in all instances ground collisions are clearly avoided. The terminal pitch angle constraint is 10 degrees for all cases while the terminal roll angle is specified to be 0. In all cases the initial yaw angle is 0 degrees and the intent is to tightly maintain 0 degrees yaw. Inspection of the MIL Case 7 results illustrates the simultaneous coordination of the roll and pitch maneuvers through large angle rotations with minimal oscillations demonstrating the effectiveness of decoupling the attitude control. The success of large angle euler steering is also demonstrated in MIL Case 2. It is evident that the terminal euler constraints are successfully met satisfying that performance objective. The acceleration radical is maintained below 1 in all cases and in general is minimal at the termination of each mission scenario. The acceleration radical growth during the mid course of each mission is induced by the actuation system control maneuvers necessary to avoid ground collisions plus the trajectory conditioning maneuvers necessary to meet the terminal attitude constraints.

The "H" or 68000 hardware based controller results in all MIL Cases (1-7) are essentially identical to the simulated hardware test cases (PE 8/32). These tests are seen as conclusive with respect to demonstrating the proper operation of the 68000 based controller algorithm demonstrating feasibility of hosting the control concept in currently available off the shelf hardware. The results of the next section only illustrate the simulated hardware performance with the PE 8/32 computer since all testing has indicated a close correspondence between the simulated hardware and the actual microprocessor hardware.

7.4 Results with Variations of the Initial Attitude.

The remaining results exercise the control strategy at various altitude, attitude and initial speeds. Table 7.2 defines the initial ejection seat flight conditions for these test cases. The corresponding figure identifiers illustrating the results of each case are also indicated in the figure. Inspection of Table 7.2 indicates that the majority of flight conditions be evaluated at a number of initial orientations in order to test controller sensitivity to initial attitude conditions. The dynamic pressure in these cases range from low for cases (4-10), moderate for cases (11-15) and high for cases (16-20). The high altitude conditions at 600 KEAS for cases (16-20) imply actual ground speeds of approximately 2300 fps. The high dynamics with respect to absolute inertial velocity in cases (16-20) leads to significant coupling of the attitude and translational controls resulting in challenging cases to deal with when a single set of parameters for all possible flight conditions to be encountered are used in the controller.

The results from the uncontrolled ejection seat in this series have negative conclusions concerning stability and containment of the acceleration radical similar to the conclusions of the previous two sections. Further discussion of the open loop, uncontrolled performance is not warranted.

The "S" or simulated hardware performance results are emphasized for this series of tests. The strip chart recordings are to be found on the ensuing pages.

TABLE 7.2

Variable Initial Attitude Conditions.

Mil Case	Attitude		Speed	Altitude	Results Illustration
	Pitch (Deg)	Roll (Deg)	(KEAS)	(Feet)	
1	0	0	0	0	Figure 7.9
2	0	0	600	0	Figure 7.10
3	0	0	700	0	Figure 7.11
4	0	0	150	5000	Figure 7.12
5	0	120	150	5000	Figure 7.13
6	0	180	150	5000	Figure 7.14
7	45	120	150	5000	Figure 7.15
8	45	180	150	5000	Figure 7.16
9	-45	120	150	5000	Figure 7.17
10	-45	180	150	5000	Figure 7.18
11	0	0	400	5000	Figure 7.19
12	45	120	400	5000	Figure 7.20
13	45	180	400	5000	Figure 7.21
14	-45	120	400	5000	Figure 7.22
15	-45	180	400	5000	Figure 7.23
16	0	0	600	45000	Figure 7.24
17	45	120	600	45000	Figure 7.25
18	45	180	600	45000	Figure 7.26
19	-45	120	600	45000	Figure 7.27
20	-45	180	600	45000	Figure 7.28

Case 1 is the standstill ejection scenario and inspection of the results illustrates the low dynamic pressure, the minimal acceleration radical plus the well conditioned attitude time histories. The altitude progresses from the initial 0 value to a terminal value of approximately 50 feet. Cases 2-3 are low altitude, high dynamic pressure conditions with conclusions quite similar in content to those of paragraph 7.2.1.

Cases 4-10 all represent low dynamic pressure scenarios with large angle variation in the initial attitude. All scenarios are exercised at 5000 feet so that the threat of ground collision is moot in these instances. The terminal pitch angle is selected to be 10 degrees for all scenarios. The ejection flight conditions do not warrant any changes in roll angles to avoid ground collisions and in these situations the control algorithm will regulate the roll angle to the initial values. Examination of the results reveals well conditioned pitch control with essentially monotonic transition from the initial to the final specified value. The variation in the acceleration radical is indicative of the varying control energy requirements required to induce pitch maneuvers and control attack angle in attaining the terminal constraint values. In all instances the acceleration radical is constained within the minimal injury region.

Cases 11-15 exercise a subset of the cases 4-10 at the indicated higher speed of 400 KEAS in Table 7.2. The attitude response is similar in form to the results of the previous paragraph with no instabilities apparent in the strip charts results. Once again the roll angles are clamped to the initial values given the threat of ground collision is ruled out by the substantial altitude. The higher control energy required to steer the angle of attack to the terminal conditions is under the influence of the higher initial speed condition.

U=UNCONTROLLED, S=SIMULATION (PE 8/32), H=HARDWARE (MC 68000)

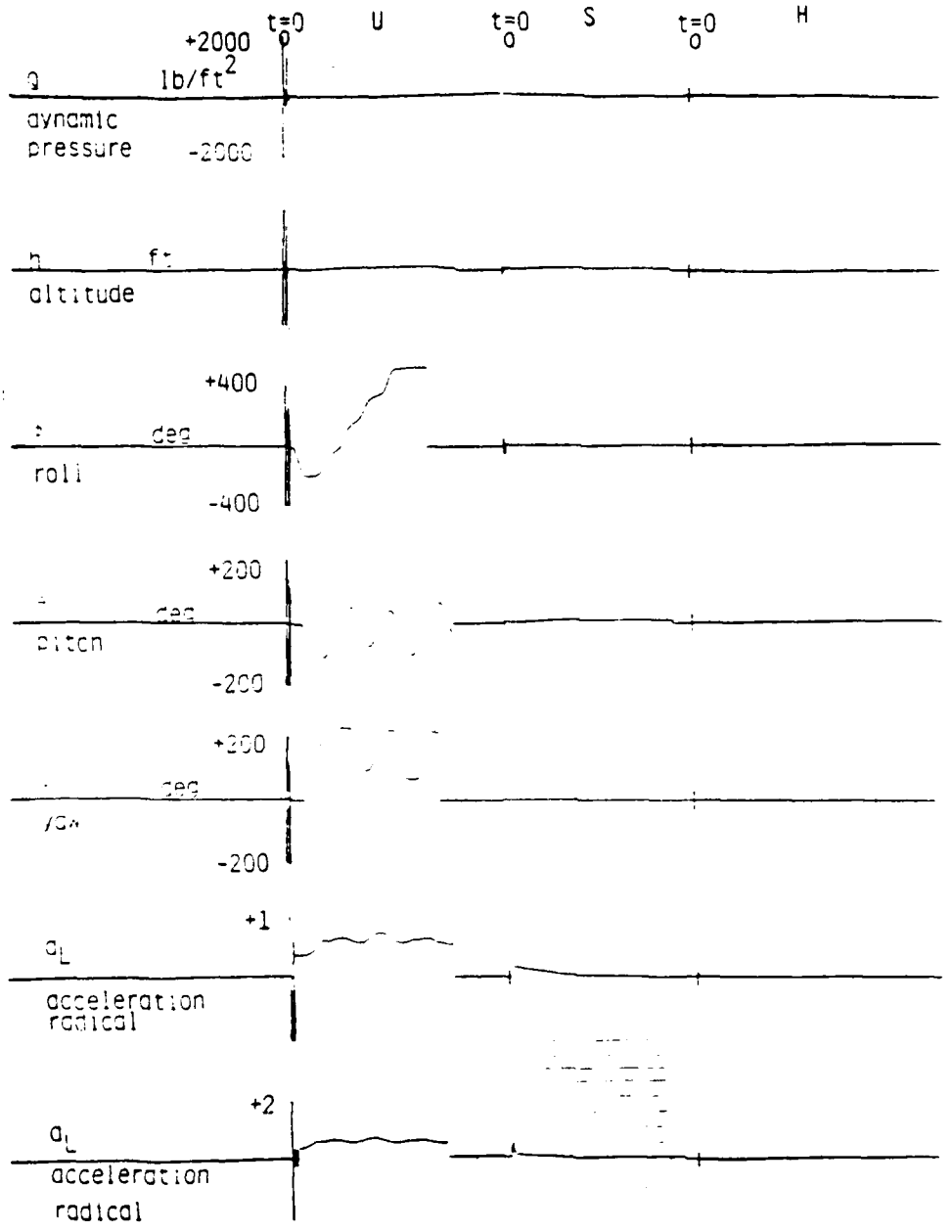

Figure 7.9 VARIABLE INITIAL ATTITUDE CONDITONS

U=UNCONTROLLED, S=SIMULATION (PE 8/32), H=HARDWARE (MC 68000)

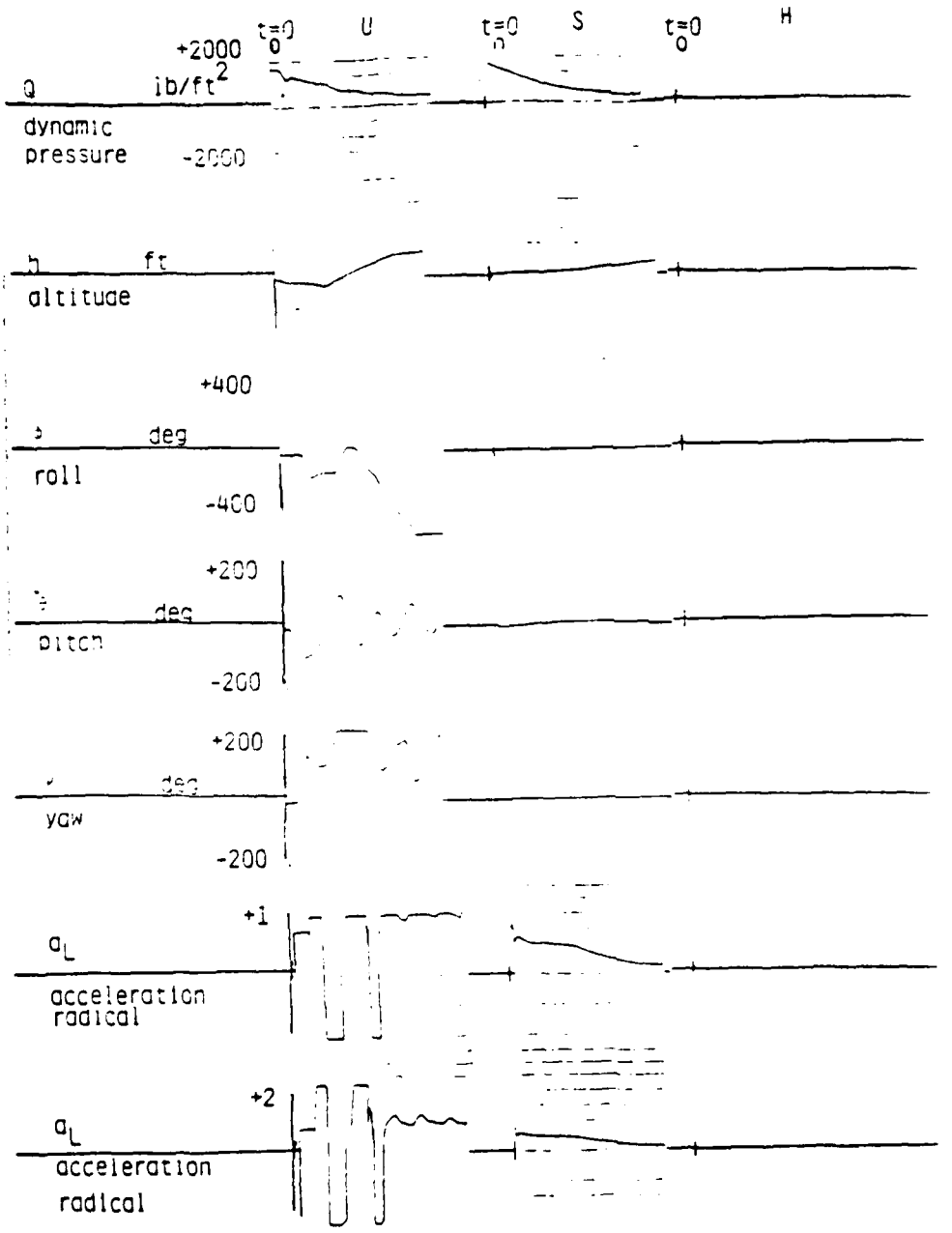

Figure 7.10 VARIABLE INITIAL ATTITUDE CONDITIONS

U=UNCONTROLLED, S=SIMULATION (PE 8/32), H=HARDWARE (MC 68000)

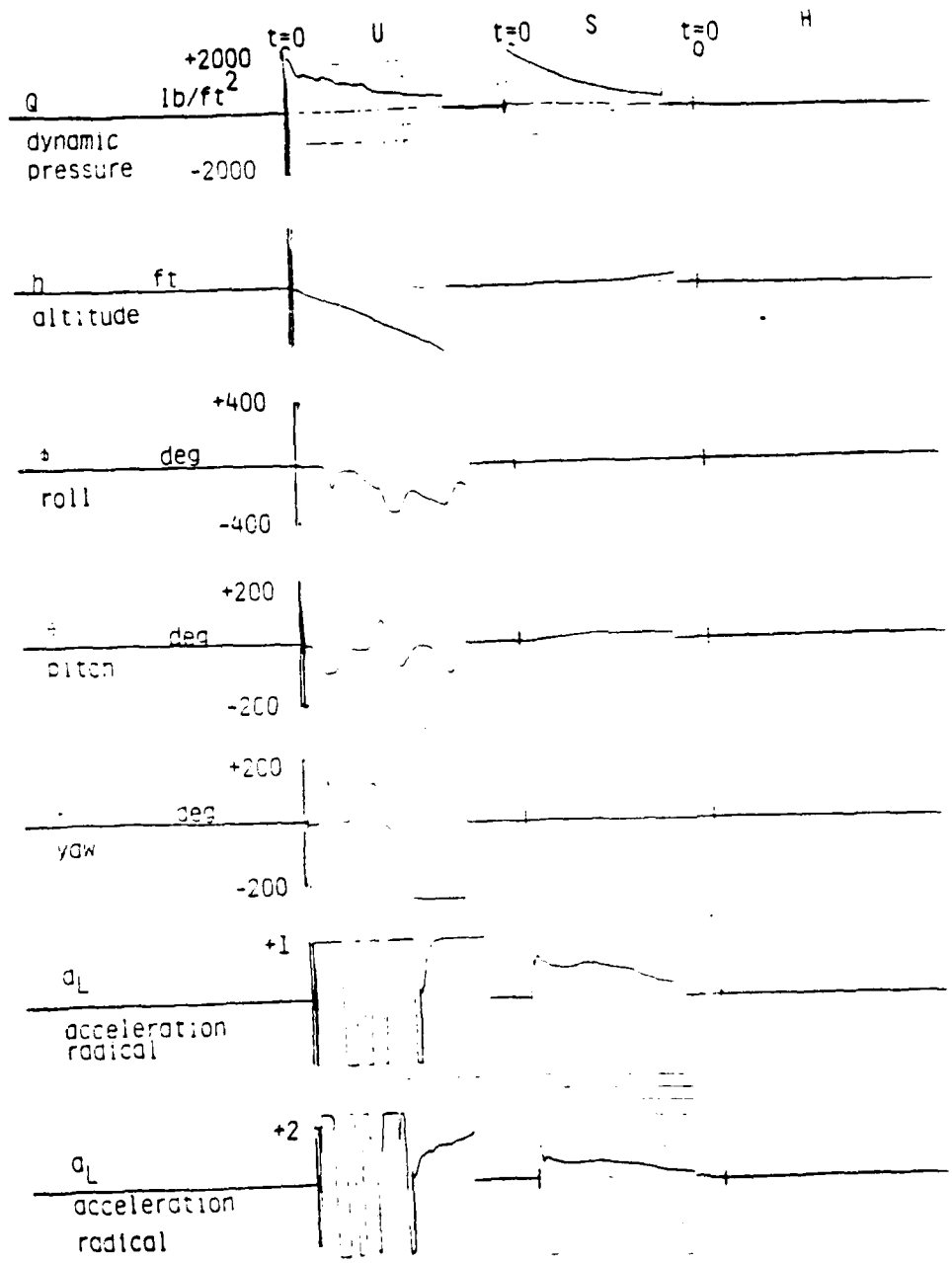

Figure 7.11 VARIABLE INITIAL ATTITUDE CONDITIONS

U=UNCONTROLLED, S=SIMULATION (PE 8/32), H=HARDWARE (MC 68000)

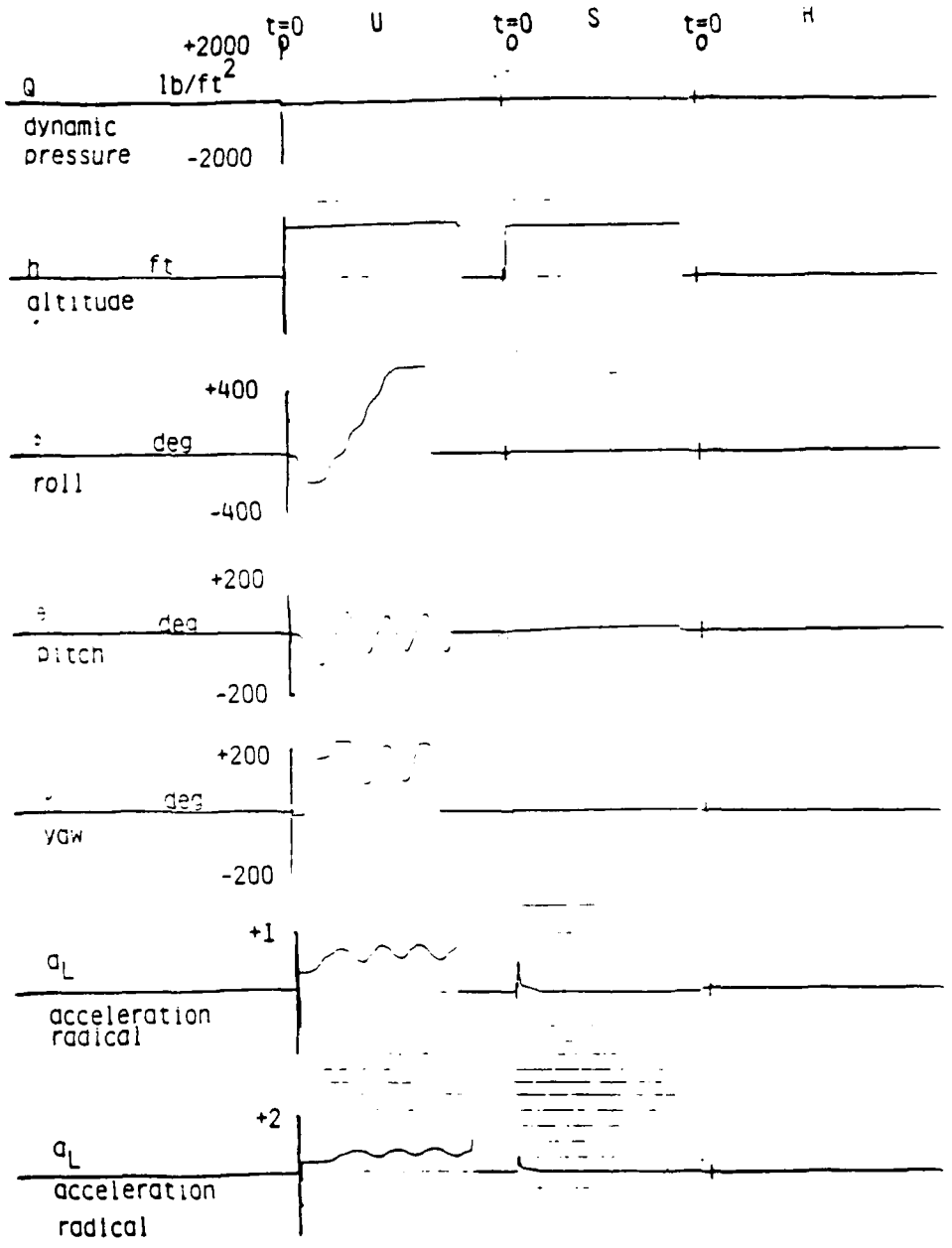

Figure 7.12 VARIABLE INITIAL ATTITUDE CONDITIONS

U=UNCONTROLLED, S=SIMULATION (PE 8/32), H=HARDWARE (MC 68000)

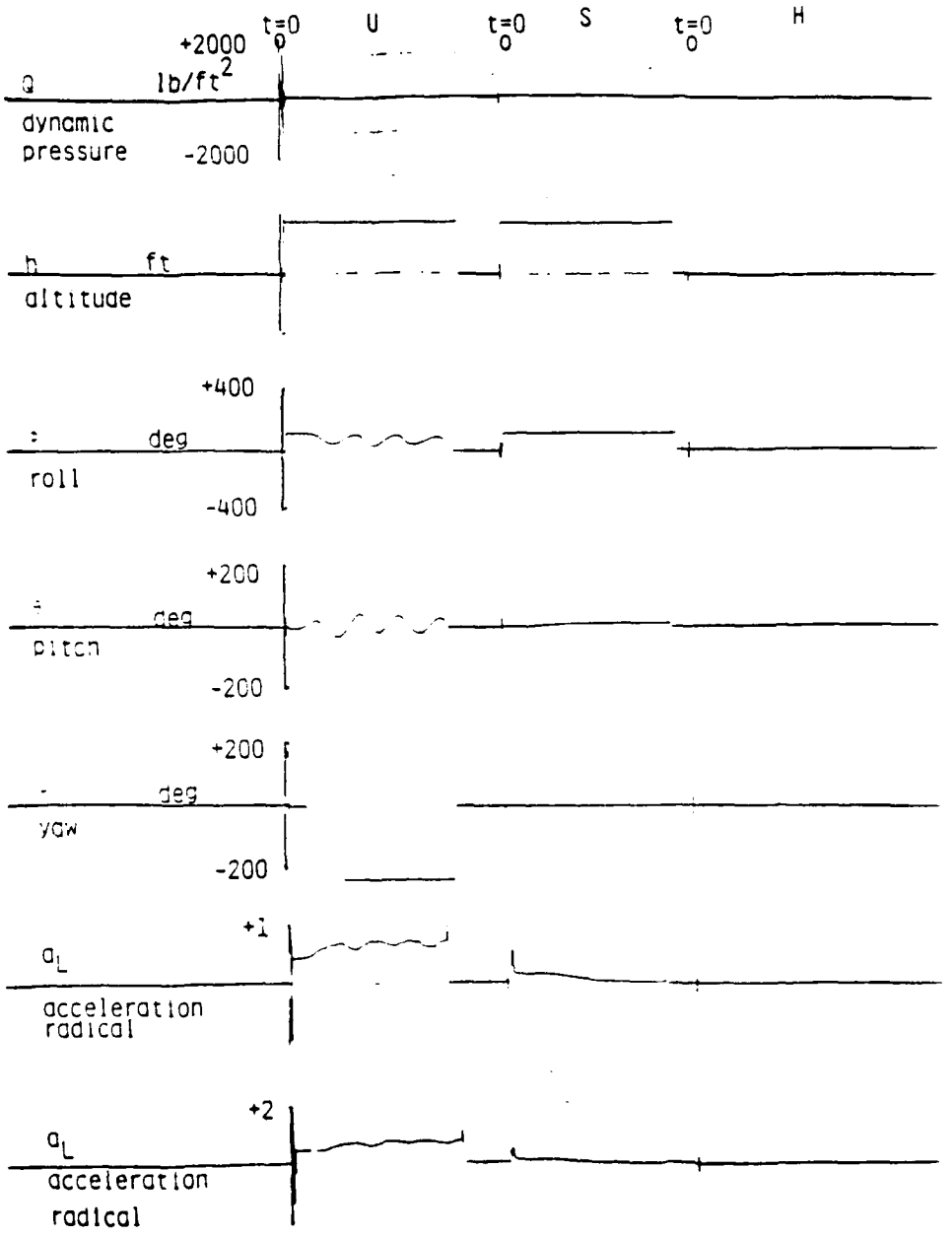

Figure 7.13 VARIABLE INITIAL ATTITUDE CONDITIONS

U=UNCONTROLLED, S=SIMULATION (PE 8/32), H=HARDWARE (MC 68000)

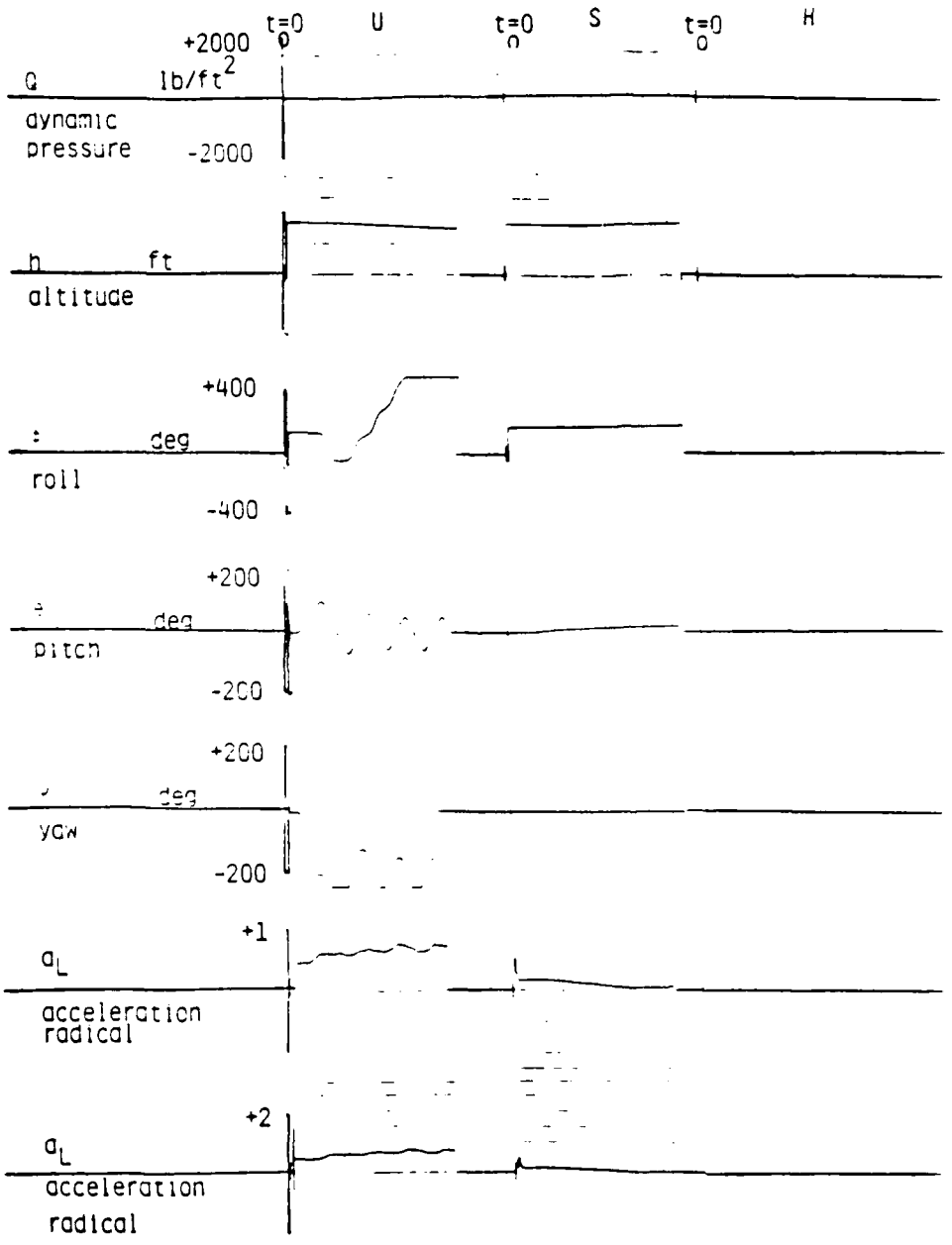

Figure 7.14 VARIABLE INITIAL ATTITUDE CONDITIONS

U=UNCONTROLLED, S=SIMULATION (PE 8/32), H=HARDWARE (MC 68000)

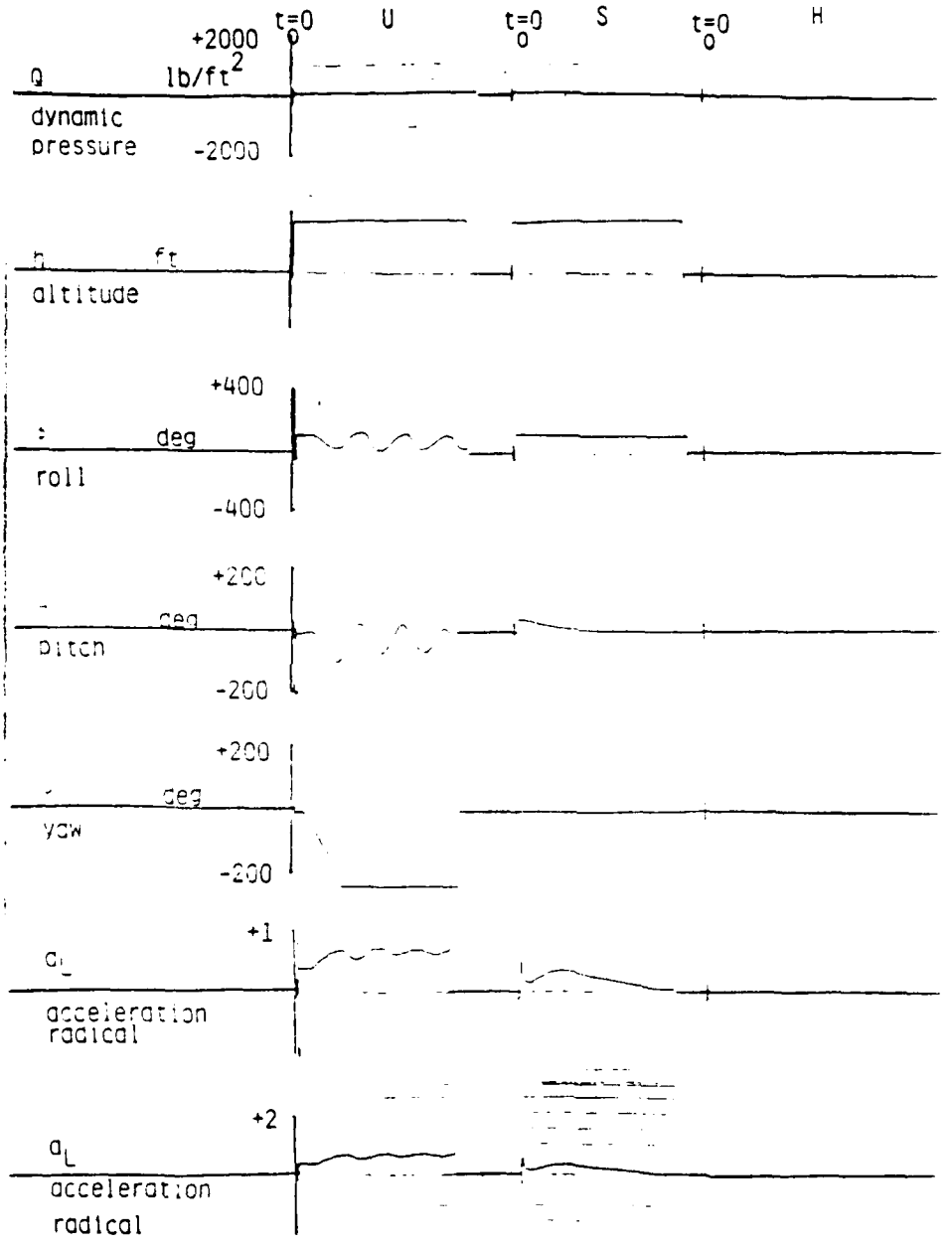

Figure 7.15 VARIABLE INITIAL ATTITUDE CONDITIONS

U=UNCONTROLLED, S=SIMULATION (PE 8/32), H=HARDWARE (MC 68000)

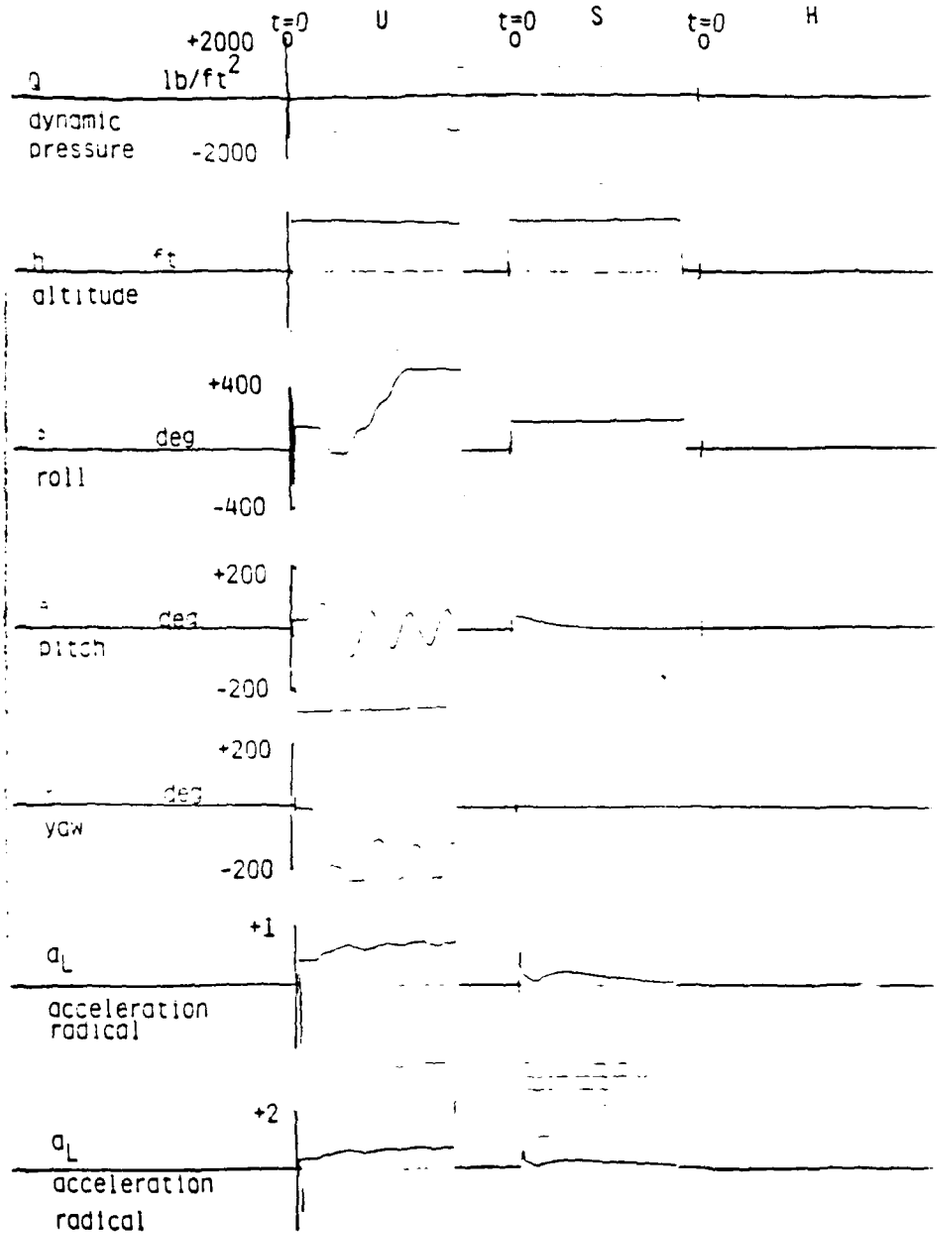

Figure 7.16 VARIABLE INITIAL ATTITUDE CONDITIONS

U=UNCONTROLLED, S=SIMULATION (PE 8/32). H=HARDWARE (MC 68000)

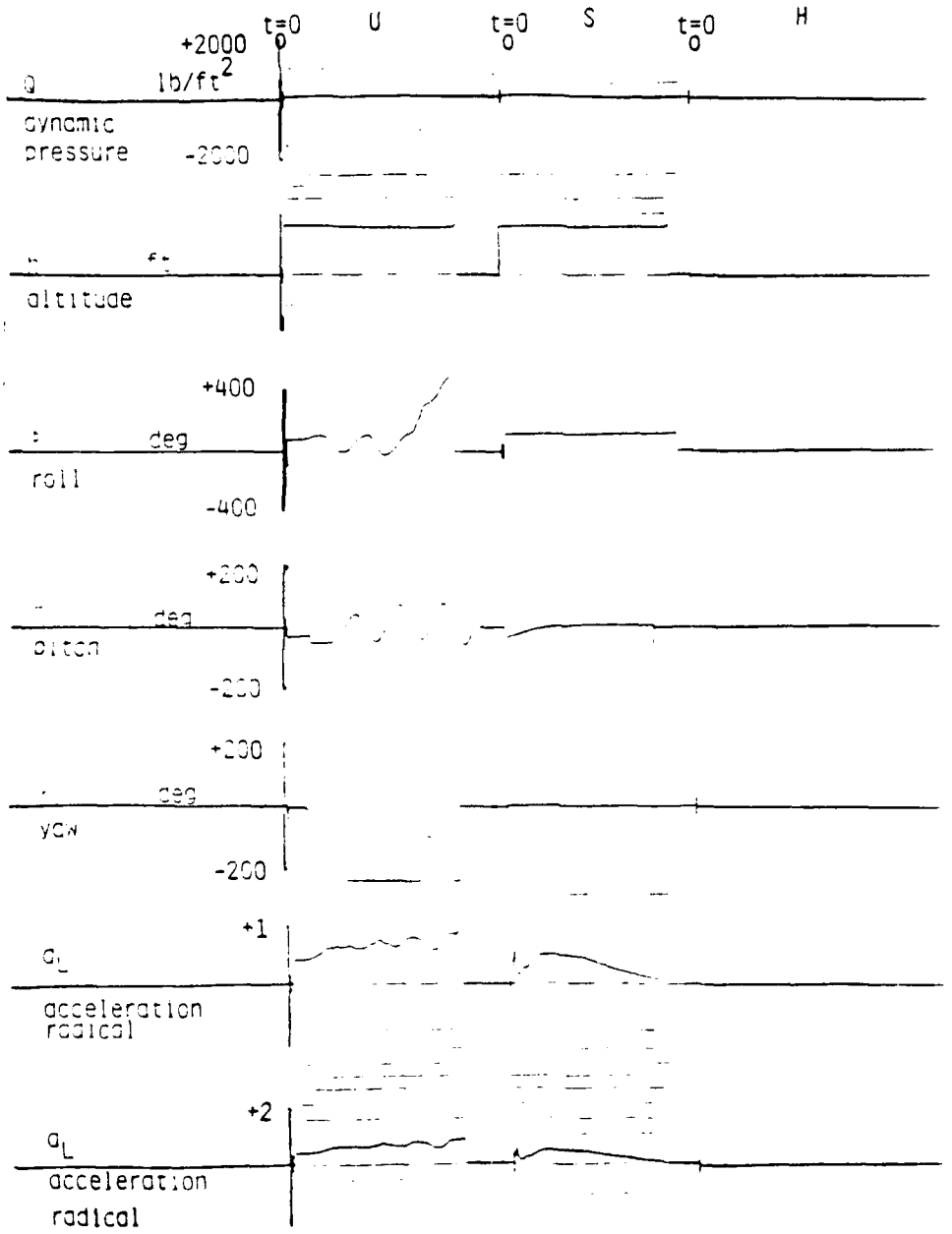

Figure 7.17 VARIABLE INITIAL ATTITUDE CONDITIONS

U=UNCONTROLLED, S=SIMULATION (PE 8/32), H=HARDWARE (MC 68000)

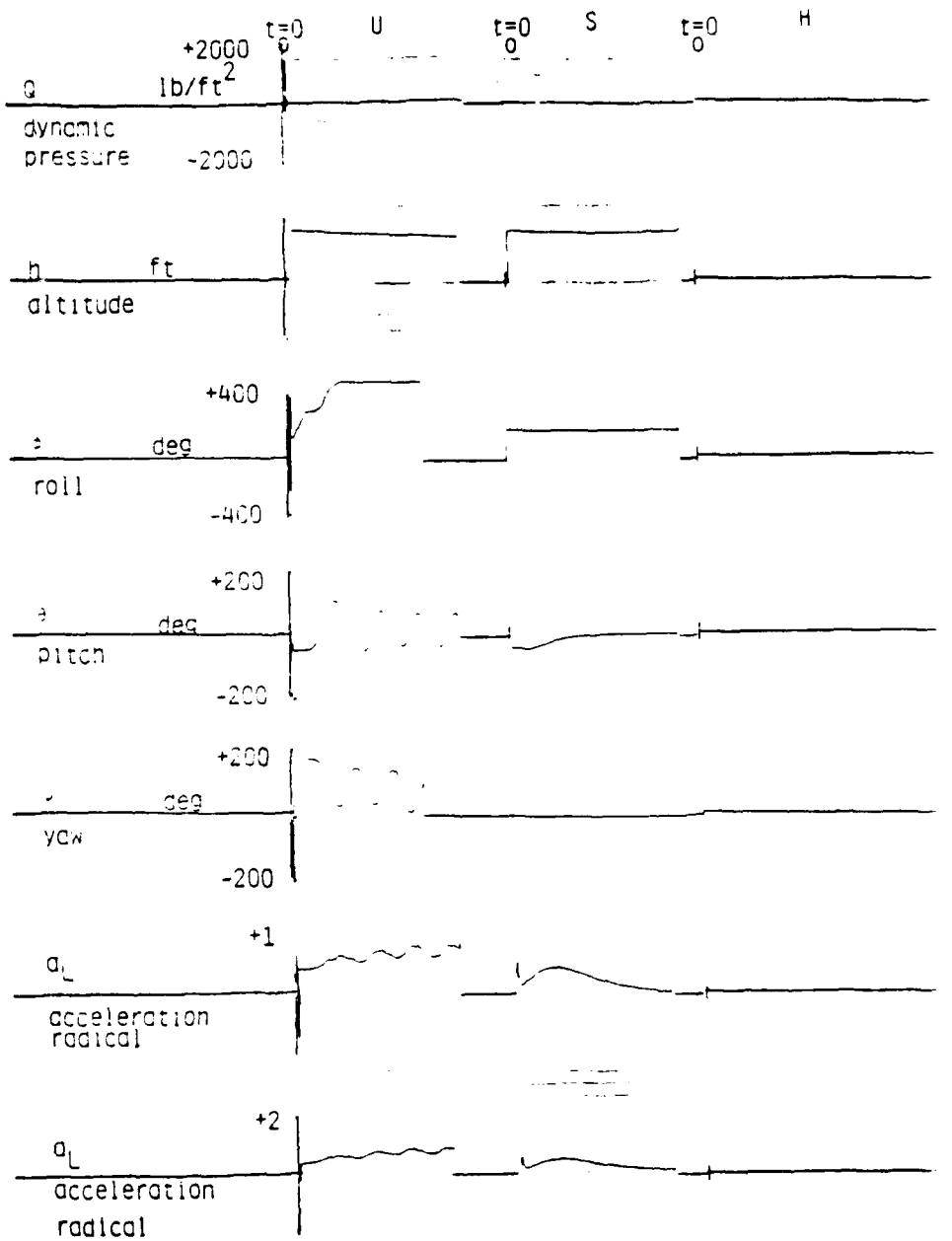

Figure 7.18 VARIABLE INITIAL ATTITUDE CONDITIONS

U=UNCONTROLLED, S=SIMULATION (PE 8/32), H=HARDWARE (MC 68000)

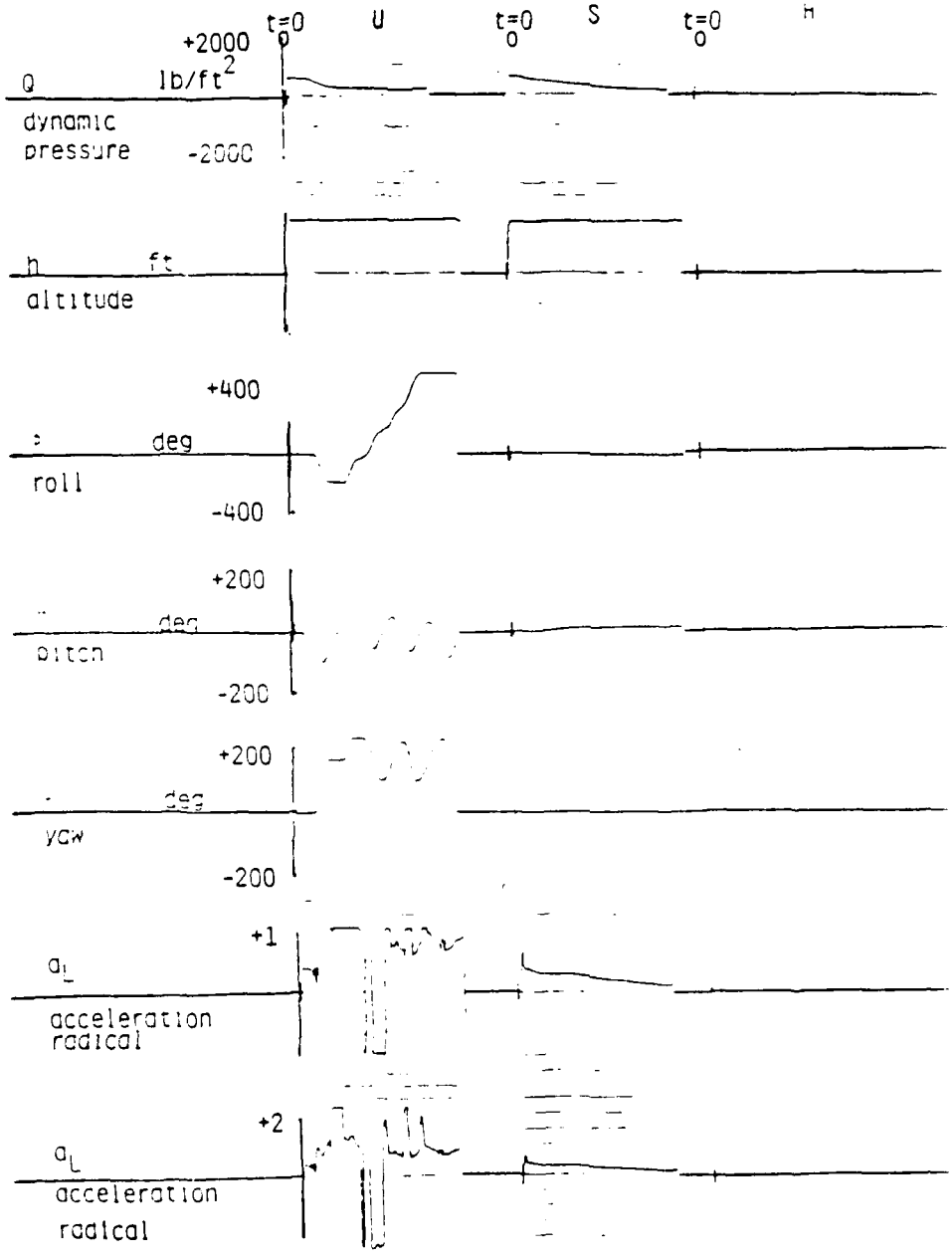

Figure 7.19 VARIABLE INITIAL ATTITUDE CONDITIONS

U=UNCONTROLLED, S=SIMULATION (PE 8/32). H=HARDWARE (MC 68000)

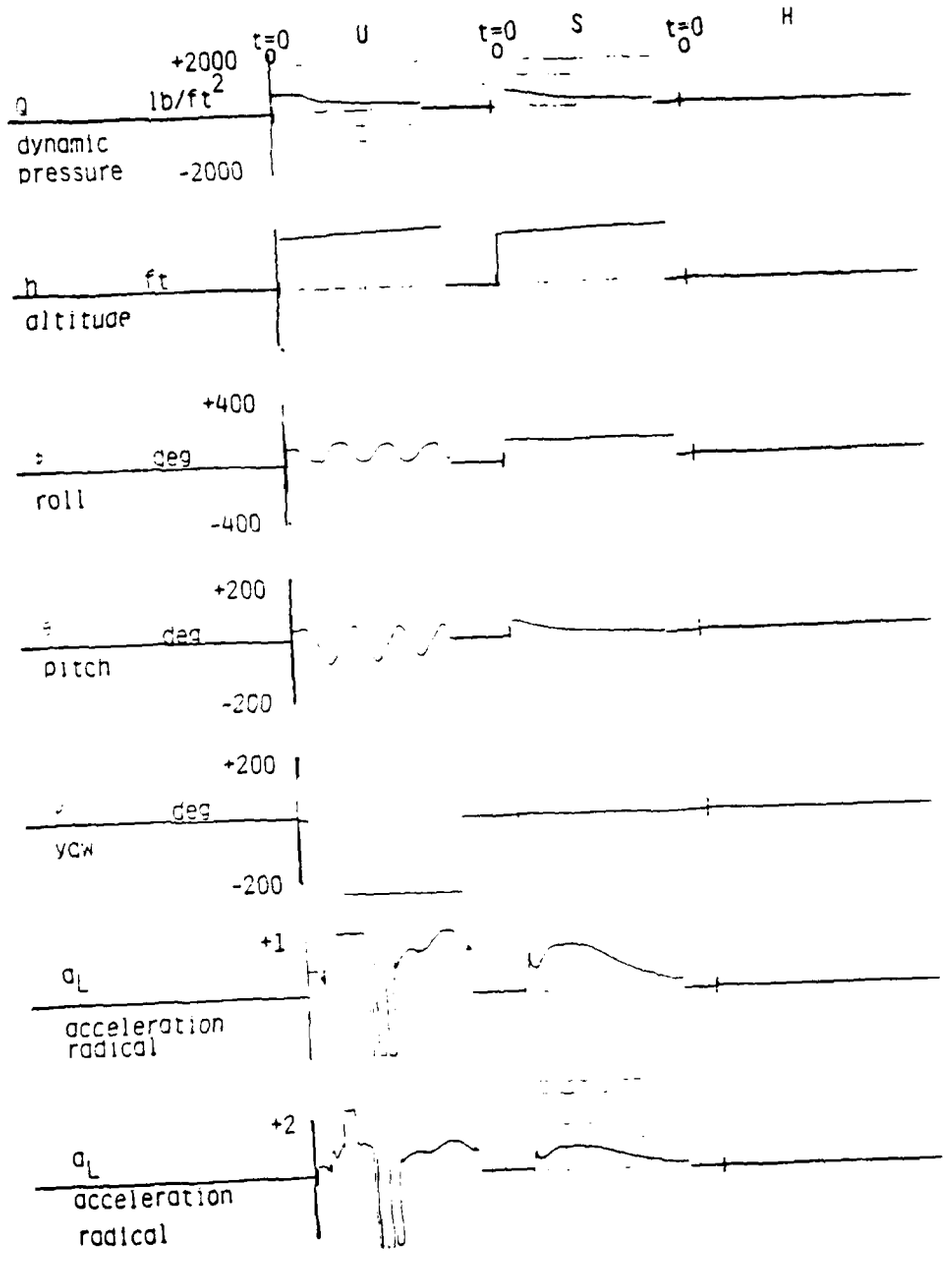

Figure 7.20 VARIABLE INITIAL ATTITUDE CONDITIONS

U=UNCONTROLLED, S=SIMULATION (PE 8/32). H=HARDWARE (MC 68000)

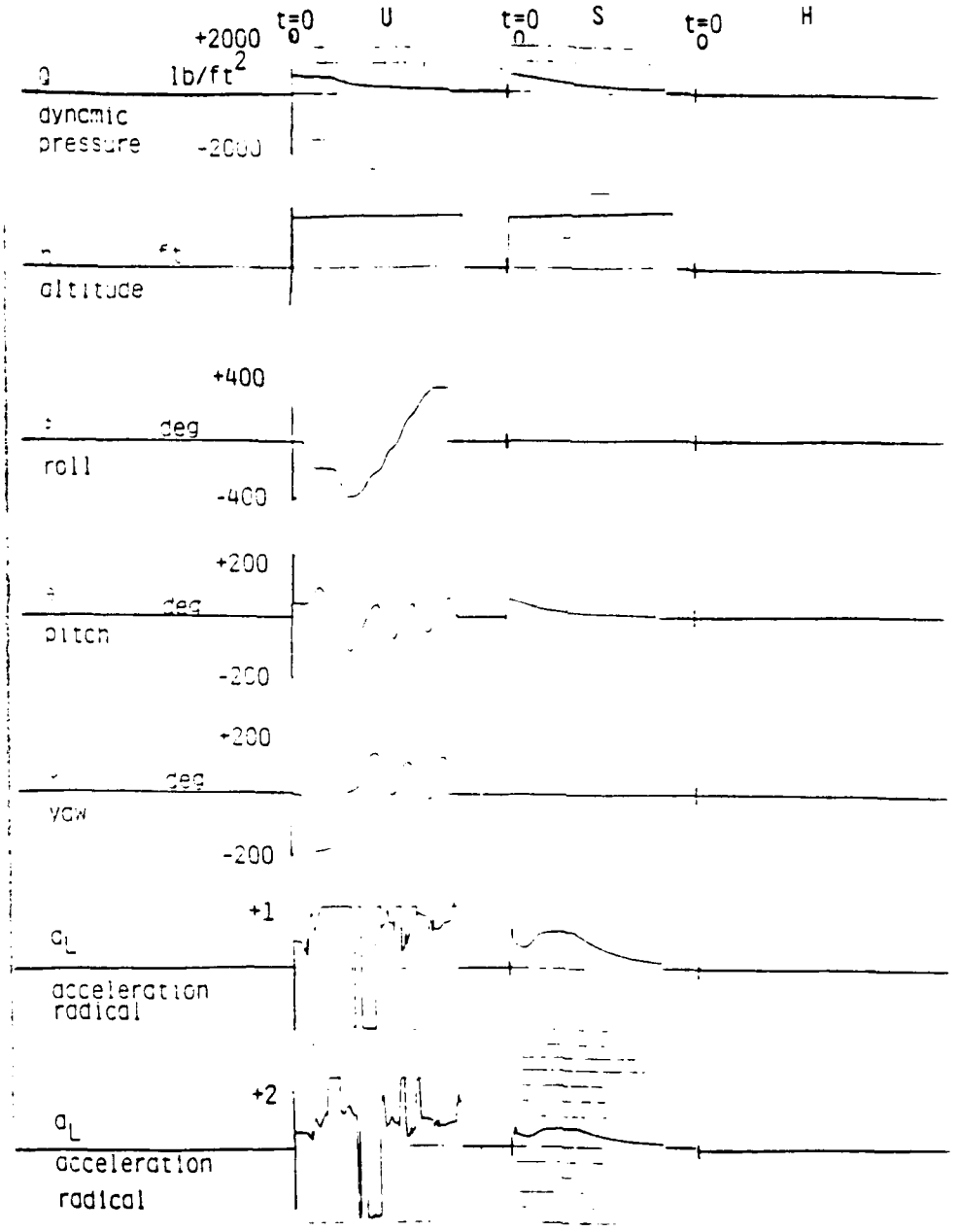

Figure 7.21 VARIABLE INITIAL ATTITUDE CONDITIONS

U=UNCONTROLLED, S=SIMULATION (PE 8/32). H=HARDWARE (MC 68000)

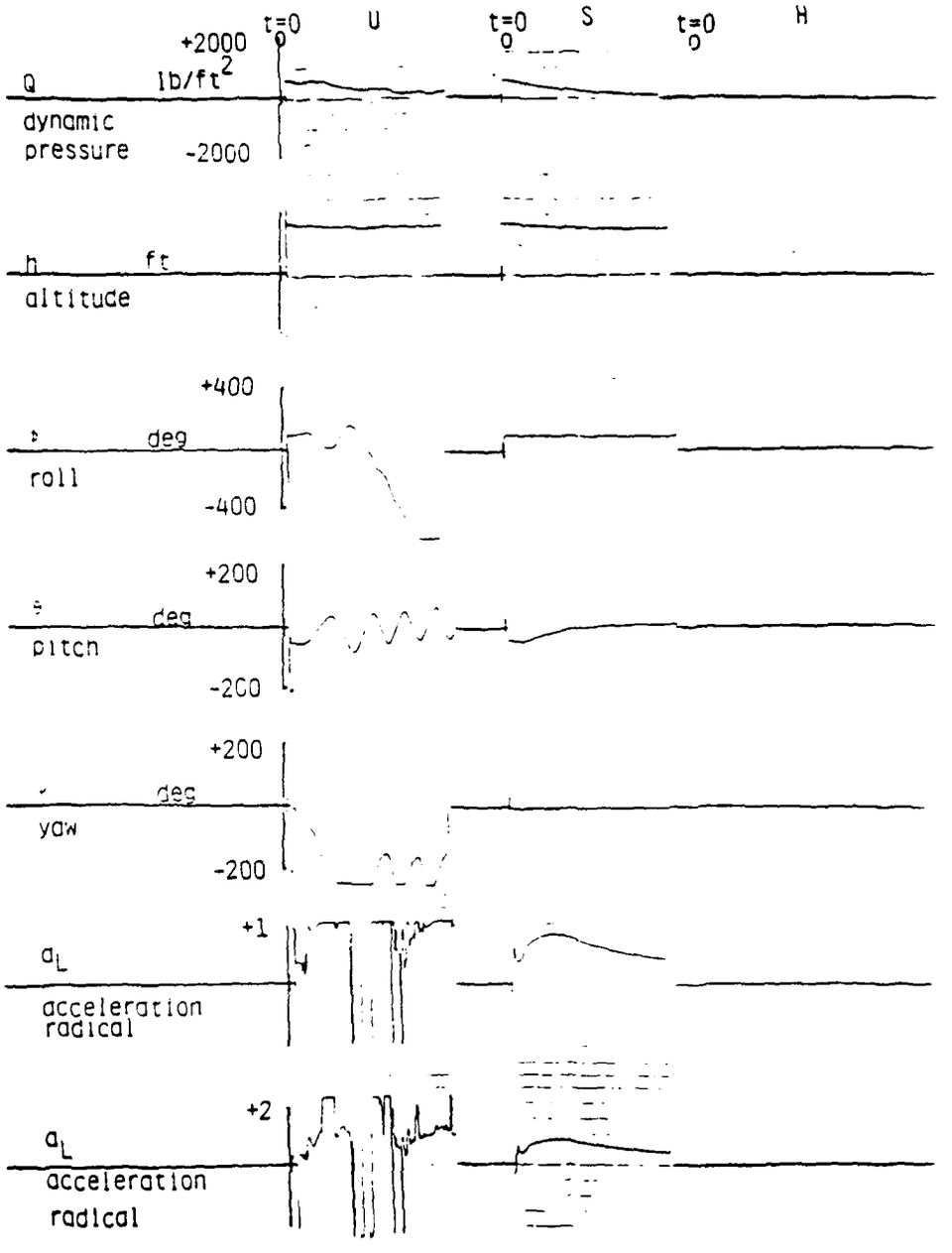

Figure 7.22 VARIABLE INITIAL ATTITUDE CONDITIONS

U=UNCONTROLLED, S=SIMULATION (PE 8/32). H=HARDWARE (MC 68000)

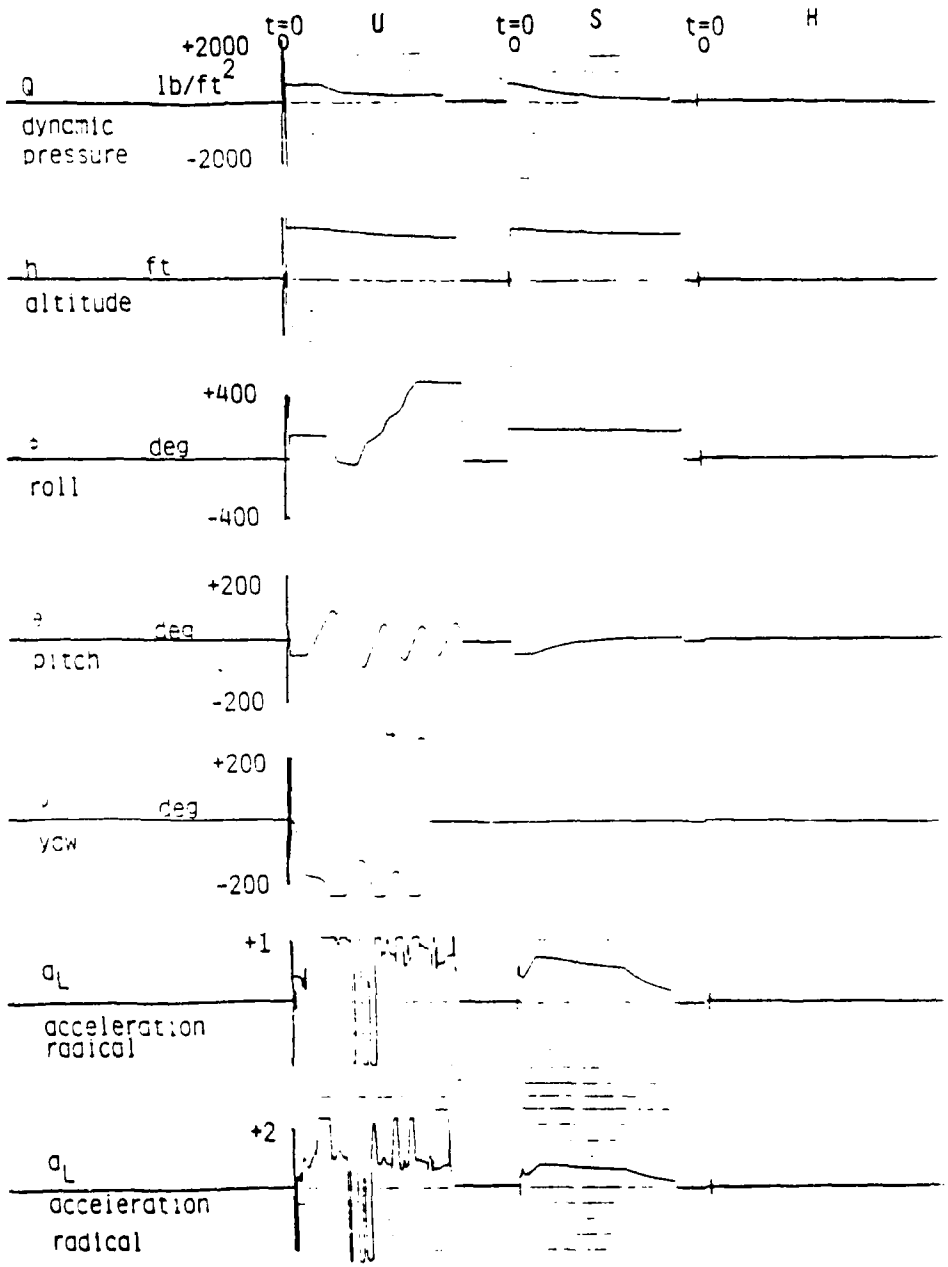

Figure 7.23 VARIABLE INITIAL ATTITUDE CONDITIONS

The final series of test cases under examination are cases 16-20 which are high altitude and high dynamic pressure ejection conditions. The 600 KEAS ed specification translates into high ground speed upwards of 2200 fps. Hence, rotation of the velocity vector in this area of the flight envelope requires very high energy requirements as evidenced by the growth in the acceleration radical for cases 19 - 20. Case results results in an excessive radical with a maximum value of approximately 1.2. The case 20 results are marginal at best. The maximum value of the acceleration radical may be contained in these cases by a more judicious choice of the terminal attitude conditions imposed on the problem. A very careful assessment of the terminal angle of attack condition for successful ejection is warranted to insure that the control energy requirements for safe ejection are minimized. The extensive testing has demonstrated the need to offer quick rotational stabilization of the seat frame while minimizing the attitude steering to insure that the control energy does not itself become the major source of pilot injury.

7.5 Basic Conclusions on the Scenarios Investigated.

Examination of the results of the last few sections indicates without doubt the specific benefits in the use of advanced control for ejection seats in improving the probability of survival over the use of simplified booster schemes. The method of control summarized in paragraph 6.3.1 yielded superior attitude control even in the instances of simultaneous large angle corrective steering of both pitch and roll (see MIL Case 7 above). The high altitude response of Cases 16-20 emphasized the need to select the terminal attitude condition carefully in order to minimize the control energy required in attitude steering. The low altitude performance in the presence of high dynamic pressure (Cases 2-3) were wholly acceptable in meeting the control objective. From a control standpoint the MIL Cases 1-7 are the most challenging, combining the effects of adverse attitude with imminence of ground collision. The ability of the control scheme

U=UNCONTROLLED, S=SIMULATION (PE 8/32), H=HARDWARE (MC 68000)

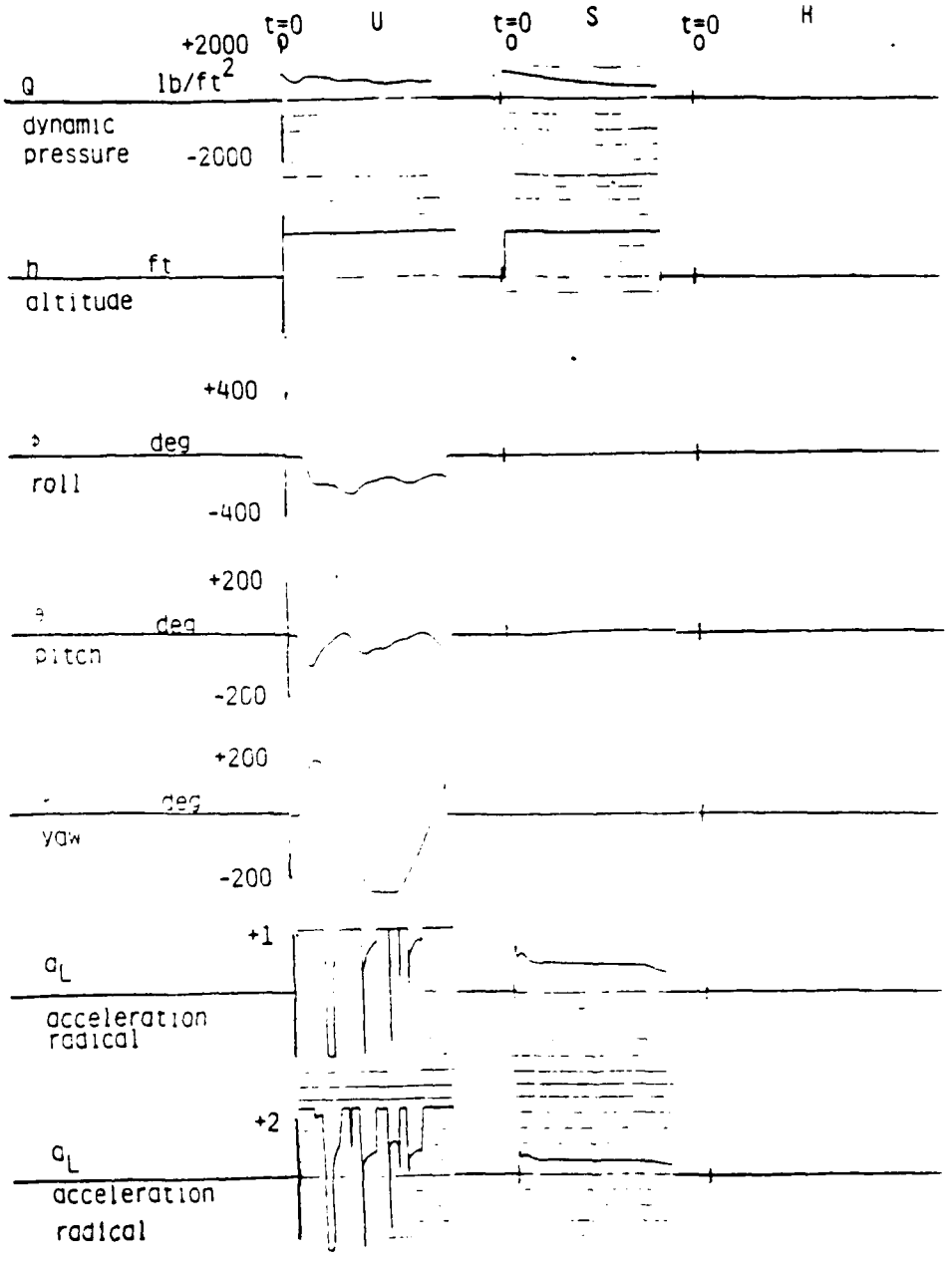

Figure 7.24 VARIABLE INITIAL ATTITUDE CONDITIONS

U=UNCONTROLLED, S=SIMULATION (PE 8/32), H=HARDWARE (MC 68000)

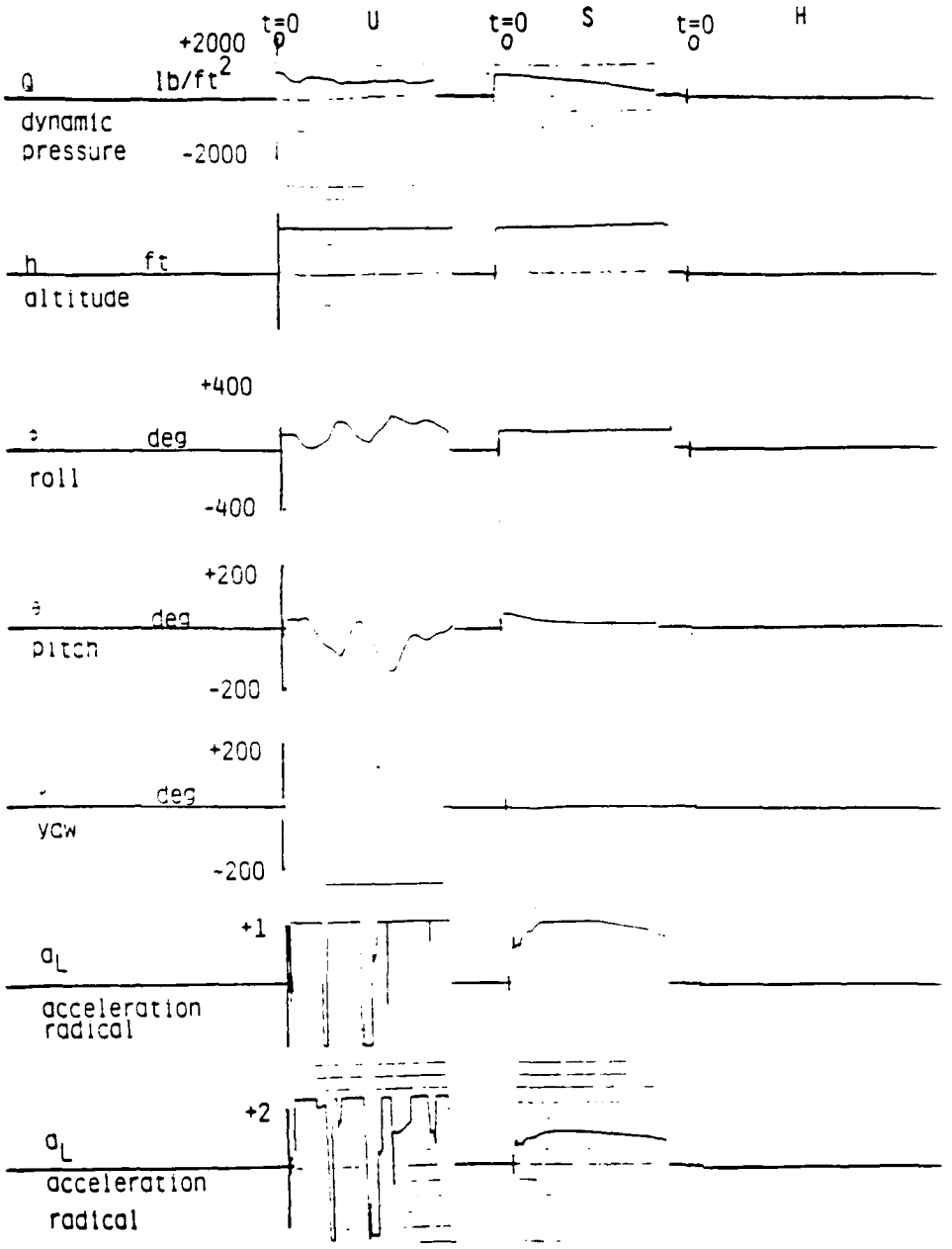

Figure 7.25 VARIABLE INITIAL ATTITUDE CONDITIONS

U=UNCONTROLLED, S=SIMULATION (PE 8/32), H=HARDWARE (MC 68000)

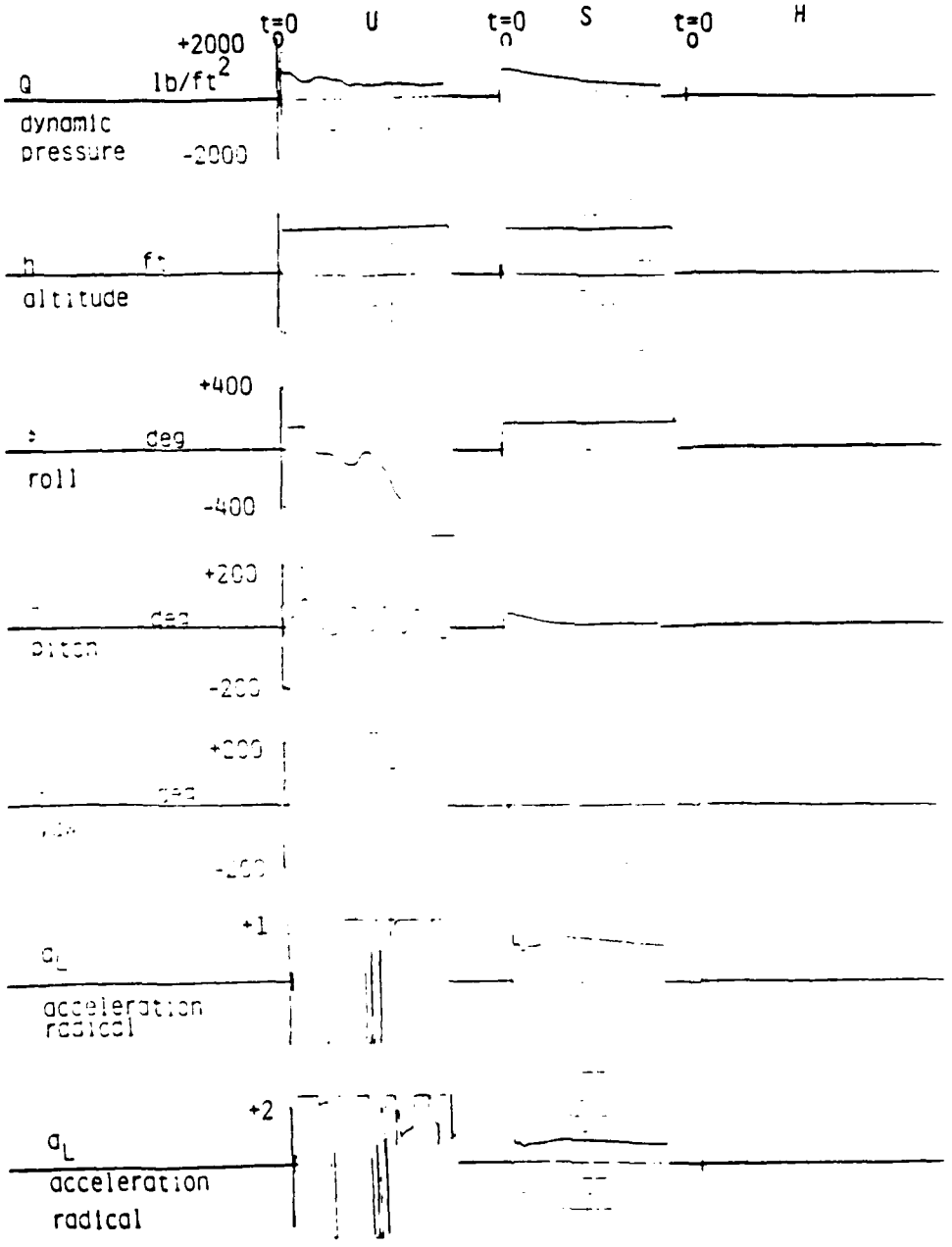

Figure 7.26 VARIABLE INITIAL ATTITUDE CONDITIONS

U=UNCONTROLLED, S=SIMULATION (PE 8/32), H=HARDWARE (MC 68000)

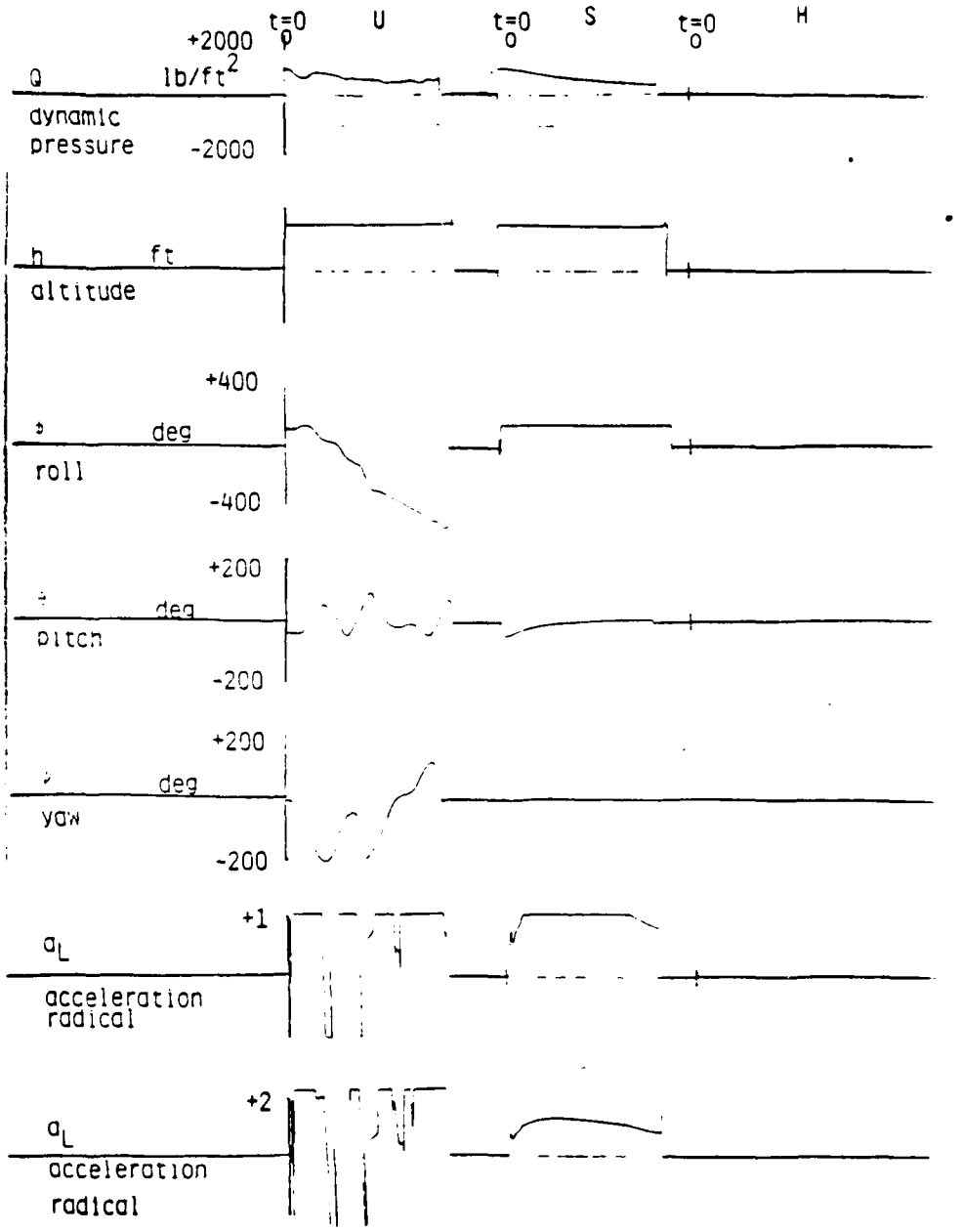

Figure 7.27 VARIABLE INITIAL ATTITUDE CONDITIONS

U=UNCONTROLLED, S=SIMULATION (PE 8/32), H=HARDWARE (MC 68000)

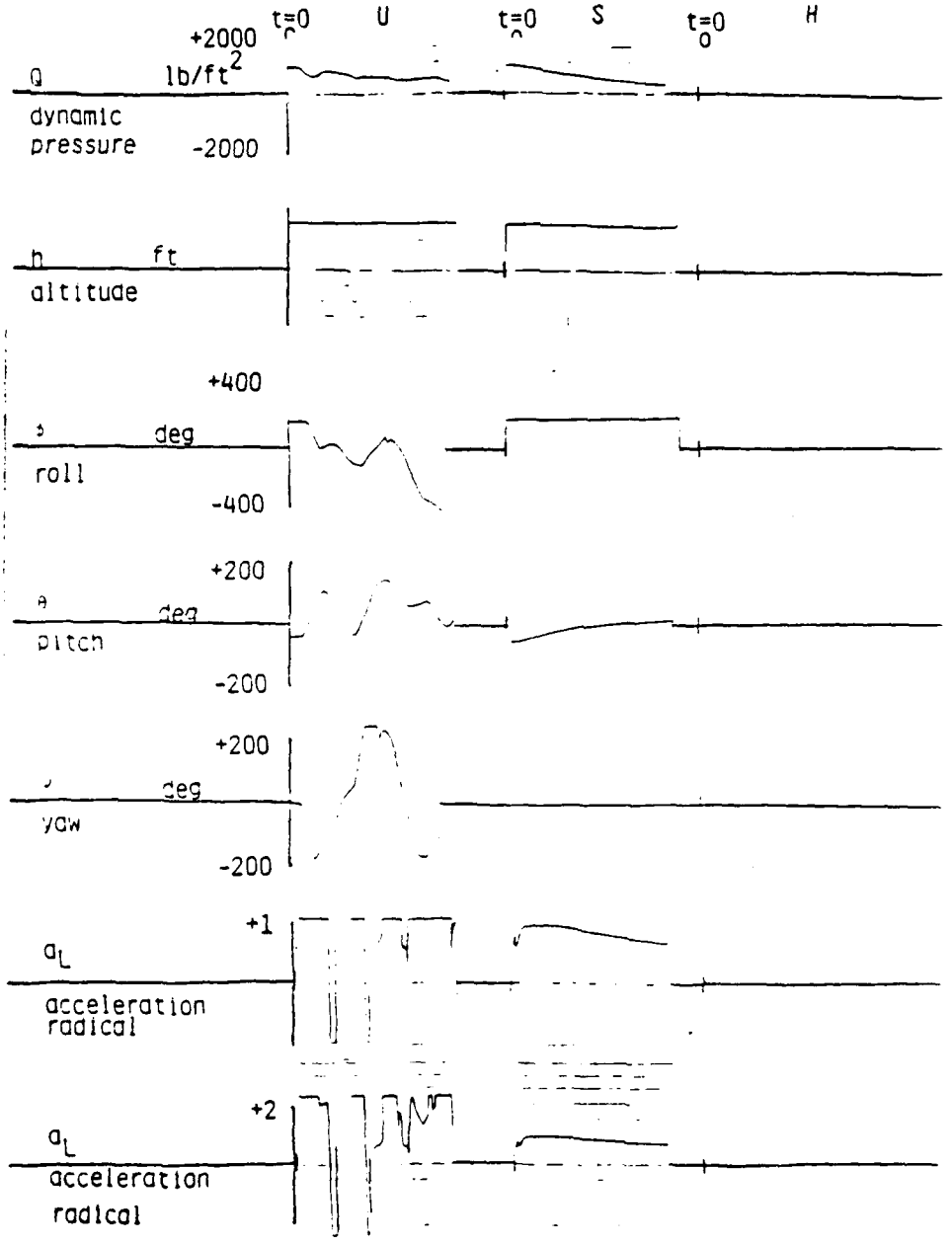

Figure 7.28 VARIABLE INITIAL ATTITUDE CONDITIONS

in dealing with those cases is significant evidence of the viability of the method in handling "difficult" ejection conditions.

7.6 Microprocessor Memory and Throughput.

In the initial program development plan, the PASCAL language was proposed in order to support the higher order language (HOL) requirement in DOD program development. An HOL environment offers the advantage of module clarity, ease of implementation and maintainance while sacrificing speed of execution. The HOL strategy leads to much lower execution rates than acceptable so that assembly code development of the control algorithm is required.

Extensive evaluation of the execution rate requirements for the proposed control system has indicated that the control algorithm need execute at a minimum of a 40-50 Hz rate. Execution rates higher than 100 Hz do little to alter system performance. The results of the previous section were all generated at the 50 Hz rate demonstrating feasibility of operation at that rate. In general it is advisable to dedicate no more than 1/2 of the available microprocessor throughput to control algorithm execution leading to the requirement of a 100 Hz algorithm in order for the scheme to be realizable in current hardware.

Table 7.3 illustrates the memory and throughput actually measured using the TEKTRONIX Microprocessor Development Lab (MDL) utilizing the Motorola 68000 emulator operating with an 8 MHz clock speed.

TABLE 7.3

Control Algorithm Throughput and Timing Measurements with Motorola 68000 Microprocessor. (8 Mhz System Clock).

	Pascal Code	Assembly Code
Memory	22 KBytes	20 KBytes
Timing	0.28 s/cycle (3.5 Hz)	0.007 s/cycles (130 Hz) (1)
		0.01 s/cycles (100 Hz) (2)

(1) No I/O Included

(2) I/O Included (ADCs & DACs)

These timing results are based on all integer arithmetic, that is, without the aid of the faster Motorola 68020 and co-processor. The original PASCAL code results indicate a nominal 3.5 Hz execution rate leading to the conclusion that HOL implementations are most likely infeasible on most available state of the art hardware components.

An assembly code version of the control software was developed to evaluate the feasibility of control algorithm use in real time applications. The measurements indicated in Table 7.3 demonstrate the capability of the algorithm to execute at 100 Hz when implemented in assembly language. The current algorithm is then feasible given 50 Hz execution rates and a 0.5 utilization factor. The 8 MHz clock speed is intermediary in the family of available Motorola 68000 system clocks. Currently the Motorola 68000 may be utilized in conjunction with any of the following clock speeds: 4, 8, 16, 32 MHz. Clearly the 16 MHz clock would not push the system clock specification to the limit and would make feasible 200 Hz algorithm execution speed leading to a 0.25 utilization factor of the processor. The 16 MHz clock speed also could allow for alternate tasks to be executed to support other functions such as pyrotechnic sequencing and drogue chute deployment.

AD-A166 596 VECTORED THRUST DIGITAL FLIGHT CONTROL FOR CREW ESCAPE 2/3
VOLUME 2(U) SCIENTIFIC SYSTEMS INC CAMBRIDGE MA
J V CARROLL ET AL. DEC 85 AFWAL-TR-85-3116-VOL-2
UNCLASSIFIED F33615-82-C-3402 F/G 1/4 NL

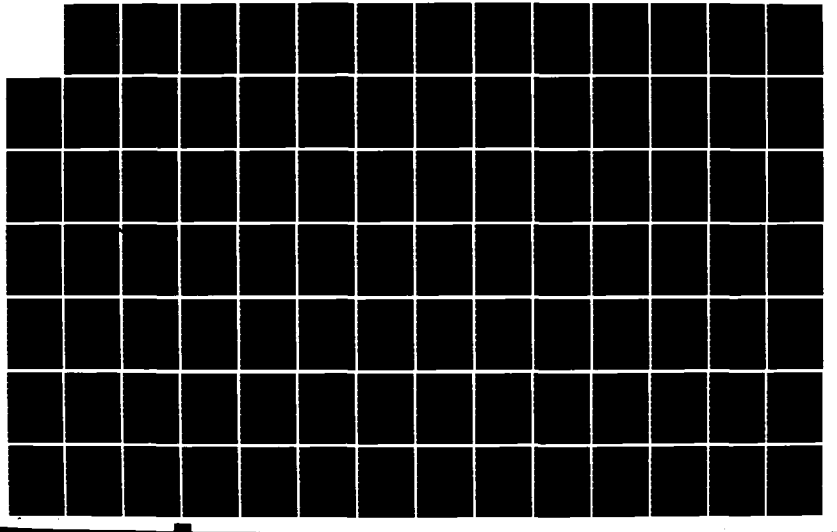

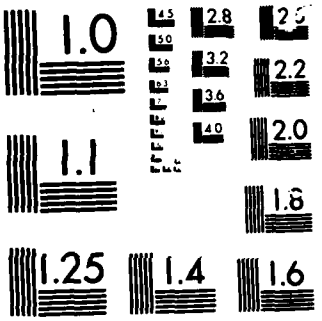

MICROCOPY CHART

Memory requirements, as indicated in Table 7.3, are currently in the 22 KByte range. These memory requirements should be considered minimal since off the shelf 64 and 256 KByte RAM chips are readily available at low cost. Note that the 22 KByte memory requirement includes the total local and global data storage requirements as well as the controller binary code.

In summary the timing and memory measurements with actual Motorola 68000 hardware demonstrates that the requirements of the control approach is currently feasible at relatively low expense for the computer hardware. The low accuracy sensor figures of Table 6.3 of the previous chapter similarly illustrate the feasibility of use of low cost inertial components in supporting the hardware requirements.

7.7 Dynamic Occupant C.g. Results

In compliance with para. 4.5.3 of the SOW, SSI has incorporated the effects of pilot motion during ejection in the all digital VAX FORTRAN simulation in order to reflect c.g. dynamics of the combined seat/occupant system. Previous work aimed at demonstrating the feasibility of attaining a desired acceleration tolerance radical, attitude and altitude given the assumption of a fixed c.g. and moment of inertia for the combined seat/occupant system. In reality elastic properties inherent in the restraint system and pilot body frame result in variations in the c.g. location and consequently in a time varying moment of inertia. This sub-task is intended to evaluate robustness of the control algorithm in maintaining stability of the plant and containment of the acceleration radical given the disturbances mentioned above.

Two modifications were necessary to upgrade the existing simulation in order to account for the dynamic occupant c.g. The first involved the implementation of the seated human slump model forwarded by R.J. Dobbek to SSI. That model represented the occupant response to forces acting on the ejection seat by a second order response model in each of the three orthogonal directions of forward, right and down. According to Dobbek, the original model was obtained from the SAFEST computer program documented in AFWAL TR-82-3013 and modified to account for non-linear characteristics in the restraint system such as the "dead-zone", "hysterises" and non symmetrical response to plus, minus x and z axis loading. Also included in the Dobbek communication were representative values for the parameters in the second order response model as well as the associated non linearities. The variations in the c.g. dynamic states (positions (δx_{cg}, δy_{cg}, δz_{cg}), velocities ($\dot{\delta x}_{cg}$, $\dot{\delta y}_{cg}$, $\dot{\delta z}_{cg}$)) driven by the second order response model for acceleration ($\ddot{\delta x}_{cg}$, $\ddot{\delta y}_{cg}$, $\ddot{\delta z}_{cg}$) were appended to the existing 6DOF flight model state vector consistent with the Dobbek model and integrated at the fundamental integration time step rate (approximately 0.001 s) to form the representation of pilot c.g. motion.

The second modification required is a consequence of the first, i.e., the mass shift of the pilot c.g. results in a time varying moment of inertia. Recall that the center of gravity of n masses at time t is expressed by:

$$\bar{r}_i(t) = \sum_{i=1}^{n} \frac{m_i r_i(t)}{\Sigma m_i} \qquad (7.1)$$

where

m_i = mass of body i

$r_i(t)$ = position vector for center of mass i at time t in some reference frame

$\bar{r}_i(t)$ = center of gravity of the composite of the system in the reference direction

The second moment of inertia for n masses about an axis b is given by:

$$I_b(t) = \sum_{i=1}^{n} I_{a_i} + m_i(r_i(t) \times R(t))^2 \qquad (7.2)$$

where

$I_b(t)$ = moment of inertia of the composite of n bodies about axis b

I_{a_i} = moment of inertia for body i with respect to the c.g. of body i about a axis a parallel to b

$r_i(t)$ = position vector of body i in some reference frame

$R(t)$ = unit vector defining the direction of axis b in some reference frame

The 6DOF dynamics equations previously defined in are valid when the moment of inertia I is respect to the system c.g. about axes defined along the orthogonal directions of motion. Hence, R(t) in equation (7.2) need be the unit vector associated with the center of mass as defined by equation (7.1) for $I_b(t)$ to be equivalent to I in the 6 DOF equations. For convenience in this implementation, $r_i(t)$, $\bar{r}_i(t)$ are referenced with respect to the SRP frame. The only time varying term in the expressions (7.1, 7.2) considered here is the pilot c.g. location in SRP units.

Table 7.4 ACES II Ejection Seat Component & Crew Data

Component	Weight lbs	C.G. x	wrt ft y	S.R.P. z	Ixx slug ft^2	Iyy slug ft^2	Izz slug ft^2	Ixy slug ft^2	Ixz slug ft^2	Iyz slug ft^2	PHI rad
Basic Configuration	91.5	-.0276	.0431	-.6005	4.1497	4.44762	2.4593	.1311	1.1391	-.3812	0.0
Rocket Propellant	5.6	-.51	0.0	-1.56	.126	.126	.006	0.0	0.0	0.0	.029
Drogue Gun slug	1.0	-.45	-.33	-1.22	0.00003	.00013	.00013	0.0	0.0	0.0	-.15
Drogue Chute	8.1	-.32	-.33	-.7	.034	.038	.014	0.0	0.0	0.0	0.0
Recovery Chute	20.19	-.2777	.0177	-2.4725	.3052	.2577	.0349	.0546	.1464	.0975	0.0
Maximum Survival Kit	66.7	.6000	0.0	.15	.1402	.034	.1542	.1416	-.0293	-.1337	0.0
Minimum Survival Kit	25.4	.6567	.0025	.3205	.2409	.5774	.4401	.0841	.286	.2079	0.0
95% Pilot *	250.7	.7204	.0197	-.10636	10.3683	10.5159	3.0416	.0974	2.029	.0311	0.0
5% Pilot *	166.38	.7376	.0432	-.8436	5.4572	3.3740	2.0973	-.8118	2.081	-.9791	0.0

*Suited for flight

The data for evaluation of the moment of inertia of the combined seat/occupant system given by equation (7.2) is taken from Air Force supplied data illustrated in Table 7.4. In particular the evaluation here assumes the 95 percentile pilot data from row 8 while the data for the ejection seat is given by the composite of rows 1-7. The initial ejection seat flight conditions are illustrated in Table 7.5 so that the dynamic pressure here is severe implying near worst case conditions.

TABLE 7.5

INITIAL EJECTION FLIGHT CONDITIONS FOR DYNAMIC OCCUPANT C.G. EVALUATION

Roll	0 degree
Pitch	0 degree
Yaw	0 degree
Speed	687 KEAS
Altitude	100 feet

In order to demonstrate the effects of the occupant c.g. dynamics two cases for preliminary evaluation were constructed. The first assumes the pilot c.g. to be fixed while the second incorporates the dynamic effects of the human slump model. To clarify, the distinction between Cases 1 and 2 is that in Case 1 the system c.g. is fixed and the control law has an exact estimate of the system c.g. and moment of inertia while in Case 2 the system c.g. and moment of inertia are time varying in the 6 DOF dynamics equations but the control law only has an estimate of the initial (an approximate time average) c.g. and moment of inertia. The two cases then directly demonstrate the differential effects of the additional dynamics due to pilot motion on the closed loop control system performance.

The Case 1 results are shown in Figure 7.29 which illustrate the evolution of the key system states and acceleration radical. Similarly the results from comparison Case 2 is depicted in Figure 7.30. Inspection of the two cases lead to the preliminary conclusion that the pilot c.g. dynamics results in minor variations in the

control system performance with respect to control of the plant and acceleration radical. Perhaps this result is not too surprising since the maximum excursion of the system c.g. during execution in Case 2 is bounded by 2 inches in the r.m.s sense with a maximum deviation of 1 slug-ft2 in the moment of inertia. Other cases with comparable level of error disturbances of the same order demonstrated a similar result.

LEGEND

RAD	Acceleration Radical	nd
P,Q,R	Inertial Rotation Rate in Body	Deg/Second
Pitch	Inertial Pitch Angle	Degrees
Roll	Inertial Roll Angle	Degrees
Yaw	Inertial Yaw Angle	Turns (1 turn=360 deg)
Xvel	X component of velocity	fps
Yvel	Y component of velocity	fps
Zvel	Z component of velocity	fps

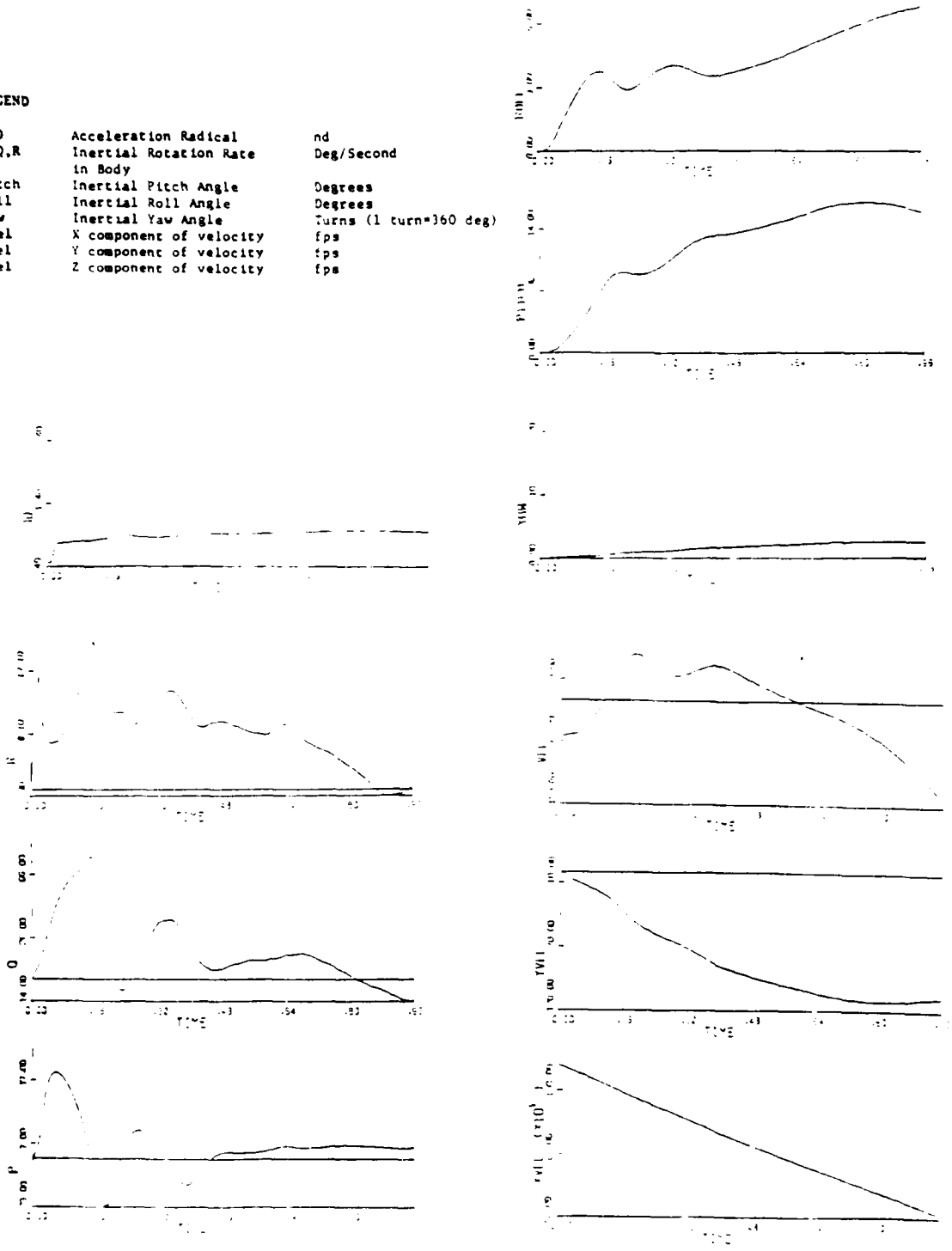

Figure 7.29. Ejection Seat Plant Assuming no Pilot C.G. Dynamics

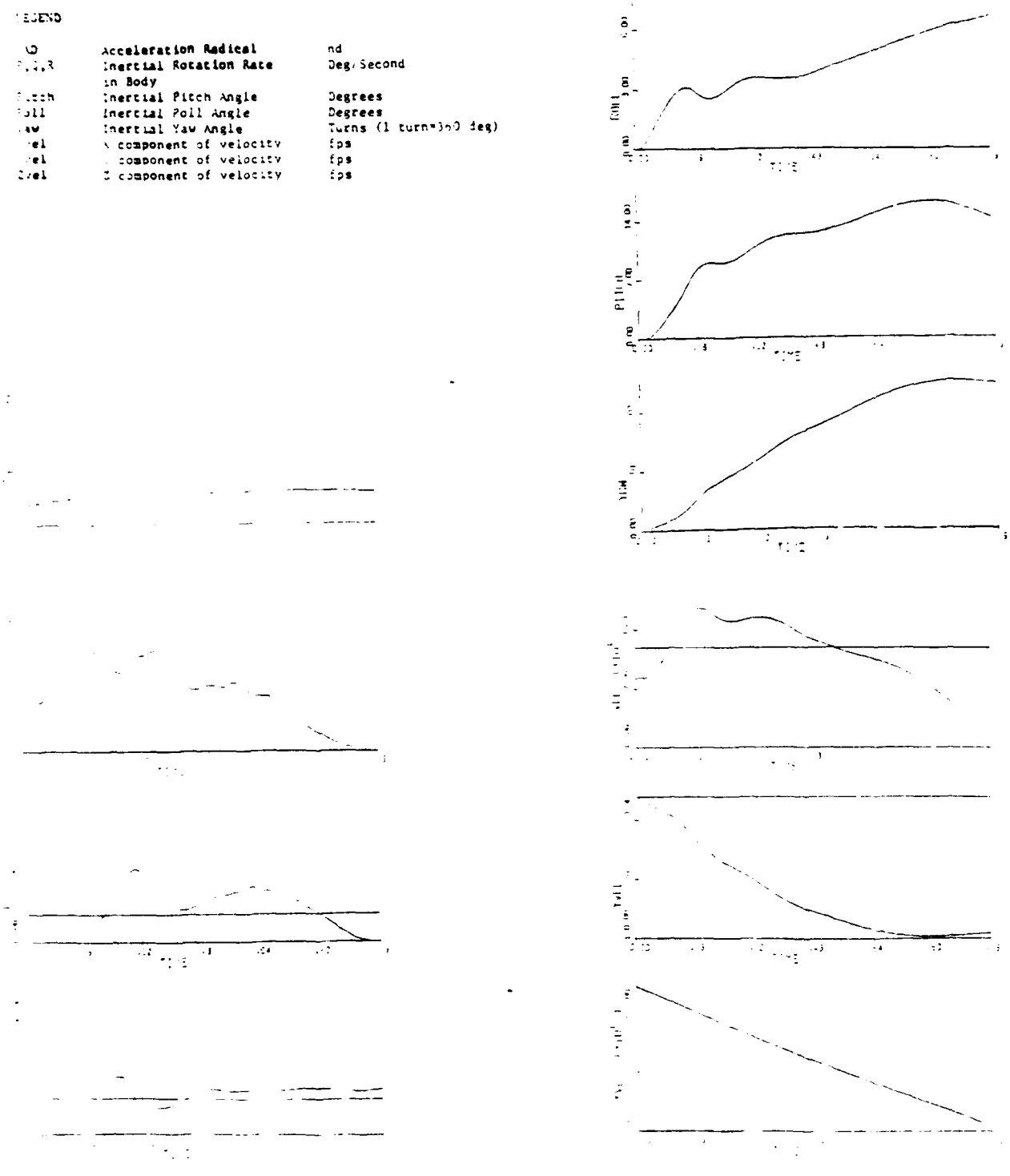

Figure 7.30. Ejection Seat Plant with Pilot C.G. Dynamics

7.8 Nominal Pilot Results.

This section examines the control performance in an all digital simulation environment for the situation when the controller assumes the parameters associated with a 50 percentile pilot while the actual 6 DOF equations are driven by parameters associated with either a 5 or 95 percentile pilot. The controller only has approximate knowledge of the seat/pilot mass and moment of inertia properties which is the case under normal conditions. The results of the previous paragraph focused on the effects of the CG dynamics due to pilot motion and the conclusion was that those dynamics were insufficient to alter the basic control system performance measures. The cases examined here represent large constant disturbances imposed on the control system when compared to pilot motion alone, a situation of potentially far greater consequences with respect to system stability.

All previous results presented so far were based on a limited definition of the acceleration radical. The results presented in this section incorporate the Dynamic Response Index (DRI) as the acceleration radical so that a more realistic evaluation of potential lethality is represented. The DRI definition and associated parameters are based on the requirements established as part of the Crew Escape Systems Technology (CREST) program. In that program the intent is to produce an actual prototype of the next generation ejection seat based on the most recent advancements in applicable technologies.

The results of two cases are presented here. Table 7.4 of the last section defined the parameters associated with the ACES II seat on a component basis. Inspection of the CG shift from a 5 to a 95 percent pilot reveals a substantial shift for the z CG location. The moment of inertia components for the respective pilot specifications indicate a substantial difference in terms of the x and y principal

moments. Any viable control scheme must be tolerant to such variations if the controller parameters are to be pilot independent.

The flight conditions and pilot case definitions are illustrated in Table 7.6. Inspection of the table indicates that the 95 percent crew case also has a large initial negative pitch rate (-72 deg/sec).

Table 7.6 Flight Conditions For Nominal Pilot Case.

Pilot Percentile	Flight Condition		Terminal Pitch
5%	Speed:	700 KEAS	
	Altitude:	0 feet	
	Pitch:	25 deg	25 deg
	Pitch Rate:	0 deg/s	
95%	Speed:	700 KEAS	
	Altitude:	0 feet	
	Pitch:	12.5 deg	25 deg
	Pitch Rate:	-72 deg/s	

5 Percent Pilot Results Discussion.

The results of the 5 % pilot test case are illustrated in Figure 7.31. It is apparent from the Figure that the usual ground collision potential associated with low altitude ejection is avoided. Due to the DRI, the radical reported in Figure 7.31 has higher dynamics than the results of Section 7.2. The radical is however always contained below the critical threat level.

95 Percent Pilot Results Discussion.

The results of the 95 % pilot test case illustrated in Figure 7.4. In spite of the large initial pitch rate the altitude results show conclusively that ground collision is avoided. The radical is bounded within the lethal limit with a temporary excursion toward the high probability of injury limit. The pitch angle is well controlled to the terminal specified value of 25 deg.

The results above represent a severe emergency case and in both instances the control approach contains the acceleration radical to acceptable bounds. Of some significance is the controller robustness to the fairly large input disturbances demonstrating the feasibility of the approach in tolerating realistic operational deviations from the nominal system parameters.

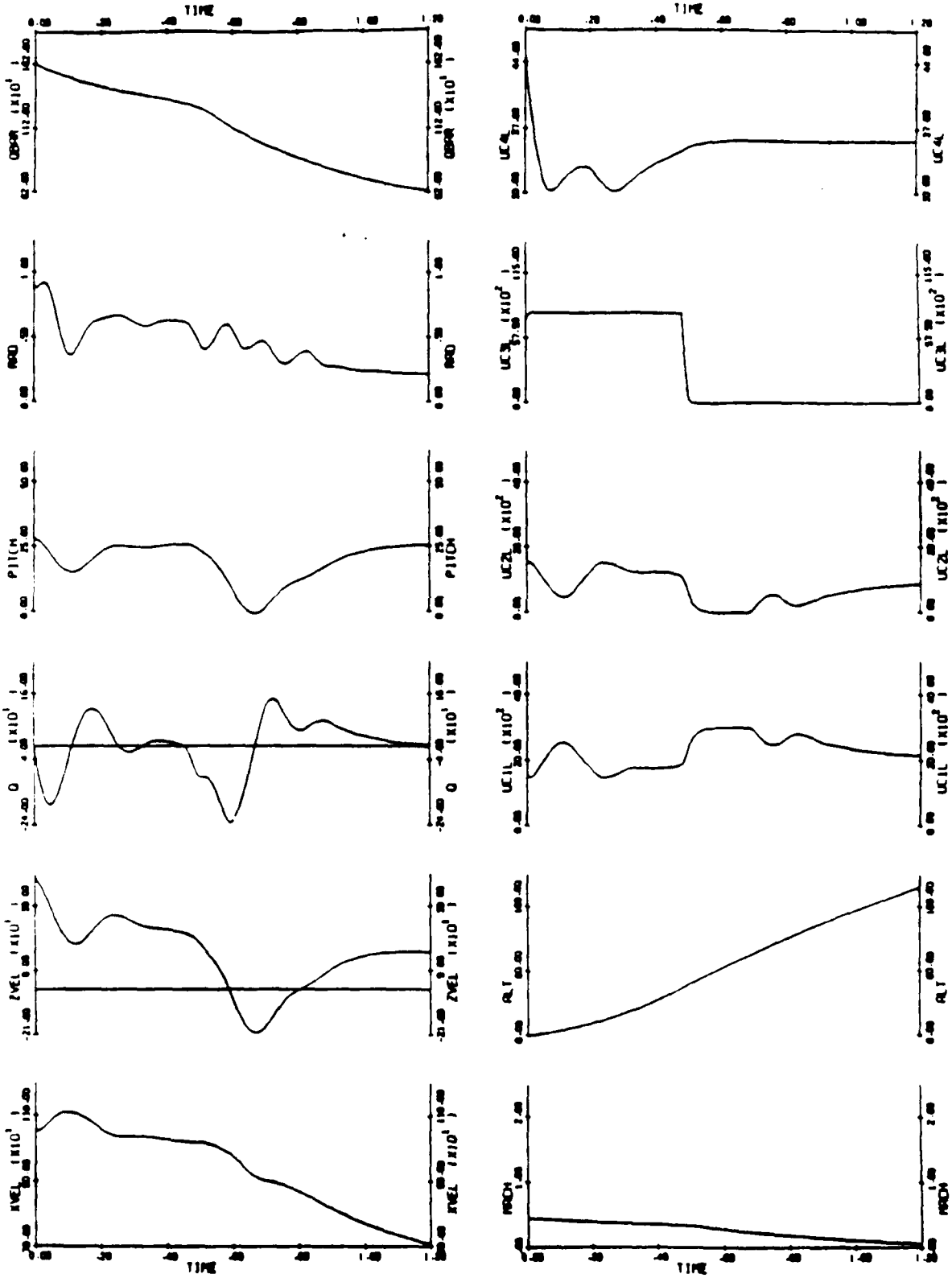

Figure 7.31. 5% PILOT RESULTS FOR NOMINAL PILOT DESIGN

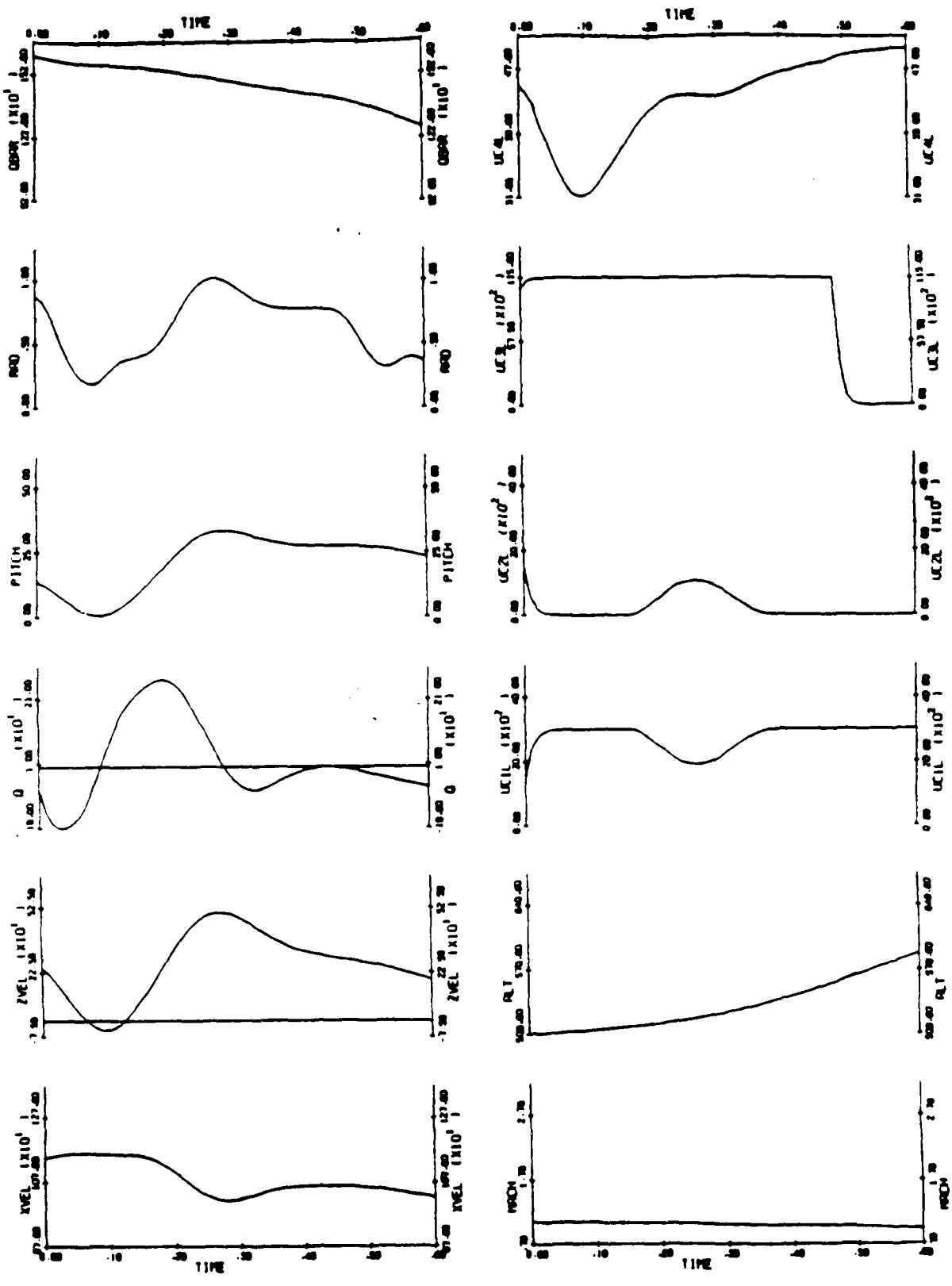

Figure 7.32. 95% PILOT RESULTS FOR NOMINAL PILOT DESIGN

7.9 Robustness; Sensitivity Analysis.

An important aspect of any control system is its robustness. That is, structural parameter changes, sensor failures and control component defects should not impede the controller from performing its essential tasks. In practice it is desired that the control system remain robust against a given set of failures and parameter changes. Such a robustness performance is usually included in the design characteristic of the control scheme.

For Vectored Thrust Digital Control, the importance of its robust behavior stems from two different, although related, requirements. First, the Vectored Thrust Control system is assumed to operate under highly uncertain and stressful conditions which are prevalent at the time that the flight crew decides to eject from the aircraft. In such conditions parameters change, sensor and component failures are commonly expected, and therefore they should be accounted for in the design phase. Second, one operational mode of the controller that has been described in previous sections relies on precomputed and stored trajectories (reference trajectories). These trajectories and the corresponding control sequences are computed off line and stored. Assuming that the structure of the seat and of the control components

remain unchanged, for each set of initial conditions (u, v, w, p, q, r, x, y, z, θ , ϕ , ψ) one trajectory and its associated control sequences have to be stored. It is clear that, unless some data reduction and simplification is done, the storage and retrieval problem would be impractical due to the large memory requirement. The data reduction and simplification has to rely on the robustness of the control system with respect to the initial conditions. That is, instead of computing and storing all the reference trajectories, a limited number of them, corresponding to typical or critical initial points, will be computed and stored, together with the corresponding control sequences. Then for any initial point, a reference trajectory and a reference control sequence will be approximated (interpolated from precomputed trajectories corresponding to the neighboring points). If the control scheme is sufficiently robust, and if a sufficient number of trajectories have been stored, it is expected that this approximation, coupled with an on-line regulation, should result in a reasonably good control strategy. In the following we will elaborate on various aspects of this issue.

7.9.1 Derivation of Sensitivity Relationships.

In this section we derive some analytical results relating the behavior of the trajectory to the change in initial conditions and to the change of the control vector.

Let us define the following notation:

$x(t)$: trajectory vector (12 dimensions)

$x(t) = (u,v,w,p,q,r,x,y,z, \theta, \phi, \psi)$

$f(.) : R^{12} \rightarrow R^{12}$

$g(x) : R^{12} \rightarrow R^{m}$

U : m dimensional control vector

x_0 : initial condition

$\dot{x} = f(x) + g(x)\, U$: nonlinear dynamic equation

Then

$$x(t) = x_0 + \int_0^t f(x)dt + \int_0^t g(x)\, U(t)dt$$

Robustness with respect to the initial vector x_0: This sensitivity matrix, the component of which are $\frac{\partial x_i(t)}{\partial x_{jo}}$ is easily computable from the trajectory equation.

Suppose that a trajectory x(t), depending on the control vector U(t) and the initial condition x_0 is computed. Assuming that the control vector remains the same, the change of x(t) relative to x_0 is easy to compute. In fact:

$$\frac{\partial x(t)}{\partial x_0} = I + \int_0^t \frac{\partial f}{\partial x}(x)dt + \int_0^t \frac{\partial g}{\partial x}(x)U(t)dt \overset{\Delta}{=} S_1 \qquad (7.3)$$

where $\frac{\partial f}{\partial x}(x)$ and $\frac{\partial g}{\partial x}(x)$ denote matices of derivative of the elements of f(x) and g(x) with respect to x. Both are available through the linearization of the dynamic equation, or can be evaluated on line.

For example, the above formula can be used to determine the sensitivity of the final altitude Z(T) with respect to different elements of the initial conditions x_0. This altitude is independent from the control and its time derivative is:

$$\dot{z} = -\sin\theta\, u + \cos\theta \sin\phi . v + \cos\theta \cos\phi . w$$

Then it follows

$$\frac{\partial Z(T)}{\partial p_0} = \frac{\partial Z(T)}{\partial q_0} = \frac{\partial Z(T)}{\partial r_0} = \frac{\partial Z(T)}{\partial x_0} = \frac{\partial Z(T)}{\partial y_0} = 0$$

And:

$$\frac{\partial Z(T)}{\partial Z_0} = 1$$

$$\frac{\partial Z(T)}{\partial \theta_0} = \int_0^T [-\cos\theta.u - \sin\theta \sin\phi.v - \cos\theta \cos\phi.w]dt$$

$$\frac{\partial Z(T)}{\partial \phi_0} = \int_0^T [\cos\theta \cos\phi\ v - \cos\theta \sin\phi.w]dt$$

$$\frac{\partial Z(T)}{\partial u_0} = \int_0^T - \sin\theta.dt$$

$$\frac{\partial Z(T)}{\partial v_0} = \int_0^T \cos\theta \sin\phi\ dt.$$

$$\frac{\partial Z(T)}{\partial w_0} = \int_0^T \cos\theta \cos\phi\ dt.$$

Note that the sensitivities of Z(T) with respect to the initial velocities depend on the angles θ, ϕ and ψ rather than on the magnitudes u_0, v_0, w_0.

In general, a function of the states x has a sensitivity with x_0 which is itself a function of the elements of Si. For example, RAD is a function of x via the relationship

$$RAD^2 = K_u \cdot lfac(1)^2 + K_v \cdot lfac(2)^2 + K_w \cdot lfac(3)^2. \qquad (7.4)$$

In (7.4), $lfac_i$ is an element of the 3-D load factor vector, lfac. This quantity is defined in the SAFEST code by the vector equation

$$lfac = \omega x(\omega x\ r_{CG}) - (\dot{u},\dot{v},\dot{w}) - \omega xv + \dot{\omega} \times r_{CG} \tag{7.5}$$

where the notation in (7.5) is standard. The K_i in (7.4) are constants which define nominal load factor limits for pilot survival (we have used a conservative value for K_W in place of the DRI); $\dot{u}$, $\dot{v}$, and $\dot{w}$, in (7.5) are elements of f(x,u), and r_{CG} is a constant vector in this analysis. Equations (7.4) and (7.5) are then used in the RAD sensitivity matrix

$$S3 = \frac{1}{RAD}\,[K_u \cdot lfac(1) \cdot \partial lfac(1)/\partial x + K_v \cdot lfac(2) \cdot \tag{7.6}$$

$$\partial lfac(2)/\partial x + K_W \cdot lfac(3) \cdot \partial lfac(3)/\partial x]$$

In deriving $(\partial lfac/\partial x)$, a 3-by-12 matrix, it is best to expand each of the four terms in (7.5), and then take explicit partials. One term is readily available: $-\partial(\dot{u},\ \dot{v},\ \dot{w})/\partial x$ is the negative of the first three rows of the system matrix A. The other terms are:

$$-\frac{\partial(\omega xv)}{\partial x} = \left[\begin{array}{cccccc|c} o & r & -q & o & -w & v & \\ -r & o & p & w & o & -u & 0_{3x6} \\ q & -p & o & -v & u & o & \end{array}\right]$$

$$\frac{\partial}{\partial x}(\dot{\omega} \times r_{CG}) = \left[\begin{array}{c} r_3 \frac{\partial \dot{q}}{\partial x} - r_2 \frac{\partial \dot{r}}{\partial x} \\ r_1 \frac{\partial \dot{r}}{\partial x} - r_3 \frac{\partial \dot{p}}{\partial x} \\ r_2 \frac{\partial \dot{p}}{\partial x} - r_1 \frac{\partial \dot{q}}{\partial x} \end{array}\right]$$

where $\partial\dot{q}/\partial x$ is the fourth row of the system matrix A, etc; and,

$$\frac{\partial}{\partial x}(\omega \times \omega \times r_{CG}) =$$

$$\left[\begin{array}{c|ccc|c} & (qy_{CG} + rz_{CG}) & (py_{CG} - 2qx_{CG}) & (pz_{CG} - 2rx_{CG}) & \\ 0_{3x3} & (qx_{CG} - 2py_{CG}) & (px_{CG} + rz_{CG}) & (qz_{CG} - 2r\ y_{CG}) & 0_{3x6} \\ & (rx_{CG} - 2pz_{CG}) & (ry_{CG} - 2qz_{CG}) & (qy_{CG} + px_{CG}) & \end{array}\right]$$

where (x_{CG}, y_{CG}, z_{CG}) are components of r_{CG}.

It is important to analyze the robustness of the control system with respect to the control input U(t). In practice it is desirable to use the same pre-stored control input U(t) for a class of system conditions, so that the storage and retrieval is reduced. On the other hand, because of possible defects and failures, the pre-stored control vector might not be exactly realizeable. If the system is sufficiently robust a crude realization of the control input U(t) should result in an acceptable (although degraded) performance.

Formally, the sensitivites of the trajectory x(t) with respect to the control vector U can be calculated from the nonlinear first order matrix differential equation:

$$\dot{x}_U = \frac{\partial f}{\partial f} x_U + \frac{\partial g}{\partial x} x_U U + g(x)$$

Or equivalently from the matrix integral equation:

$$x_U = \int_0^t \frac{\partial f}{\partial x} x_U \, dt + \int_0^t \frac{\partial g}{\partial x} n_U \, U \, dt + \int_0^t g(x)dc \triangleq S2$$

where

$$S2 = x_U = \frac{\partial x}{\partial U} : \text{n x m sensitivity matrix}$$

The above equations can be solved numerically. In most cases an approximate value of the sensitivity factors is sufficient, and can be easily obtained either by numerical methods or by simulation.

Our experience with the control solutions has shown that the control law is very robust with respect to both initial conditions and control input. We now discuss a typical example.

Let us consider a typical example of a seat trajectory during the course of the ejection. For a three degree of freedom model, the optimal solution in the sense of maximizing the altitude of the seat at the end of the first phase of the ejection is shown on the plots of Figure 7.33 (a,b,c) to Figure 7.36. The state vector and the corresponding plot symbols are defined as follows:

	Plot Symbol
u: velocity along the x axis	XVEL
w: velocity along the z axis	ZVEL
θ : pitch angle	PITCH
x: position along x axis	XPOS
z: position along z axis	ZPOS

The control vector is two dimensional and is defined as

U_1 : Thrust level (magnitude)	THRUST
U_2 : Nozzle Angle	NZLANG

The instantaneous DRI is plotted on Figure 7.35a (denoted by DOBJ) and its integral (OBJFCN) is plotted on Figure 7.36. The DRI is constrained to remain below the value of 1, although in practice the violation of this limit for short period of time is tolerated.

Using the above solution as the base case trajectory for high speed ejection we will study its variation in response to changes of initial conditions and of inputs.

Test 1

The control inputs remain the same. The initial velocities u and w are decreased by 10%, which correpsonds to a decrease of 100 f/s. Figures 7.37 (a,b,c), 7.38 (a,b,c), 7.39 (a,b,c) and 7.40 correspond to this test case. It is clearly seen that the pitch rate is very sensitive to these initial velocities. The two most important functions to monitor, howerver, are the final altitude z(T) and the DRI. The altitude z(T) decreases, in absolute value, from 15 to 13 feet; that is a decrease of 13% in response to 10% in initial velocities. The final altitude of 13 feet is acceptable. The DRI function change is on the other hand very significant. A decrease of 25 to 30% is apparent on the instantaneous values of the DRI, and a 30% decrease in achieved on the accumulated (integrated DRI) value (Figure 7.38a and Figure 7.40). The results are reasonable and agree with intuition. In fact the thrust level being maintained at its previous while the initial speed is decreased, it is natural to expect the seat to decelerate more rapidly, i.e., the DRI decrease. The same is not time if the velocities were to increase. This is illustrated in the next test case.

Test 2

The control inputs remain the same. The initial velocities are increased by 10%, which corresponds to a 100 f/s increase.

Plots of Figures 7.41, 7.42, 7.43 and 7.44 illustrate the trajectories corresponding to these test case. It can be observed that the final altitude z(T) is increased in absolute value, by 14%. This is natural since the altitude depends directly on the initial velocity in z direction. On the other hand the DRI function increases by 30% resulting in an unacceptably high level of pressure on the pilot. In fact since the thrust level has not been augmented to compensate for the change in velocity, the acceleration radial remains relatively high on the pilot. These results combined with the ones of the previous run suggest that to make the control performance robust against increase of initial velocity, one has to apply more thrust level than what is exactly needed by the ESOP program.

Test 3

The initial conditions remains unchanged. The thrust level is smoothed.

As plots of Figure 7.35 display, the optimal inputs (optimal thrust and nozzle angle) computed by the ESOP programs are not smooth. It is important to study the behaviour of the solution when a rather crude smoothing of these inputs is performed.

Figures 7.45 through 7.48 correspond to a test in which the thrust level is smoothed (see Figure 7.46b). The essential features of the trajectory are not degraded. In particular the altitude z(T) is decreasd by 1 ft. which corresponds to 7% decrease in absolute value. The performance of the DRI is slightly superior to the base case. It is interesting to notice that the discontinuties of the DRI are closely correlated with those of the thrust level afnd the nozzle angle.

Test 4

The initial conditions remain unchanged. Both the thrust level and the nozzle angle are smoothed.

Figures 7.49, 7.50, 7.51 and 7.52 correspond to the case where both the thrust level and the nozzle angle are smoothed (Figure 7.49b,c). As expected the DRI performance remains almost similar to the previous case, with somehow less discontinutities. The final altitude z(T) is not significantly altered by the smoothing of the nozzle angle. The overall trajectory remains accpetable and the seat can be safely ejected using these two smoothed controls instead of the ones generated by the ESOP program.

7.9.2. Some Implementation Details. It is noted that the expressions for S1, S2 and S3 are matrix integral equations. In a linear system, closed form solutions exist or, equivalently, frequency domain results are obtainable via the Laplace transform. Previously, we have been integrating a system of 12 equations. The introduction of the equations for the S greatly expands the system order to

$$12 + 12^2 + (12 \times 8) = 252$$

$$(x) \quad (S1) \quad (S2)$$

(S3 is derived algebraically). In order to maintain a basic level of efficiency, the S1 system was made more compact. Several elements of S1 remain identically 0 or 1, thereby requiring no integration. These can be eliminated from the system. Doing this reduces the overall dimension from 252 to 175, a 30% savings.

The rest of the mechanization is straightforward; the new integration equations depend strongly on the linear system matrices, A and B. These are available from existing SSI software (as well as from EASIEST), at any point in time along the trajectory. The

appropriate initial conditions are, for S1, the 12-by-12 identity matrix I, and S2(0) = B Δt; S3(0) is derived algebraically once other quantities are developed.

The expanded sensitivity system runs at a noticeably slower rate than the basic system, but can still be run effectively interactively. The same IMSL DGEAR algorithm used before is still good, with much the same parameter values.

7.9.3. Results. The high Q (dynamic pressure)-low altitude case and MIL-S Case 1 (no dive, 60 deg. bank, 120 KEAS at ground level) were used as references. The state trajectory is in agreement with the original result to within 1%. The variation is felt to be due to the automatic changes in integration step size generated by DGEAR. Tables 7.7 to 7.10 show typical results.

Table 7.7 shows S1 for the high Q case at t = 0.96 second. Each element of S1, $\partial x_i/\partial x_{0_j}$, indicates the sensitivity of x_i (row i of S1) to a unit change in x_{0_j} (column j of SI), at time t (0.96 sec.). Only 67 of the 144 S1 elements are actually integrated, because the others remain constant, as noted above; however, all 144 S1 elements are displayed for convenience. Note also that columns defined by angular quantities (e.g., q, pitch rate) typically have larger values than the other columns. This is due to the radian measure used for angles. For example, the change in y (row 10 of S1) due to a one degree change in ψ, heading angle (column 12) is about 15 feet at 0.96 seconds.

Table 7.8 shows MIL-S Case 1 at 0.25 second. While this is a different case, it is generally true that the elements of S1 increase with time. Table 7.9 shows the same S1, with S3 now added to the printout. Analyzing one of the elements of S3, we note tat the sensitivity of RAD to a unit change in r_0 (yaw rate) is -0.0943. In general, this is reasonable, because the slideslip angle is positive, and thus a positive yaw rate would point the seat's x axis more into the wind direction, thus reducing RAD.

Table 7.7. High Q, Low Altitude, T = 0.96 sec.

HI-Q/LO-ALT ; T = 0.96

```
time =       0.960
      dfr,dtr,frc,trc:
         -12.753        0.14343        2.0162        -1.2340        -4.3502        0.17815E-01
         -910.14        173.22        -7300.3        39.443        954.21        -77.501
```

GADAG:	u	v	w	p	q	r	ϕ	θ	x	y	z	ψ
$\dot{u}$	-0.2509	0.1746	-0.3555	0.0000	5.0369	-5.4670	0.0000	-29.9856	0.0000	0.0000	0.0000	0.0000
$\dot{v}$	-0.0385	0.4639	0.1492	-5.5549	0.0000	-380.5776	29.9594	-0.1476	0.0000	0.0000	0.0000	0.0000
$\dot{w}$	0.6243	-0.0715	0.9234	55.4670	580.6775	0.0000	-0.6362	-6.7488	0.0000	0.0000	0.0000	0.0000
$\dot{p}$	-0.0159	0.2171	-0.0353	0.5526	0.7065	0.1516	0.0000	0.0000	0.0000	0.0000	0.0000	0.0000
$\dot{q}$	-0.2305	0.0039	-0.1735	-0.0456	0.0369	0.0030	0.0000	0.0000	0.0000	0.0000	0.0000	0.0000
$\dot{r}$	0.0439	-0.1927	-0.0021	-0.2541	-0.0305	0.7438	0.0000	0.0000	0.0000	0.0000	0.0000	0.0000
$\dot{\phi}$	0.0000	0.0000	0.0000	0.9000	0.0367	0.2177	1.0769	0.0539	0.0000	0.0000	0.0000	0.0000
$\dot{\theta}$	0.0000	0.0000	0.0000	0.0000	0.9592	-0.0274	-0.0549	1.0000	0.0000	0.0000	0.0000	0.0000
$\dot{x}$	0.9296	-0.2615	0.2104	0.0000	0.0000	0.0000	-13.8221	-187.9638	1.0000	0.0000	0.0000	-0.2616
$\dot{y}$	0.0035	0.9568	-0.0034	0.0000	0.0000	0.0000	4.9022	-14.6239	0.0000	1.0000	0.0000	859.5017
$\dot{z}$	-0.2100	0.0198	0.9312	0.0000	0.0000	0.0000	-54.3519	-855.2708	0.0000	0.0000	1.0000	0.0000
$\dot{\psi}$	0.0000	0.0000	0.0000	0.0000	0.0210	0.9893	0.2729	0.0008	0.0000	0.0000	0.0000	1.0000

```
CNTRLR: acc_d(1), vel_d(1):
         -560.00        0.00000E+00        -300.00        615.64        0.00000E+00        -341.53
      acc_d(3), vel_d(4):
         -459.76        9.0239        -478.31        643.29        -40.251        -164.79
      omegadot_d(B), omega_d(B):
         -0.59426        -3.9303        0.70399        0.00000E+00        0.00000E+00        0.00000E+00
       (B) aib, dacc; vib, dvel:
         -458.27        7.8035        -438.52        -1.5150        1.2174        0.20398
         693.79        -43.155        -166.45        -10.497        -0.94797E-01        1.6747
      dtr acc, rate components:
         -1.9005        -5.3326        -0.14925        0.78273        0.83007        0.10040
      frd, trd:        -1004.5        138.56        -7299.8        30.340        937.34        -78.397
time =       0.970
      dfr,dtr,frc,trc:
         -13.070        0.17993        2.0761        -1.1177        -4.4725        -0.48848E-01
         -1017.5        138.74        -7297.7        29.223        932.86        -78.445
GADAG:
     -0.2702        0.1740        -0.3592        0.0000        6.7235        -58.9759        0.0000        -30.2956        0.0000        0.0000        [illegible]        [illegible]
```

Table 7.8. MIL-S Condition 1, T=0.25

	u	v	w	p	q	r	φ	θ	x	y	[illegible]	[illegible]
u̇	0.9277	-0.0774	-0.0187	0.0000	-4.8796	9.6150	0.0000	-7.8786	0.0000	0.0000	0.0000	0.0000
v̇	0.0616	0.9439	1.0213	4.8796	0.0000	-49.8120	6.0908	0.9064	0.0000	0.0000	0.0000	0.0000
ẇ	0.0503	-1.0293	0.9766	-9.6150	49.8120	0.0000	4.3225	-1.2616	0.0000	0.0000	0.0000	0.0000
ṗ	0.0015	0.0172	0.0349	1.0013	0.1234	-0.0356	0.0000	0.0000	0.0000	0.0000	0.0000	0.0000
q̇	-0.0162	0.0004	-0.0005	-0.3137	0.9675	-0.5653	0.0000	0.0000	0.0000	0.0000	0.0000	0.0000
ṙ	-0.0025	0.0026	0.0025	0.1520	-0.2133	0.9455	0.0000	0.0000	0.0000	0.0000	0.0000	0.0000
φ̇	0.0000	0.0000	0.0000	0.2530	-0.0287	0.0394	0.9927	-0.0792	0.0000	0.0000	0.0000	0.0000
θ̇	0.0000	0.0000	0.0000	0.0000	0.1932	0.1373	0.0759	1.0000	0.0000	0.0000	0.0000	0.0000
ẋ	0.2444	-0.0166	0.0461	0.0000	0.0000	0.0000	2.6718	-11.1896	1.0000	0.0000	0.0000	-9.9319
ẏ	-0.0129	0.1939	0.1345	0.0000	0.0000	0.0000	1.0649	0.6882	0.0000	1.0000	0.0000	49.1965
ż	-0.0565	-0.1344	0.1595	0.0000	0.0000	0.0000	12.2614	-49.5763	0.0000	0.0000	1.0000	0.0000
ψ̇	0.0000	0.0000	0.0000	0.0000	-0.1402	0.1972	-0.0365	-0.3162	0.0000	0.0000	0.0000	1.0000

MIL-S CONDITION #1, T = 0.25

```
CNTRLR: acc_d(1), vel_d(1):
          0.00000E+00   0.00000E+00   -140.00        199.51        37.149        -57.973
        acc_d(3), vel_d(3):
          26.933        -3.91759      -137.75        203.25        52.224        -22.476
        omegadot_d(B), omega_d(B):
          -29.739       2.1774        -3.48106       0.00000E+00   0.00000E+00   0.00000E+00
         (B) aib, docc, vib, avel:
          46.381        5.7322        -190.52        -19.149       -6.6198       52.766
          203.80        57.367        -35.575        -0.54525      -5.1427       13.099
        dtr acc, rate components:
          1.0367        9.3597        -1.8451        -17.305       2.2556        3.2517
       frd, trd:       763.48         38.436        -2197.6       -597.52       153.47        114.75
  time =  0.260
        dfr,dtr,frc,trc:
          -116.52       -45.293       335.13        -16.395       11.535        1.4067
          934.82        64.423        -2233.0       -614.22       165.10        116.15

 TIME
  U         V         W         P         Q         R         PHI       THETA     X_E
  Y_E       ALT       TURNS     ALPHA     BETA      VEL       UDOT      VDOT      WDOT
  PDOT      QDOT      RDOT      PSIDOT    THCOT     PHIDOT    VNDOT     QBAR      MACH
  PAERO     QAERO     RAERO     PRKT      QRKT      RRKT      XRKT      YRKT      ZRKT
  XAERO     YAERO     ZAERO     CX        CY        CZ        CL        CM        CN
  ALTDOT    UC1       UC2       UC3       UC4       UC5       UC6       UC7       UC8
  RADIT     PCMAG     TCMAG     MOMARM    FANGX     FANGY     FANGZ
```

TABLE 3

Table 7.9. MIL-S Condition 1, T=0.25

S1, S3 Printout

trd, trd:

time = 0.25 [illegible] 760.55 [illegible] 172.36 [illegible] -2178.0 -581.33 147.27 112.56

dfr,dtr,frc,trc:

-113.63	-62.563	335.34	-15.513	12.891	1.5536
992.21	158.52	-2525.1	-599.84	150.16	114.12

TIME

U	V	W	P	Q	R	PHI	THETA	X_E
[illegible]	ALT	TURNS	ALPHA	BETA	V_L	UDOT	VDOT	WDOT
[illegible]	[illegible]	[illegible]	[illegible]	THETT	PHIDOT	VMDOT	QBAR	MACH
[illegible]	[illegible]	[illegible]	[illegible]	[illegible]	PFRT	XFRT	YFRT	ZFRT
[illegible]	[illegible]	[illegible]	[illegible]	[illegible]	CL	CL	CM	CN
[illegible]	[illegible]	[illegible]	[illegible]	[illegible]	[illegible]	UCA	UC7	UC8
[illegible]	[illegible]	[illegible]	[illegible]	[illegible]	[illegible]	[illegible]		

β = 15.9°

[illegible]								
[illegible]	[illegible]	[illegible]	[illegible]	[illegible]	[illegible]	[illegible]	10.45	49.20
-1040.	[illegible]	[illegible]	[illegible]	[illegible]	[illegible]	[illegible]	-120.6	-493.7
56.81	[illegible]	-12.5	-599.5	[illegible]	251.4	504.5	54.33	0.1915
[illegible]	[illegible]	[illegible]	[illegible]	[illegible]	114.1	992.2	168.5	-2826.
[illegible]	[illegible]	11.[illegible]	[illegible]	-0.[illegible]17	[illegible]	-0.3474E-01	0.1257	-0.5965E-01
[illegible]	[illegible]	531.3	0.275[illegible]	[illegible]	[illegible]	[illegible]	58.84	1712.
[illegible]	[illegible]	[illegible]	1.[illegible]2	70.6[illegible]	[illegible]	16[illegible]		
[illegible]				[illegible]	-5.[illegible]27	0.1731E-01		

	u	v	w	p	q	r	φ	θ	x	y	z	ψ	
DADXO:	[illegible]	[illegible]	[illegible]	[illegible]	[illegible]	[illegible]	0.0075	-0.0015	0.0000	0.0000	0.0000	0.0000	S3
	[illegible]	[illegible]	[illegible]	[illegible]	[illegible]	[illegible]	[illegible]	-7.5736	0.0000	0.0000	0.0000	0.0000	S1
	[illegible]	[illegible]	[illegible]	[illegible]	[illegible]	-49.[illegible]126	6.0908	0.9644	0.0000	0.0000	0.0000	0.0000	
	[illegible]	-1.[illegible]	[illegible]	-2.[illegible]	[illegible]	[illegible]	4.3226	-1.2416	0.0000	0.0000	0.0000	0.0000	
	[illegible]	[illegible]	[illegible]	[illegible]	[illegible]	[illegible]	0.0000	0.0000	0.0000	0.0000	0.0000	0.0000	
	[illegible]	[illegible]	[illegible]	[illegible]	0.9575	[illegible]	0.0000	0.0000	0.0000	0.0000	0.0000	0.0000	
	[illegible]	[illegible]	[illegible]	[illegible]	[illegible]	0.9445	0.0000	0.0000	0.0000	0.0000	0.0000	0.0000	
	[illegible]	[illegible]	[illegible]	[illegible]	[illegible]	[illegible]	0.9927	-0.5792	0.0000	0.0000	0.0000	0.0000	
	[illegible]	[illegible]	[illegible]	[illegible]	[illegible]	.1373	0.5759	1.0000	0.0000	0.0000	0.0000	0.0000	
	[illegible]	[illegible]	[illegible]	[illegible]	[illegible]	[illegible]	2.6718	-11.1896	1.0000	0.0000	0.0000	-9.9319	
	[illegible]	[illegible]	[illegible]	[illegible]	[illegible]	[illegible]	1.0649	0.6652	0.0000	1.0000	0.0000	49.1965	
	[illegible]	[illegible]	[illegible]	[illegible]	[illegible]	[illegible]	12.2614	-48.5763	0.0000	0.0000	1.0000	0.0000	
	[illegible]	[illegible]	[illegible]	[illegible]	[illegible]	.1372	-1.[illegible]365	[illegible]	0.0000	0.0000	0.0000	1.0000	

UNTNKR: acc_s(1), vel_s(1):

[illegible] [illegible] -14[illegible] 129.51 37.149 -57.373

acc_s(2), vel_s(2):

[illegible] [illegible] -1[illegible]7.75 203.25 52.224 -22.476

omegadot_a(2), omega_a(2):

[illegible] 2.1774 [illegible] 0.0000E+00 0.00000E+00 0.00000E+00

(B) aaba dacc vio, ival:

44.[illegible]1	5.7[illegible]	-120.52	-19.149	-6.6198	52.764
403.80	57.367	-35.575	-0.54526	-5.1427	13.099

dtr acc, rate components:

1.4069 9.3599 -1.6451 -17.505 2.2654 3.2517

trd, trd:

time = 0.260 760.48 58.406 -2187.6 -597.82 153.47 114.75

dfr,dtr,frc,trc:

-116.52	-46.280	335.13	-16.398	11.635	1.4067
984.82	64.623	-2833.0	-614.22	165.10	116.16

Table 7.10 shows the MIL-S Case 1 at t = 0.09 second, with S2 added to the printout. The columns of S2 correspond to the 8 control vector elements. Columns 3, 6 and 8 of S2 are much smaller than the others, due again to the fact that the latter are nozzle deflection commands (radians), and that columns 3, 6 and 8 are thrust magnitudes (pounds).

7.9.4. Conclusions. The above analysis and example reveals that the robustness of the control scheme should be studied and taken into account in the design level. More precisely, the robustness of the control structure with respect to initial conditions can be used both for data reduction and storage, and also for deducing on line approximative control adjustment. These adjustment procedures are of simple regression type and can be implemented on line.

The robustness of the control structure with respect to the control inputs should be taken into consideration in conjunction with the technological feasibility and the cost of generating the desired control sequences. For instance, a rapidly oscillating thrust level may not be easily realizable, and one would like to replace it with a less demanding thrust level variations without vitally imparring the overall control performances. The robustness of the control strategy can be taken advantage of in investigating and defining such a control law.

Table 7.10. MIL-S Case 1, T=0.09, S2.

[illegible]

[illegible]	[illegible]	[illegible]	[illegible]	[illegible]	[illegible]	[illegible]	[illegible]	0.0000	0.0000	0.0000	0.0000	S_3

[illegible]

[illegible]	[illegible]	[illegible]	[illegible]	[illegible]	[illegible]	[illegible]	[illegible]	0.0000	0.0000	0.0000	0.0000	S_1
[illegible]	[illegible]	[illegible]	[illegible]	[illegible]	[illegible]	[illegible]	[illegible]	0.0000	0.0000	0.0000	0.0000	
[illegible]	[illegible]	[illegible]	[illegible]	[illegible]	[illegible]	2.3165	-1.3444	0.0000	0.0000	0.0000	0.0000	
[illegible]	[illegible]	[illegible]	[illegible]	[illegible]	[illegible]	0.0000	0.0000	0.0000	0.0000	0.0000	0.0000	
[illegible]	[illegible]	[illegible]	[illegible]	[illegible]	[illegible]	0.0000	0.0000	0.0000	0.0000	0.0000	0.0000	
[illegible]	[illegible]	[illegible]	[illegible]	[illegible]	[illegible]	0.0000	0.0000	0.0000	0.0000	0.0000	0.0000	
[illegible]	[illegible]	[illegible]	[illegible]	[illegible]	[illegible]	0.9980	[illegible]	0.0000	0.0000	0.0000	0.0000	
[illegible]	[illegible]	[illegible]	[illegible]	[illegible]	[illegible]	0.5484	1.0000	0.0000	0.0000	0.0000	0.0000	
[illegible]	[illegible]	[illegible]	[illegible]	[illegible]	[illegible]	0.7936	[illegible]	1.0000	0.0000	0.0000	-3.4619	
[illegible]	[illegible]	[illegible]	[illegible]	[illegible]	[illegible]	-1.1415	[illegible]	0.0000	1.0000	0.0000	17.7192	
[illegible]	[illegible]	[illegible]	[illegible]	[illegible]	[illegible]	[illegible]	-17.5495	0.0000	0.0000	1.0000	0.0000	
[illegible]	[illegible]	[illegible]	[illegible]	[illegible]	[illegible]	[illegible]	[illegible]	0.0000	0.0000	0.0000	1.0000	

[illegible]

[illegible]	[illegible]	[illegible]	[illegible]	[illegible]	[illegible]	115.1992	[illegible]	S_2 $(t=0.09)$
[illegible]	[illegible]	[illegible]	[illegible]	[illegible]	[illegible]	-96.7295	-0.0014	
[illegible]	[illegible]	[illegible]	[illegible]	[illegible]	[illegible]	[illegible]	[illegible]	
-28.0575	[illegible]	[illegible]	[illegible]	[illegible]	[illegible]	[illegible]	[illegible]	
[illegible]	[illegible]	[illegible]	[illegible]	[illegible]	[illegible]	-29.4586	-0.0020	
-47.2982	[illegible]	[illegible]	[illegible]	[illegible]	[illegible]	[illegible]	[illegible]	
[illegible]	[illegible]	[illegible]	[illegible]	[illegible]	[illegible]	0.3791	[illegible]	
-3.5591	[illegible]	[illegible]	[illegible]	[illegible]	[illegible]	-1.1920	[illegible]	
[illegible]	[illegible]	[illegible]	[illegible]	[illegible]	[illegible]	0.8122	[illegible]	
[illegible]	[illegible]	[illegible]	[illegible]	[illegible]	[illegible]	-4.5707	[illegible]	
[illegible]	[illegible]	[illegible]	[illegible]	[illegible]	[illegible]	-2.9143	[illegible]	
[illegible]	1.1713	[illegible]	[illegible]	[illegible]	[illegible]	[illegible]	[illegible]	

[illegible]

[illegible]	[illegible]	[illegible]	[illegible]	[illegible]	[illegible]	-0.7046	[illegible]	$S_2(0)$
[illegible]	[illegible]	[illegible]	[illegible]	[illegible]	[illegible]	[illegible]	[illegible]	
[illegible]	[illegible]	[illegible]	[illegible]	[illegible]	[illegible]	-0.1135	[illegible]	
[illegible]	[illegible]	[illegible]	[illegible]	[illegible]	[illegible]	-0.0079	0.0000	
[illegible]	[illegible]	0.0001	[illegible]	[illegible]	[illegible]	-0.3900	-0.0002	
-1.1565	0.3059	0.0002	[illegible]	[illegible]	[illegible]	0.0141	0.0000	
0.0000	0.0000	0.0000	[illegible]	[illegible]	[illegible]	0.0000	0.0000	
0.0000	0.0000	0.0000	[illegible]	[illegible]	[illegible]	0.0000	0.0000	
0.0000	[illegible]	0.0000	[illegible]	[illegible]	0.0000	0.0000	0.0000	
0.0000	0.0000	0.0000	[illegible]	0.0000	0.0000	0.0000	0.0000	
0.0000	0.0000	0.0000	0.0000	0.0000	0.0000	0.0000	0.0000	
0.0000	0.0000	0.0000	0.0000	0.0000	0.0000	0.0000	0.0000	

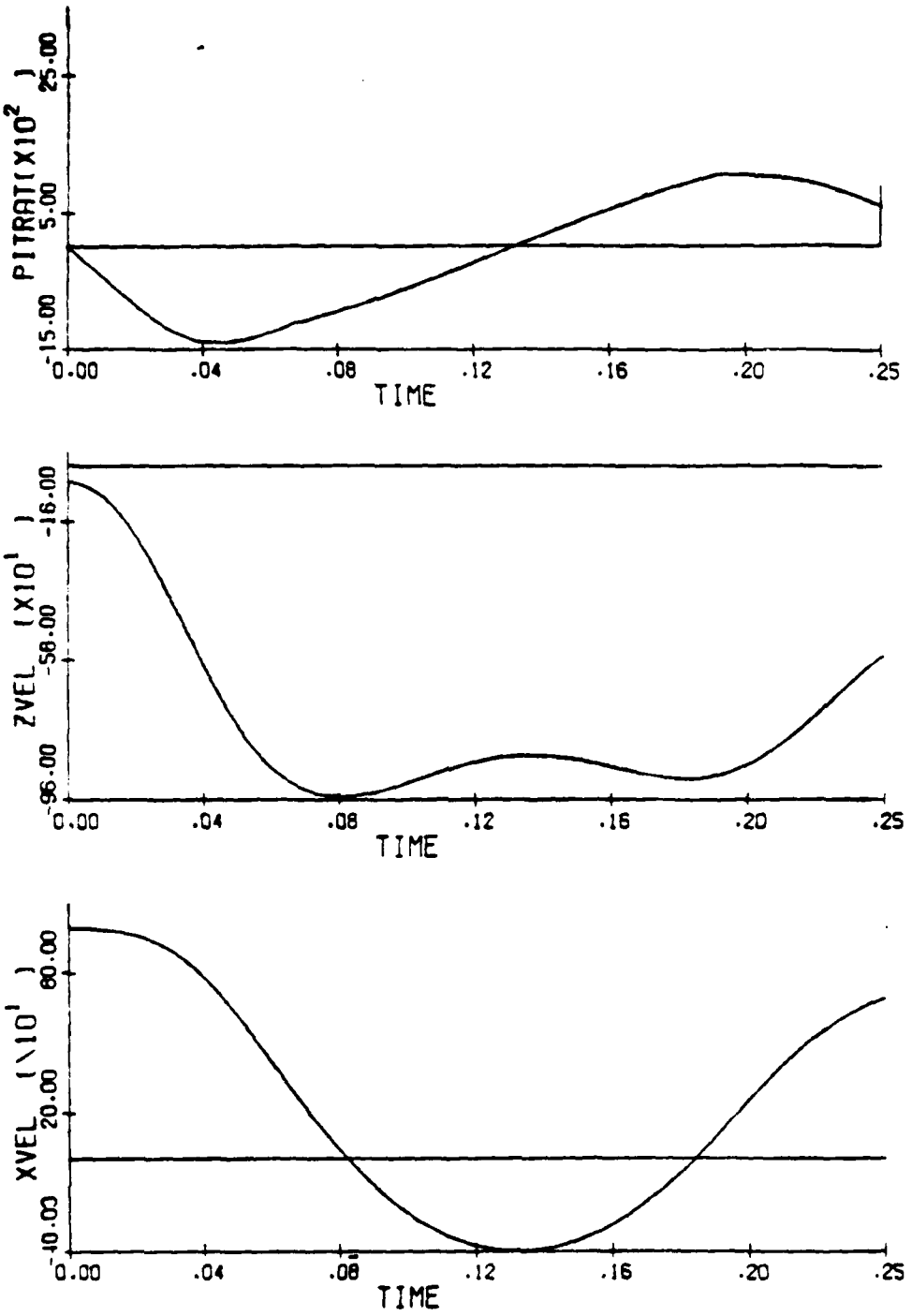

Figure 7.33 (a,b,c). High Q Case 3 DOF ESOP Solution

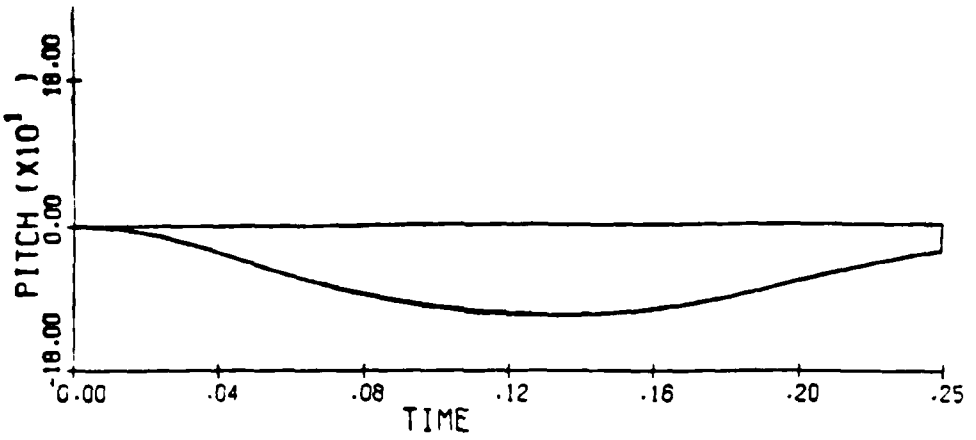

(a)

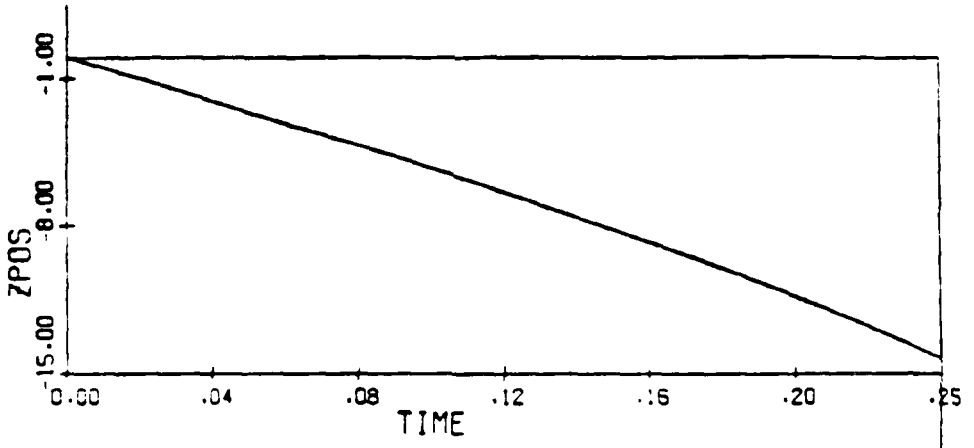

(b)

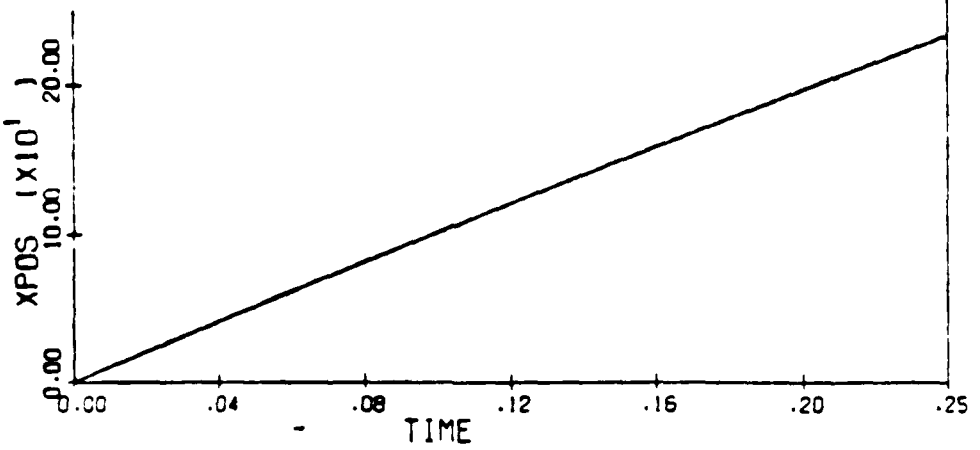

(c)

Figure 7.34 (a,b,c). High Q Case (continued)

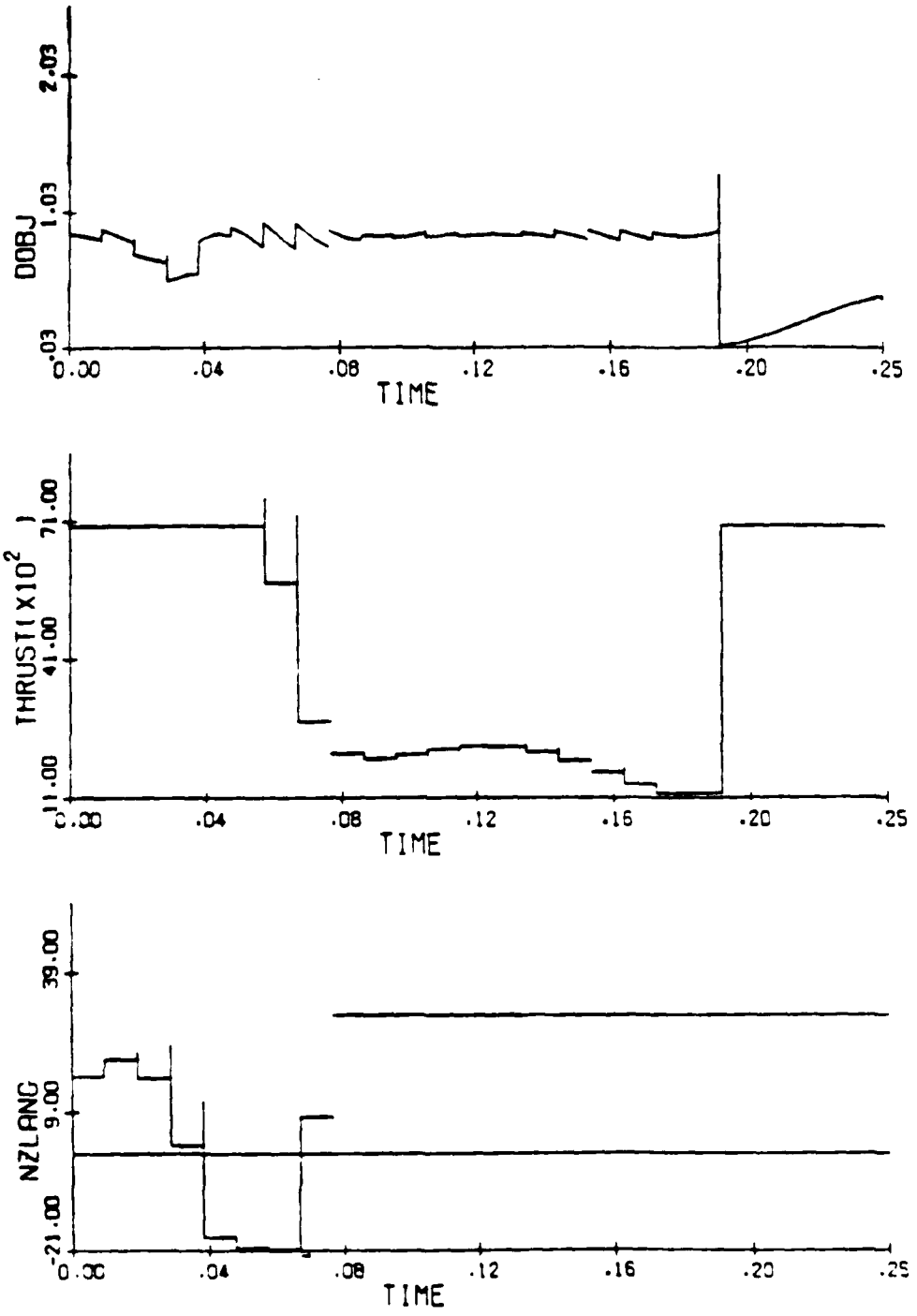

Figure 7.35 (a,b,c). High Q Case (continued)

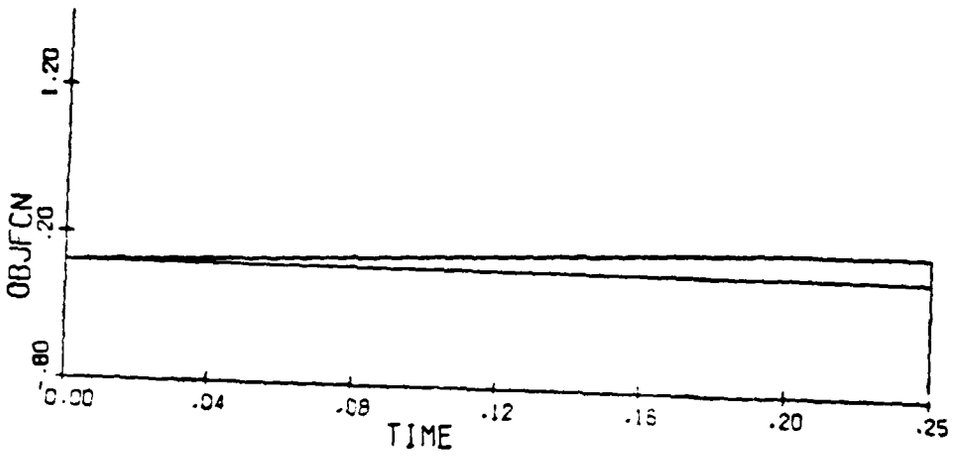

Figure 7.36. High Q Case

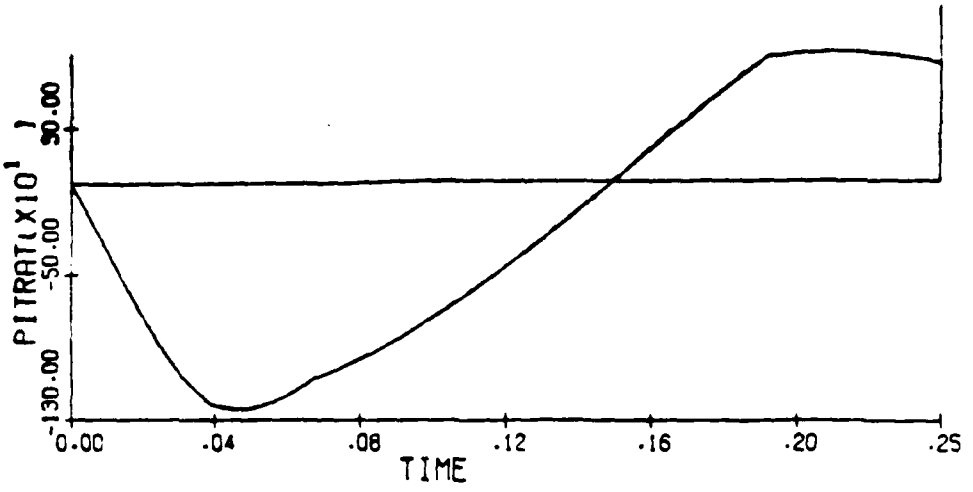

(a)

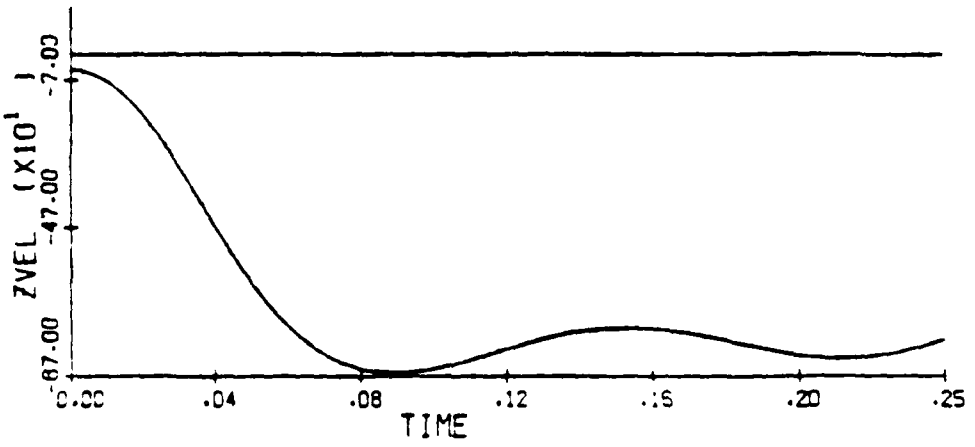

(b)

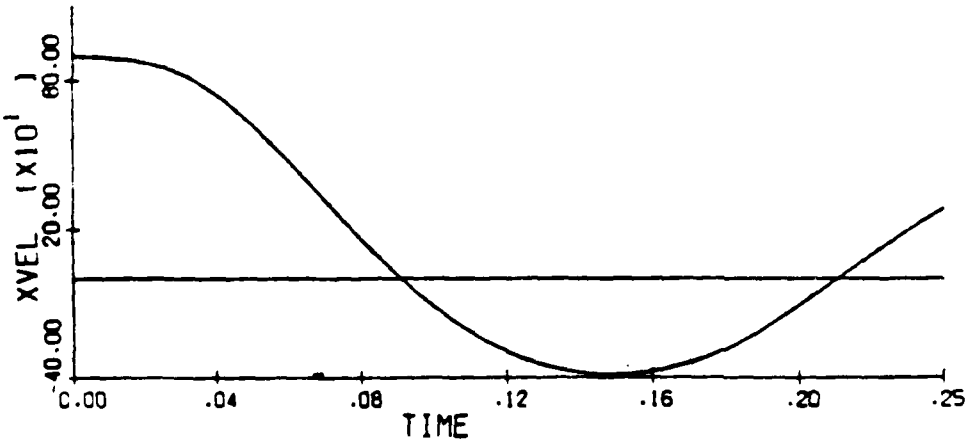

(c)

Figure 7.37 (a,b,c). High Q; 10% Decrease in u and w

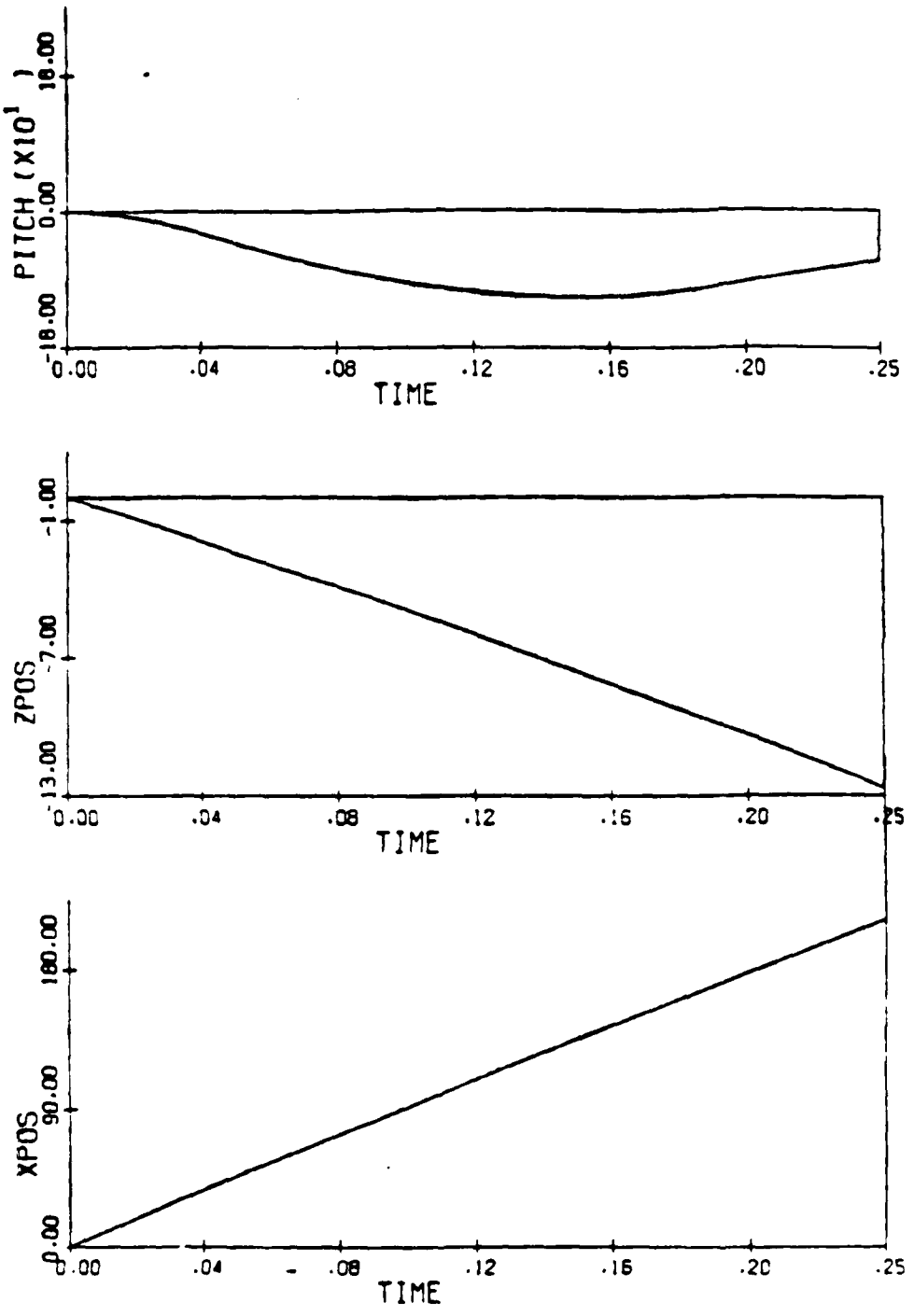

Figure 7.38 (a,b,c). High Q; 10% Decrease in u and w

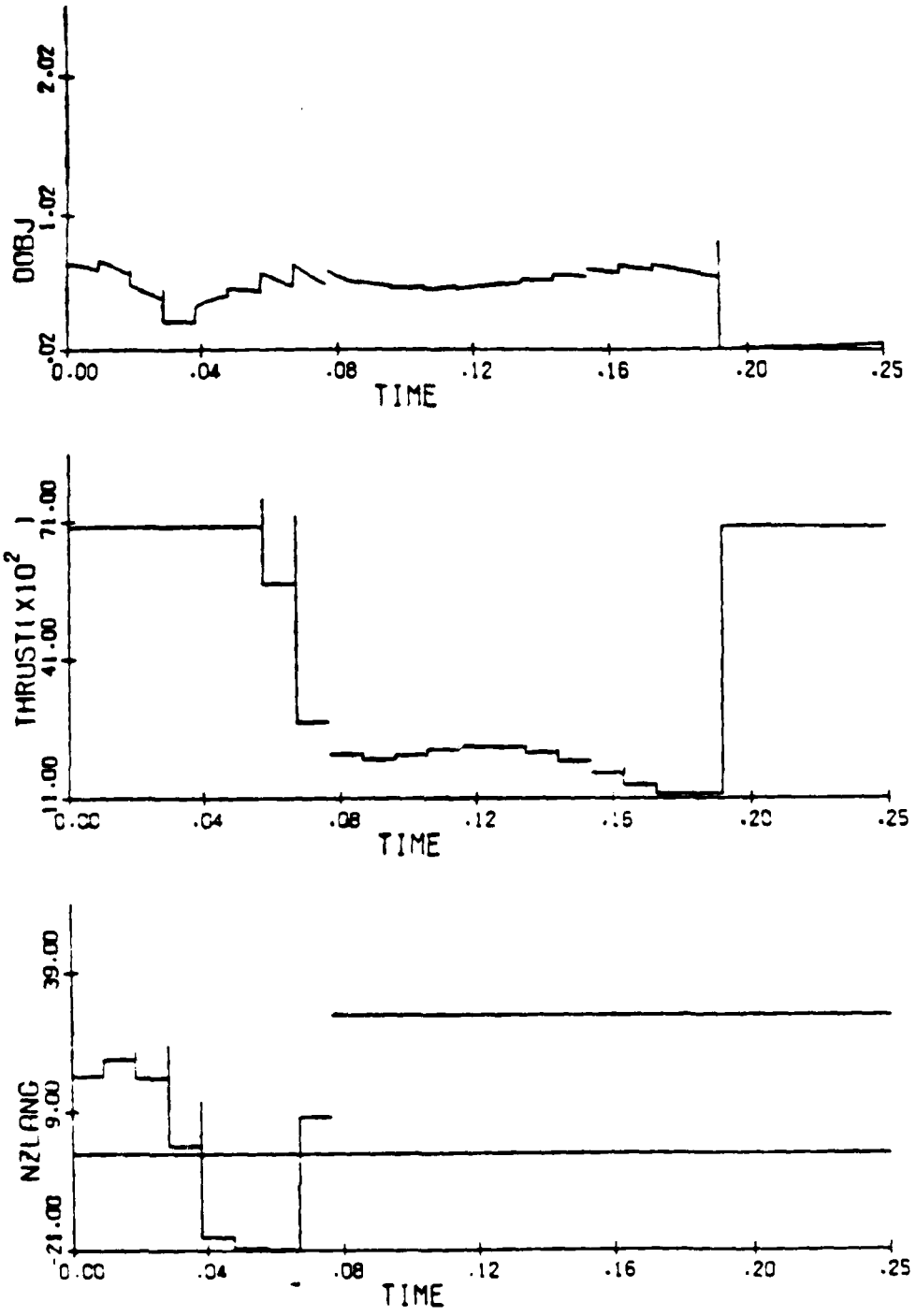

Figure 7.39 (a,b,c). High Q: 10% Decrease in u and w

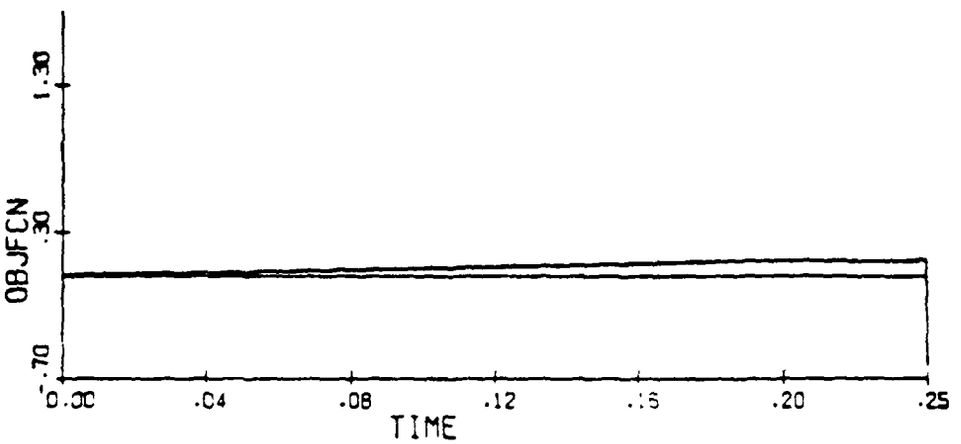

Figure 7.40. High Q; 10% Decrease in u and w

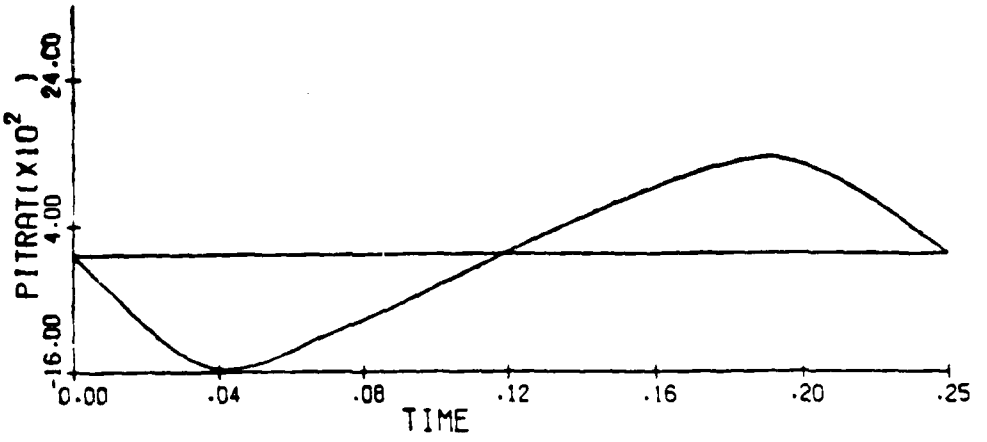
PITRAT(X10^2)
24.00
4.00
-16.00
0.00
.04
.08
.12
.16
.20
.25
TIME

(a)

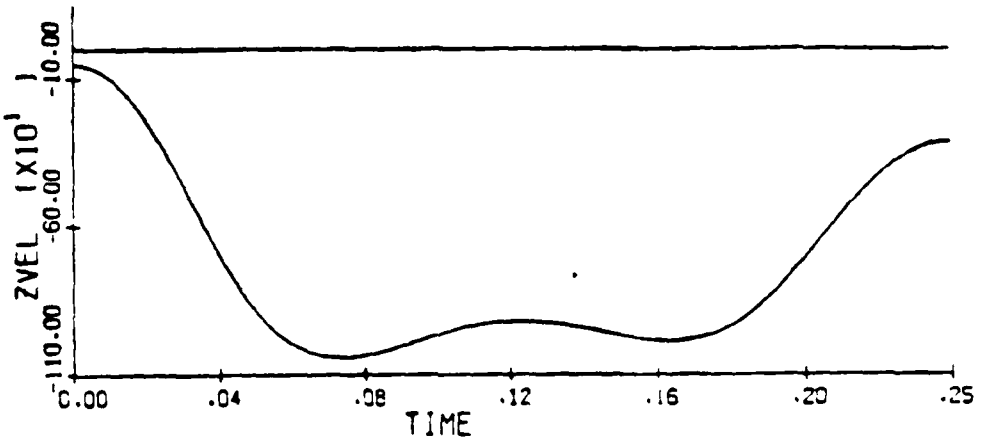
ZVEL (X10^1)
-10.00
-60.00
-110.00
0.00
.04
.08
.12
.16
.20
.25
TIME

(b)

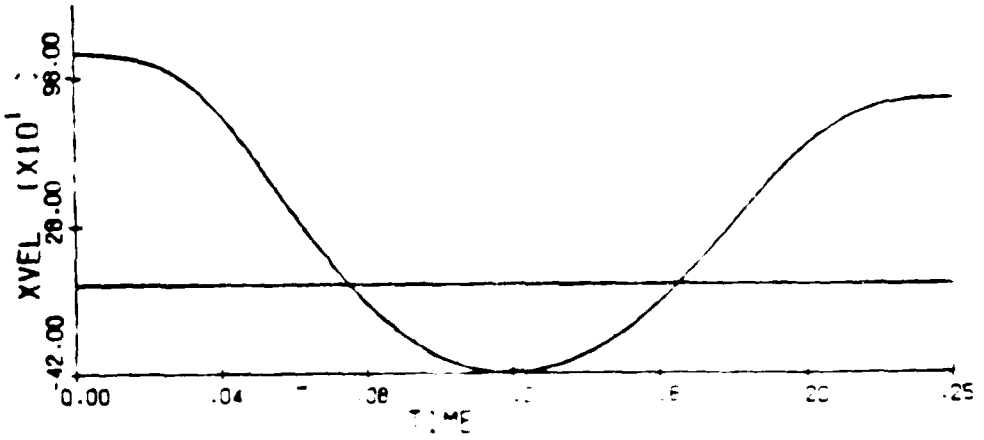
XVEL (X10^1)
98.00
28.00
-42.00
0.00
.04
.25

(c)

Figure [illegible]

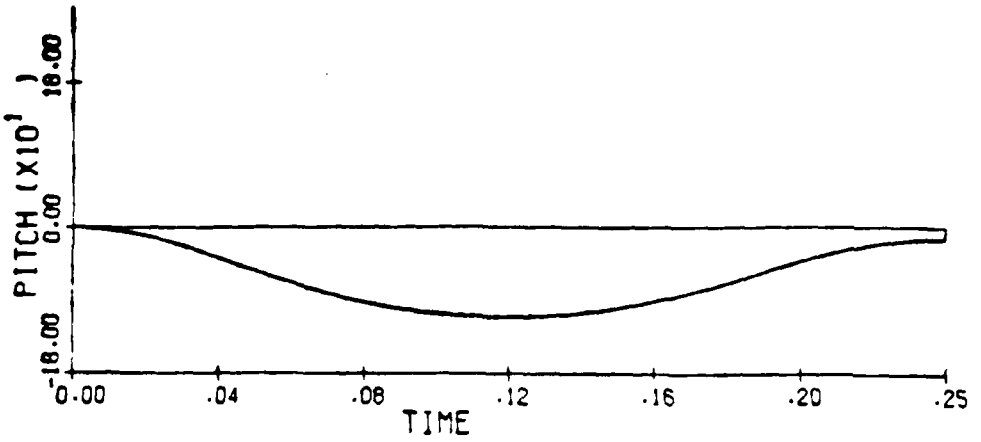

(a)

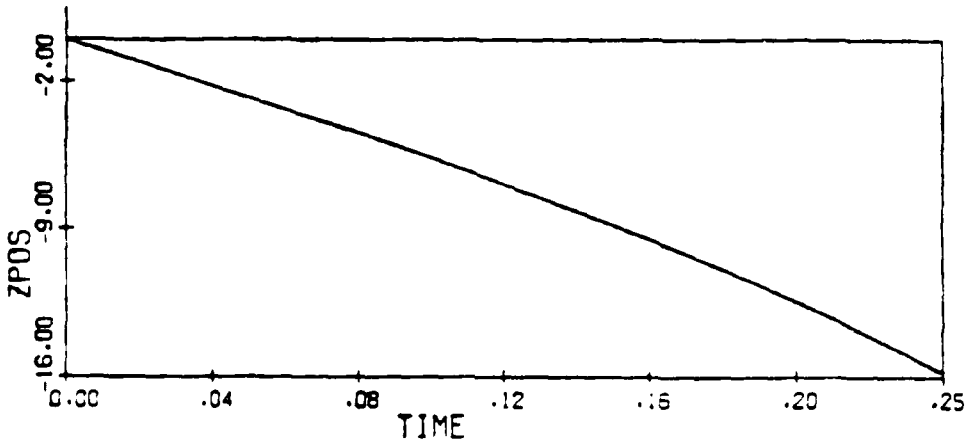

(b)

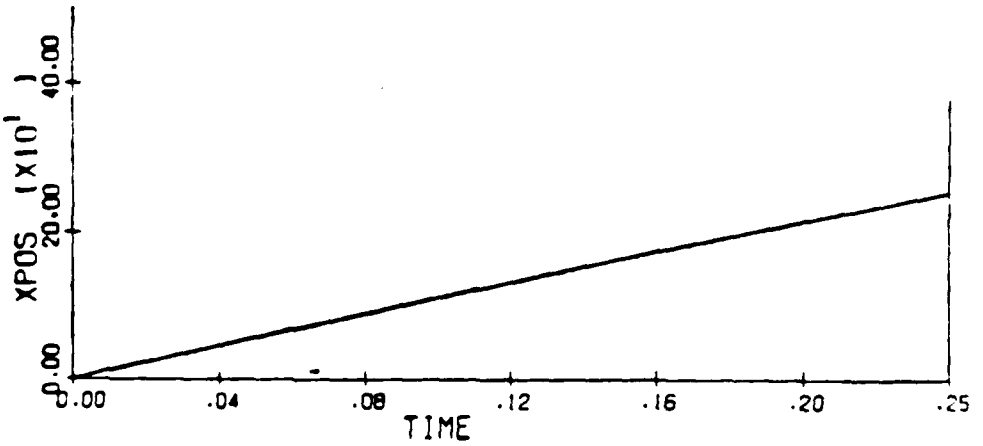

(c)

Figure 7.42 (a,b,c). High Q: 10% Increase in u and w

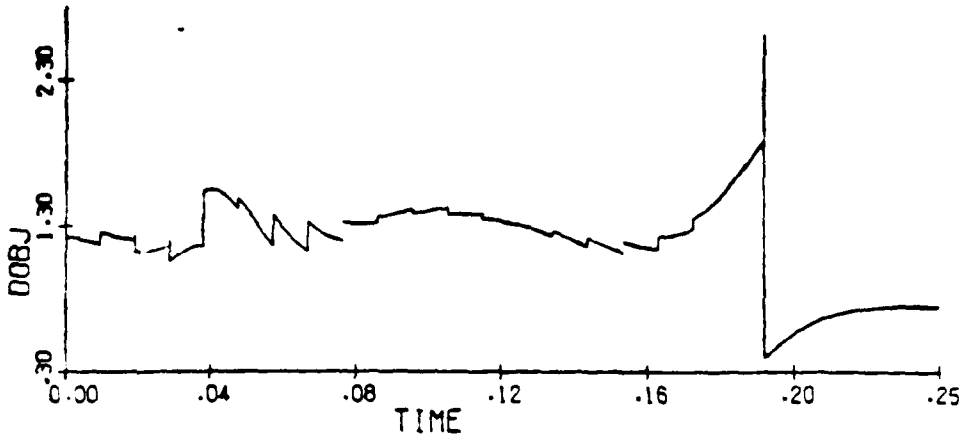

(a)

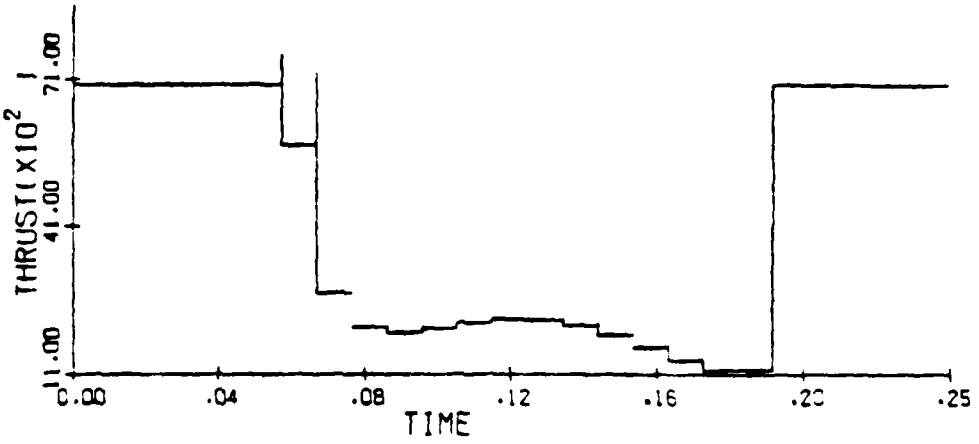

(b)

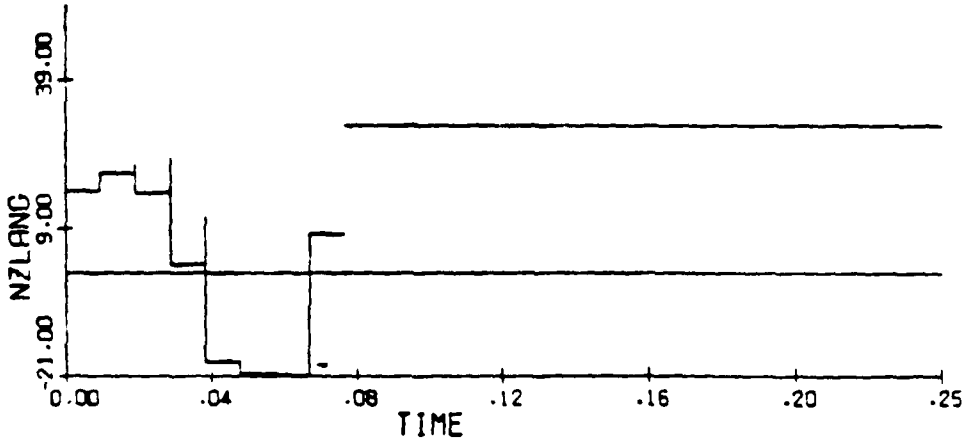

(c)

Figure 7.43 (a,b,c). High Q: 10% Increase in u and w

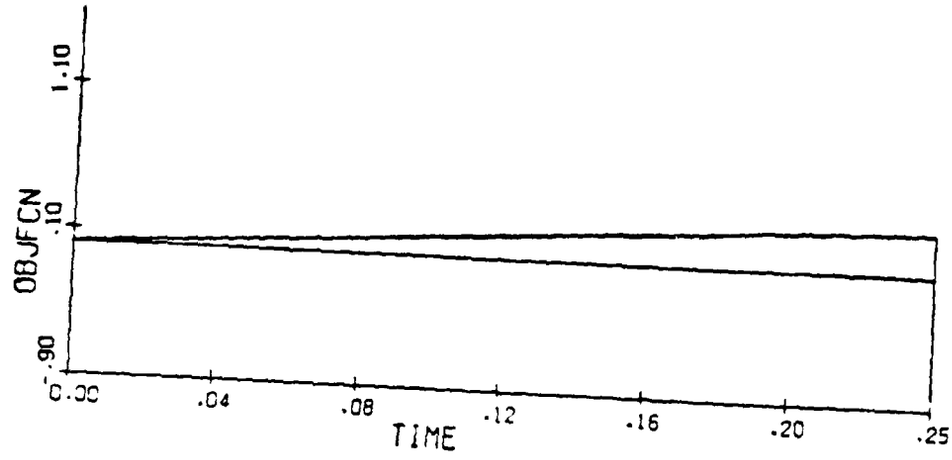

Figure 7.44. High Q; 10% Increase in u and w

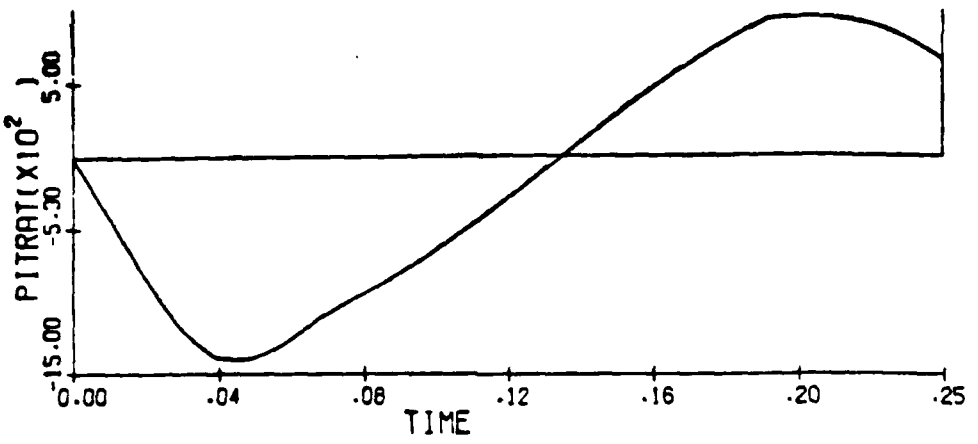

(a)

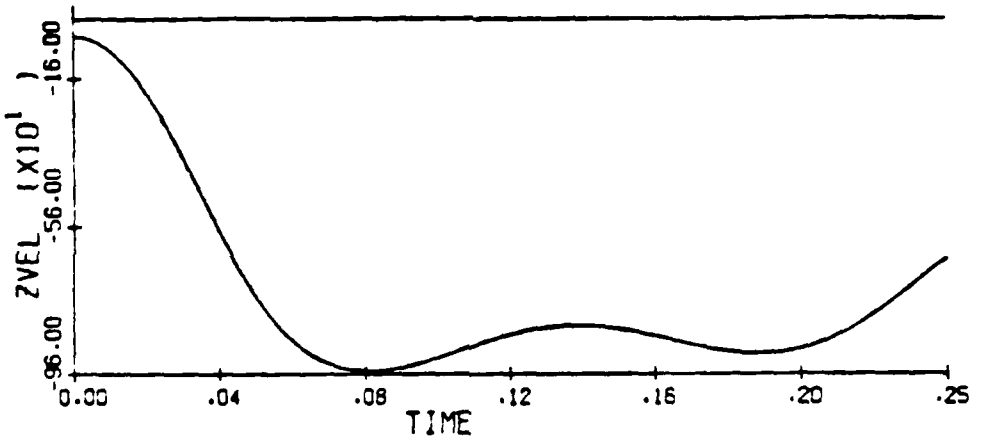

(b)

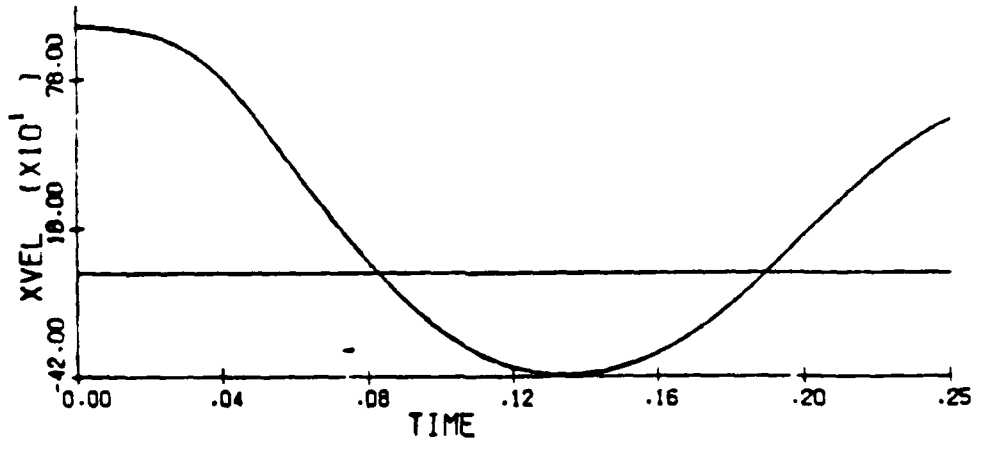

(c)

Figure 7.45 (a,b,c). High Q: Smooth Thrust

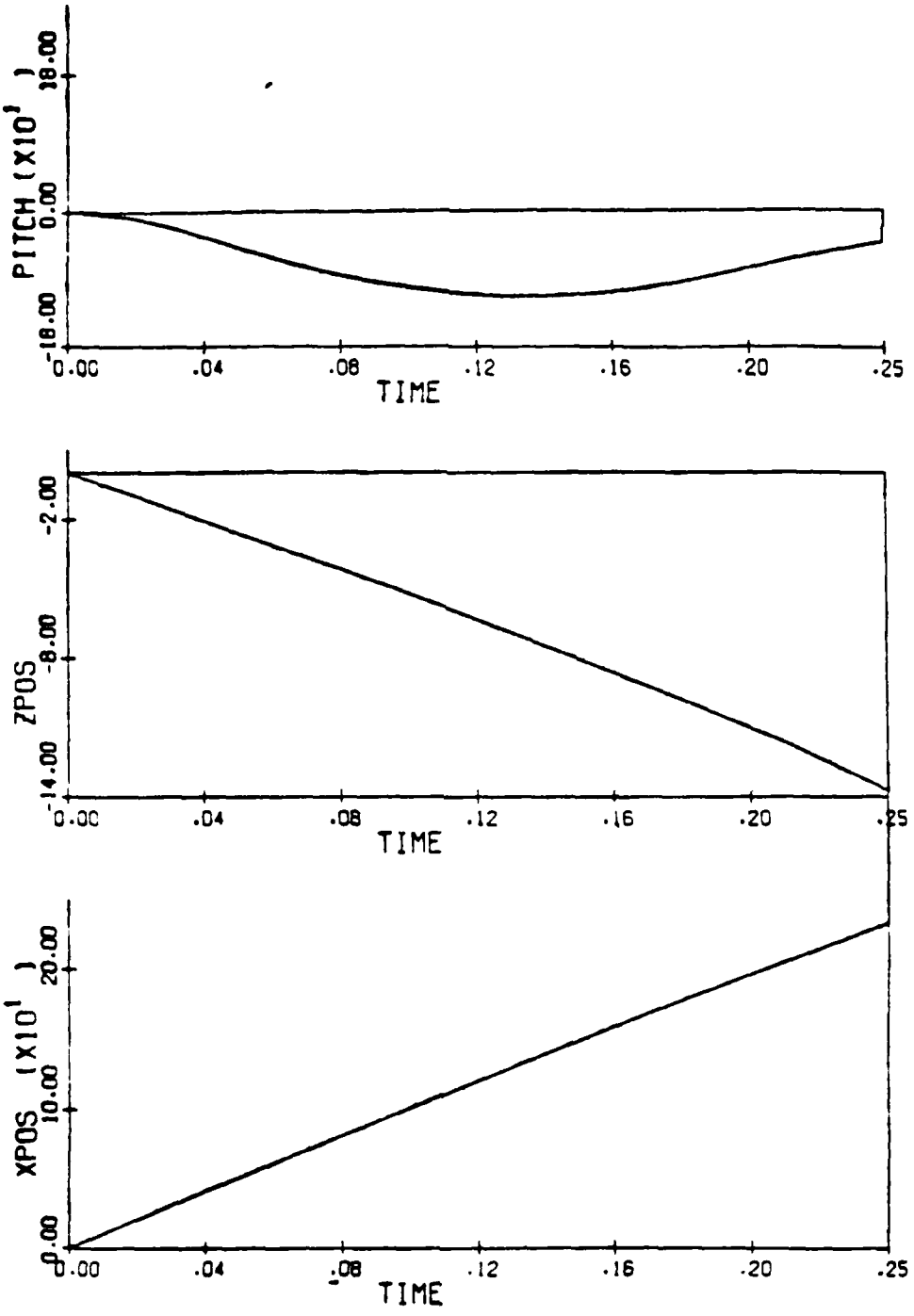

Figure 7.46 (a,b,c). High Q; Smooth Thrust

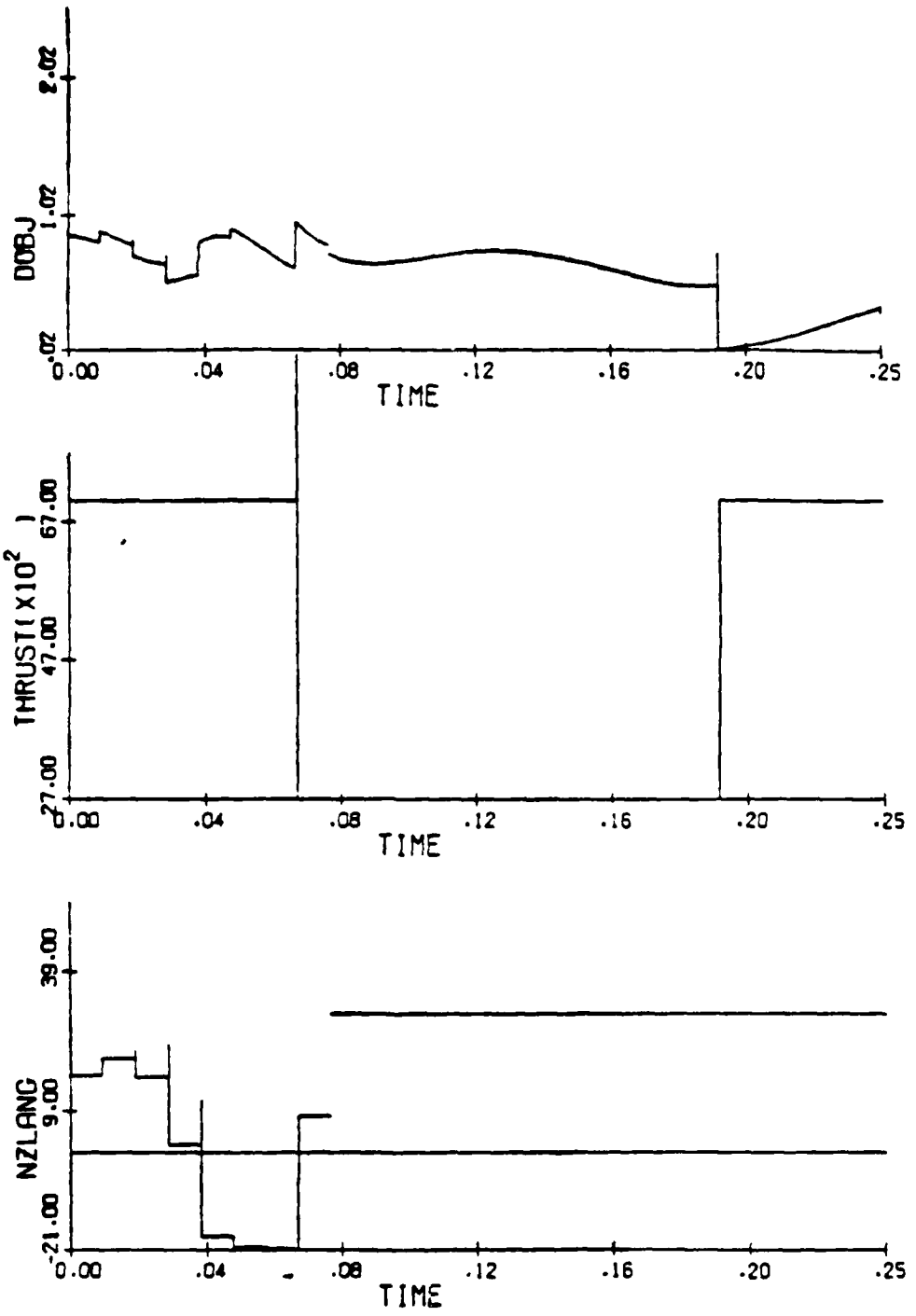

Figure 7.47 (a,b,c). High Q; Smooth Thrust

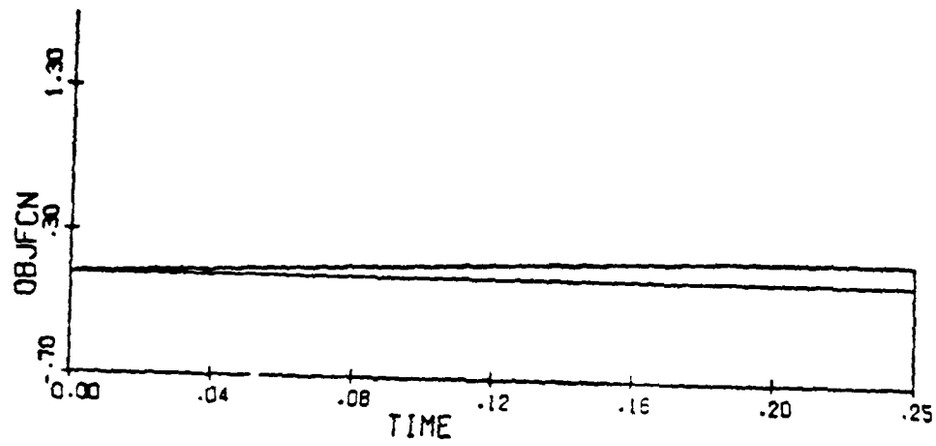

Figure 7.48. High Q: Smooth Thrust

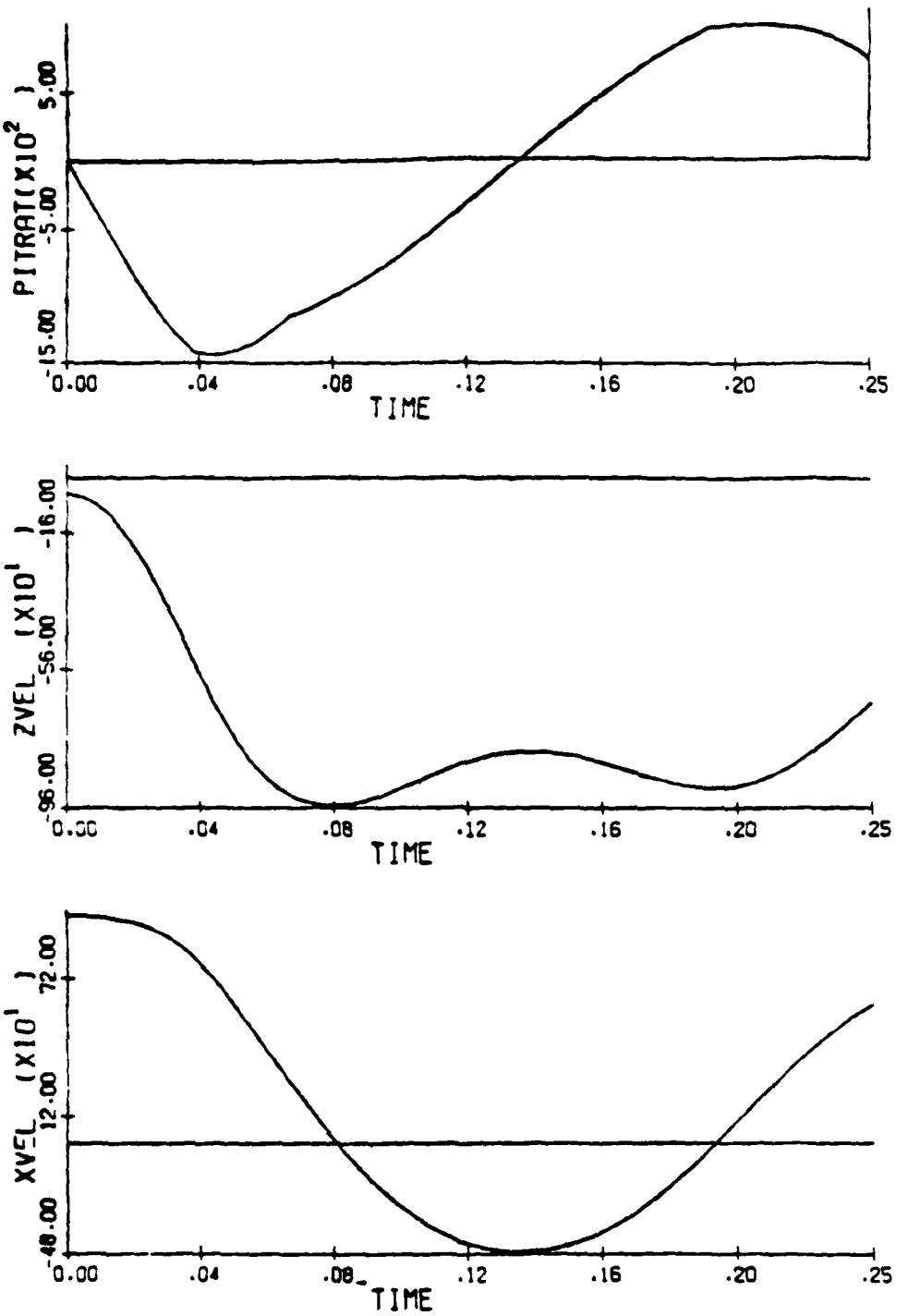

Figure 7.49 (a,b,c). High Q: Smooth Thrust and Gimbal Angle

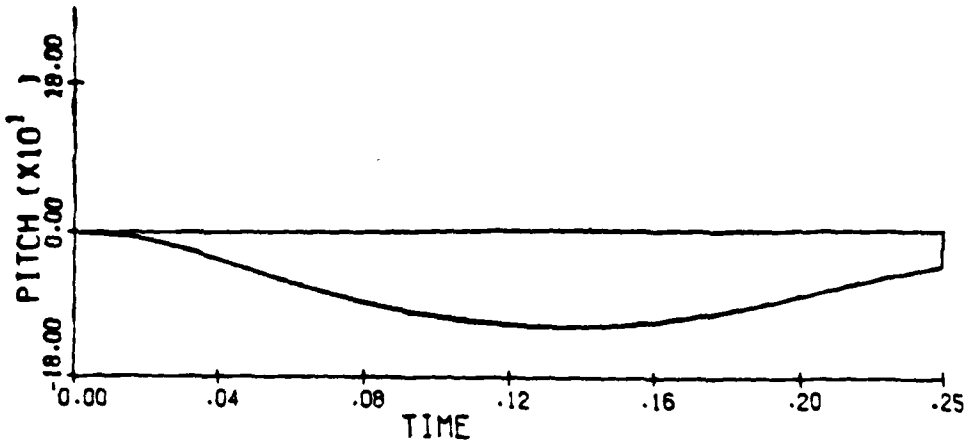

(a)

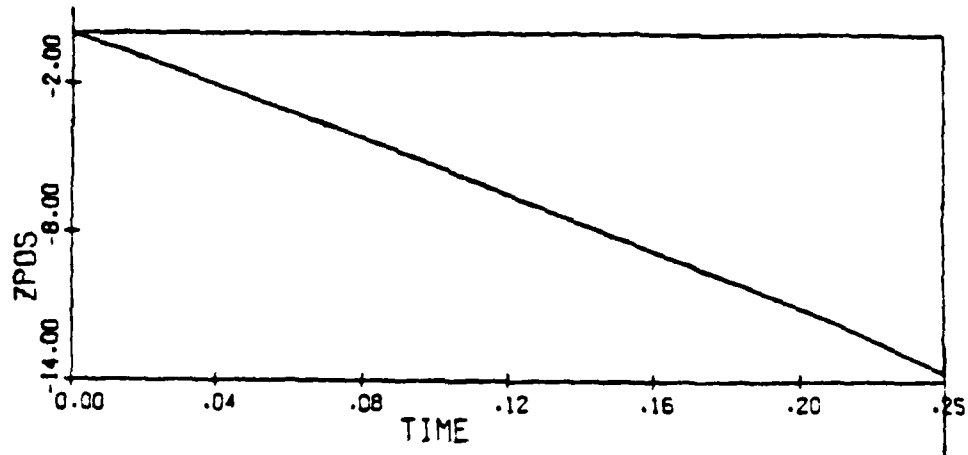

(b)

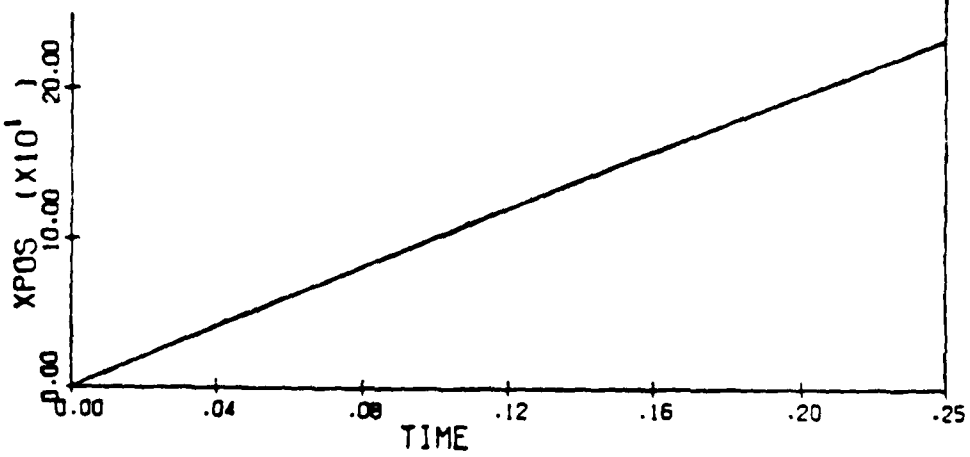

(c)

Figure 7.50 (a,b,c). High Q: Smooth Thrust and Gimbal Angle

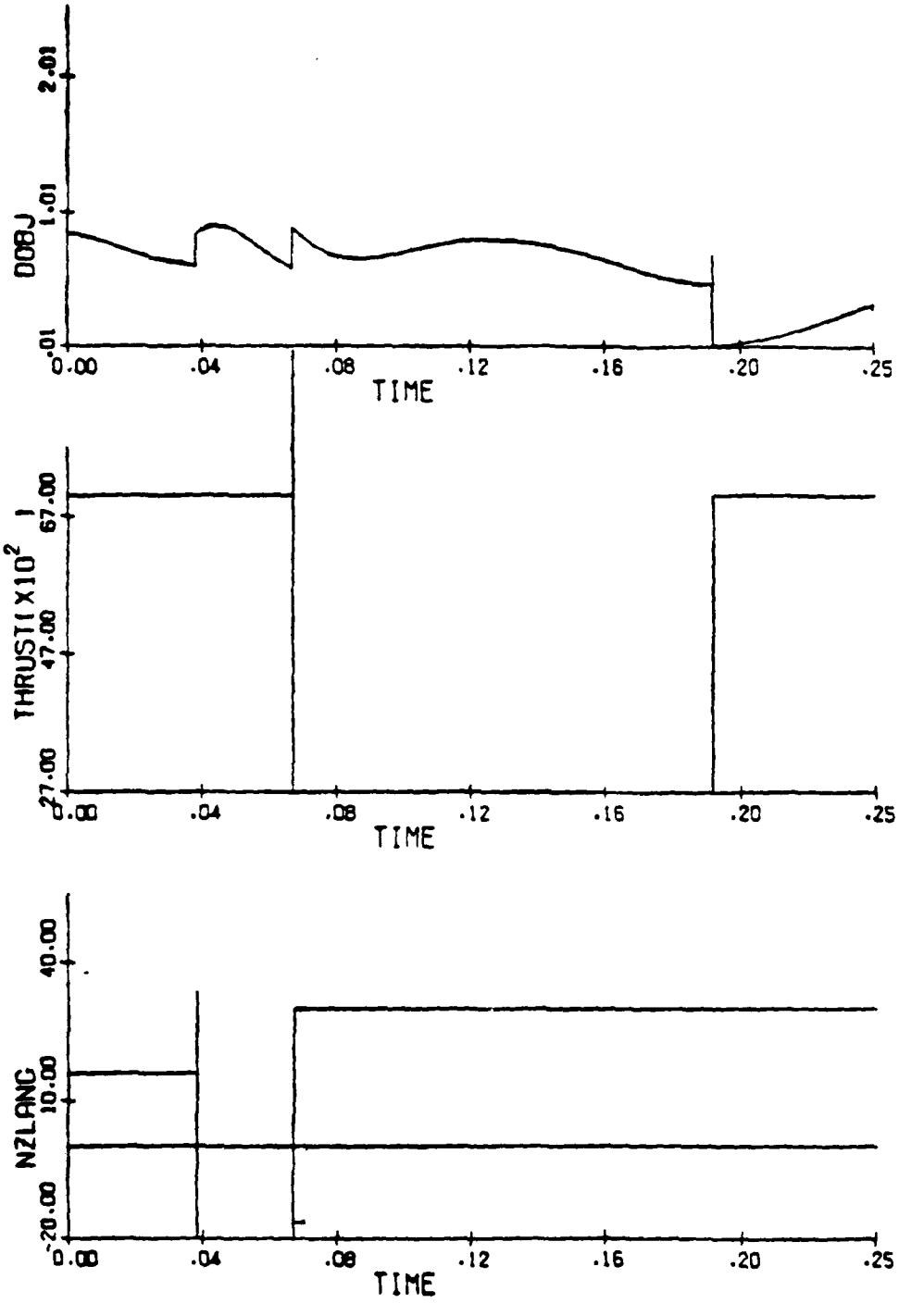

Figure 7.51 (a,b,c). High Q: Smooth Thrust and Gimbal Angle

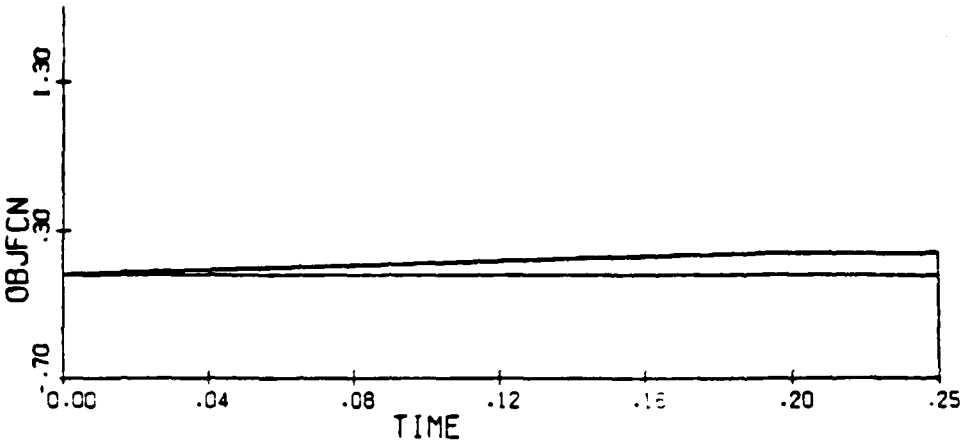

Figure 7.52. High Q: Smooth Thrust and Gimbal Angle

TABLE 1. LOW ALTITUDE ESCAPE CONDITIONS (1)

MIL CASE	ATTITUDE PITCH (DEG)	ATTITUDE ROLL (DEG)	SPEED (KNOTS)	ALTITUDE (FEET)
1	0	60	120	0 (2)
2	0	180	150	200
3	0	0	150	300 (3)
4	-60	0	200	500
5	-30	0	450	500
6	-60	60	200	550
7	-45	180	250	600

(1) CONDITIONS AT START OF ESCAPE SEQUENCE

(2) IMPACT OCCURS AT INSTANT OF SEAT/AIRCRAFT SEPARATION

(3) 10000 FEET PER MINUTE SINK RATE

TABLE 2. VARIABLE ATTITUDE INITIAL CONDITIONS

CASE	ATTITUDE		SPEED	ALTITUDE
	PITCH (DEG)	ROLL (DEG)	(KEAS)	(FEET)
1	0	0	0	0
2	0	0	600	0
3	0	0	700	0
4	0	0	150	5000
5	0	120	150	5000
6	0	180	150	5000
7	45	120	150	5000
8	45	180	150	5000
9	-45	120	150	5000
10	-45	180	150	5000
11	0	0	400	5000
12	45	120	400	5000
13	45	180	400	5000
14	-45	120	400	5000
15	-45	180	400	5000
16	0	0	600	45000
17	45	120	600	45000
18	45	180	600	45000
19	-45	120	600	45000
20	-45	180	600	45000

EJECTION SEAT CONTROL

SUMMARY OF HYBRID SIMULATION RESULTS

- LOW ALTITUDE (100 FT), HIGH DYNAMIC PRESSURE (1600 LB/FT^2)
  - UNCONTROLLED PERFORMANCE (OPEN LOOP RESULTS)
    - —NO DIRECT ALTITUDE CONTROL LEADING TO IMMEDIATE GROUND COLLISION
    - —TOTALLY UNSTABLE ATTITUDE CONTROL
      - SEVERE PITCH OSCILLATION
      - COMPLETE YAW REVERSAL
    - —ACCELERATION RADICAL MUCH GREATER THAN 1
    - —SIMULATION QUICKLY LOSES MATHEMATICAL MEANING DUE TO VARIABLE SATURATIONS

EJECTION SEAT CONTROL

SUMMARY OF HYBRID SIMULATION RESULTS

- LOW ALTITUDE (100 FT), HIGH DYNAMIC PRESSURE (1600 LB/FT^2)
- CONTROLLED PERFORMANCE (HARDWARE AND SIMULATED)
  - SMOOTH VARIATION WITH ORDER OF MAGNITUDE REDUCTION IN DYNAMIC PRESSURE
  - MONOTONICALLY INCREASING ALTITUDE RESULTING IN GROUND COLLISION AVOIDANCE
  - TIGHT ATTITUDE CONTROL
    - MINIMAL TRANSIENT AND CROSS COUPLING EFFECTS
      TERMINAL PITCH, YAW, ROLL CONSTRAINTS ACHIEVED
  - ACCELERATION RADICAL BOUNDED TO ALLOWABLE REGION

EJECTION SEAT CONTROL

SUMMARY OF HYBRID SIMULATION RESULTS

- MIL CASES 1-7 (TABLE 1)
  - LOW DYNAMIC PRESSURE CASES
  - HIGH PROBABILITY OF GROUND COLLISIONS
  - ADVERSE ATTITUDE IN SEVERAL CASES (UPSIDE DOWN, ADVERSE PITCH)
- UNCONTROLLED RESPONSE
  - ALTITUDE AND ATTITUDE RESPONSE QUICKLY BECOME MEANINGLESS DUE TO VARIABLE SATURATION
  - INITIAL MIGRATION OF VARIABLES BEST FOR EXTRAPOLATING RESULTS
- CONTROLLED RESPONSE
  - GROUND COLLISION AVOIDANCE IN ALL CASES
  - SMOOTH, DECOUPLED ATTITUDE RESPONSE EVEN FOR LARGE ATTITUDE CORRECTION CASES (FOR EXAMPLE MIL 2,6,7)
  - RADICAL WELL WITHIN LETHALITY BOUNDS

EJECTION SEAT CONTROL

SUMMARY OF HYBRID SIMULATION RESULTS

- CASES 2-3 OF TABLE 2
  - HIGH Q CASES SIMILAR TO LOW ALTITUDE, HIGH DYNAMIC PRESSURE CASE PREVIOUSLY DISCUSSED
  - SIMILAR CONCLUSIONS TO LOW ALTITUDE, HIGH PRESSURE CASE

- CASES 4-10 OF TABLE 2
  - EXERCISES INITIAL LARGE ATTITUDE VARIATIONS
  - CONTROLLED SITUATIONS DEMONSTRATE DECOUPLED ATTITUDE CONTROL
  - SOME SENSITIVITY OF RADICAL TO INITIAL PITCH

    (NOTE THAT TERMINAL PITCH ANGLE SAME IN ALL CASES)
  - ROLL ANGLE INTENTIONALLY STABILIZED TO INITIAL VALUE

EJECTION SEAT CONTROL

SUMMARY OF HYBRID SIMULATION RESULTS

- CASES 11-15 (TABLE 2)
  - "MEDIUM" DYNAMIC PRESSURE CASES
  - LARGE INITIAL ATTITUDE VARIATIONS
  - SIMILAR CONCLUSIONS AS IN CASES 4-10
- CASES 16-20 (TABLE 2)
  - HIGH ALTITUDE (45000 FT), HIGH DYNAMIC PRESSURE CASES (600 KEAS)
  - TRANSLATIONAL DYNAMICS MUCH MORE SEVERE THAN SIMILAR KEAS LOW ALTITUDE CASES
  - ACCELERATION RADICAL EXCESSIVE IN CASES 17, 19
  - IMPROVEMENT IN PERFORMANCE EASILY OBTAINABLE BY MORE JUDICIOUS SELECTION OF TERMINAL PITCH ANGLE

EJECTION SEAT CONTROL

MC 68000 μP LIMITATIONS

- NO FLOATING POINT CO-PROCESSOR AVAILABLE
  - REQUIRES USE OF FIXED POINT ARITHMETIC IN IMPLEMENTATION OF CONTROL ALGORITHM
  - TRANSCENDENTAL FUNCTIONS (SIN^{-1}, TAN^{-1}, SIN, COS) GENERATED BY THE FOLLOWING STEPS:
    1. CURVE FITTING OF FUNCTIONS TO POLYNOMIAL OF THIRD ORDER
    2. ADJUSTMENT OF INPUT ARGUMENTS
    3. CONVERSION TO INTEGER FORM BY SCALING
  - EACH VARIABLE ACHARACTERIZED BY MAXIMUM VALUE AND BITS OF PRECISION
  - LEADS TO MUCH ADDITIONAL WORK

EJECTION SEAT CONTROL

MC 68000 µP LIMITATIONS

- HOL IMPLEMENTATION OF CONTROL ALGORITHM
  - —ALGORITHM WRITTEN IN PASCAL WITH FIXED POINT ARITHMETIC
  - —PASCAL TO C LANGUAGE CONVERSION
  - —COMPILATION OF C LANGUAGE INTO ASSEMBLY
  - —LINK OF ALL OBJECT MODULES
  - —CONVERSION OF LINK FILE TO HEXADECIMAL FORMAT

- CONVERSION STEPS LEADS TO INEFFICIENT EXECUTABLE CODE
  - —NON-OPTIMIZED CROSS COMPILER
  - —INEFFICIENT MATRIX/VECTOR OPERATIONS
  - —SLOW EXECUTION OF TRANSCENDENTAL FUNCTIONS
  - —UNACCEPTABLE TIMING RESULTS

EJECTION SEAT CONTROL

MC 68000 μP LIMITATIONS

- DIRECT IMPLEMENTATION OF ALGORITHM IN ASSEMBLY LANGUAGE ONLY
  OBVIOUS MEANS OF PRODUCING EFFICIENT CODE WITH CURRENT CONFIGURATION

- ASSEMBLY LANGUAGE ADVANTAGES
  - IMMEDIATE ACCESS TO MEMORY AND DATA REGISTERS
  - CONSTANTS BUILT INTO TRANCENDENTAL FUNCTION EVALUATIONS
  - REDUCTION OF OVERHEAD IN ACCESS OF PRIMITIVE FUNCTIONS (+,-,x,/)
    BY ELIMINATING "JUMP TO SUBROUTINE" INSTRUCTIONS
  - GREAT IMPROVEMENT IN EXECUTION SPEED

EJECTION SEAT CONTROL

MC 68000 µP MEASUREMENTS

- MEMORY AND TIMING ESTIMATES (8 MHZ SYSTEM CLOCK)

	PASCAL CODE	ASSEMBLY CODE
MEMORY	22K	20K
TIMING	0.28 s/cycles (3.5 HZ)	0.007 s/cycles (130 HZ)*
		0.01 s/cycles (100 HZ)**

*NO I/O INCLUDED

**I/O INCLUDED

- ALGORITHM REQUIREMENT

  ALGORITHM EXECUTES AT 50 HZ SO THAT ASSEMBLY CODE IS FEASIBLE

  HOL IMPLEMENTATION NOT FEASIBLE WITH CURRENT COMPILER

EJECTION SEAT CONTROL

MODELING RESTRICTIONS WITH CURRENT HYBRID SIMULATION

- IDEALIZED AERODYNAMIC MODEL
  - SLED TESTS USUALLY INDICATE STOCHASTIC VARIATION IN AERODYNAMIC MOMENTS AND FORCES
- IDEALIZED ACTUATOR CONFIGURATION
  - NO LIMITS IMPOSED ON THRUST MAGNITUDES OF ROCKETS
  - ARBITRARY ROCKET POINTING ANGLES
- FIXED PARAMETERS
  - NO VARIATION IN MASS, MOMENT OF INERTIA PROPERTIES
  - CONSTANT C.G. LOCATION
- SIMPLIFIED RESPONSE MODELS FOR SENSORS AND ACTUATORS
  - LIMITED TO FIRST ORDER

EJECTION SEAT CONTROL

DIGITAL RESULTS WITH MMOA ROCKET CONFIGURATION

- DESIGN AS PROPOSED BY AL CIAPONI, MMOA
- MAIN THRUSTER GIMBALLED
- 6 ATTITUDE CONTROL ROCKETS (2 PITCH, 2 ROLL, 2 YAW)
- CASES INVESTIGATED
  - LOW ALTITUDE, HIGH DYNAMIC PRESSURE
  - HIGH ALTITUDE, HIGH DYNAMIC PRESSURE
  - SELECTED MIL CASES

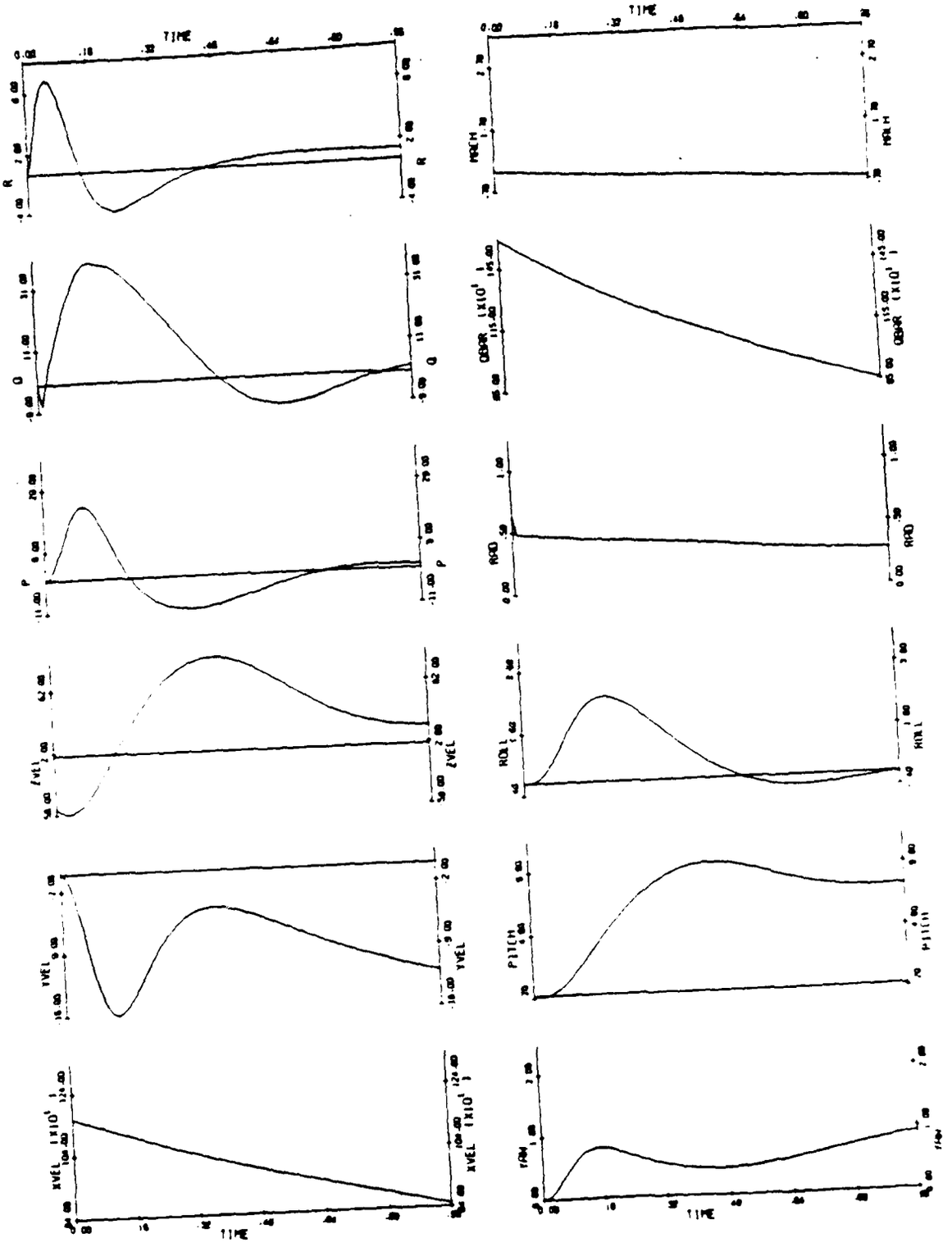

Figure 7.53. LOHHIQ02

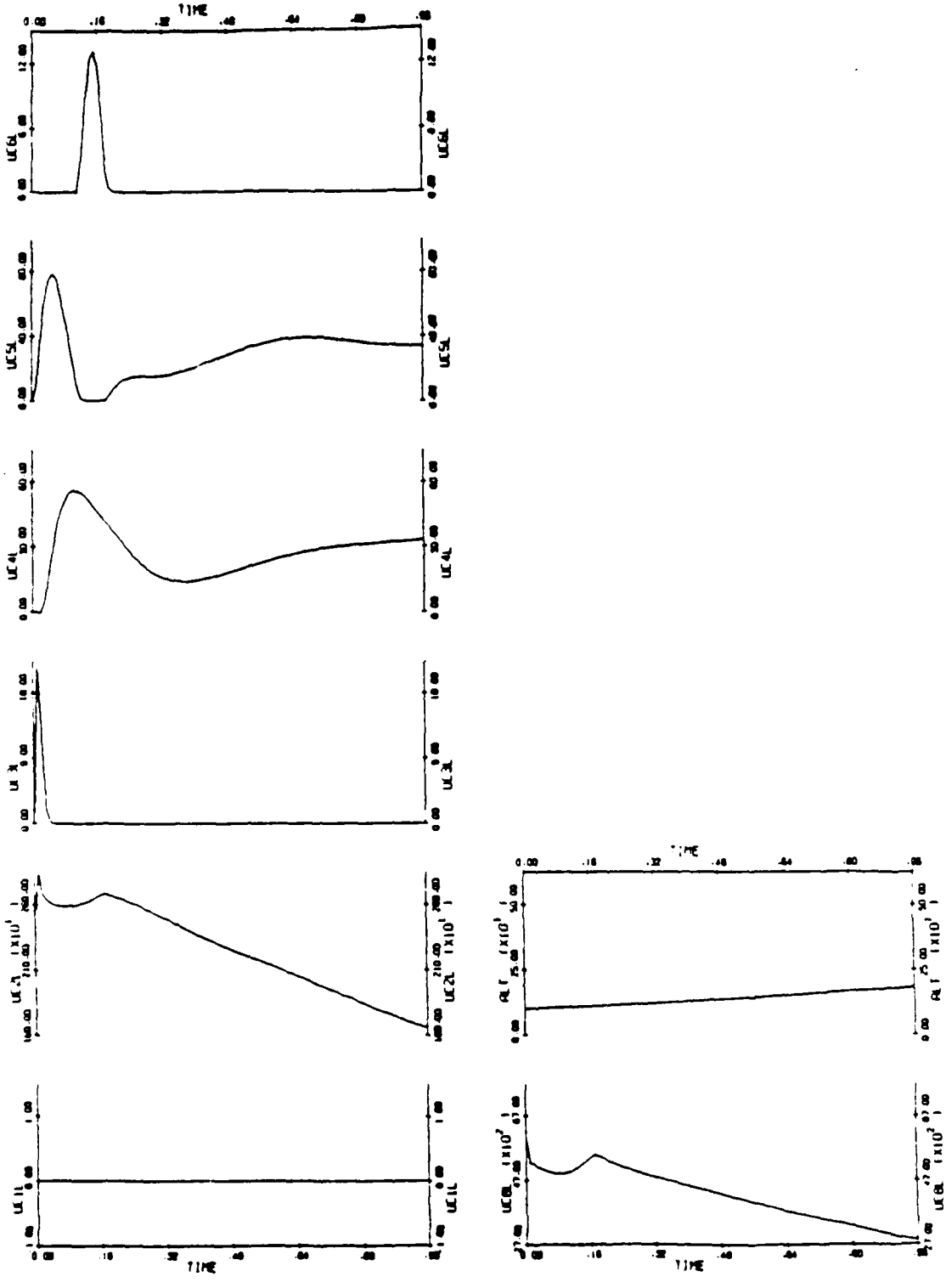

Figure 7.54. LOHHIQ02 (Continued).

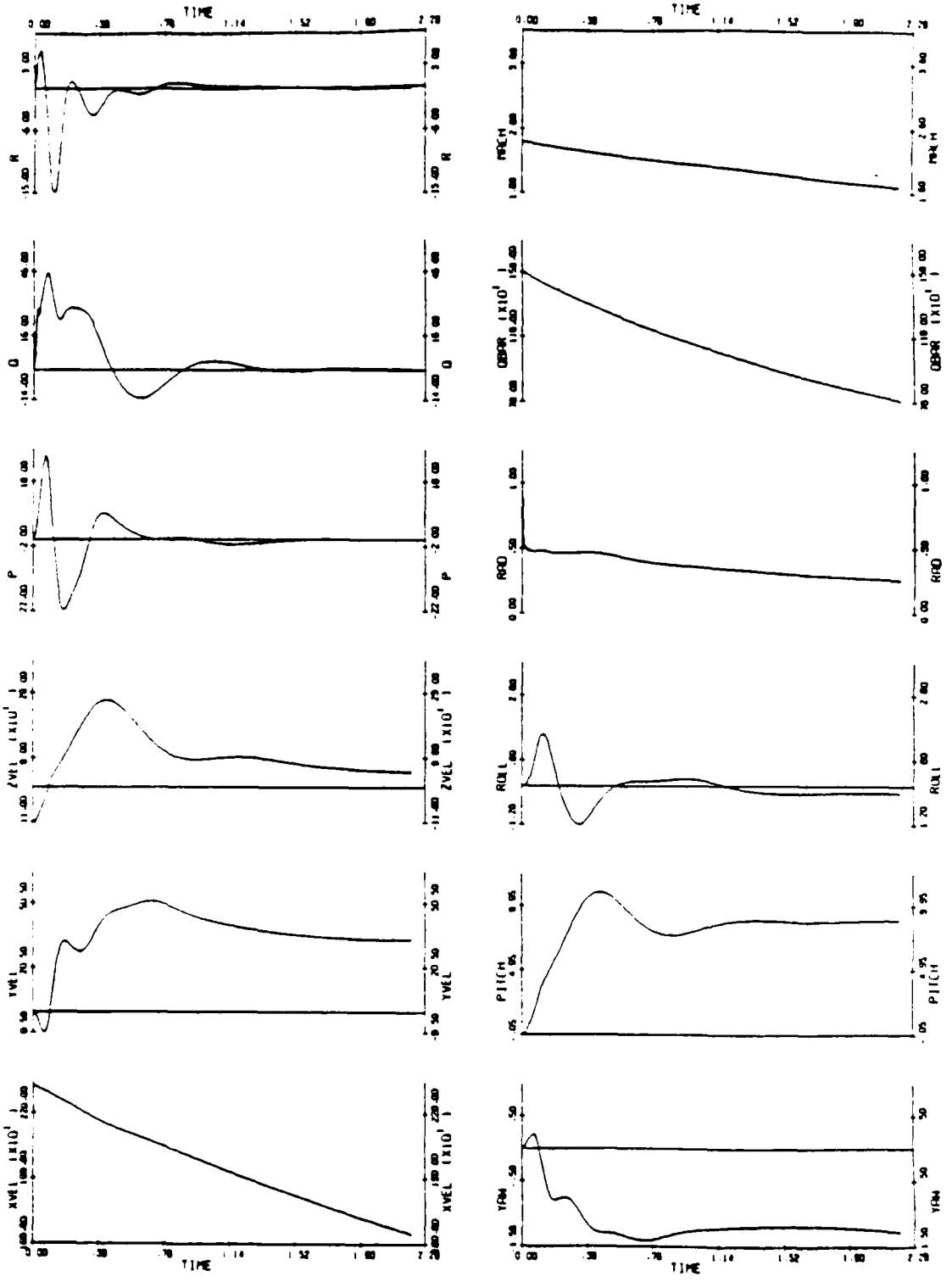

Figure 7.55. HIHHIQ02

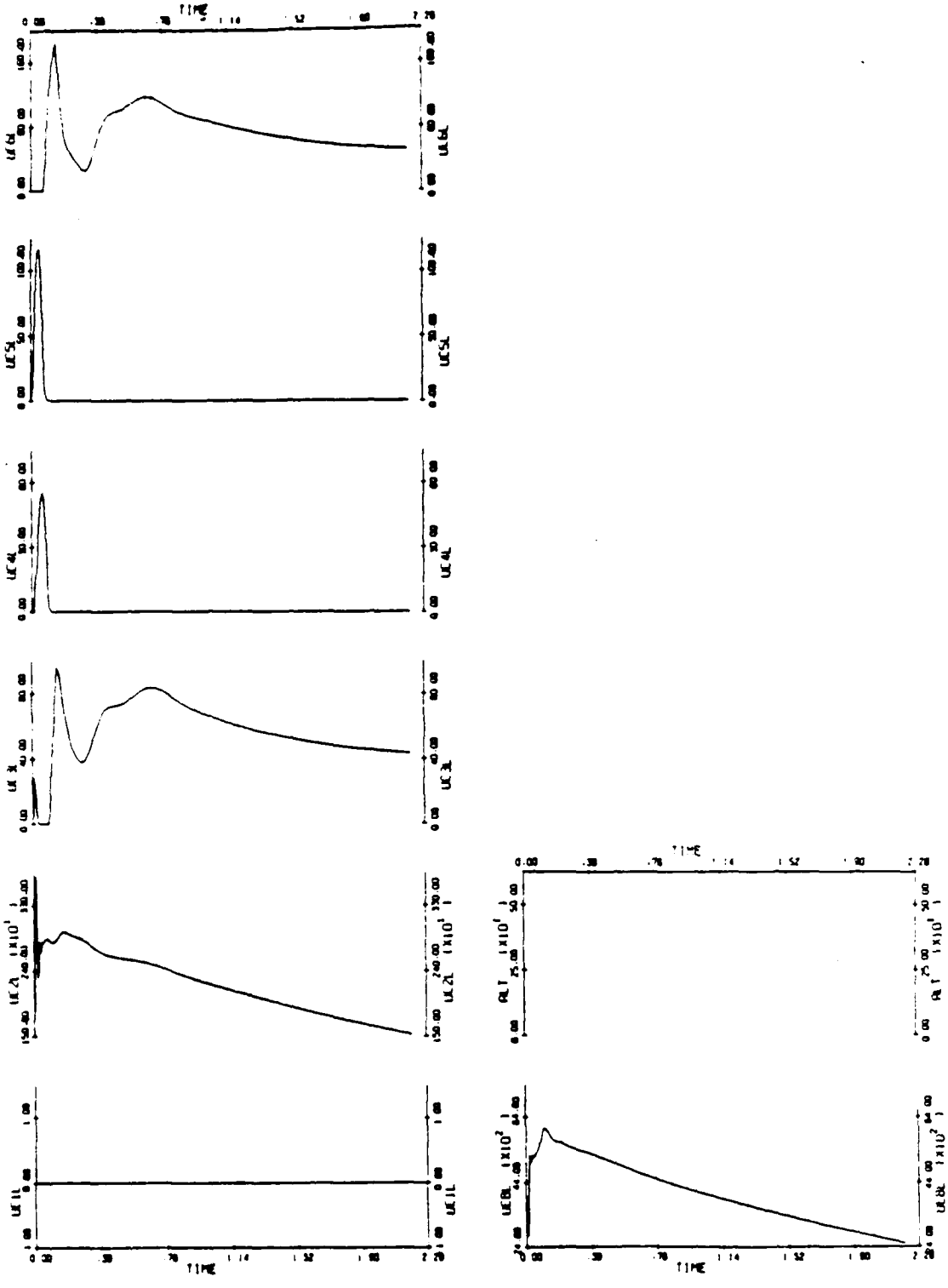

Figure 7.56. HIHHIQ02 (Continued).

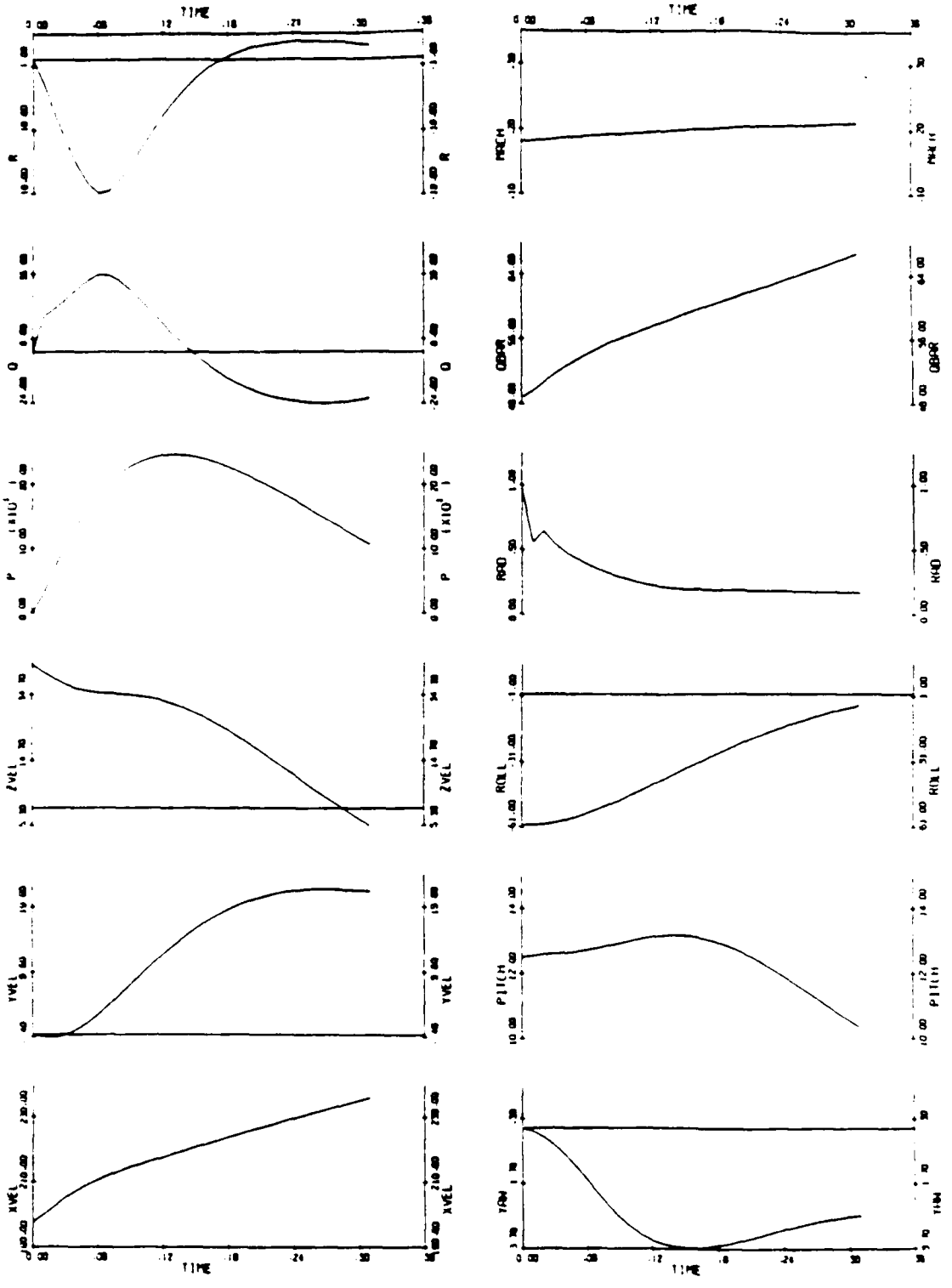

Figure 7.57. MIL102

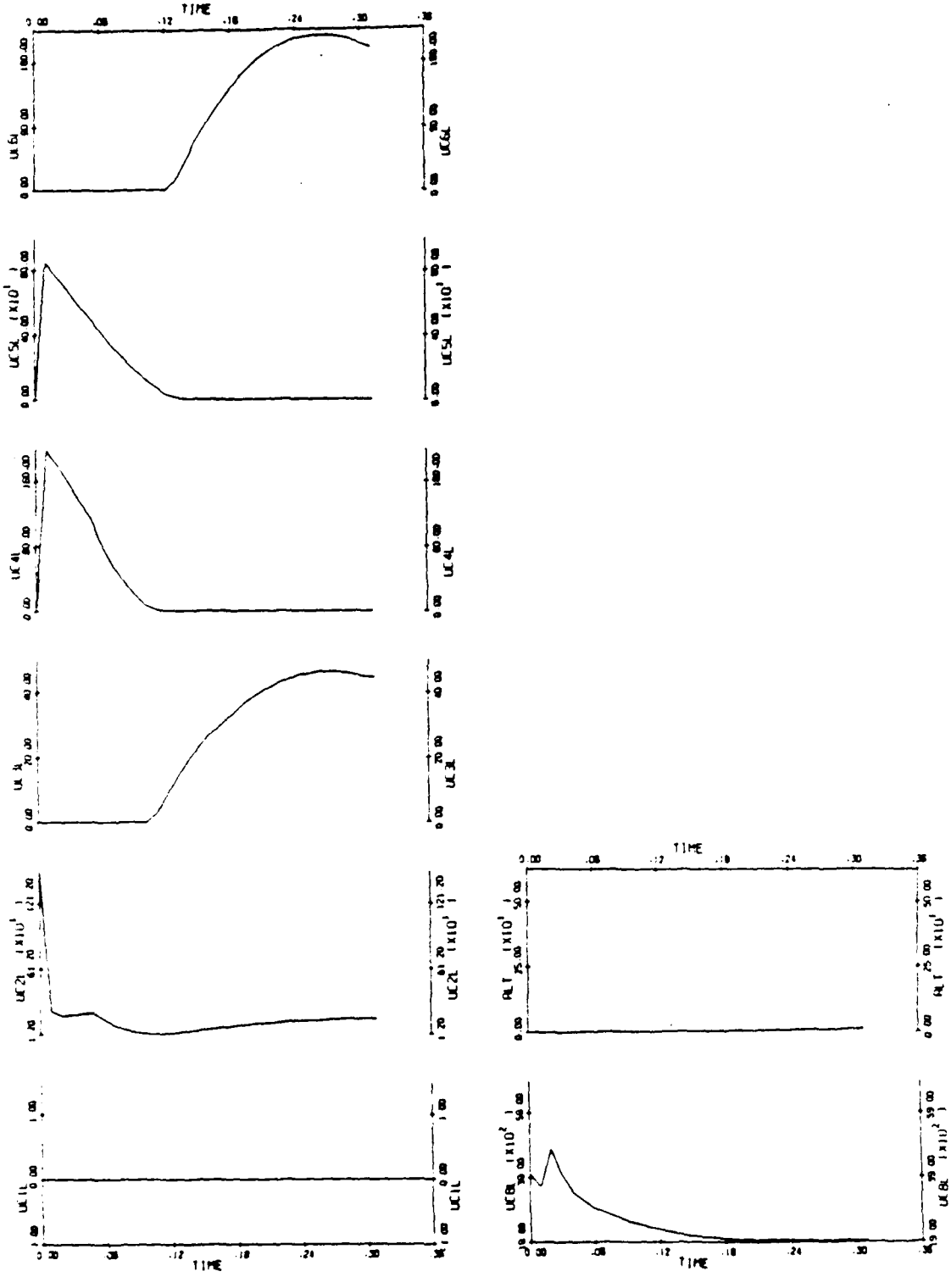

Figure 7.58. MIL102 (Continued).

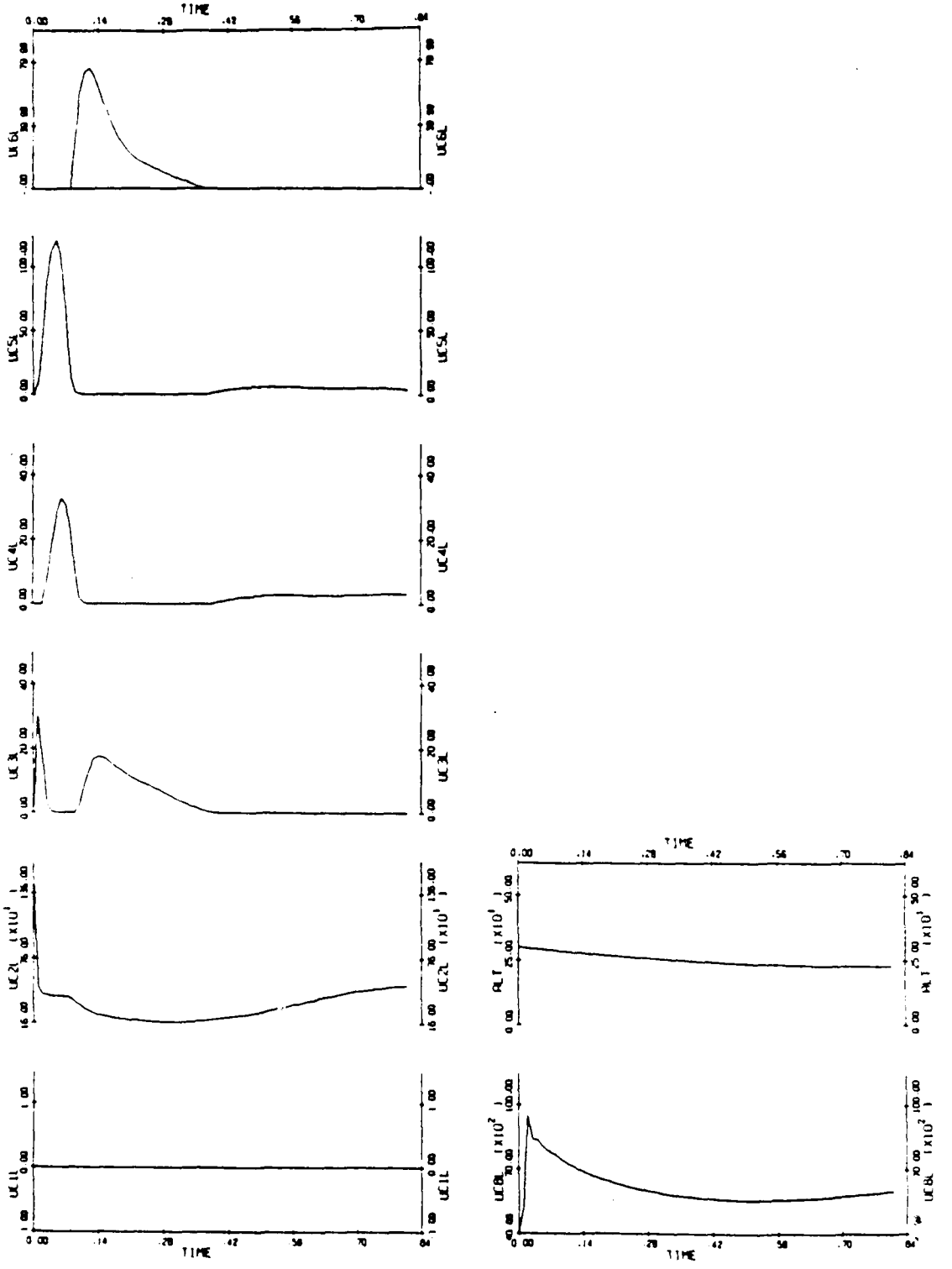

Figure 7.59. MIL302

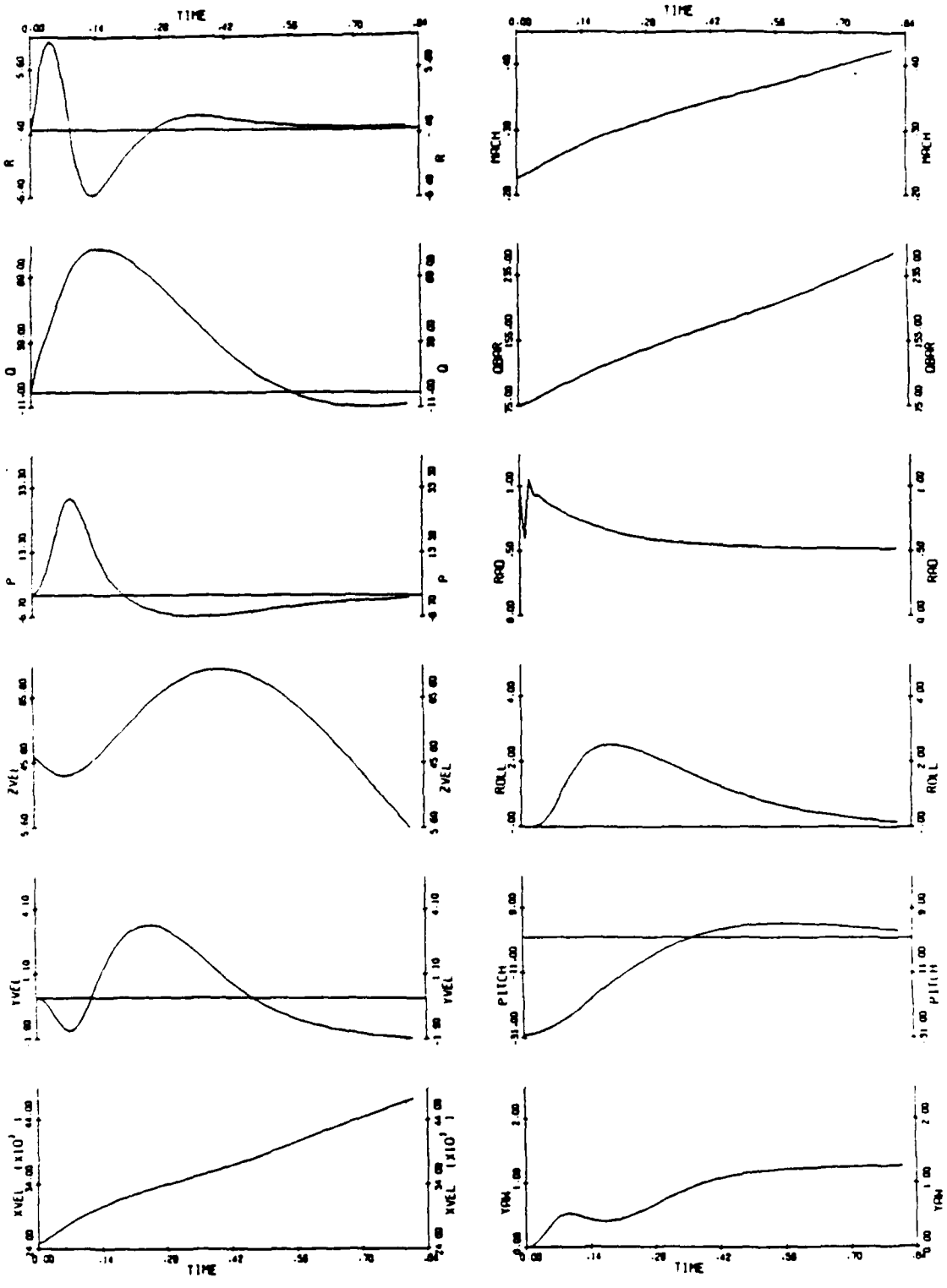

Figure 7.60. MIL302 (Continued).

EJECTION SEAT CONTROL

CONTROL SCHEME EXTENSIONS

- WORK PERFORMED UNDER CONTRACT WITH BOEING AEROSPACE TO INVESTIGATE BOEING EJECTION SEAT DESIGN FOR CREST
- NOT AT LIBERTY TO DISCUSS CONFIGURATION DESIGN OR SIMULATION RESULTS
- EFFECTS MODELED
  - REALISTIC ACTUATION SYSTEM
  - WIND GUSTS
  - MODEL/CONTROLLER MISMATCH IN ESTIMATE OF MASS/MOMENT OF INERTIA
    (MODEL: 99 %, CONTROLLER: 50 % PILOT)
  - PILOT DYNAMIC RESPONSE INDEX
  - AVOIDANCE OF TAIL COLLISIONS

U=UNCONTROLLED, S=SIMULATION (PE 8/32), H=HARDWARE (MC 68000)

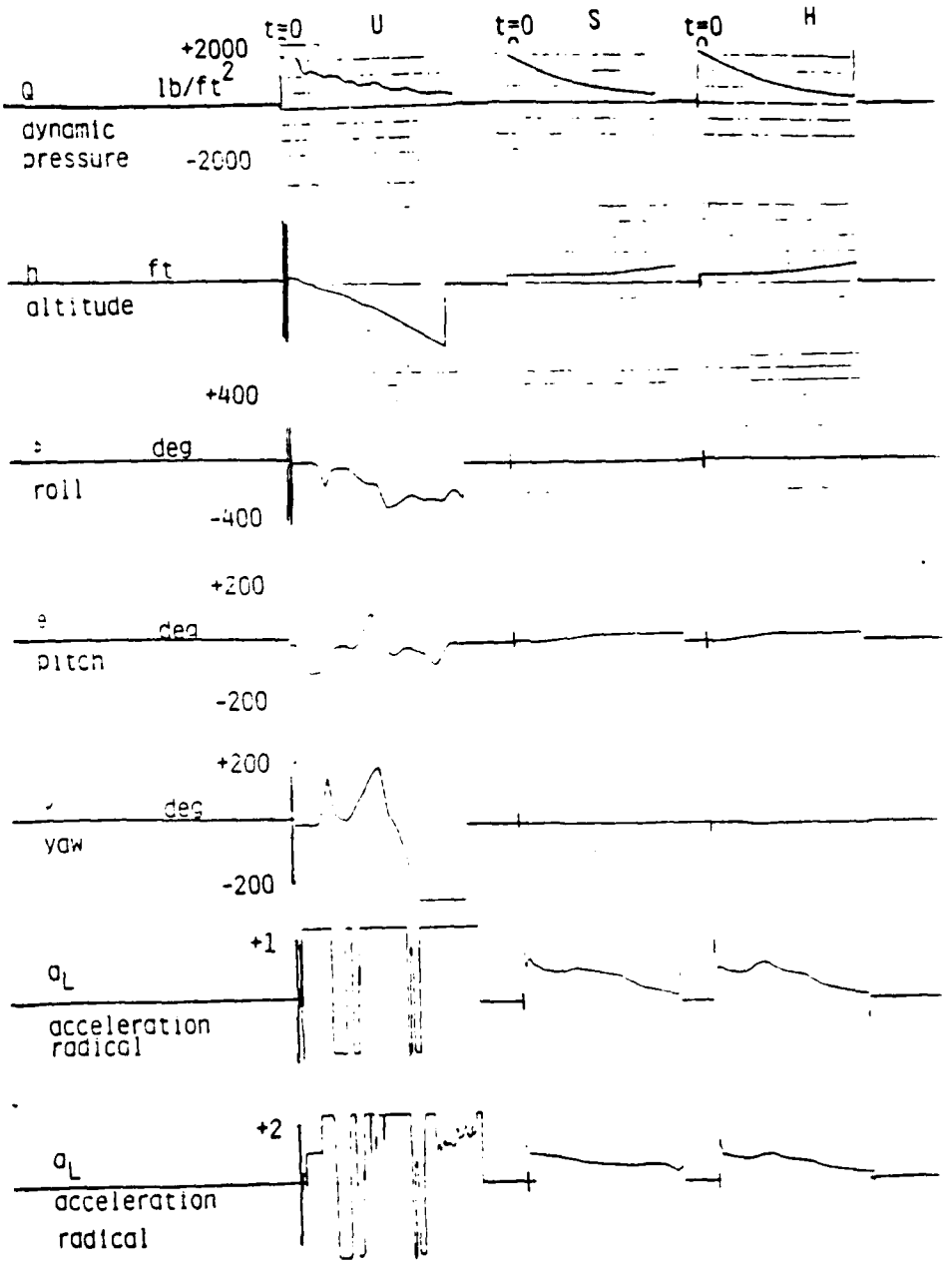

Figure 7.61 Low Altitude, High Q

U=UNCONTROLLED, S=SIMULATION (PE 8/32), H=HARDWARE (MC 68000)

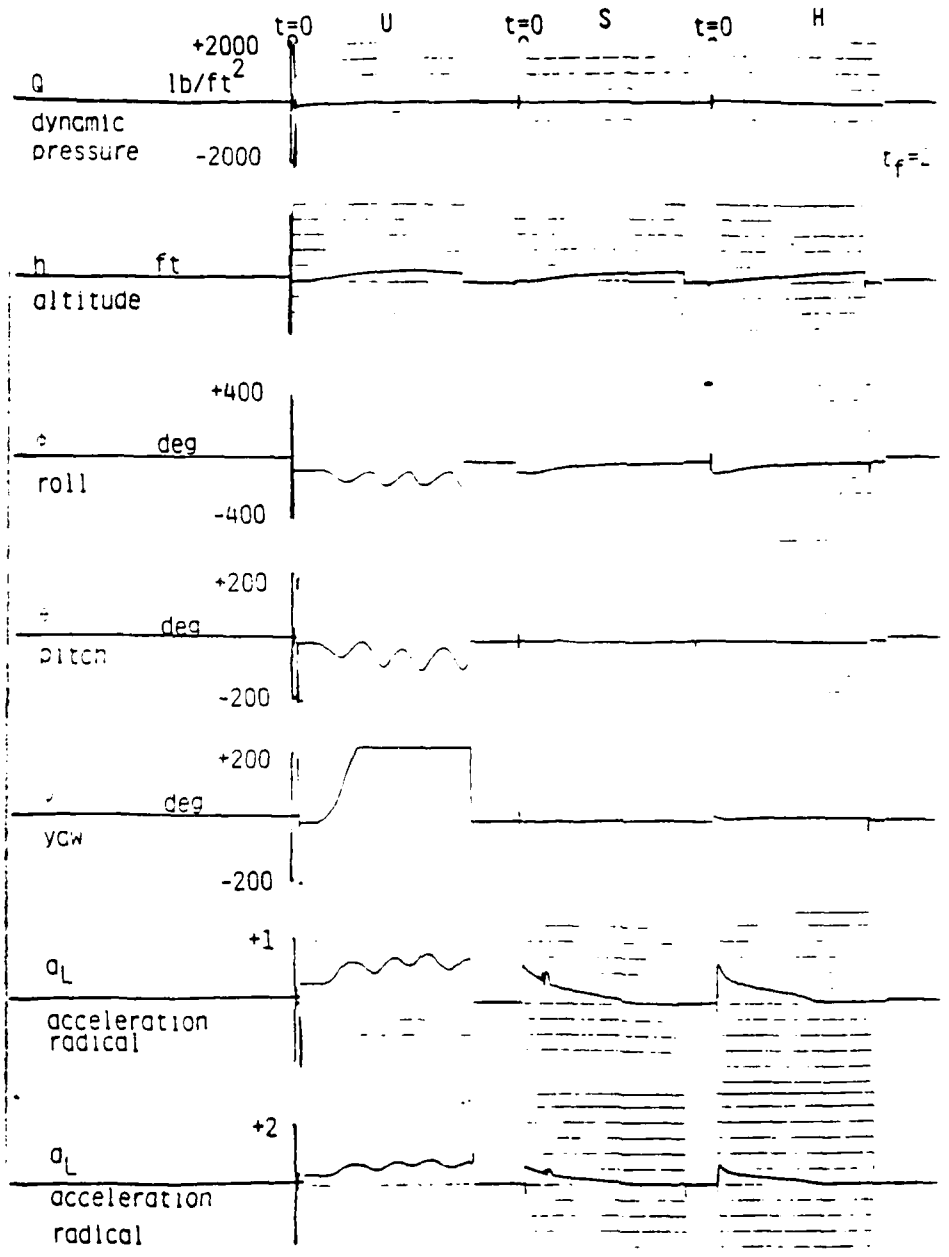

Figure 7.62 MIL 1 (Table 1)

U=UNCONTROLLED, S=SIMULATION (PE 8/32), H=HARDWARE (MC 68000)

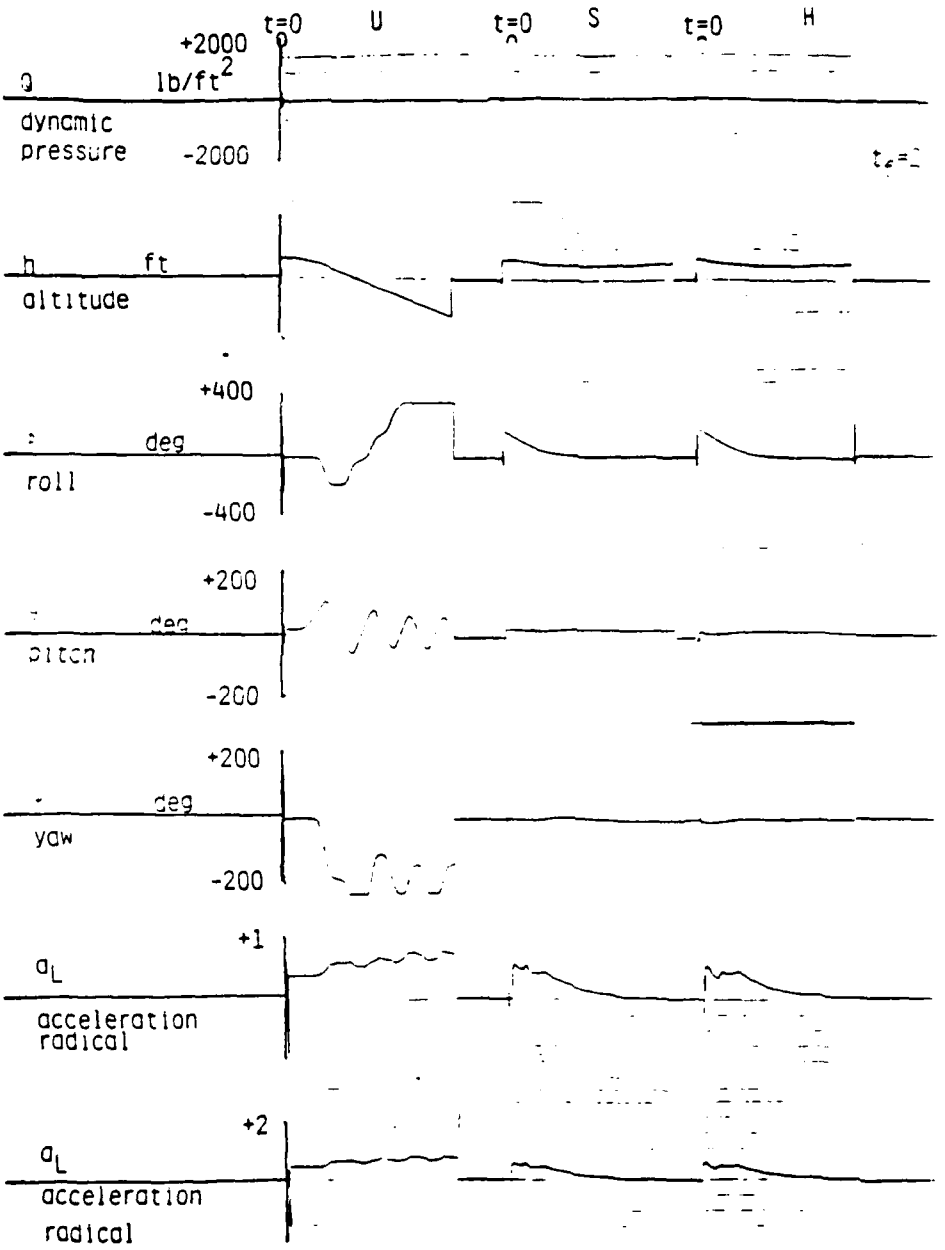

Figure 7.63 MIL 2 (Table 1)

U=UNCONTROLLED, S=SIMULATION (PE 8/32), H=HARDWARE (MC 68000)

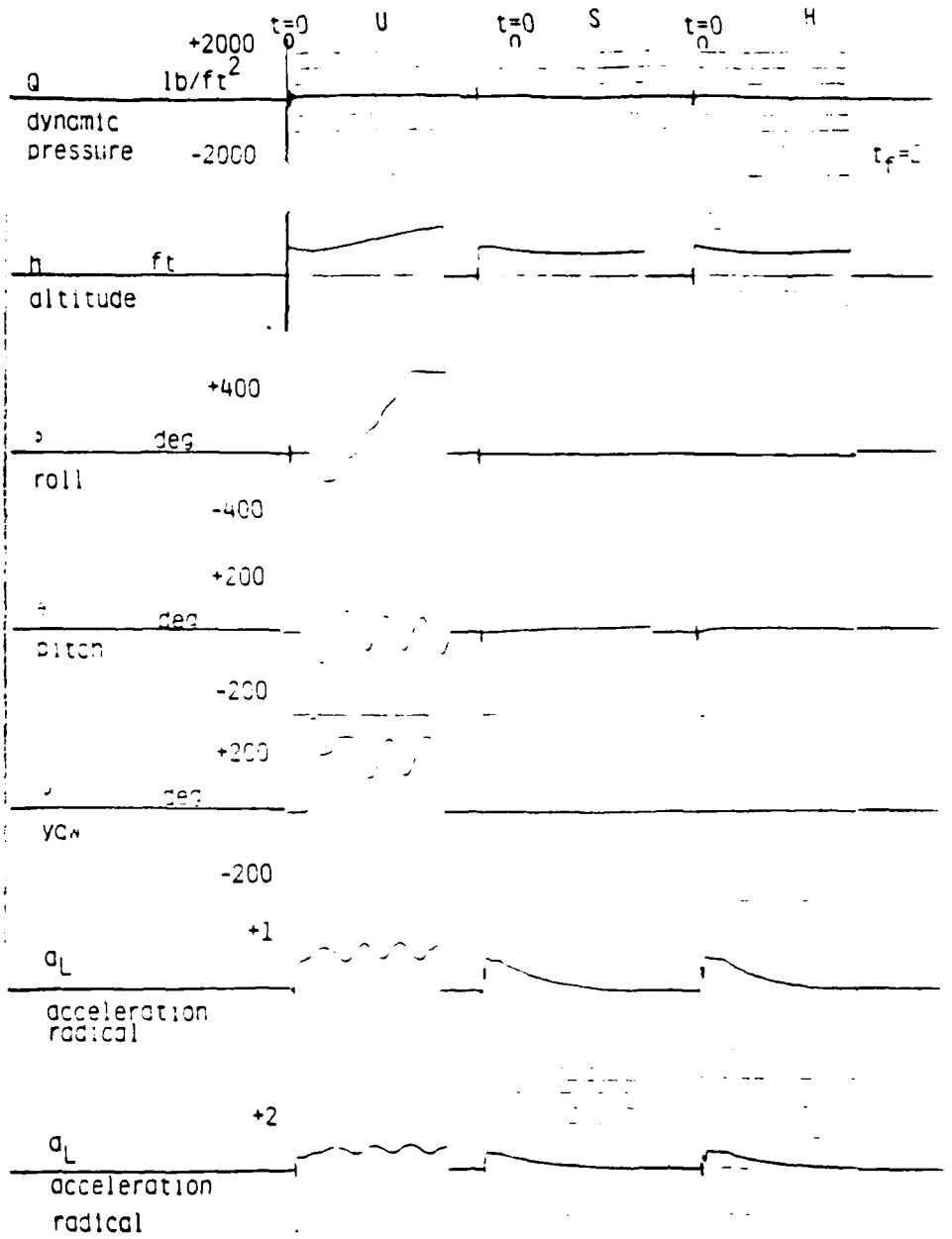

Figure 7.64 MIL 3 (Table 1)

U=UNCONTROLLED. S=SIMULATION (PE 8/32). H=HARDWARE (MC 68000)

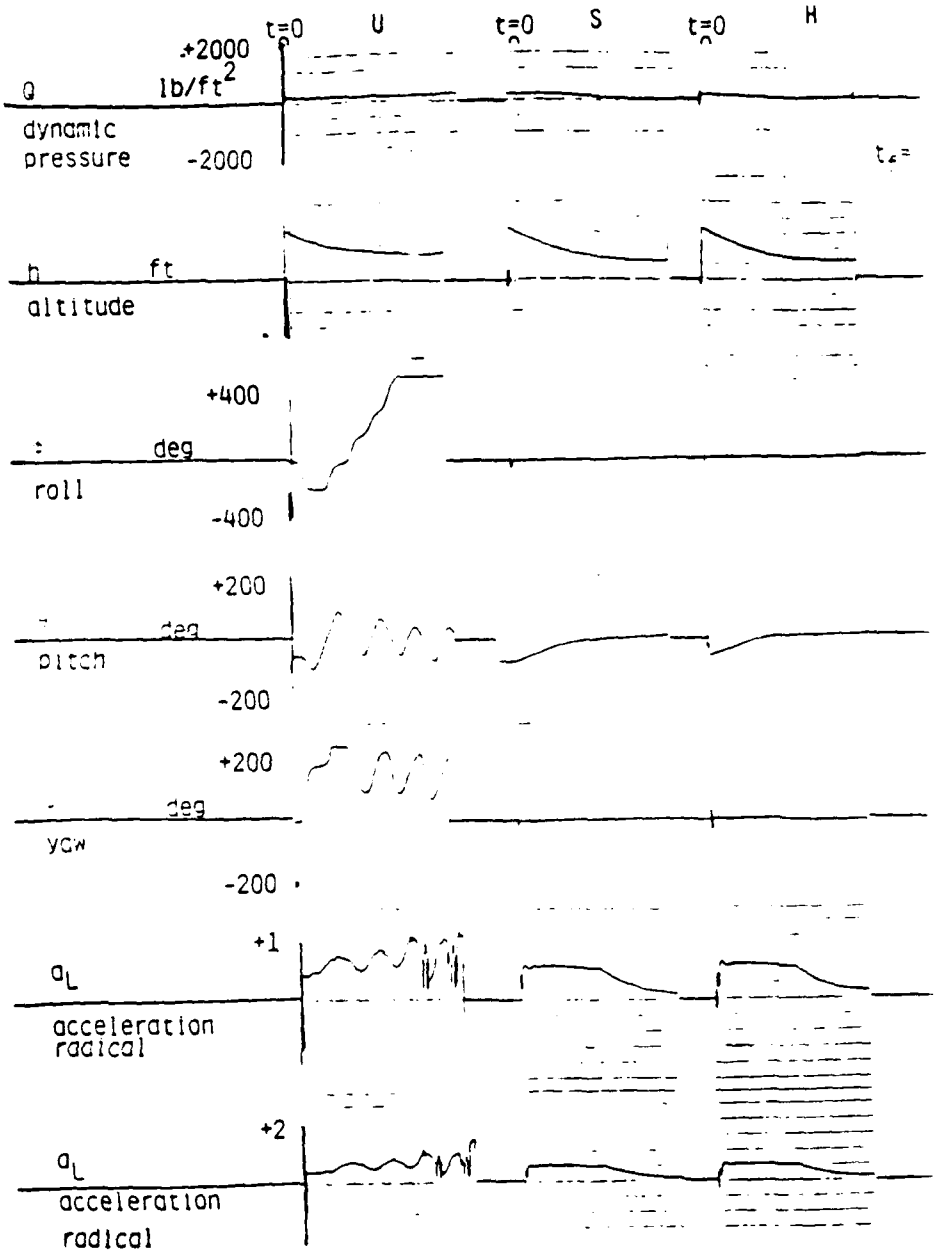

Figure 7.65 MIL 4 (Table 1)

U=UNCONTROLLED, S=SIMULATION (PE 8/32). H=HARDWARE (MC 68000)

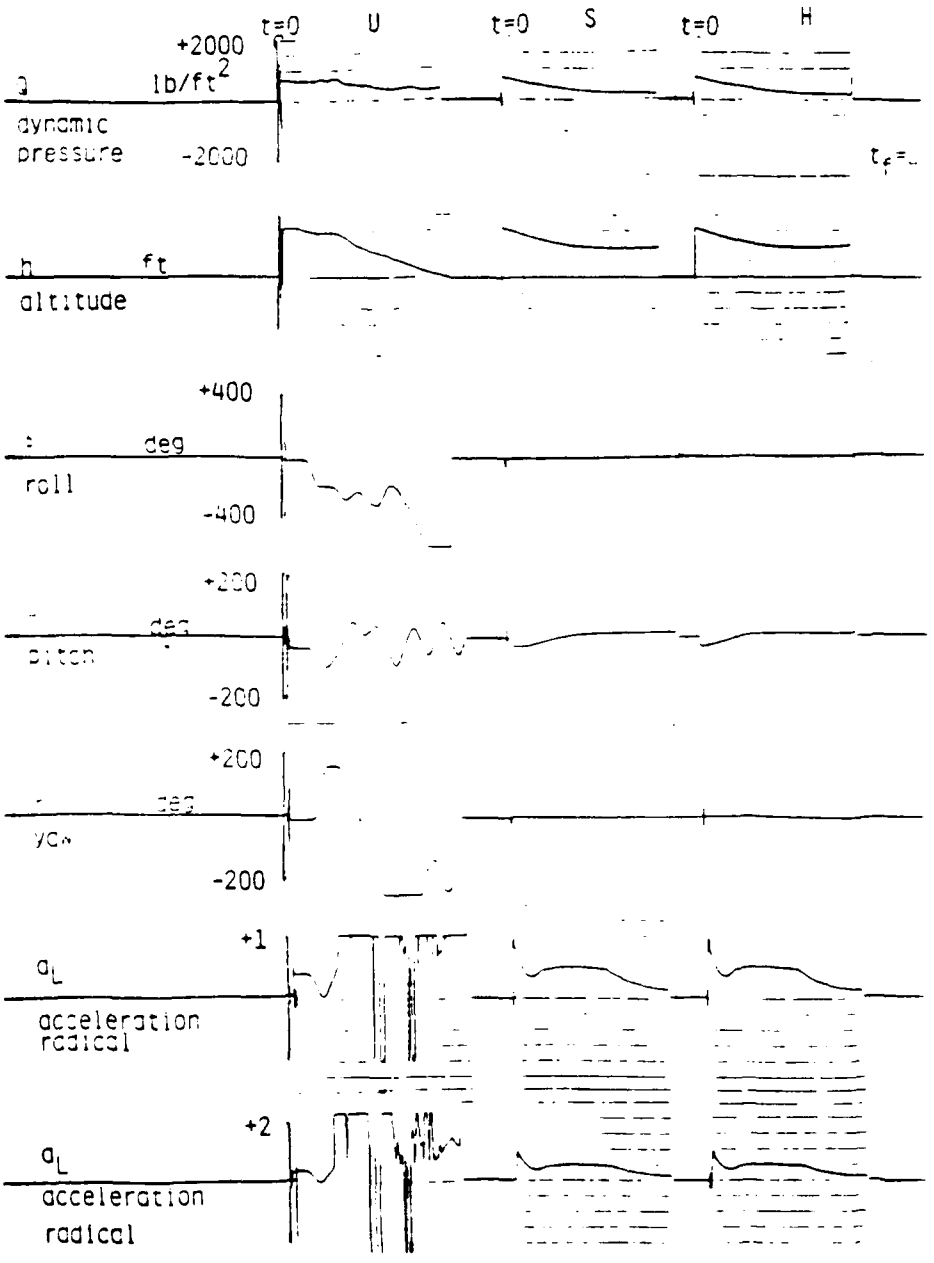

Figure 7.66 MIL 5 (Table 1)

U=UNCONTROLLED, S=SIMULATION (PE 8/32), H=HARDWARE (MC 68000)

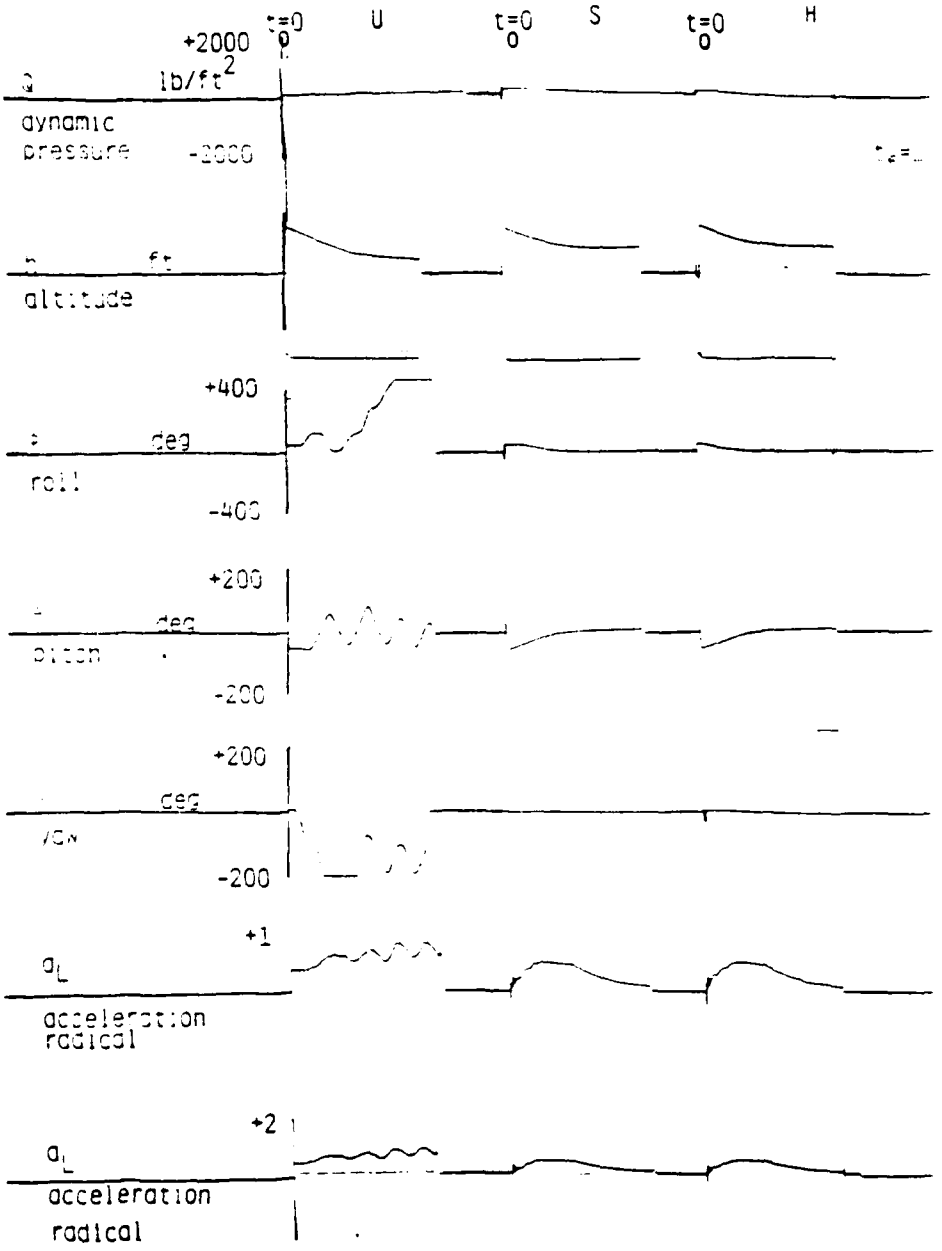

Figure 7.67 MIL 6 (Table 1)

U=UNCONTROLLED, S=SIMULATION (PE 8/32), H=HARDWARE (MC 68000)

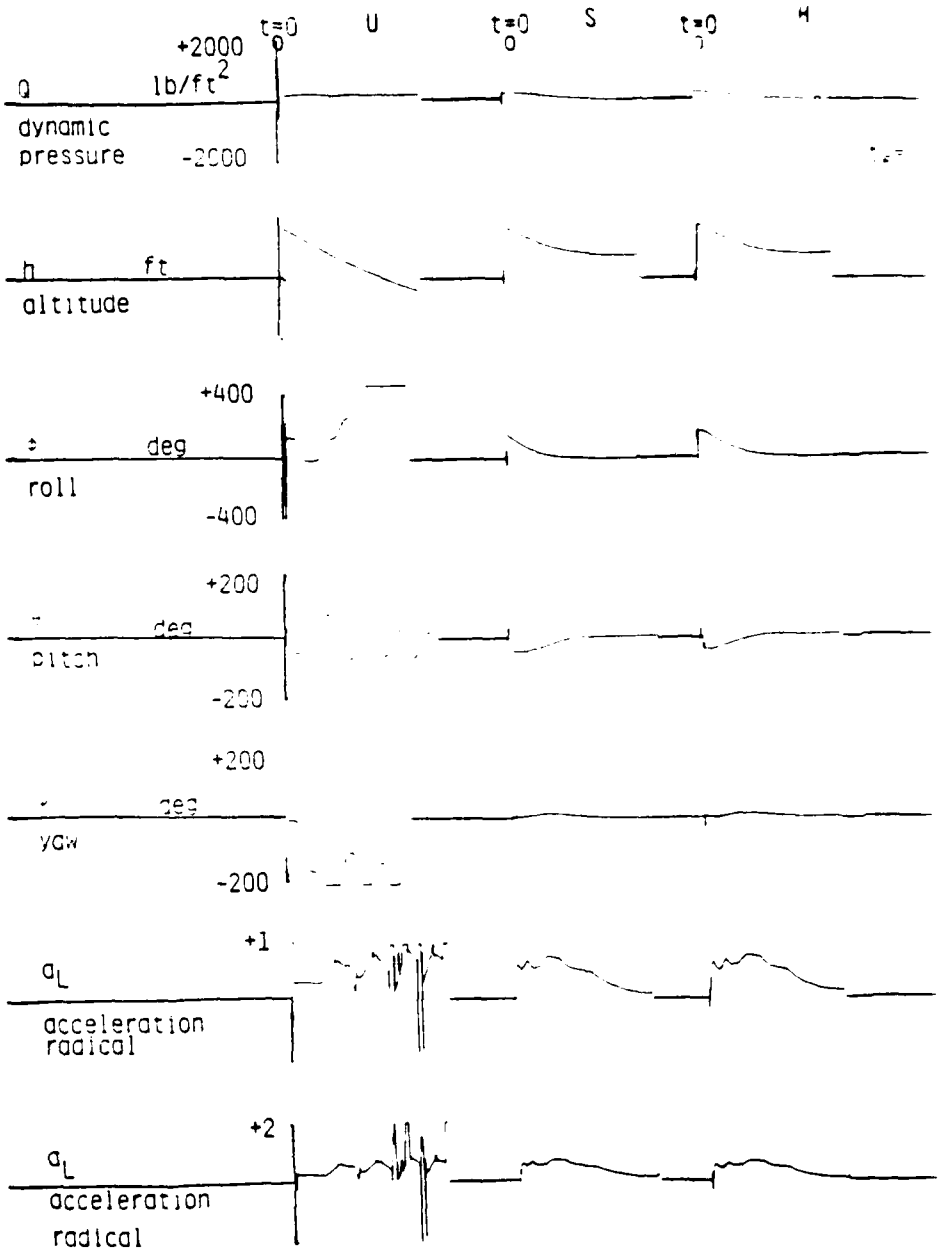

Figure 7.68 MIL 7 (Table 1)

U=UNCONTROLLED, S=SIMULATION (PE 8/32), H=HARDWARE (MC 68000)

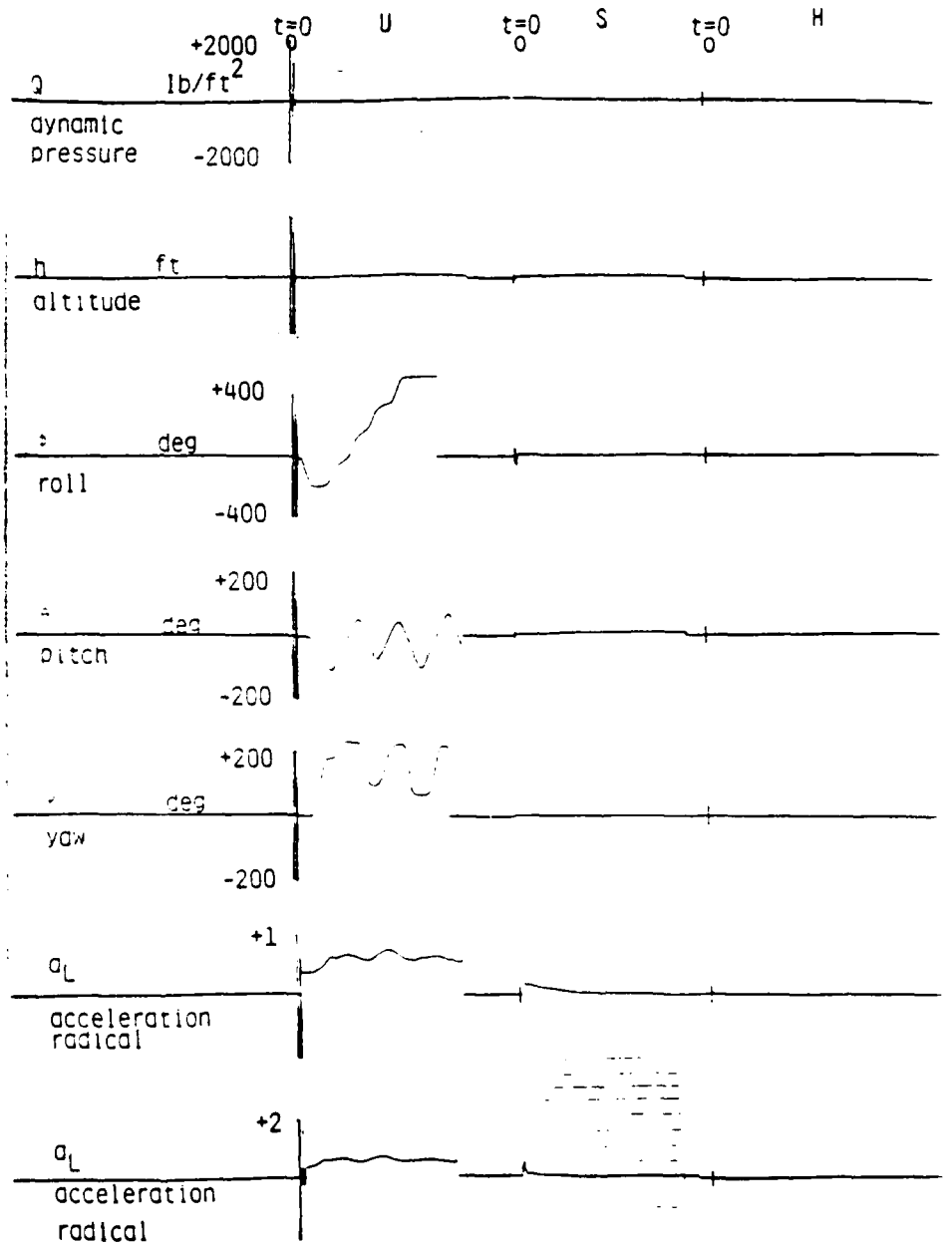

Figure 7.69 Case 1 (Table 2)

U=UNCONTROLLED, S=SIMULATION (PE 8/32), H=HARDWARE (MC 68000)

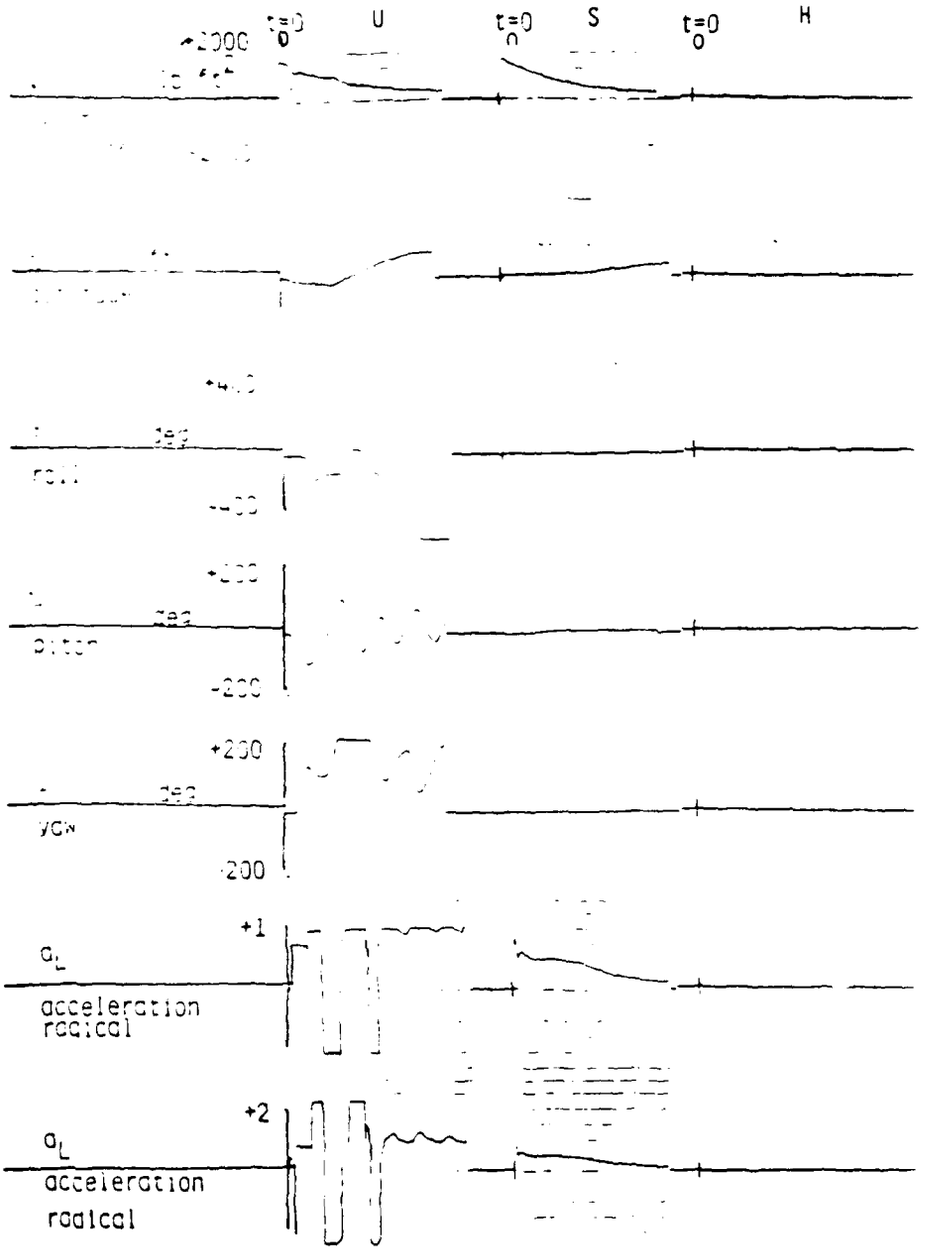

Figure 7.70 Case 2 (Table 2)

U=UNCONTROLLED, S=SIMULATION (PE 8/32). H=HARDWARE (MC 68000)

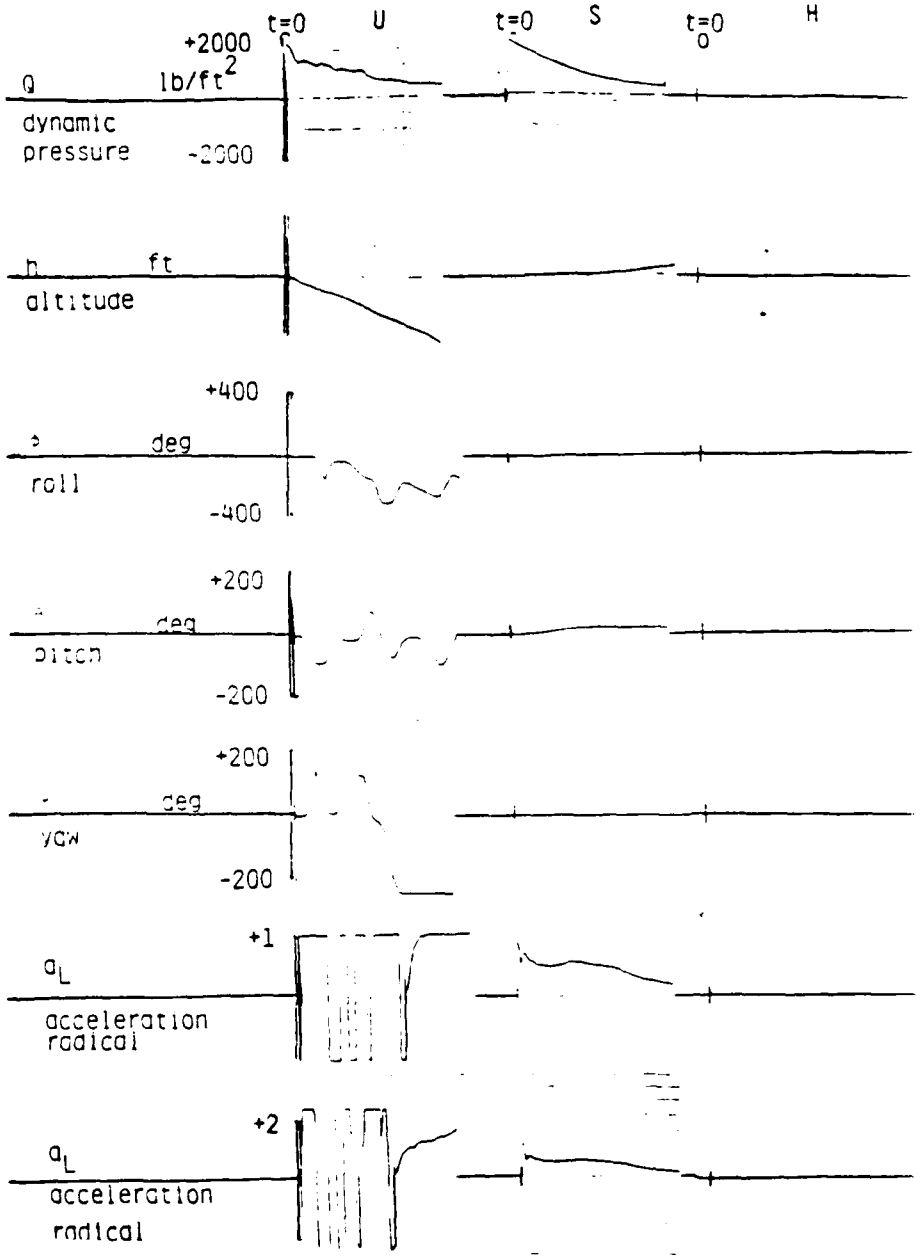

Figure 7.71 Case 3 (Table 2)

U=UNCONTROLLED, S=SIMULATION (PE 8/32), H=HARDWARE (MC 68000)

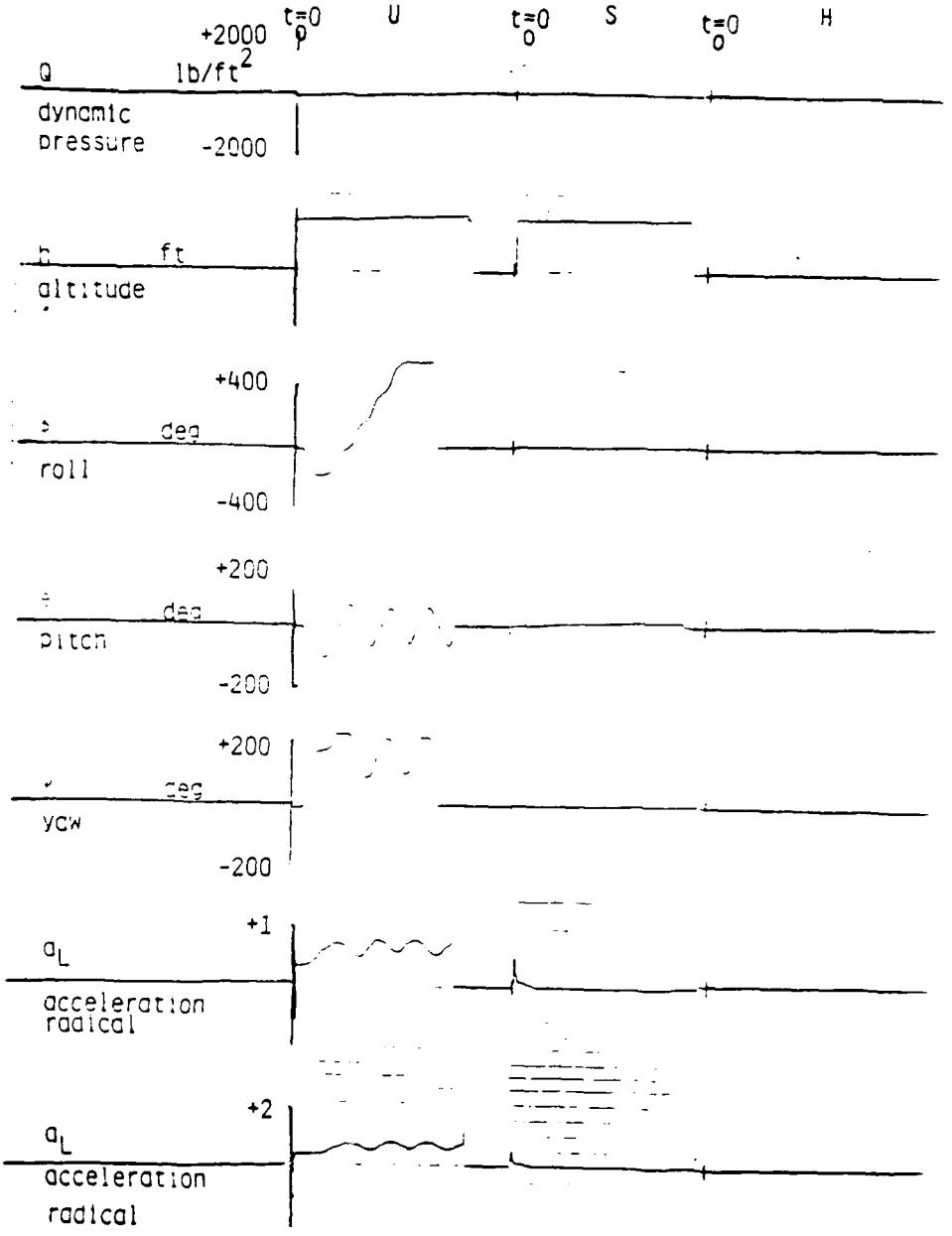

Figure 7.72 Case 4 (Table 2)

U=UNCONTROLLED, S=SIMULATION (PE 8/32), H=HARDWARE (MC 68000).

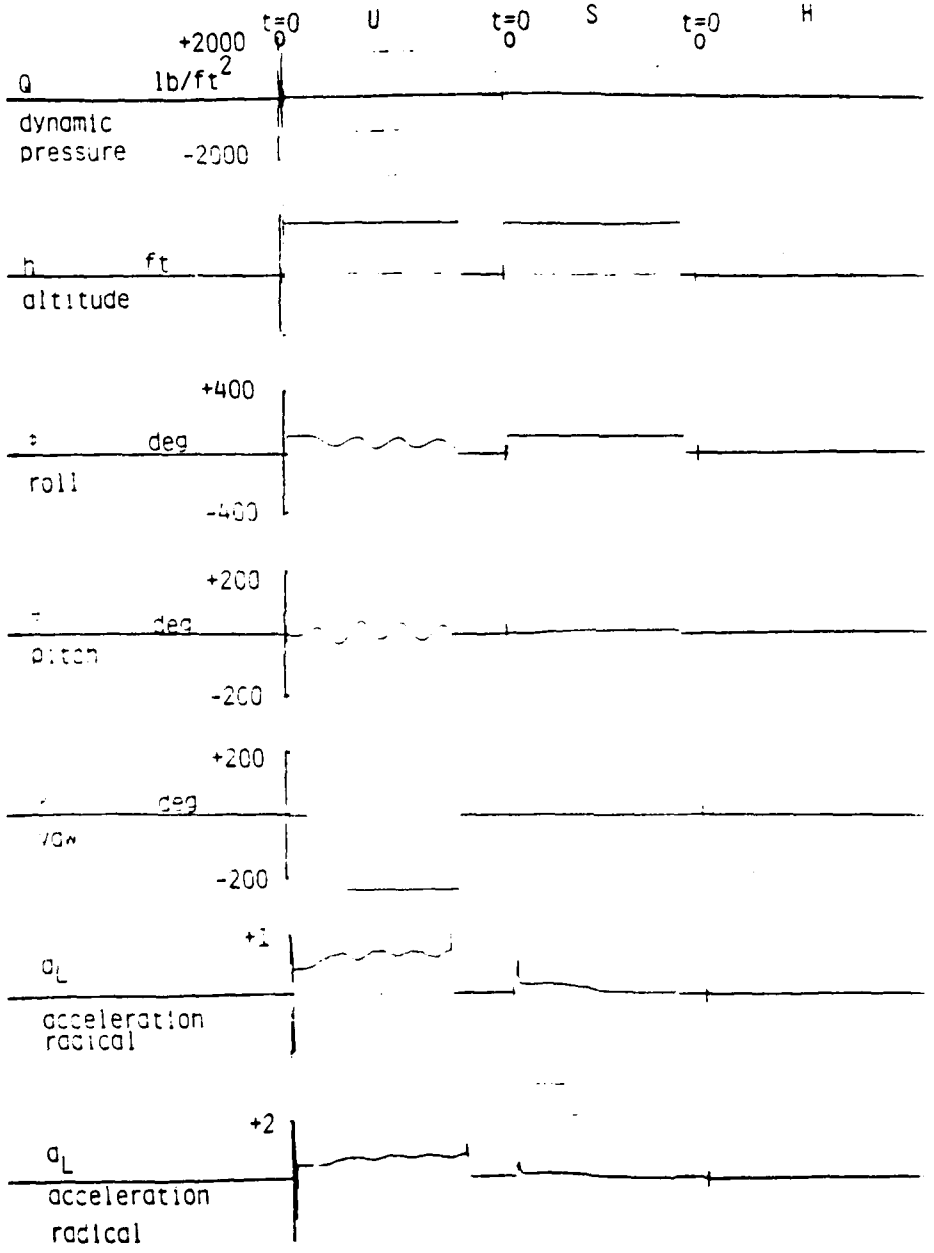

Figure 7.73 Case 5 (Table 2)

U=UNCONTROLLED, S=SIMULATION (PE 8/32), H=HARDWARE (MC 68000).

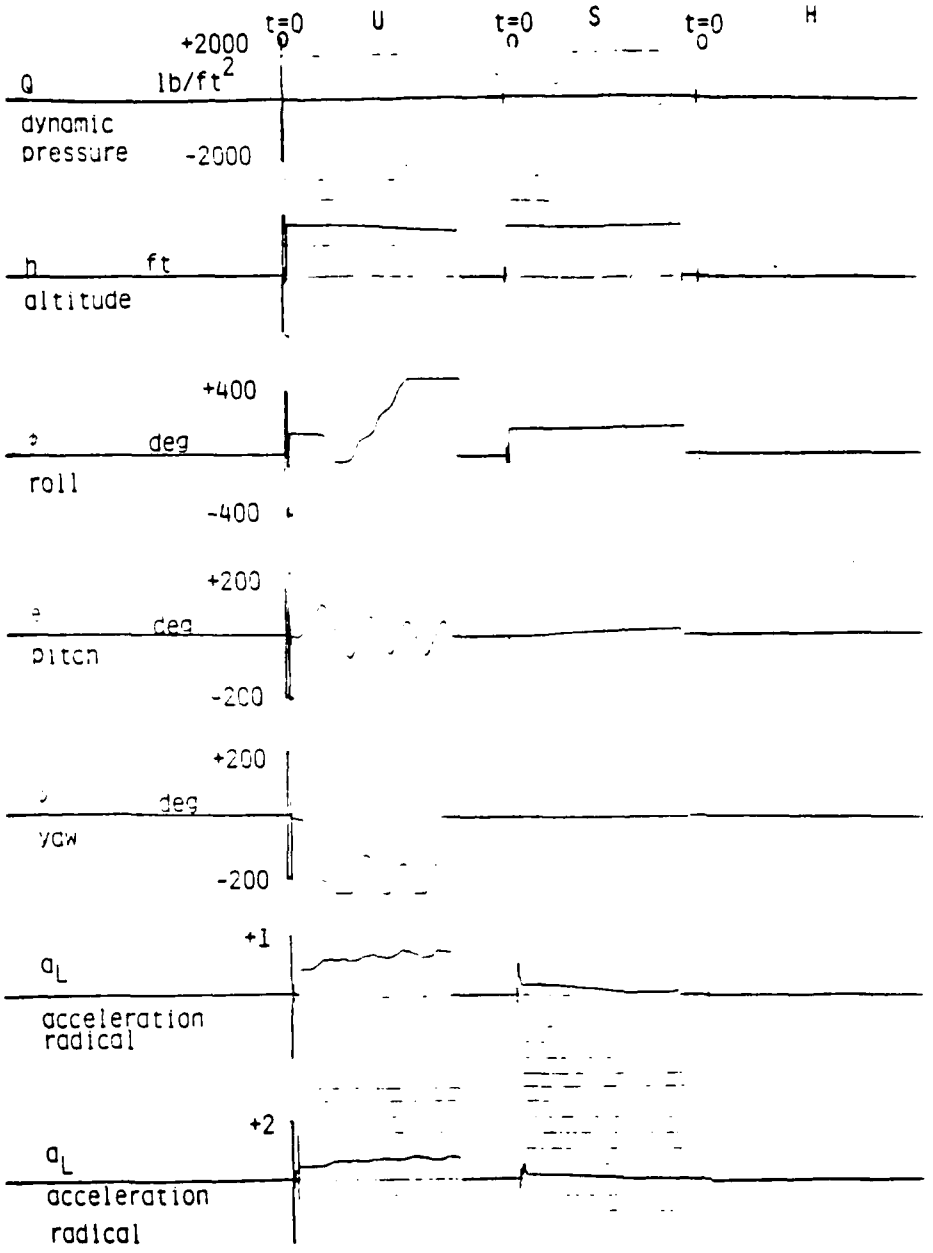

Figure 7.74 Case 6 (Table 2)

U=UNCONTROLLED, S=SIMULATION (PE 8/32). H=HARDWARE (MC 68000)

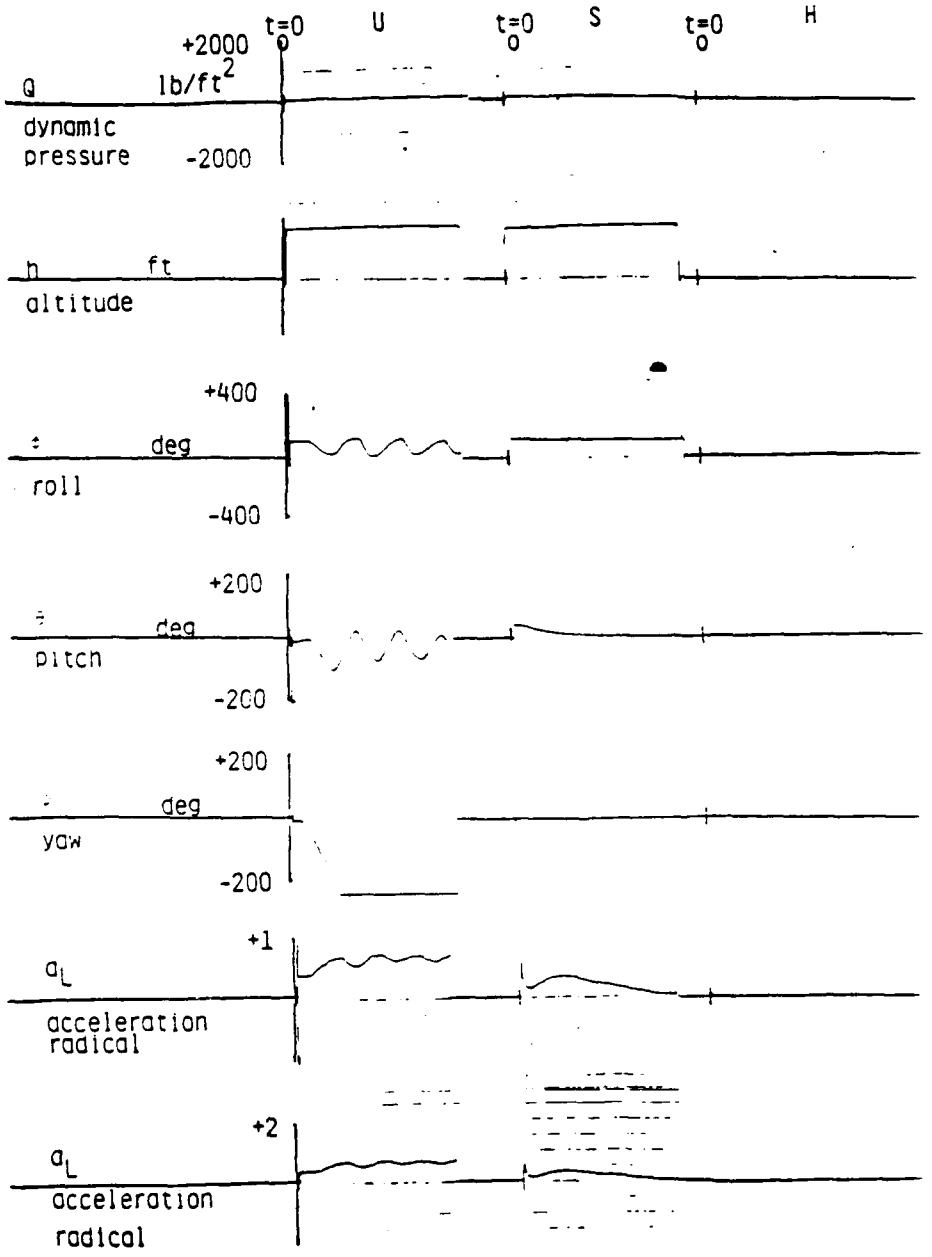

Figure 7.75 Case 7 (Table 2)

U=UNCONTROLLED, S=SIMULATION (PE 8/32), H=HARDWARE (MC 68000)

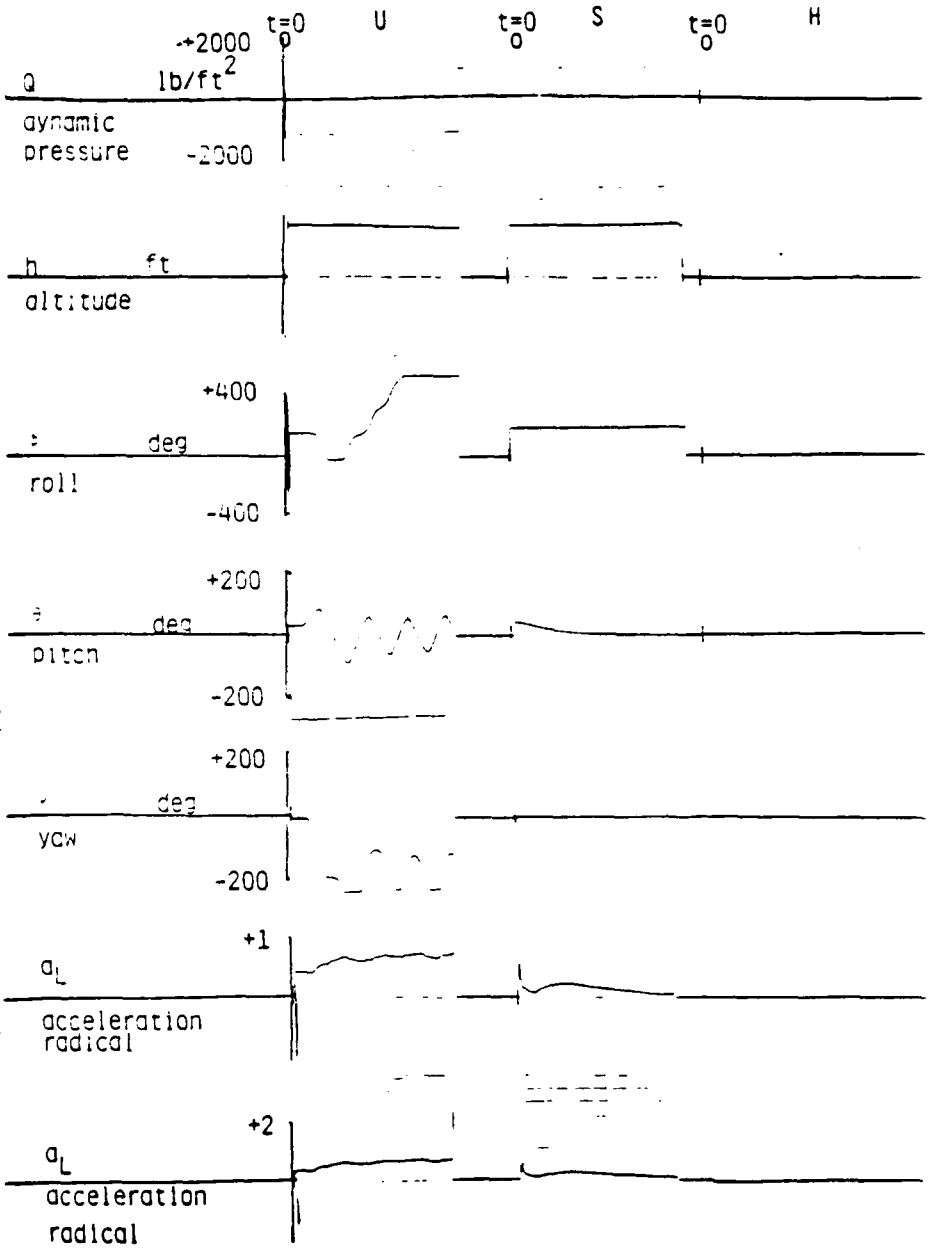

Figure 7.76 Case 8 (Table 2)

U=UNCONTROLLED, S=SIMULATION (PE 8/32), H=HARDWARE (MC 68000)

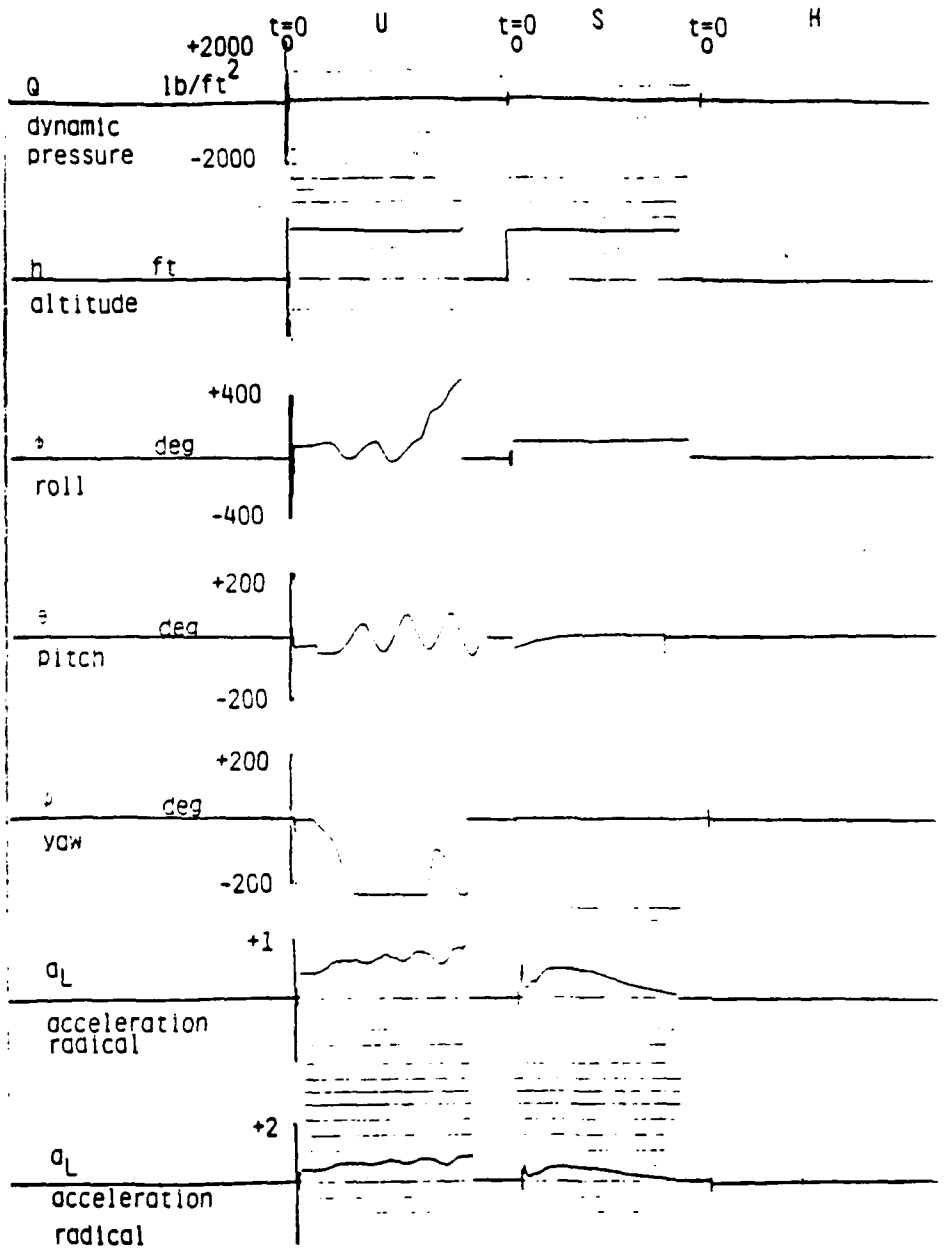

Figure 7.77 Case 9 (Table 2)

U=UNCONTROLLED, S=SIMULATION (PE 8/32). H=HARDWARE (MC 68000) .

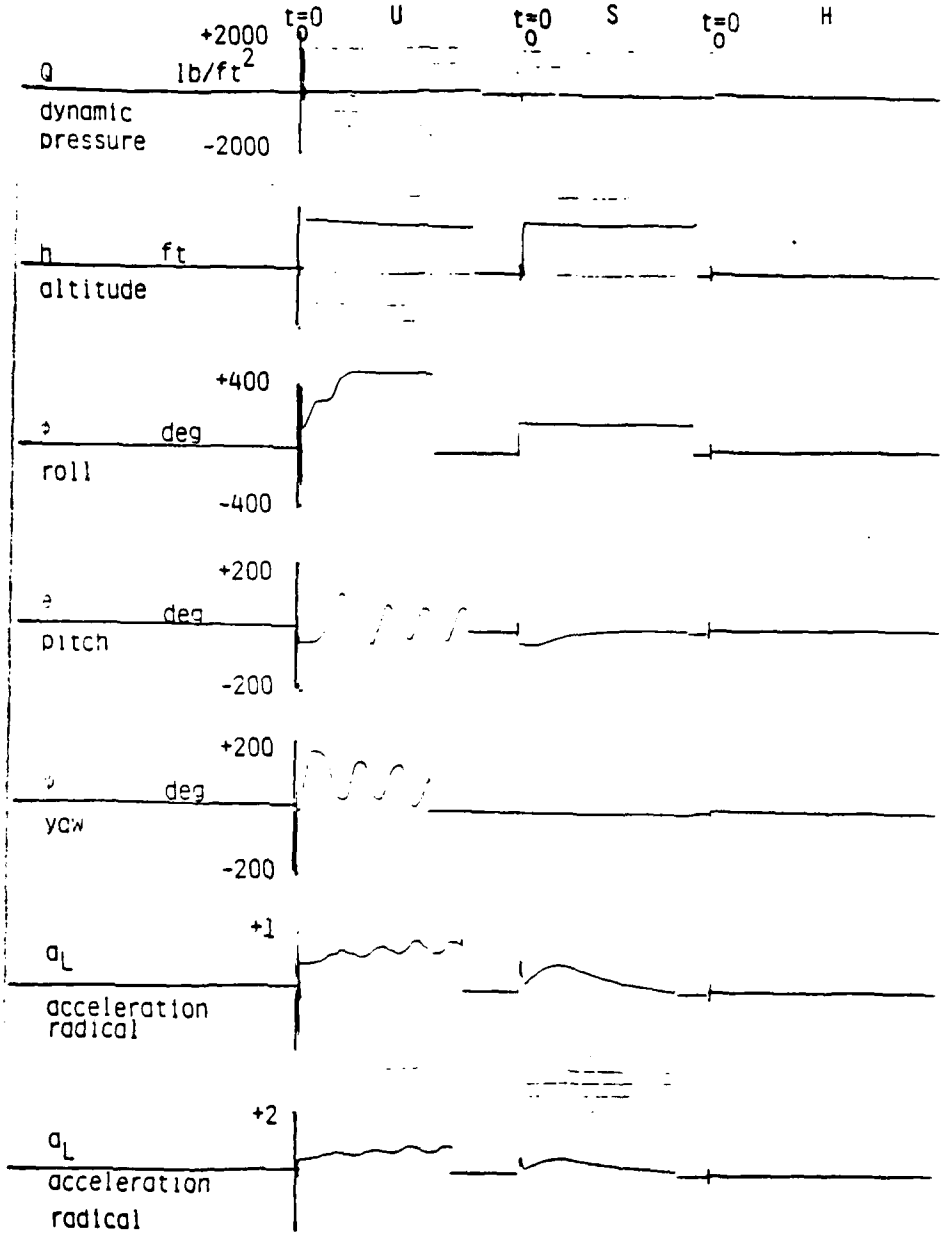

Figure 7.78 Case 10 (Table 2)

U=UNCONTROLLED, S=SIMULATION (PE 8/32), H=HARDWARE (MC 68000)

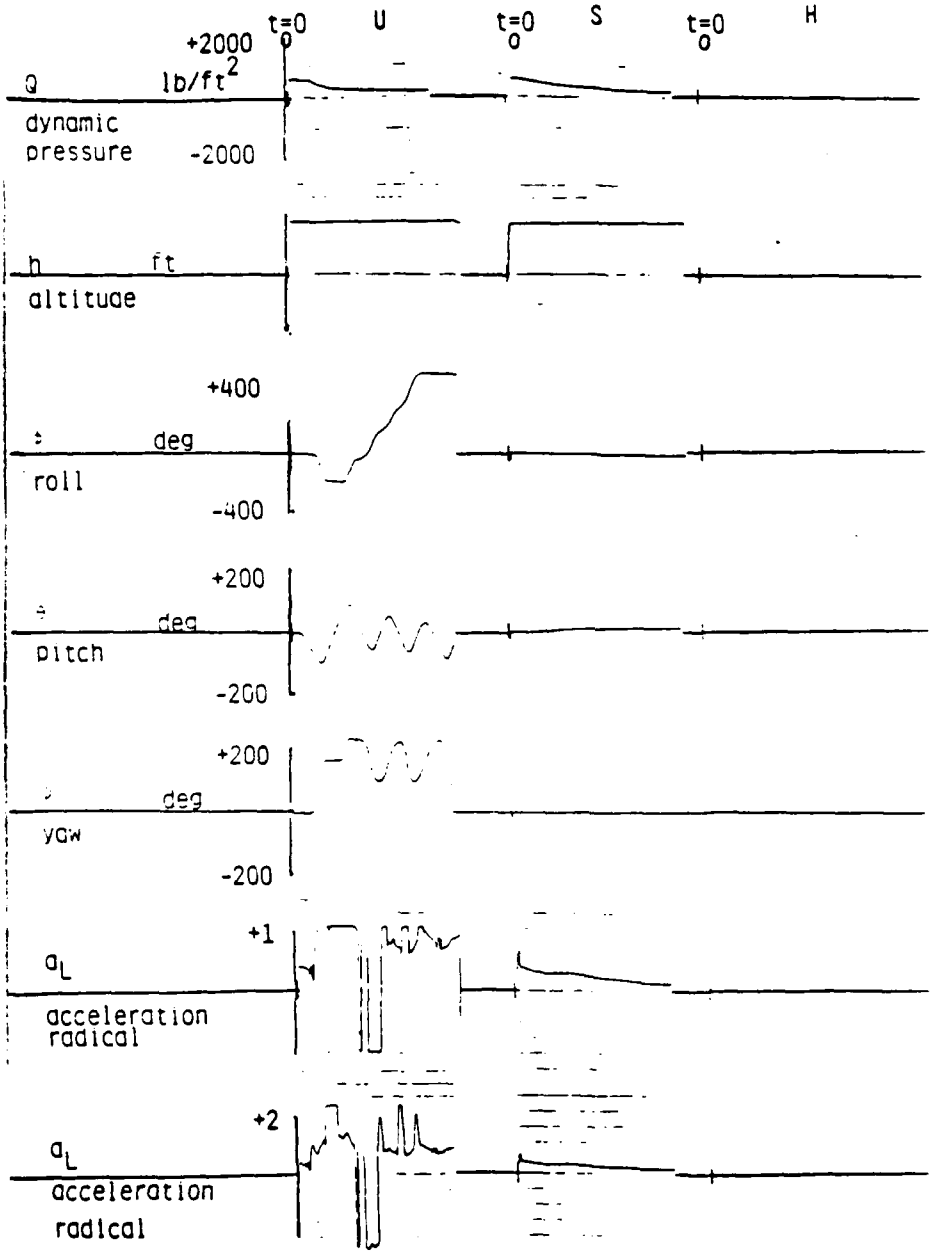

Figure 7.79 Case 11 (Table 2)

U=UNCONTROLLED, S=SIMULATION (PE 8/32), H=HARDWARE (MC 68000)

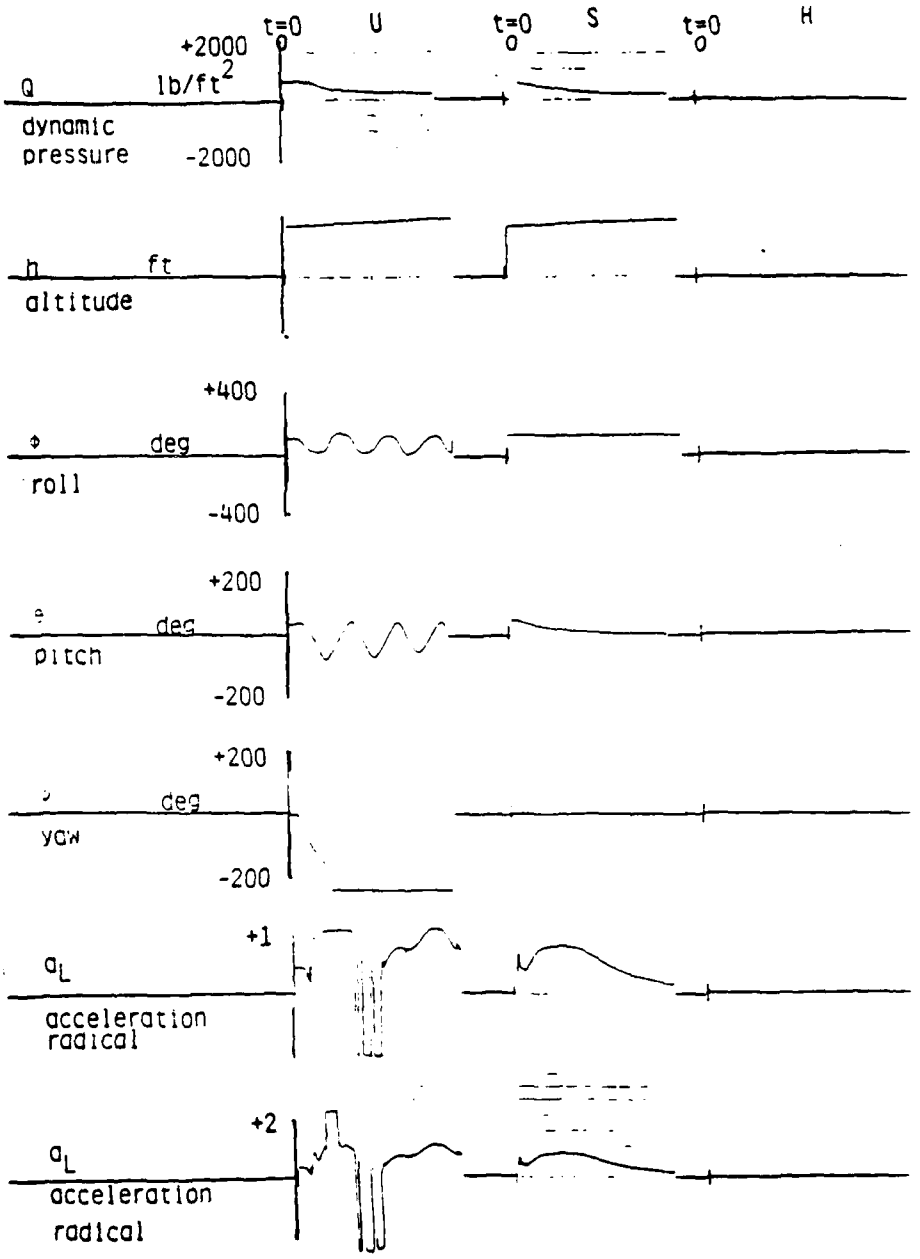

Figure 7.80 Case 12 (Table 2)

U=UNCONTROLLED, S=SIMULATION (PE 8/32), H=HARDWARE (MC 68000).

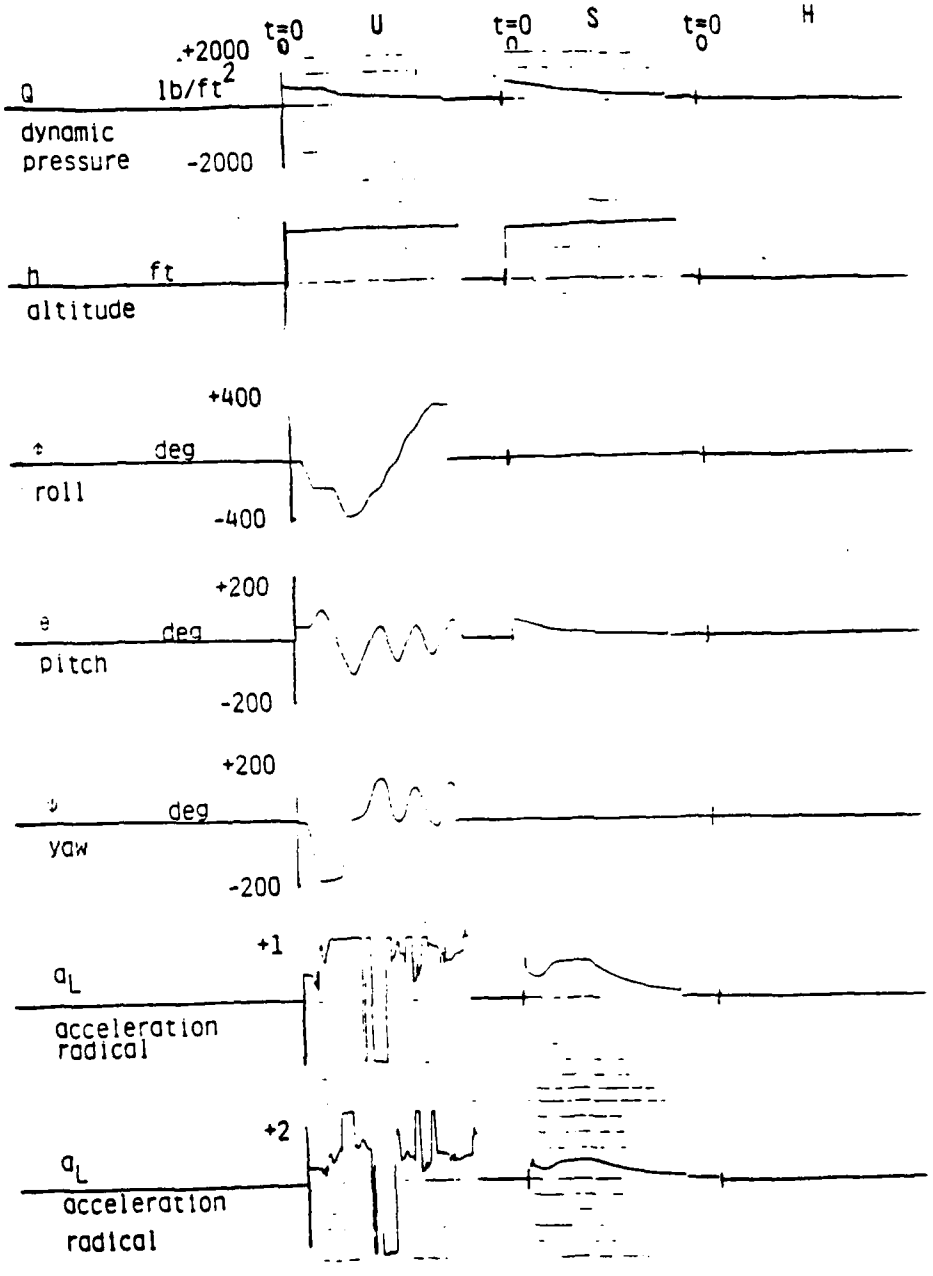

Figure 7.81 Case 13 (Table 2)

U=UNCONTROLLED, S=SIMULATION (PE 8/32), H=HARDWARE (MC 68000)

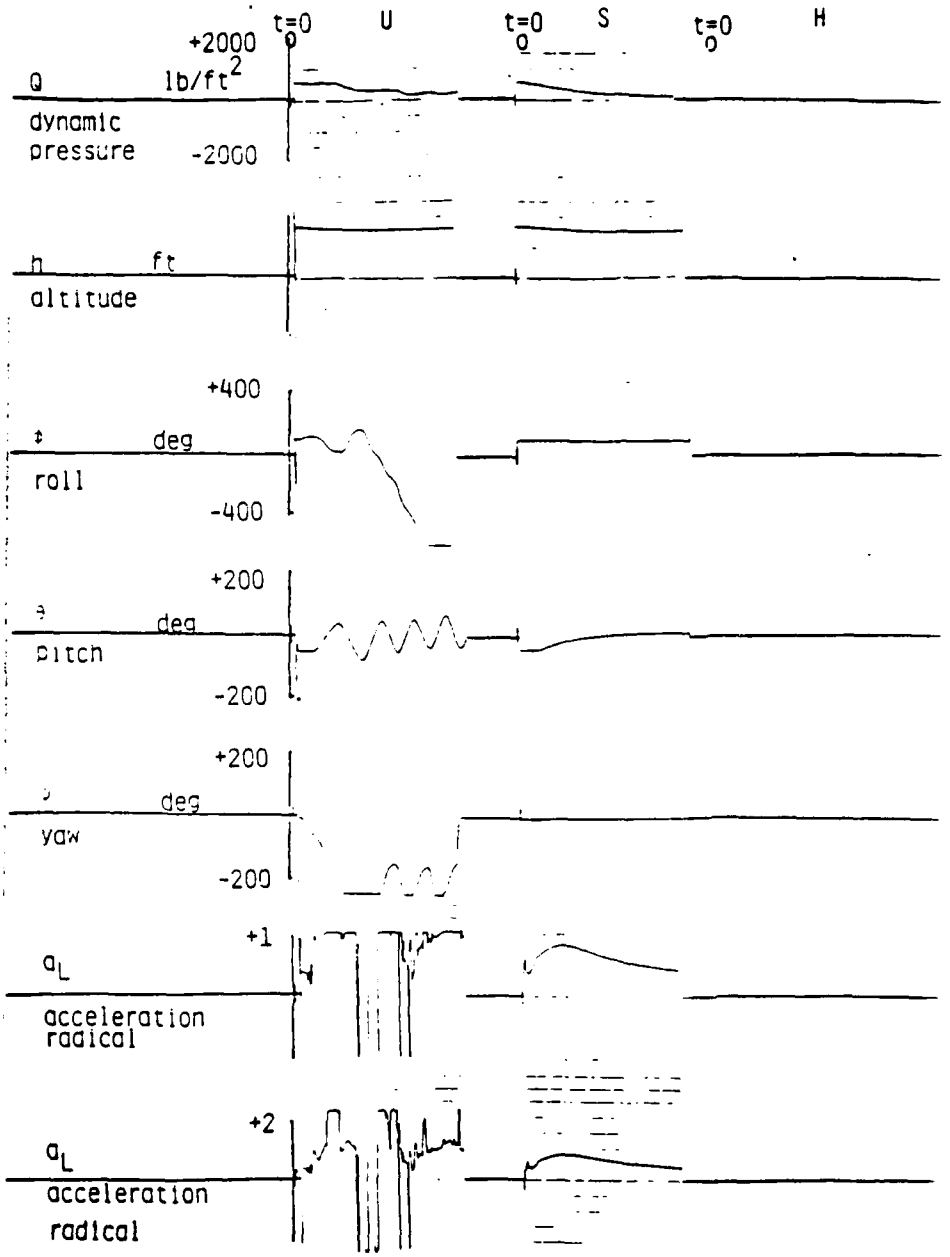

Figure 7.82 Case 14 (Table 2)

U=UNCONTROLLED, S=SIMULATION (PE 8/32). H=HARDWARE (MC 68000)

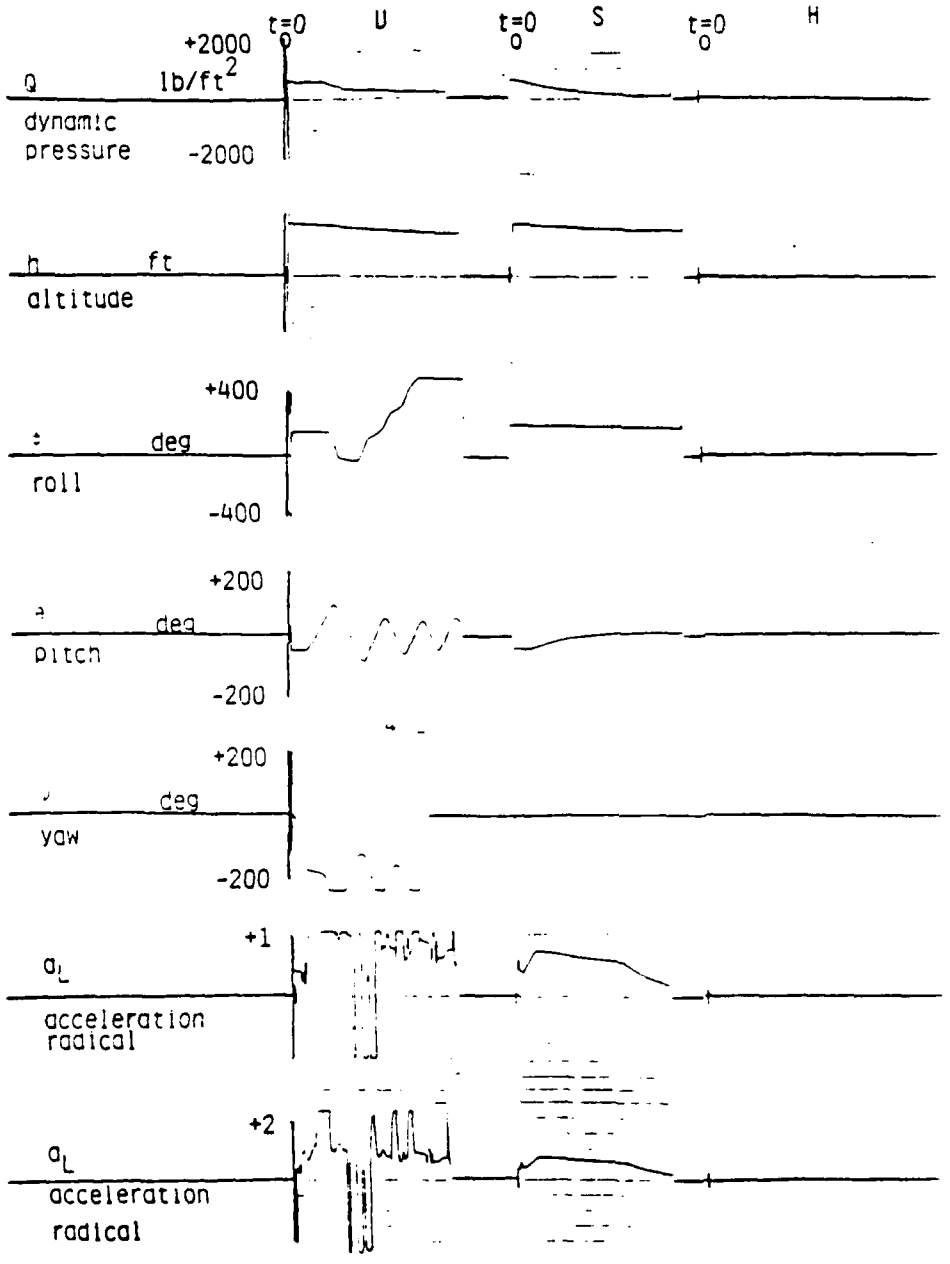

Figure 7.83 Case 15 (Table 2)

U=UNCONTROLLED, S=SIMULATION (PE 8/32), H=HARDWARE (MC 68000)

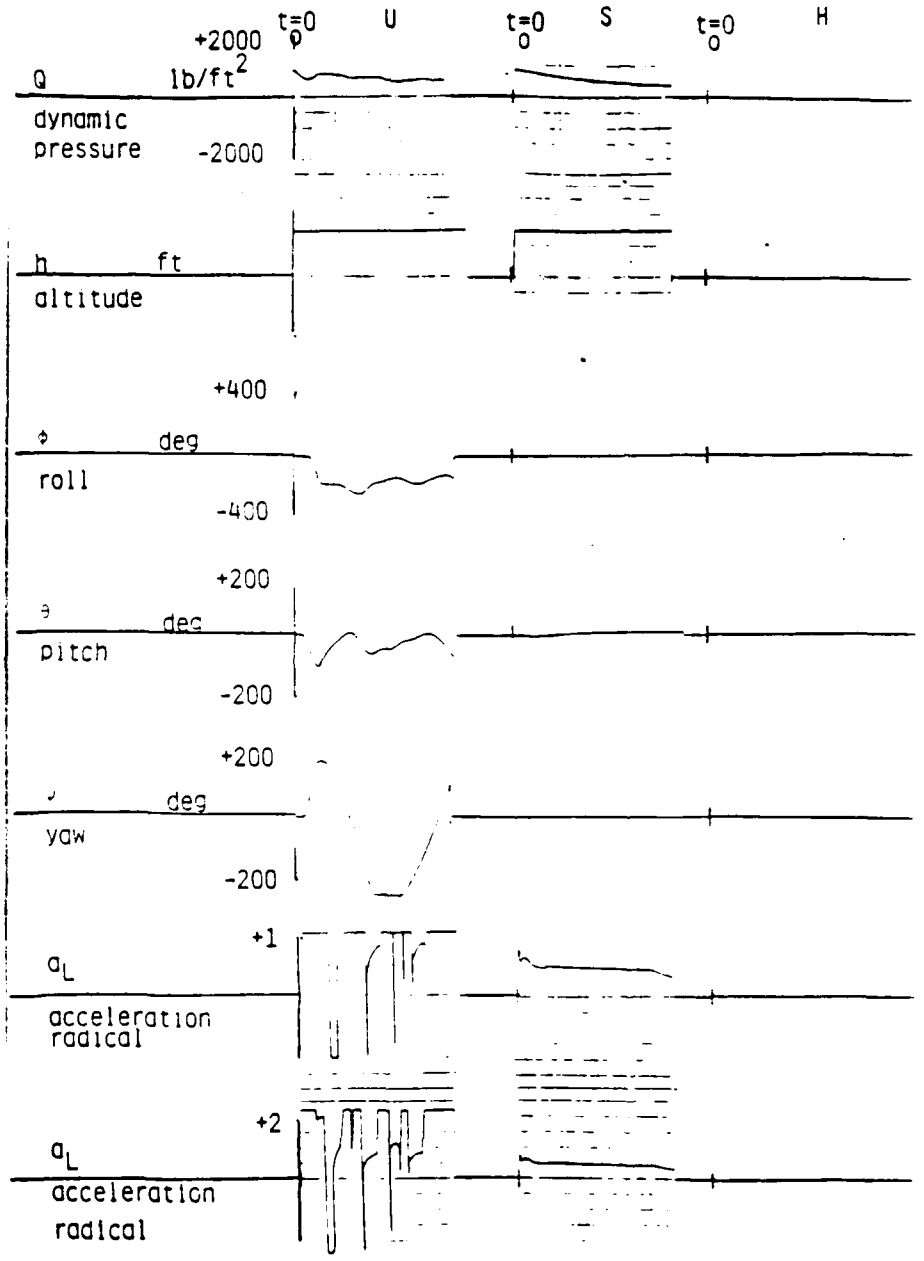

Figure 7.84 Case 16 (Table 2)

U=UNCONTROLLED, S=SIMULATION (PE 8/32), H=HARDWARE (MC 68000)

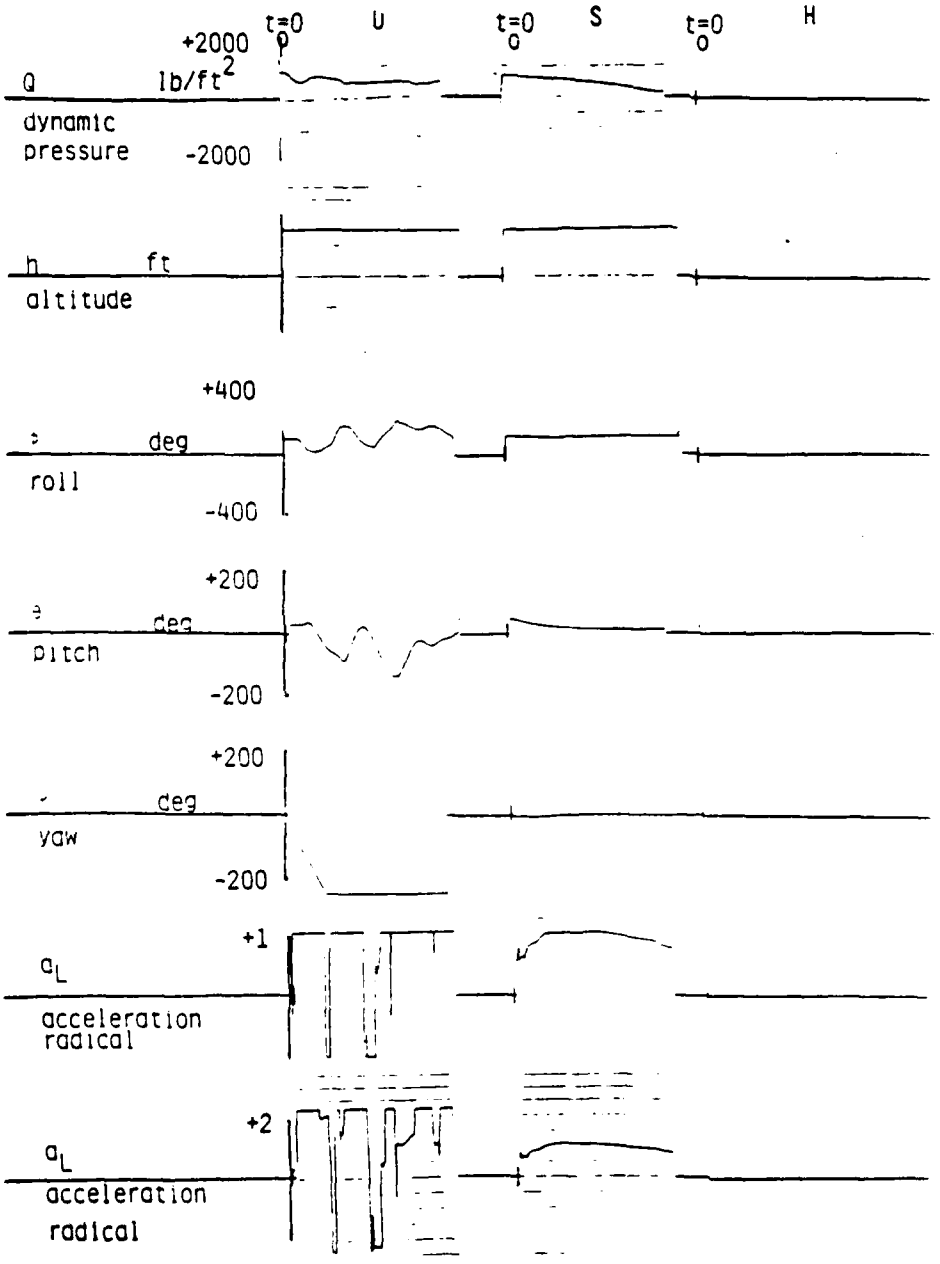

Figure 7.85 Case 17 (Table 2)

AD-A166 596 VECTORED THRUST DIGITAL FLIGHT CONTROL FOR CREW ESCAPE 3/3
VOLUME 2(U) SCIENTIFIC SYSTEMS INC CAMBRIDGE MA
J V CARROLL ET AL. DEC 85 AFWAL-TR-85-3116-VOL-2
UNCLASSIFIED F33615-82-C-3402 F/G 1/4 NL

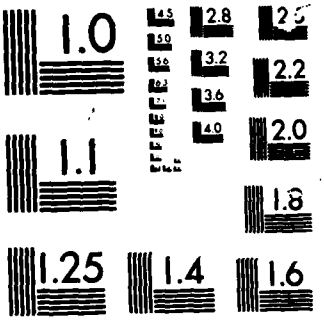

MICROCOPY CHART

U=UNCONTROLLED, S=SIMULATION (PE 8/32), H=HARDWARE (MC 68000)

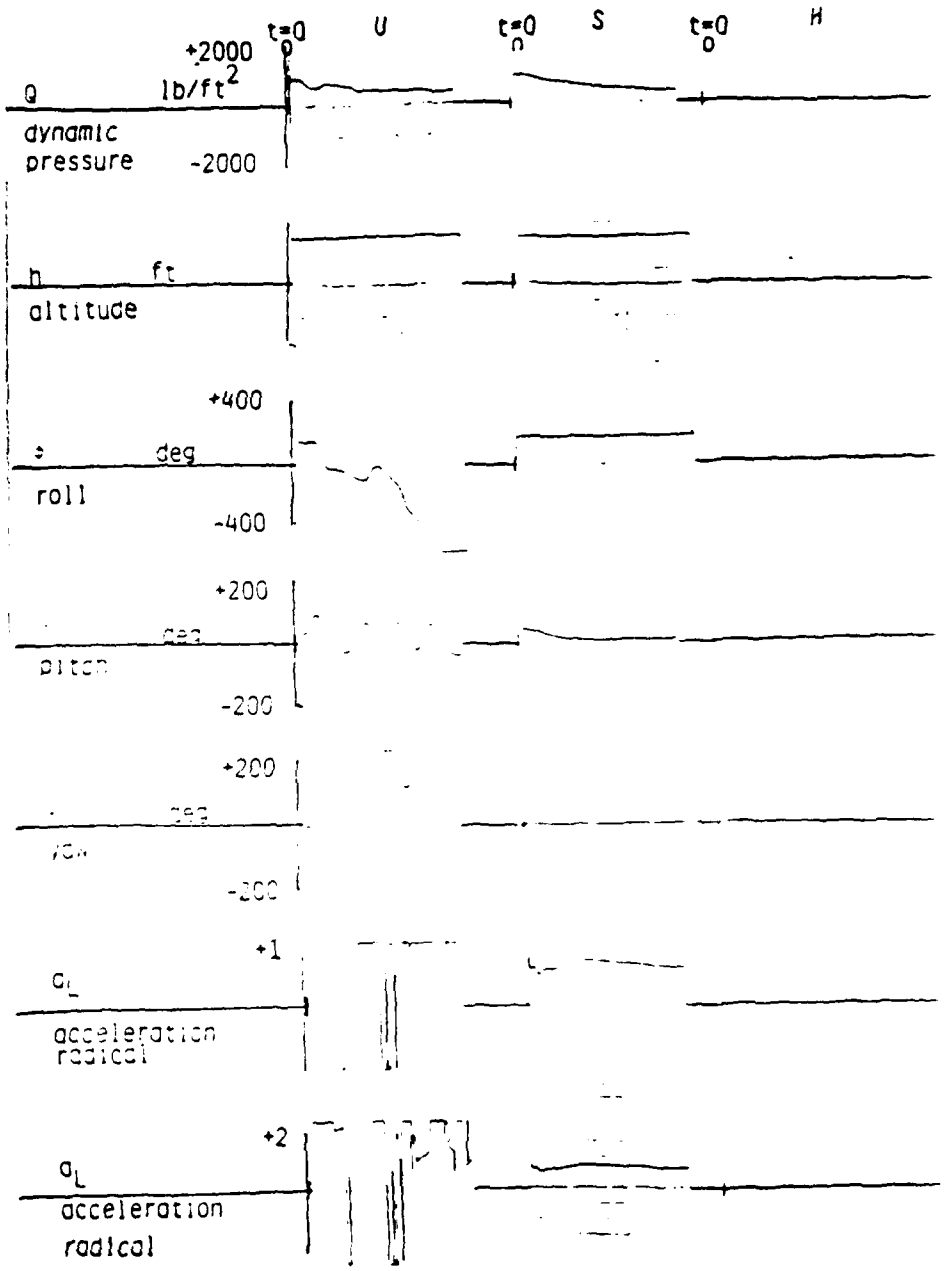

Figure 7.86 Case 18 (Table 2)

U=UNCONTROLLED, S=SIMULATION (PE 8/32). H=HARDWARE (MC 68000)

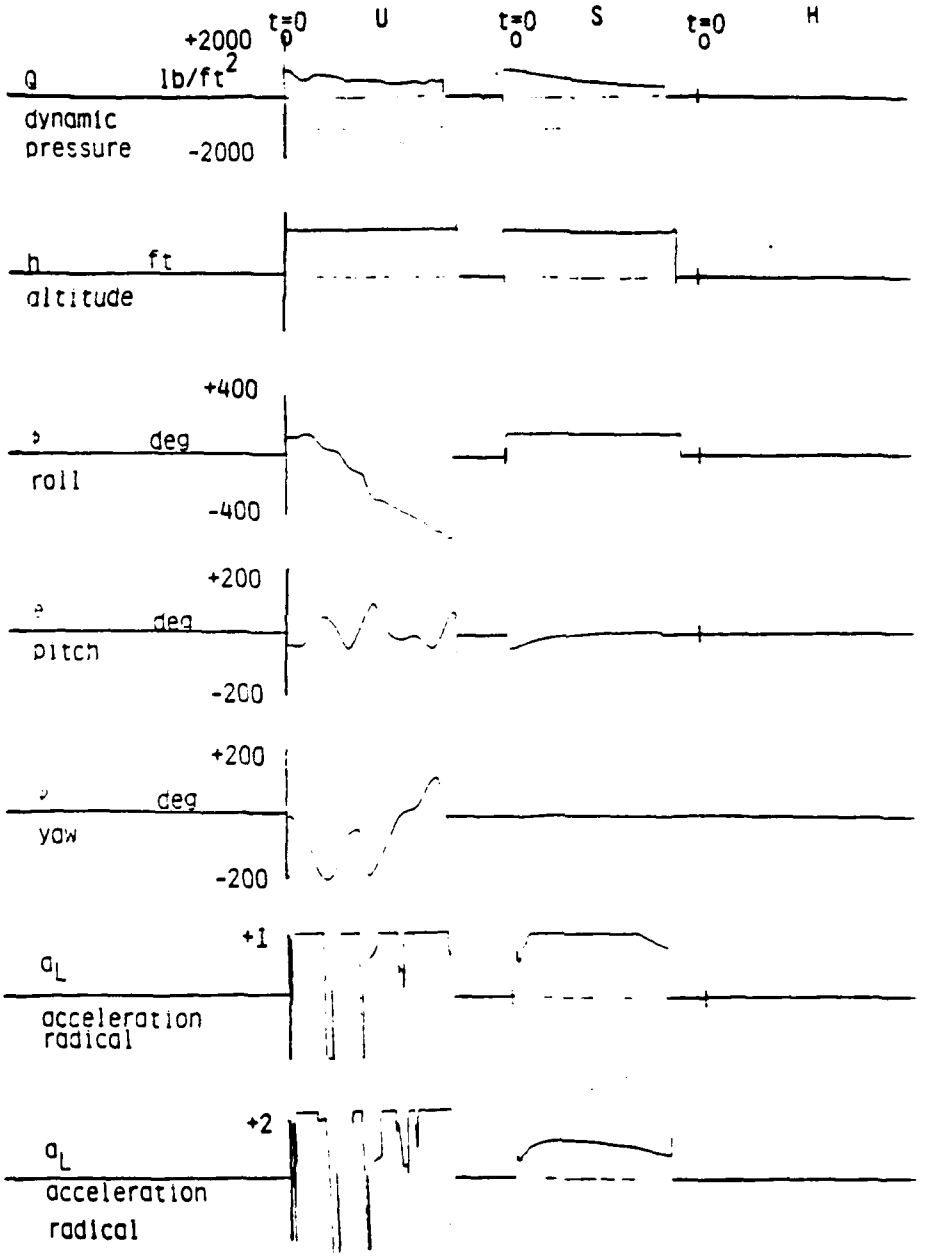

Figure 7.87 Case 19 (Table 2)

U=UNCONTROLLED, S=SIMULATION (PE 8/32), H=HARDWARE (MC 68000)

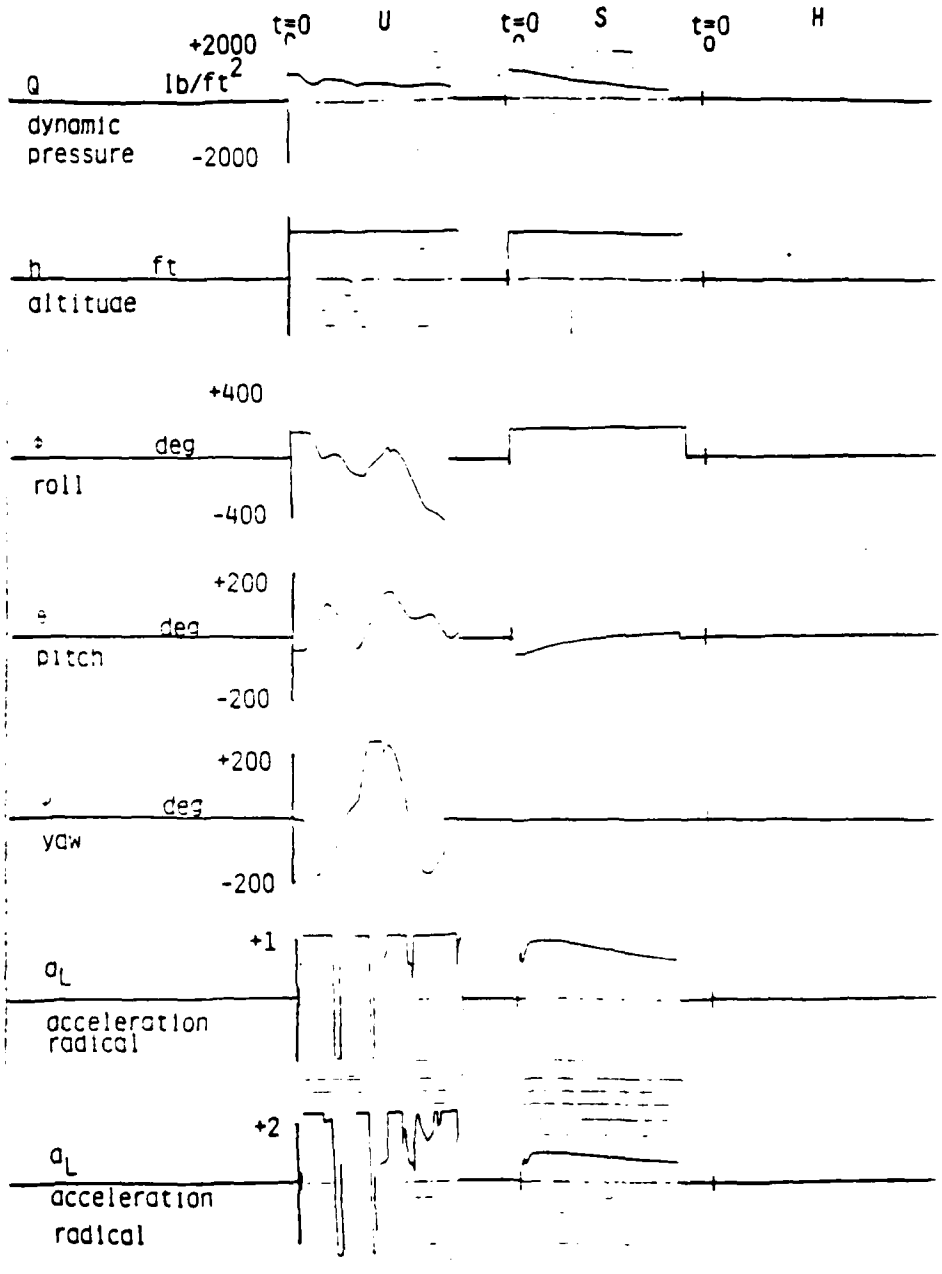

Figure 7.88 Case 20 (Table 2)

CHAPTER 8

CONCLUSIONS AND RECOMMENDATIONS

We now present the main conclusions from the design effort presented in this report:

8.1 Conclusions.

The Ejection Seat vectored thrust control problem is highly nonlinear and cannot be solved effectively or efficiently by standard linear and most modern control design methods. Other multivariable design approaches of merit are worthy of consideration for augmenting the approach presented here. All reasonable approaches are based on the same underlying principles of robustness, disturbance rejection and predictive behavior. Also, the nonlinear equations of motion have been derived, and an analytical derivation of the linearized equations has been accomplished and partially verified, so that a practical and comprehensive ejection seat control design and analysis package now exists. Also, specification of three hierarchical levels of the ejection seat control problem, and determination of the methods and software required for optimal control design at all levels has been completed.

The EASIEST program has been used extensively for computing flight trajectories, linearizing models, and performing simple feedback control strategies. In addition, much attention was given to quantification of propulsion system energy requirements (Volume I, Chapter 3), and our analysis presented here shows that high Q conditions will dictate the energy needed by the propulsion system, although some low speed, low altitude adverse attitude cases also require considerable energy. At least 8500 pounds of total force capability will be needed, and very close to this number in pound-seconds of impulse. This number could be revised upward if thrust vectoring falls much below 600 deg/sec in rate. Also, the results are very dependent on required reduction in dynamic pressure on the seat. If the required pressure for chute

deployment is much less than 600 Q, then there would again have to be an upward revision.

Performance results in Volume II, Chapter 7 show that the safe recovery of the pilot under extreme ejection conditions is feasible using vectored thrust control for an ACES II type of seat. This conclusion is based on examination of at least thirty extreme escape conditions using the real time hybrid simulator designed for this project (Volume II, Chapter 6). The thrust levels required are achievable and the control solutions are robust. Further improvements are possible by using a flexible propulsion sytem with additional thrust rockets and vernier jets, which, most likely, would be used to achieve the required degree of reliability. An example of such a system has been presented in Volume I, Section 3.2.2.4.

Our numerical studies to date have pointed out the following:

High Q ejections will almost certainly be aided by some type of deployable fin, to exploit aerodynamic energy for attitude stabilization. Such surfaces would not have to be movable, but they should reduce propulsion system required thrust capacity.

The control algorithm has been successfully implemented and tested in a real time, hybrid environment, hosted on a wire-wrapped controller designed by SSI and fabricated by Unidynamics. The simulations confirm the validity of the design, and also the need to operate the controller at a minimum sample rate of 50 Hz. In addition, the microprocessor architecture should require no more than about half of available microprocessor throughput to be dedicated to controller processing. Memory requirements are about 20 Kbytes for assembly code, a bit higher for Pascal code. Pascal code will not execute the controller in real time on the Motorola 68000 chip. These results confirm that the controller processing requirements can be met with current hardware.

A final note: the control concept presented in this report has become a part of the major technology follow-on project, the Crew Escape Technologies (CREST) Program. Working as a subcontractor to Boeing, SSI has overseen the application of its control approach to an actual test bed seat. This project is still underway, but the preliminary results are that the control logic performs very capably on the BMAC baseline design, under somewhat more difficult performance criteria than those in use for the project described here.

8.2 Recommendations.

Even though significant progress has been made in demonstrating feasibility of the vectored thrust control concept, further testing and refinements are necessary. These are not expected to be technical barriers in any sense, since the most difficult issues have already been addressed.

The major recommendation is that the breadboard simulation system developed under this project at Martin Orlando be improved and expanded upon. At this time, it is unique in terms of simulation realism for analyzing ejection seat performance. The design of this system allows for efficient progression from just the wire-wrapped controller as the breadboard hardware element (the current design), to breadboard systems with more control system hardware components added. The MMOA High Force Gain Valve is an example of such a component whose integration into the system can be readily analyzed. The simulation capability described in Appendix F is able to provide timely and cost effective support of advanced design projects such as the CREST program.

Table 8-1

A

T=0.

Eigenvalues (λ_i)

$-2.00 \pm j\ 1.838$
-3.400
$+3.419$
$+1.453$
$-.5945$
$-2.846\ E\text{-}4$
$-2.081\ E\text{-}5$

$\lambda_9=\lambda_{10}=\lambda_{11}=\lambda_{12}=0$

Table 8-2

A

-1.4[illegible]E+0[illegible]	[illegible]	9.1[illegible]1E-01	[illegible]	5.5[illegible]E+01
6.9[illegible]E-03	-[illegible].[illegible]1[illegible]E-01	[illegible]E-03	-[illegible]E-01	0.000E+00
[illegible].[illegible]61E-02	-[illegible]E-07	-[illegible].[illegible]7[illegible]E-02	-1.[illegible]E-01	[illegible].[illegible]7[illegible]E+02
-6.438E-03	1.[illegible]E-0[illegible]	[illegible].702E-04	-[illegible].[illegible]5[illegible]E-01	4.[illegible]74E-0[illegible]
-3.213E-01	5.555E-04	1.[illegible]7[illegible]E-02	-1.[illegible]E-0[illegible]	-1.[illegible]E+0[illegible]
1.137E-02	-1.[illegible]E-0[illegible]	-6.5[illegible]E-04	-1.50[illegible]E-01	1.112E-01
0.000E+00	0.000E+00	0.000E+00	1.000E+00	-5.532E-06
0.000E+00	0.000E+00	0.000E+00	0.000E+00	1.000E+00
9.942E-01	3.[illegible]7[illegible]E-04	-4.[illegible]11E-02	0.000E+00	0.000E+00
-3.131E-04	1.000E+00	-1.257E-04	0.000E+00	0.000E+00
4.001E-02	1.561E-04	9.992E-01	0.000E+00	0.000E+00
0.000E+00	0.000E+00	0.000E+00	0.000E+00	1.3[illegible]3E-04

1.995E-01	0.000E+00	-3.215E+01	0.000E+00	0.000E+00
-9.676E+02	3.215E+01	1.7[illegible]9E-04	0.000E+00	0.000E+00
0.000E+00	-4.[illegible]E-03	1.237E+00	0.000E+00	0.000E+00
-3.050E-01	0.000E+00	0.000E+00	0.000E+00	0.000E+00
-2.[illegible]E-02	0.000E+00	0.000E+00	0.000E+00	0.000E+00
4.934E-02	0.000E+00	0.000E+00	0.000E+00	0.000E+00
-4.004E-02	1.749E-02	-7.214E-03	0.000E+00	0.000E+00
-1.382E-04	7.202E-03	0.000E+00	0.000E+00	0.000E+00
0.000E+00	9.144E-03	-1.6[illegible]E+01	0.000E+00	0.000E+00
0.000E+00	5.564E+01	5.290E-03	0.000E+00	0.000E+00
0.000E+00	[illegible].07[illegible]E-01	-9.690E+02	0.000E+00	0.000E+00
1.001E+00	-4.[illegible]7[illegible]E-01	2.[illegible]E-04	0.000E+00	0.000E+00

0.000E+00	0.000E+00
0.000E+00	0.000E+00
0.000E+00	0.000E+00
0.000E+00	0.000E+00
0.000E+00	0.000E+00
0.000E+00	0.000E+00
0.000E+00	0.000E+00
0.000E+00	0.000E+00
0.000E+00	[illegible].[illegible]E-02
0.000E+00	[illegible].[illegible]9[illegible]E+02
0.000E+00	0.000E+00
0.000E+00	0.000E+00

T=0.1

Eigenvalues (λ_i)

$-5.870 \pm j\ 1.702$
4.306
-3.272
3.325
$-.5900$
$1.159\ E{-4} \pm j\ 7.610\ E{-3}$
$1.049\ E{-8} \pm j\ 3.049\ E{-8}$, $\lambda_{11} = \lambda_{12} = 0$

Table 8-3

A

T=0.2

Eigenvalues (λ_i)

$-3.120 \pm j\ 4.021$
3.916
3.101
-3.122
$-.5346$
$-1.974\ E\text{-}3 \pm j\ 1.795\ E\text{-}2$
$\pm j\ 3.357\ E\text{-}6$

$\lambda_{11} = \lambda_{12} = 0$

Table 8-4

Input matrix B:

B

-1.6538+02	0.000E+00	0.000E+00	-5.396E+01	-1.304E+00
0.000E+00	1.000E+02	0.000E+00	0.000E+00	1.243E+00
-1.111E+02	0.000E+00	0.000E+00	1.033E+02	-1.304E+00
0.000E+00	-2.143E+02	-8.836E+01	0.000E+00	-1.043E+00
-2.020E+02	0.000E+00	0.000E+00	0.000E+00	0.000E+00
0.000E+00	-1.431E+02	1.331E+02	0.000E+00	-6.966E-01
0.000E+00	0.000E+00	0.000E+00	0.000E+00	0.000E+00
0.000E+00	0.000E+00	0.000E+00	0.000E+00	0.000E+00
0.000E+00	0.000E+00	0.000E+00	0.000E+00	0.000E+00
0.000E+00	0.000E+00	0.000E+00	0.000E+00	0.000E+00
0.000E+00	0.000E+00	0.000E+00	0.000E+00	0.000E+00
0.000E+00	0.000E+00	0.000E+00	0.000E+00	0.000E+00
-5.4[illegible]E+02	0.000E+00	9.959E-01		
0.000E+00	7.000E+03	0.000E+00		
-6.978E+03	0.000E+00	-7.835E-02		
0.000E+00	-2.000E+02	0.000E+00		
-2.591E+02	0.000E+00	4.357E-14		
0.000E+00	-2.828E+00	0.000E+00		
0.000E+00	0.000E+00	0.000E+00		
0.000E+00	0.000E+00	0.000E+00		
0.000E+00	0.000E+00	0.000E+00		
0.000E+00	0.000E+00	0.000E+00		
0.000E+00	0.000E+00	0.000E+00		
0.000E+00	0.000E+00	0.000E+00		

Table 8-5

THE OPTIMAL CONTROL GAIN MATRIX

-6.7243304459295751D-01	-9.0114226104133627D-02	1.5057790719462127D-03
1.6010146434815330D-05	-4.6997361439111306D-02	-1.0192425755671530D-03
-2.2271362595854734D-05	1.1735604170551733D-01	-1.7417298322532962D-03
-7.3327351295028575D-01	-1.4844039511340111D-05	-4.9535157146371190D-02
-2.2130233978380375D-03	-1.1327397913399904D-05	-5.0544772559646398D-03
-5.6561614564161510D-02	-3.3573040923375511D-05	-9.9527026423427595D-01
6.4353223352710535D-07	9.9472431770234075D-01	-2.2215373689345167D-04
1.4272019525139950D-02	-1.3264945315925049D-03	2.4985970167711513D-07

-2.7459906772523458D-03	-3.2362575835031250D-06	-8.4733599135334734D+01
-1.3555716993065454D-01	-2.4262631373425105D+00	3.7635711352610840D-03
3.6004337129459327D-01	2.5742254523584459D+00	2.6959007785972752D-03
-4.6063775342342312D-05	2.0507945140544459D-04	1.0833544015382247D+02
-2.5453977305179503D-04	-3.0374837995532361D-05	5.7031932307259523D+00
-1.6932951257035771D-03	-1.0573404403953015D-05	-7.2722631027158968D-01
-3.2331871583707330D-01	-1.6590368252232151D-01	1.8170261141513265D-04
-3.3120950245835781D-03	-6.9249657535799309D-05	-3.1533869253352959D+00

4.3053511117485589D-05	-3.3584594343194746D-01
-8.9683557213949225D-01	3.1429640152912349D-05
-4.4483428228559693D-01	4.8433299935438371D-05
1.1315160387852223D-05	3.2304370523900037D-01
-4.3717053393975398D-03	1.7795034276898495D-02
1.4174499551439706D-05	-3.1121471952635105D-01
-4.0567503732220345D-03	5.1574244766908823D-06
-3.9995688265675514D-03	-9.7467455163373282D-03

-6.4302248181259570D-01	-7.8854437505536964D-05
1.6355983637749319D-05	-4.5783301166044751D-01
-8.7902854307579683D-05	8.8773397592616192D-01
-7.5987228995273525D-01	-1.0284670837733706D-05
-2.3774566407198307D-02	-1.1083278463558361D-03
-4.3227037311251963D-02	-1.1957047082817350D-05
5.3944516344952102D-07	-4.8957324797333152D-02
1.5071570543010143D-02	-1.9057873537811355D-07

7.6050917761191307D-01	-5.5391589127991719D-05
-4.0213047240615140D-05	-3.3547397434349065D+01
-7.3701651032203314D-05	6.5923756574453159D+01
-6.4709595031407650D-01	-5.3241957561206212D-04
-5.7451694351124685D-02	-7.9469349159427551D-02
1.0554049721067536D-02	-6.6561302146333455D-04
-1.0703778321050221D-05	-4.0759617516495370D+00
2.0312338913102283D-02	-1.7204696730214875D-05

t=0.0

Closed loop eigenvalues:

-7.459 E3; -7.459 E3; -3.938 E2; -3.809 E2; -1.433 E2;
-2.240 E2; -7.380 ± j 7.149; -1.397 E1 ± j 1.398 E1; -1; -1

Table 8-6

THE OPTIMAL CONTROL GAIN MATRIX C

-6.7362873404590245D-01	-1.0406695395345019D-04	1.5723888576551926 3D-01
1.2313120030900298 1D-03	-4.5314641.9391094 5D-02	4.5914672708033214D-04
4.0773511597928215D-04	1.1592130517044769D-01	2.0344771314215521D-04
-7.2465412133736484 0D-01	-5.0364274557454251D-05	-4.4013532564312560D-02
-2.1939528965959395 0D-02	-1.7963023930327536D-05	-4.9469011303798452D-03
-1.0509959195412413 0D-01	-1.6577523047470230D-05	-9.9557928321757464D-01
-2.0502330707979539 3D-04	9.9444067542903750 9D-01	-2.8963443357734773D-05
1.4037200724604925D-02	6.6539553.0997532 90D-07	2.4255354027391703D-05

-2.6574973004255500D-04	-1.3025631550535271D-02	-8.2450972376243839D+01
-1.3103078407910939D-01	-2.5575301230437574D+00	-4.9650336319922934D-01
3.6855415251479297D-01	2.0371759165549765D+00	-2.7374805239833951D-01
-1.6325994221532120D-04	4.0305529720452350D-02	1.0705251121291497D+02
-2.2927719093457500D-04	-7.1382936041733284D-05	5.6221958976419513D+00
-5.0692349730845190D-05	6.0235635220758323D-04	7.1384715379576402D-01
-3.2035922485397557 2D-01	-1.4351054765135573D-01	3.4423705564755453D-02
2.4324890114350393D-05	-1.0974834502350777D-03	-3.1115441506529715D+00

-1.0263455525247133D-06	-3.5305403326178947D-01
-8.9644031593724288D-01	-1.4950300354100375D-03
-4.5095099333315867D-01	-7.4215539190526343D-04
2.4683595213650001D-04	3.0885874796528503D-01
-4.3645281773240614D-03	1.7420317328578833D-02
4.9612337492307865D-05	-3.0313675192735033D-01
-6.9452909929306472D-03	1.3327954397177265D-04
-6.6987043533673985D-05	-9.4987149211152762D-03

-6.7450425503136607D-01	-1.4217753925935937D-04
1.1933690359530855D-03	-4.6191700589794392D-01
9.6557568996758930D-04	8.8547298440210223D-01
-7.3632473300822223D-01	5.8177574364139347D-04
-2.2425075359241819D-02	-1.1024593216900272D-03
-4.6406811195636462D-02	-1.1024549132158251D-05
-7.3113404713001477D-05	-5.0682320027681360D-02
1.4341046793747081D-02	-1.5159237313259110D-05

7.3749351762605437D-01	-3.9994300224311070D-02
4.2134134423150263D-05	-3.0492157765355020D+01
5.2590447530314016D-04	6.5016739029314036D+01
-6.7594599315436329D-01	8.3981594701040425D-02
-3.3270601932432527D-02	-6.3354452195246997D-02
-9.0079540571232392D-04	2.0592378371872353D-04
-2.2911758305063241D-04	-4.0735205254199530D+00
2.0333130311559512D-02	-2.3001231752437073D-03

t=0.1

Closed loop eigenvalues:

-7.459 E3; -7.459 E3; -3.822 E+2; -3.710 E2;
-1.476 E2; -2.238 E2; -7.258 ± j 7.039;
-1.393 E1 ± j 1.396 E1; -1.; -1.43

Table 8-7

THE OPTIMAL CONTROL GAIN MATRIX C

-6.6225703471959347D-01	-2.2815015723617430D-04	1.4704702355984093D-01
3.1501512163839937D-03	-5.2106474639740110D-02	1.2154615442136311D-03
2.9167590336647502D-03	1.1595555719329455D-01	6.5713572585498575D-04
-7.4532330375976515D-01	-1.7741323347309371D-04	-5.4545579523271330D-02
-2.2984811290490568D-02	-3.4420865309783582D-03	-5.2361106391216123D-03
-7.4964237525552688D-02	-3.4541623357340330D-05	-9.9459142335794490D-01
-8.5530633517460884D-04	9.9410930729447540D-01	-5.9572605537670279D-03
1.4644936525802033D-02	2.7377256534731980D-05	2.6264164389355570D-03

-7.6681351734014377D-04	-3.2322519615513163D-02	-7.7387325769278462D+01
-1.4839959380335275D-01	-2.4398329550916781D+00	-1.1954177383060225D+00
3.0783857223152560D-01	1.8769607350273610D+00	-7.0777629052527792D-01
-5.5354252545449323D-04	9.7384226463301500D-02	9.7213380537332247D+01
-3.1540055265443792D-04	-4.5454059443011934D-03	5.1322044301252292D+00
-3.5531661533356917D-05	-1.3384050243873397D-04	-2.0924438176155141D+00
-3.1580805979562410D-01	-1.4313603315903734D-01	8.7644066156972289D-02
9.1362148075920653D-05	-2.3430254264231967D-03	-2.8383969080119635D+00

-3.0645643536109621D-04	-3.2715903487229831D-01
-9.0040262923125333D-01	-3.9283571359916344D-03
-4.4133945713514643D-01	-2.3791865701690970D-03
6.7115984534087378D-04	3.4232271790101098D-01
-4.3505792713293695D-03	1.8484432772153987D-02
1.8424637570467315D-04	-3.0613303156493377D-01
-1.2955971111505258D-03	3.3961897311935813D-06
-1.8383416164472568D-05	-1.0175176365821123D-02

-6.8757612585213326D-01	3.2987572147001164D-06
2.4015039701376534D-03	-4.5137638324847691D-01
3.3562039521158413D-03	8.9072434157491540D-01
-7.2404586540627312D-01	2.6550245979123751D-03
-2.1725536212070364D-02	-9.6474646913494443D-04
-4.8089536309425623D-02	5.4915558229079521D-05
-1.6330428319726271D-04	-5.3492634253576339D-02
1.3964239567516063D-02	-6.5755663380751867D-05

7.2442622322469577D-01	-1.0901233154552240D-01
4.6031312259545064D-04	-3.2260110053786449D+01
2.2053990657245788D-03	6.0322875552048390D+01
-6.3765111016555139D-01	2.6903392583257913D-01
-3.8553452355540516D-02	-6.7077191799176392D-02
1.9507934285598377D-02	-1.3573839345609430D-04
-6.7515155745794185D-04	-4.0914705915952770D+00
2.1087903745218260D-02	-7.2597394277534440D-05

t=0.2

Closed loop eigenvalues:

-7.460 E3; -7.460 E3; -3.740 E2; -3.564 E+2; -2.240 E2;
-1.330 E2; -7.558 ± j 7.311; -1.387 E1 ± j 1.390 E1; -1; -1.318

REFERENCES

Astrom, K.J. (1980), "Self-Tuning Regulators - Design Principles and Applications," in Narendra, K.S. and R.V. Monopoli (eds.), Applications of Adaptive Control, New York: Academic Press.

Athans, M., R.P. Wishner and A. Bertolini (1968), "Suboptimal State Estimation for Continuous-time Nonlinear Systems from Discrete Noisy Measurements," IEEE Trans. Automatic Control.

Beale, R.B. (1975), "Fluidic Thrust Vector Control for the Stabilization of Man/ Ejection Seat Systems," Report AFFDL-TR-75-105.

Bierman, G.J. (1977), Factorization Methods for Discrete Sequential Estimation, New York: Academic Press.

Bryson, A.E. (1978), "Kalman Filter Divergence and Aircraft Motion Estimators," J. Guidance and Control, vol. 1, pp. 71-79.

Bryson, A.E. and Y.C. Ho (1975), Applied Optimal Control, Wash. DC: Hemisphere.

Buzan, F.T. and J.K. Hendrick (1983), "Lateral Active Suspensions for Rail Vehicle Ride Control," presented at the Amer. Control Conf. (ACC), San Francisco, CA.

Carroll, J.V., D.P. Martin, R.K Mehra and D.E. Gustafson (1982), "Vectored Thrust Digital Flight Control for Crew Escape," Interim Report No. 1, Scientific Systems, Inc.

Chou, S.I. (1976), "Projected Surface Ship Anti-Submarine Warfare Target Motion Analysis," NVC TN1717, Naval Undersea Center, San Diego, CA.

Craig, J.N., R.L. Barron and F.J. Cook (1980), "A Priori Training of Guidance and Control Algorithms for Tactical Missiles, Task I: Air-to-Air Guidance Law Implementation," Final Report, AFATL-TR-80-102.

Cutler, C.R. and B.L. Ramaker (1980), "Dynamic Matric Control - A Computer Control Algorithm," (presented at the AICHE National Mtg., 1979), Joint Automatic Control Conf. Proc., San Francisco, CA.

Daclin, E. (1980), "Design Studies for the Automatic Piloting of the Tripartite Mine Hunter Boat," Paper no. FA9-E, JACC.

Doyle, J.C., J.E. Wall, and G. Stein (1982), "Performance and Robustness Analysis for Structured Uncertainty," Proc. Conf. Decision and Control.

Doyle, J.C. and G. Stein (1981), "Multivariable Feedback Design: Concepts for a Classical/Modern Synthesis," IEEE Trans. Automatic Control, vol. AC-26, no. 1, pp 4-16.

Etkin, B. Dynamics of Atmospheric Flight, Wiley and Sons, Inc., 1972.

Gear, C.W. (1971), "Numerical Inertial Value Problems in Ordinary Differential Equations," New Jersey: Prentice-Hall.

Goldstein, H., Classical Mechanics Addison Wesley, 1965.

Gully, S.W. and N. Coleman (1981), "Microcomputer Control Algorithms for Weapon Pointing and Stabilization," IEEE Control Systems Mag.

Gupta, N.K. and R.K. Mehra (1974), "Computational Aspects of Maximum Likelihood Esitmation and Reduction in Sensitivity Function Calculations," IEEE Trans. Automatic Control, vol. AC-19, pp. 774-783.

Horowitz, I., B. Golubev, T. Kopelman and S. Britman (1980), "Research in Advanced Flight Control Design," AFFDC-TR-79-3120.

Jines, L.A. (1982), "SAFEST Computer Program User Guide," AFWAL-TR-82-3013.

Landau, I.D. (1974), "A Survey of Model Reference Adaptive Techniques (Theory and Applications)," Automatica, vol. 10, pp. 353-379.

Lecamus, F. and J. Richalet (1968), "Identification des Systemes Discrets Linearies Monovariables por Minimisation d'une Distance de Structure," Electronics Letters, vol. 4, no. 24.

Lecrique, J., A. Rault, M. Tessier and J.L. Testud (1978), "Multivariable Regulation of a Thermal Power Plant Steam Generator," presented at the IFAC World Congress, Helsinki.

Mehra, R.K. (1970), "On the Identification of Variances and Adaptive Kalman Filtering," IEEE Trans. Automatic Control, vol. AC-15, pp. 175-184.

Mehra, R.K. (1971), "A Comparison of Several Nonlinear Filters for Reentry Vehicle Tracking," IEEE Trans. Automatic Control, vol. AC-16, pp. 307-319.

Mehra, R.K. (1972), "Approaches to Adaptive Filtering," IEEE Trans. Automatic Control, vol. AC-17, pp. 693-698.

Mehra, R.K., P. Mereau and D. Guillaume (1978), "Flight Control Application of Model Algorithmic Control with IDCOM," Proc. IEEE Conf. Decision and Control, pp. 977-982.

Mehra, R.K. and R. Rouhani (1980), "Theoretical Considerations on Model Algorithmic Control for Non-minimum Phase Systems," Proc. JACC.

Mehra, R.K., R. Rouhani and L. Praly (1980), "New Theoretical Developments in Multivariable Predictive Algorithmic Control," Proc. JACC, paper FA9-B.

Mehra, R.K., Rault, J., J. Richalet, R. Papon and W.C. Kessel (1978), "Model Algorithmic Control using IDCOM for the F-100 Jet Engine Multivariable Control Design Problem," in Sain et.al (eds.), Alternatives for Linear Multivariable Control, Chicago: NEC, Inc.

Mehra R.K. and R.E. Davis (1970), "A Generalized Gradient Method for Optimal Control Problems With Inequality Constraints and Singular Arcs," Research Report 2, Systems Control Inc.

Mehra, R.K. (1977), "Group Method of Data Handling; Review and Experience," IEEE Decision and Control Conf., New Orleans.

Mehra, R.K., et al (1979), "Study of the Application of Singular Perturbation Theory," Scientific Systems NASA Contract Report 3167.

Mehra, R.K., et al, (1980), "Basic Research in Digital Stochastic Model Algorithmic Control," Technical Report AFWA2-TR-80-3125, Air Force Wright Aeronautical Laboratories, Wright-Patterson AFB, OH, DTIC Document AD-A102145.

Mehra, R.K., et al., (1980), "Application of Model Algorithmic Control to Fossil-Fueled Power Plants," Scientific Systems Interim Report for Contract DE-AC01-78ET29328.

Mereau, P. and J.P. Littman (1978), European Transonic Wind Tunnel, Dynamics Simplified Model, Adersa/Gergios.

Meyer, G. (1980), "Use of System Inverses in the Design of Flight Control Systems for Aircraft of Nonlinear Characteristics," Preprints JACC, San Francisco.

Meyer, G. and Cicolani, L. (1975), "A Formal Structure for Advanced Automatic Flight Control Systems," NASA Technical Note, NASA TN D-7940.

Porter, B. and A. Bradshaw (1982), "Design of Direct Digital Adaptive Flight Mode Control Systems for High-Performance Aircraft," Proc. NAECON Conf., Dayton, OH.

Praly, L. (1975), "General Study of Single Input Single Output Linear Time Variant Conrol Laws: Application to an Adapted Model Algorithmic Control (AMAC), Adersa/Gergios, pp. 75-195.

Rault, A., J. Richalet and P. LeRoux (1975), "Commands Auto-Adaptive d'un Avion," Adersa/Gergios, pp. 75-195.

Reid, J.G., D.E. Chaffin and J.T. Silverthorn (1981), "Output Predictive Algorithmic Control: Precision Tracking with Application to Terrain Following," AIAA J. Guidance and Control, vol. 4, no. 5, pp. 502-509.

Richalet, J., (1980), "General Principles of Scenario Predictive Control Techniques," Proc. JACC.

Richalet, J. and B. Gimonet (1968), "Identification des Systemes Discrets Linearines Monovariables par Minimisation d'une Distance de Structure," Electronics Letters, vol. 4, no. 24.

Richalet, J., F. Lecamus and P. Hummel (1970), "New Trends in Identification, Minimization of a Structural Distance," Weak Topology, 2nd IFAC Symp. on Identification, Prague.

Richalet, J., A. Rault and R. Pouliquen (1971), "Identification des Processus par la Methode du Modele, Gordon and Breach.

Speyer, J.L. and T.L. Song (1981), "A Comparison Between the Pseudomeasurement and Extended Kalman Observers," presented at the Conf. Decision and Control, San Diego, CA.

Testud, J.L. (1977), Commande Numerique Multivariable du Ballon de Recuperation de Vapeur, Adersa/Gergios.

West, C.L., B.R. Ummel and R.F. Yurczyk (1980), "Analysis of Ejection Seat Stability using EASY Program," AFWAL-TR-80-3014.

White, B.J. (1974), "Aeromechanical Properties of Ejection Seat Escape Systems," Report AD-787-194, AF Flight Dynamics Lab.

Wishner, R.P., R.E. Larson and M. Athans (1970), "Status of Radar Tracking Algorithms," presented at the Symp. Nonlinear Estimation Theory and Its Application, San Diego, CA.

U.S. GPO: 646-066

END

FILMED

5-86

DTIC